Correlation analyses of deep galaxy samples

Phillips, Steven

CORRELATION ANALYSES OF DEEP GALAXY SAMPLES

by

Steven Phillipps, B.Sc., M.Sc., F.R.A.S.

A thesis submitted to the
University of Durham
for the degree of
Doctor of Philosophy

April 1979

To my parents

and

Mr B.M. Hogbin

without whom this thesis would never have been completed

ABSTRACT

Methods are set out for the study of galaxy correlations using deep Schmidt plates and an automatic measuring procedure.

The covariance function is defined and shown to be an objective measure of galaxy clustering. The work of previous authors on the angular covariance function and the conversion of this to the spatial covariance function is reviewed. The clustering of clusters is discussed.

The form of the data used is described and the procedure for calculating the angular covariance function is set out. The form of the angular covariance function is found to be consistent with a power law of index $-0{\cdot}8$, in agreement with previous estimates.

In order to compare the amplitude of the angular covariance function for the very deep samples with that obtained from the earlier shallow samples, a cosmological generalization of Limber's formula is derived. In order to evaluate this, the distribution in distance of the galaxies in the sample is required.

This is obtained via the distribution of angular diameters of the galaxies. A detailed model of the galaxy population is used to determine the expected distribution of angular diameters and the best fit to

the observed counts gives the most likely parameters for the model. This in turn gives the distance distribution of the visible galaxies.

It is found that the amplitude is lower than expected and it is judged that this is due to the use of very small areas which may not truly reflect the overall clustering pattern. Nonetheless, it is felt that the methods described will prove a valuable and powerful means of exploring the large scale distribution of galaxies.

PREFACE

The work presented in this thesis was carried out between 1975 and 1977 while the author was a research student under the supervision of Professor A.W. Wolfendale and later Dr.R. Fong, in the Department of Physics at the University of Durham.

Some of the research was carried out in collaboration with Dr. Fong and Dr. R.S. Ellis, but the majority is the author's own work.

Certain results have been published in the following papers :

Dodd, R.J., MacGillivray, H.T., Ellis, R.S., Fong, R. and Phillipps, S., 1976, Mon.Not.R.astr.Soc., 176, 33P

Ellis, R.S., Fong, R. and Phillipps, S., 1977, Mon.Not.R. astr.Soc., 181, 163.

Phillipps, S., 1978, in IAU Symposium No.79. The Large Scale Structure of the Universe (Dordrecht, Reidel), p280.

Phillipps, S., Fong, R., Ellis, R.S., Fall, S.M. and MacGillivray, H.T., 1978, Mon.Not.R.astr.Soc., 182, 673.

CONTENTS

CHAPTER ONE

INTRODUCTION

'But if the matter was evenly disposed throughout an infinite space, it could never convene into one mass; but some of it would convene into one mass, and some into another, so as to form an infinite number of great masses, scattered at great distances from one another throughout all that infinite space'.

Isaac Newton.

1.1 HISTORICAL BACKGROUND TO THE STUDY OF GALAXY CLUSTERING

In 1784 Messier published his famous catalogue of objects to be avoided when hunting comets. Whether or not he remarked on the fact is not recorded, as far as the present writer is aware, but a remarkable number of these objects appear in the constellation of Virgo and several more in Coma Berenices.

Concentrations of nebulae in these areas were noted by Herschel (1811), however, and the cataloguing of nebulae during the following century, much of it by the Herschels between about 1780 and 1860 (Herschel 1864) culminating in the New General Catalogue of Dreyer (1888), revealed several concentrations of nebulae. Two of these, in Coma and Perseus were described in some detail by Wolf (1902, 1906).

By 1918 progress in the observation of spiral nebulae especially by Slipher enabled Wirtz to suggest that they were generally moving away from the solar neighbourhood, and after Hubble (1924) proved that the spiral nebulae were extragalactic, Wirtz, Lundmark (1924) and Hubble (1927) himself, established that the velocity of recession (the redshift) increased linearly with distance, thus enabling astronomers to find the distance of a galaxy and hence distinguish between chance alignments and genuine clusters of galaxies at the same distance.

Wirtz (1924) had called attention to several

conspicuous centres of clustering, and at least four clusters - Virgo, Ursa Major and two in Fornax - are apparent among the bright galaxies in the Shapley-Ames catalogue (1932).

Shapley (1933) described 25 individual clusters and further Harvard surveys revealed more and more clustering, which suggested from its uneven distribution the possibility of superclustering, i.e. the existence of clusters of clusters.

Hubble (1934) investigated what he called the great clusters of about 500 members each and estimated that one per cent of all galaxies belong to such a cluster. Hubble also studied the galaxy distribution outside the great clusters. He found that these were also non-randomly distributed and inferred the presence of small scale clustering (Hubble 1936).

As more clusters were discovered, Zwicky (1938) was led to propose that all galaxies belong to clusters, and that the universe was divided into cluster cells of diameter around 75 Mpc (on the present estimate of the distance scale, $H_o = 50$ km s^{-1} Mpc^{-1}, given by Sandage 1975).

From the Lick Astrographic Survey, Shane and his collaborators were able to point out many clusters and apparent superclusters and these plates gave the first sample large enough for statistical analyses to be applied meaningfully to the galaxy distribution (see

section 1.4 below).

Abell (1958) catalogued 2712 rich clusters visible on the Palomar Sky Survey prints, and analysed the distribution of 1682 of these which comprised a more or less homogeneous sample, while Zwicky and his associates prepared the far more comprehensive Catalogue of Galaxies and Clusters of Galaxies (Zwicky et al 1961-1968).

1.2 TYPES OF CLUSTERS

There exists a wide variety of forms of galaxy cluster, ranging from rich compact clusters like the Coma cluster containing several thousand members down to small groups like the local group which has about 20 members, only three of which are conspicuous giant galaxies.

De Vaucouleurs (1975) has studied the nearby small groups of galaxies and found 54 within about 35 Mpc (for $H_o = 50$ km s^{-1} Mpc^{-1} ; this value will be assumed henceforth) of the local group. He also concluded that at most 10% of the galaxies in this volume were not in a group of some size. Holmberg (1962) however, claims that only 50% of galaxies are in clusters.

Clusters can also be divided into regular and irregular; regular clusters having populations upward of 1000 and showing a central concentration and spherical

symmetry, while irregular clusters may have any number of members but have no central concentration or symmetry of shape. Regular clusters are usually found to be dominated by elliptical and lenticular galaxies, whereas all types are present in the irregular clusters (Abell 1975).

The Virgo cluster and other rich irregular clusters such as Hercules have diameters around 3 to 5 Mpc with some as large as 10 Mpc, while small groups like the local group range from about 1 to 3 Mpc. The sizes of the regular clusters are somewhat more difficult to judge, but Abell (1975) suggests that they are also of the order of 3 to 5 Mpc, while Zwicky and Rudnicki (1963) claim that the largest clusters have diameters of around 10 Mpc. Many irregular clusters appear to possess sub-concentrations with characteristic scales less than 1 Mpc (Abell, Neyman and Scott 1964).

1.3 SUPERCLUSTERING AND HIERARCHICAL MODELS

Holmberg (1937) suggested the existence of a metagalactic cloud with a centre in the general direction of the north galactic pole and about 18 Mpc from the Galaxy. The idea of a local supercluster has been vigorously followed by de Vaucouleurs (1953, 1956, 1958, 1971, 1975a), who considers it to have a diameter of about 75 Mpc, centred on Virgo and to contain the local group the Ursa Major cloud and many smaller clusters and groups.

Bahcall and Joss (1976) consider the 'supercluster effect' to be due merely to the chance proximity of the Virgo cluster.

Shane (1956) noted several apparent aggregates of clusters on the Lick Survey plates which have dimensions of 15 to 60 Mpc. Abell (1961) also noted groupings among the clusters in his catalogue comprising about 10 members each.

As long ago as 1908, Charlier proposed that the structure of the universe could be hierarchical, that is, galaxies belong to clusters, which themselves aggregate in superclusters, the superclusters then being part of higher order clusters and so on.

Support for this view has been given by de Vaucouleurs (1970) and the possibility of hierarchical models has also been considered by Peebles (1974a), but the majority of observers believe that the largest clustering scale is the supercluster of dimensions up to perhaps 100 Mpc. Thus on scales of several 100's of Mpc the universe may be considered to be statistically homogeneous and isotropic, as is required in the derivation of the usual Friedmann models and in particular for the Robertson-Walker metric (see e.g. Weinberg 1972, chapter 14, and appendix A).

1.4 STATISTICAL METHODS FOR STUDYING GALAXY CLUSTERING

When the Lick Astrographic Survey was made it produced a wealth of data amenable to statistical analysis.

Neyman and Scott (1952) and Neyman, Scott and Shane (1953, 1954) found serial correlations in the counts in $1^{\circ} \times 1^{\circ}$ cells and derived parameters to describe the scale and degree of the clustering. They then produced artificial fields of galaxies with these parameters, assuming that all galaxies were in clusters, and found that the synthetic fields were extremely similar to the real galaxy fields. Their conclusions were that most galaxies belong to clusters a few Mpc in diameter (with around 100 members).

Limber (1953, 1954) also used the Lick Counts and by considering the density of galaxies to be a smoothly varying function of position, comprising a mean density $\bar{\rho}$ and fluctuation $\bar{\rho}\, D(\underline{r})$ where r is the distance from the observer in some given direction in space, deduced a further estimate of the scale of clustering which was in general agreement with Neyman and Scott's. Limber's technique was essentially similar to the covariance analysis later developed by Peebles which uses the numbers of pairs of objects separated by some angle θ. Limber further derived a formula for comparing the results found from surveys complete to different limiting apparent magnitudes.

Rubin (1954) also considered a fluctuating term $D(\underline{r})$ and by dividing the sky into small areas computed the mean square fluctuations $\overline{N^2} / \overline{N}^2$, where N is the number of galaxies brighter than some limiting magnitude in one of the small areas of the sky, for various assumed forms for the autocorrelation of $D(\underline{r})$.

The indeterministic approach of Neyman (1962) assumes the observable universe to be one realization of a stationary stochastic process which determines whether a galaxy is present at any particular point and if so what its luminosity, size, mass etc., are. This approach has also been adopted by Peebles (1973), but unlike Neyman and Scott's attempt to derive as many parameters of the galaxy distribution as possible, Peebles' aim was to evaluate the autocovariance of the two dimensional distribution (the covariance function) and its Fourier transform, the power spectrum, and hence to determine a limited number of simple statistical measures of the clustering process.

Totsuji and Kihara (1969) had already evaluated the angular covariance function for the Lick Counts and deduced the form of the spatial covariance function, and Peebles and his collaborators (Peebles 1973, Hauser and Peebles 1973, Peebles and Hauser 1974, Peebles 1974a, Peebles 1974b, Peebles 1975, Davis, Groth and Peebles 1977, Groth and Peebles 1977, Seldner and Peebles 1977) have since analysed the distributions of galaxies in the Zwicky and

Shane-Wirtanen catalogues and in the Jagellonian field (Rudnicki et al 1972) as well as the distribution of clusters in the Abell catalogue and the cross-correlations between the clusters and the Shane-Wirtanen galaxies. A further analysis was the evaluation of the 3-point covariance function for the Shane-Wirtanen catalogue (Peebles and Groth 1975, Groth and Peebles 1977) and the Jagellonian field (Peebles 1975). Even a somewhat obscure four-point correlation function has been evaluated for part of the Zwicky catalogue by Kalinkov, Kuneva and Gelovska (1976) in an attempt to find superclustering statistically.

Abell (1958) used a simple χ^2 test on the number of clusters from his catalogue, in small areas of the sky and deduced the existence of superclusters of dimensions ~ 60 Mpc and containing $\sim$ 10 clusters each. The applicability of this test, especially for estimating scales was challenged by Yu and Peebles (1969), who, from a power-spectrum analysis (Blackman and Tukey 1959), concluded that although there was very significant evidence for non-randomness in the distribution of clusters, not more than 10% of clusters could be in the type of superclusters envisaged by Abell.

In a further analysis of the distribution of Abell clusters using the power-spectrum, Hauser and Peebles (1973) found 'clear and direct evidence' for superclusters with small angular scales, in agreement with the results of Bogard and Wagoner (1973) who used nearest neighbour

distributions (Wagoner 1967). Using both the power-spectrum and covariance function, Hauser and Peebles deduced the existence of superclusters containing 2 or 3 clusters each and of typical scale $\sim$ 40 Mpc. Large scale irregularity of the distribution was also noted, but most of the power at small wavenumbers, i.e. large separations, appeared to be due to a zone of depletion - either real or due to obscuration.

--

CHAPTER TWO

THE COVARIANCE FUNCTION

'The general subject of study in the theory of clustering of galaxies may be described as the search for formulas connecting the various characteristics of the model described, that is to say, the presumed happenings in space, with the statistical characteristics of the observations'.

Jerzy Neyman.

2.1 DEFINITIONS AND LIMBER'S FORMULA

In chapter 1 the angular covariance function or autocorrelation function was introduced as an objective measure of clustering. In this chapter, the concepts involved in this form of correlation analysis and the results obtained by previous authors are described. Interpretation is postponed until a later chapter when the relevant parts of the present analysis can also be incorporated.

Following Peebles (1973) define the angular covariance function $w(\theta)$ through the conditional probability

$$\delta P(\theta) = \mathcal{N}(1 + w(\theta))\,\delta\Omega \qquad (2.1)$$

of observing another galaxy in the solid angle $\delta\Omega$ at an angular separation θ from an arbitrary galaxy in a sample with mean number density $\mathcal{N}$ per unit solid angle.

Similarly define the spatial covariance function at cosmic time t, $\xi(y,t)$, through the conditional probability

$$\delta P_1(y,t) = n(1 + \xi(y,t))\,\delta V \qquad (2.2)$$

of there being another galaxy in the comoving volume δV a comoving distance y from an arbitrary galaxy at the cosmic time t, where n is the mean number density per unit comoving volume (a constant providing there is no creation or annihilation of galaxies). It is assumed

that the universe is isotropic and homogeneous on large scales and can be described by the Robertson-Walker metric (see appendix A).

Now if the volume δV subtends a solid angle $\delta\Omega$ it is easily seen from the R-W metric that

$$\delta V = \frac{r_2^2 \delta r_2}{(1 - kr_2^2)^{1/2}} \delta\Omega \qquad (2.3)$$

where r_2 is the comoving distance from the observer to δV. Hence

$$\delta P_1(y,t) = n\,(1 + \xi(y,t)) \frac{r_2^2 \delta r_2}{(1 - kr_2^2)^{1/2}} \delta\Omega \qquad (2.4)$$

Let the probability that a galaxy at distance r is included in the sample be $\Phi(r)$. This is known as the selection function.

Then the probability that an arbitrary galaxy in the sample is at a distance $r \in (r_1, r_1 + \delta r_1)$ from the observer is

$$\delta P_2(r_1) = \frac{\Phi(r_1)\, r_1^2 \delta r_1}{(1 - kr_1^2)^{1/2}} \Big/ \int_0^\infty \frac{\Phi(r)\, r^2\, dr}{(1 - kr^2)^{1/2}} \qquad (2.5)$$

and the probability that there is a galaxy in δV in the sample is

$$\delta P_3(r_2) = n\,(1 + \xi(y,t)) \frac{\Phi(r_2)\, r_2^2 \delta r_2\, \delta\Omega}{(1 - kr_2^2)^{1/2}} \qquad (2.6)$$

Also

$$\mathcal{N} = n \int_0^\infty \phi(r) \frac{r^2\, dr}{(1 - kr^2)^{1/2}} \qquad (2.7)$$

Now if the distance y subtends an angle θ at the observer (see figure 2.1), then it follows, by integrating over all possible r_1 and r_2, that

$$\delta P(\theta) = \int_0^\infty \int_0^\infty n(1 + \xi(y,t)) \frac{\phi(r_1)\, r_1^2\, dr_1}{(1 - kr_1^2)^{1/2}} \frac{\phi(r_2)\, r_2^2\, dr_2}{(1 - kr_2^2)^{1/2}} \qquad (2.8)$$

i.e.

$$w(\theta) = \frac{\int_0^\infty \int_0^\infty \xi(y,t) \frac{\phi(r_1)\, r_1^2\, dr_1}{(1 - kr_1^2)^{1/2}} \frac{\phi(r_2)\, r_2^2\, dr_2}{(1 - kr_2^2)^{1/2}}}{\left(\int_0^\infty \frac{\phi(r_1)\, r_1^2\, dr_1}{(1 - kr_1^2)^{1/2}} \right)^2} \qquad (2.9)$$

where $y = y(\theta, r_1, r_2)$

and $t = t(\frac{1}{2}(r_1 + r_2))$

Since the observer sees the two galaxies as they were at times $t(r_1)$ and $t(r_2)$, the cosmic time at which ξ should be taken strictly depends on both. However, in all cases $t(r_1) \approx t(r_2)$, since correlations exist only on scales small compared to the Hubble radius, so the time at the mid-point of r_1 and r_2 is a convenient choice.

This is the cosmological generalization of the

Figure 2.1

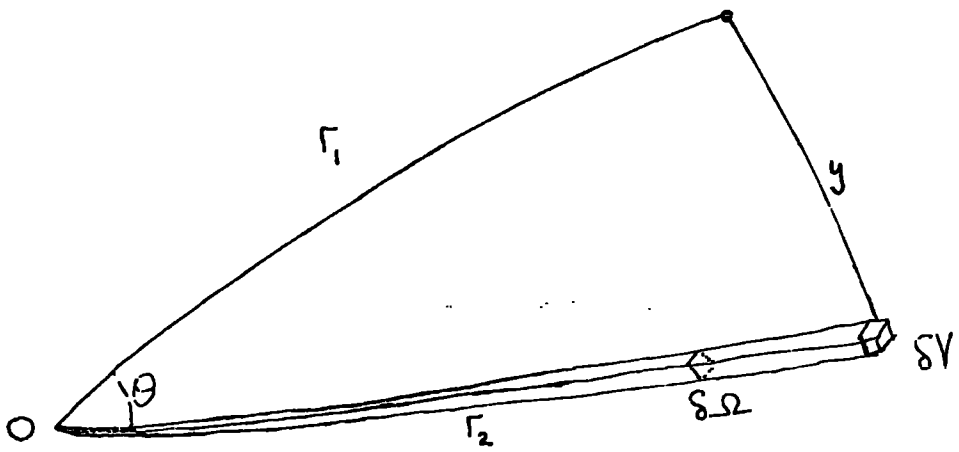

Relationship between comoving coordinates r_1, r_2 and y and the parameters θ, $\delta\Omega$ and δV.

formula first derived by Limber (1953) to relate w and ξ. Alternative derivations of generalized versions of Limber's formula are given by Fall (1976) and Phillipps *et al* (1977).

If correlations exist only on small scales, the R-W line element may be used to give the approximation

$$y^2 = \frac{(r_1 - r_2)^2}{1 - kr^2} + r^2\theta^2 \qquad (2.10)$$

where the choice of $r = \frac{1}{2}(r_1 + r_2)$ as the radial co-ordinate is arbitrary since $r_1 \approx r_2$ when r is small, and it is easy to see that equations (2.9) and (2.10) reduce to the usual formula (Peebles 1973) in the limit of small r_1, r_2.

It is now convenient to change from co-ordinate distances to redshifts, in which case equation (2.9) becomes

$$w(\theta) = \frac{\int_0^\infty \int_0^\infty \xi(y,t)\phi(z_1)\phi(z_2)\, f^2(z_1)g(z_1)(1+z_1)^3\, f^2(z_2)g(z_2)(1+z_2)^3\, dz_1\, dz_2}{\left(\int_0^\infty \phi(z)\, f^2(z)\, g(z)\, (1+z)^3\, dz\right)^2} \qquad (2.11)$$

and

$$y^2 = \left[g^2(z)\,(z_1 - z_2)^2 + f^2(z)\,\theta^2\right](1+z)^2\, R_0^{-2} \qquad (2.12)$$

where

$$f(z) = zq_0 + (q_0 - 1)\left((2q_0 z + 1)^{1/2} - 1\right) cH_0^{-1}(1+z)^{-2} q_0^{-2} \qquad (2.13)$$

is the angular diameter distance,

$$g(z) = c\, H_0^{-1}(1+z)^{-2}\,(2q_0 z + 1)^{-1/2} \qquad (2.14)$$

is the derivative of proper distance with respect to

redshift, and H_o , q_o and R_o are the Hubble parameter, deceleration parameter and cosmic scale factor at the present epoch (c.f. Weinberg 1972, equations 15.3.4 and 15.3.23), z, z_1 and z_2 being the redshifts corresponding to r, r_1 and r_2 respectively.

If the galaxy distribution is not time independent, it is convenient to replace $\xi(y,t)$ in equation (2.12) by $\xi(s,z)$ where s is the proper separation at the redshift z, corresponding to co-ordinate separation y,

$$s = y R_o (1+z)^{-1}$$

$$= \left[g^2(z) (z_1 - z_2)^2 + f^2(z) \theta^2 \right]^{1/2} \qquad (2.15)$$

In the simplest approximation, take $\xi(s,z)$ to be separable i.e. of the form

$$\xi(s,z) = \xi_o(s) h(z) \qquad (2.16)$$

(see section 2.3), then

$$w(\theta) = \frac{\int_0^\infty \int_0^\infty h(z) \xi_o(s) \phi(z_1) \phi(z_2) f^2(z_1) f^2(z_2) g(z_1) g(z_2) (1+z_1)^3 (1+z_2)^3 \, dz_1 dz_2}{\left(\int_0^\infty \phi(z) f^2(z) g(z) (1+z)^3 \, dz \right)^2} \qquad (2.17)$$

Changing variables from (z_1, z_2) to (z,x) where $x = z_1 - z_2$ and using the approximation $z_1 \approx z_2 \approx z$, we have

$$w(\theta) = \frac{\int_0^\infty (1+z)^6 h(z) \phi^2(z) f^4(z) g^2(z) dz \int_{-2z}^{2z} \xi_o((g^2(z)x^2 + f^2(z)\theta^2)^{1/2}) dx}{\left(\int_0^\infty \phi(z) f^2(z) g(z) (1+z)^3 \, dz \right)^2} \qquad (2.18)$$

and again using the assumption that ξ_o is zero except for small separations, we can change the limits of the inner integral to $(-\infty, +\infty)$ since the added contribution from large x is negligible. Then, with $u = g\,x/f\theta$

$$w(\theta) = \frac{\int_0^\infty (1+z)^6\, h(z)\, \phi^2(z)\, f^5(z)\, g(z)\, \theta\, F(f(z)\,\theta)\, dz}{\left(\int_0^\infty \phi(z)\, f^2(z)\, g(z)\, (1+z)^3\, dz \right)^2} \qquad (2.19)$$

with

$$F(v) = \int_{-\infty}^{\infty} \xi_o(v\sqrt{1+u^2})\, du \qquad (2.20)$$

2.2 THE POWER LAW COVARIANCE FUNCTION

The angular covariance function has been previously evaluated for various samples of galaxies as mentioned in Chapter 1. Totsuji and Kihara (1969) using the Lick Counts (Shane and Wirtanen 1967), found that $w(\theta)$ was well represented by a power law of index - 0·8. Peebles and co-workers (Peebles and Hauser 1974, Peebles 1975) subsequently analysed the Shane-Wirtanen and Zwicky Catalogues (Zwicky et al 1961-1968) and the Jagellonian Catalogue (Rudnicki et al 1972), concluding that a power law of this form was indeed a good fit to all the estimates of the angular covariance function (see also Peebles 1974a).

If we put $$\xi_o(s) = \alpha\, s^{-\gamma} \qquad (2.21)$$

in equation (2.20) then with $\gamma = 1 + \delta$

$$F(v) = \alpha I(\delta)\, v^{-(1+\delta)} \tag{2.22}$$

where

$$I(\delta) = \int_{-\infty}^{\infty} (1 + u^2)^{-\left(\frac{1+\delta}{2}\right)} du$$

$$= \sqrt{\pi}\, \Gamma\left(\frac{\delta}{2}\right) \Big/ \Gamma\left(\frac{\delta+1}{2}\right) \tag{2.23}$$

$$\therefore \quad w(\theta) = G\, S(\phi)\, \theta^{-\delta} \tag{2.24}$$

with $$G = \alpha I(\delta) \tag{2.25}$$

and

$$S(\phi) = \frac{\int_0^{\infty} (1 + z)^6\, h(z)\, \phi^2(z)\, g(z)\, f^{4-\delta}(z)\, dz}{\left(\int_0^{\infty} (1 + z)^3\, \phi(z)\, g(z)\, f^2(z)\, dz \right)^2} \tag{2.26}$$

Thus we see that a power law spatial covariance function gives rise to a power law angular covariance function, with the index raised by one. Note that for a given δ, G is independent of the survey, while S is determined solely by the selection function for the sample, so to compare the angular covariance functions from different surveys it is only necessary to consider the factor S.

First consider a simple case where ϕ (z, sample) = $\phi\,(z/z^*)$ where z^* is a representative redshift for galaxies in the survey, which for convenience can be taken to be the greatest redshift at which a galaxy of

some particular absolute magnitude M^* will be visible. In a shallow magnitude limited sample this will be a good approximation since $\phi(z)$ is then simply the fraction of galaxies brighter than $M = M^* - 5 \log z/z^*$ (as the luminosity distance is essentially linear in z), and is clearly only a function of z/z^*. Thus

$$S(z^*) = \frac{\int_0^\infty \phi^2\left(\frac{z}{z^*}\right)\left(\frac{c}{H_0}\right)^{5-\delta} z^{4-\delta}\, dz}{\left(\int_0^\infty \phi\left(\frac{z}{z^*}\right)\left(\frac{c}{H_0}\right)^{3} z^2\, dz\right)^2}$$

$$= \left(\frac{c\, z^*}{H_0}\right)^{-1-\delta} \frac{\int_0^\infty \phi^2(a)\, a^{4-\delta}\, da}{\left(\int_0^\infty \phi(a)\, a^2\, da\right)^2}$$

$$\therefore \quad w(\theta) = K\,(D^*)^{-1-\delta}\,\theta^{-\delta} \qquad (2.27)$$

where K is a constant independent of the survey and $D^* = cz^*/H_0$ is a representive depth for the survey (c f. Peebles 1974a equation (2)). Equation (2.27) may also be written in the useful form

$$w(\theta) = K_1\, \mathcal{N}^{-\left(\frac{1+\delta}{3}\right)}\, \theta^{-\delta} \qquad (2.28)$$

since $\mathcal{N} \propto (D^*)^3$ in this simple case, K_1 being another constant.

The determination of S for a deep sample is considered in chapter 6. This is a non-trivial extension of the above, because the luminosity distance

is no longer linear in z and k-corrections (see footnote) and cosmological effects become important in determining ϕ.

FOOTNOTE:

The k-correction is the change in apparent luminosity of a source at redshift z, due to (a) the fact that for a fixed bandpass in the observed frame, the bandwidth in the emitter's frame is reduced by a factor $(1 + z)$ and (b) the possible difference in flux between the emitted wavelength and the observed wavelength in the spectrum of the source. It is thus defined by

$$k(z) = 2{\cdot}5 \log(1 + z) + 2{\cdot}5 \log\left(\int_0^\infty F(\lambda)S(\lambda)d\lambda \Big/ \int_0^\infty F(\lambda/(1+z))S(\lambda)d\lambda \right)$$

where $F(\lambda)$ is the flux at wavelength λ and $S(\lambda)$ is the detector response. This may be approximated for all usual purposes by

$$k(z) = 2{\cdot}5 \log(1 + z) + 2{\cdot}5 \log\left[F(\bar{\lambda}) \,/\, F(\bar{\lambda}/(1 + z)) \right]$$

where $\bar{\lambda}$ is the wavelength at the peak of the detector response.

2.3 A SIMPLE MODEL FOR CORRELATION EVOLUTION

In section 2.1 a simple functional form to represent the evolution of the spatial covariance function was introduced. Using the power law form of section 2.2 this gives

$$\xi(s,z) = B\, s^{-\gamma}\, h(z) \tag{2.29}$$

Now consider a region of space where proper separations between galaxies vary with cosmic time according to

$$s(t) = s(t_o)\left[\frac{R(t)}{R(t_o)}\right]^{\beta} \tag{2.30}$$

where $R(t)$ is the cosmic scale factor. Note that if the galaxies expand with the universe $\beta = 1$, if they maintain constant proper separations $\beta = 0$ and if they collapse together $\beta < 0$. The number of galaxies in a volume which collapses according to equation (2.30) and is a proper distance $s(t)$ from an arbitrary galaxy in the region is

$$n(t)\, V(t)\left[1 + \xi(s(t),t)\right] = \text{constant}$$

where $n(t)$ is the proper density at time t, so

$$\left[\frac{R(t)}{R(t_o)}\right]^{-3}\left[\frac{R(t)}{R(t_o)}\right]^{3\beta}\left(1 + B\, s(t_o)^{-\gamma}\left[\frac{R(t)}{R(t_o)}\right]^{-\beta\gamma} h(t)\right) = 1 + B\, s(t_o)^{-\gamma}$$

$$\therefore \quad h(t) \approx \left[\frac{R(t)}{R(t_o)} \right]^{\beta\gamma - 3\beta + 3} \qquad \text{for } t \approx t_o$$

or

$$h(z) \approx (1 + z)^{3\beta - 3 - \beta\gamma} \tag{2.31}$$

Thus as a simple, one parameter model we may use

$$h(z) = (1 + z)^{-\eta} \tag{2.32}$$

with $\eta = \gamma$ if all galaxies move with the expansion of the universe (the expanding model), $\eta = 3$ if all the galaxies remain at fixed proper distances from each other (the non-evolving model) and $\eta = 6 - \gamma$ if clusters contract with $\beta = 1$ (a representative collapsing model with a 'reasonable' collapse rate).

2.4 COMPARISON OF ANGULAR COVARIANCE FUNCTION ESTIMATES

The first use of the covariance function, as such, in the study of galaxy clustering, was made by Totsuji and Kihara (1969). They used the Shane-Wirtanen counts and obtained a power law form for the correlations, with an index - 0·8.

In their study of the Zwicky Catalogue, Peebles and Hauser (1974) used a sample with photographic magnitude limit of $15^{m}\cdot 0$. They randomly sampled pairs

of galaxies and used as their estimate of the angular covariance function

$$w\left(\frac{\theta_1 + \theta_2}{2}\right) = f \frac{\Delta\Omega}{\delta\Omega} - 1 \qquad (2.33)$$

where f is the fraction of the chosen pairs of galaxies which have angular separations between θ_1 and θ_2, and $\delta\Omega$ is the average solid angle within the survey area $\Delta\Omega$ which is between θ_1 and θ_2 from a random galaxy in the survey, $\delta\Omega$ being determined empirically. Here and elsewhere w is used both for the covariance function and for its estimates.

In order to see the possible effects of galactic obscuration on the correlations, the analysis was repeated with the galaxies chosen for the pairs with a probability which decreased from 1 at the edge of the area used ($b \geq 40^\circ$) to 0·73 at the north galactic pole, to attempt to compensate for the apparent increase of density with galactic latitude, assuming a cosecant law for the absorption. They found that the large scale correlations were reduced but that $w(\theta)$ was essentially unchanged for $\theta \leq 10^\circ$.

Peebles (1974a) also considered a shallow subset of the Zwicky catalogue, which had a magnitude limit of $13^m.0$. He found that the distribution was dominated by the nearby Virgo cluster and to remove its effect, he then restricted the sample to include only those galaxies

more than 14° from the centre of the Virgo cluster.

With the inclusion of the central region of Virgo the estimates of w for angles in the range $\sim 0^{\circ}.4$ to $\sim 10^{\circ}$ are larger by factors around 2 or 3.

In the Shane-Wirtanen catalogue the data is given as counts of galaxies in $1^{\circ} \times 1^{\circ}$ cells, with various correction factors estimated by the authors (Shane and Wirtanen 1967) for emulsion variations, zenith distance, atmospheric effects and so on. If the corrected number of galaxies in cell i is n_i then Peebles and Hauser's estimator for the angular covariance function is

$$w\left(\frac{\theta_1 + \theta_2}{2}\right) = \frac{\langle n_k\, n_j \rangle}{\langle \frac{1}{2}(n_k + n_j) \rangle^2} - 1 \qquad (2.34)$$

where the averages are taken over all pairs of cells k, j such that the angular separation of their centres is between θ_1 and θ_2 .

The effect of galactic absorption was then taken into account by a correction factor for the cell counts appropriate for the cosecant model. As for the Zwicky catalogue the large scale correlations were reduced but for $\theta \lesssim 4^{\circ}$ the estimates of $w(\theta)$ were unchanged.

Groth and Peebles (1977; also Davis, Groth and Peebles 1977) have recently re-analysed the Shane-Wirtanen data, using the original observations in cells of size $10' \times 10'$, corrected by various factors to

reduce them all to the same effective depth as in the earlier analysis (Seldner et al 1977). If the correction factor for cell i, which contains n_i galaxies, is c_i then their estimate of w is (neglecting errors in the estimates of the c_i)

$$w\left(\frac{\theta_i + \theta_i}{2}\right) \qquad \frac{\langle (c_i n_i - \bar{n})(c_j n_j - \bar{n}) \rangle}{\bar{n}^2 \langle c_i^{(\delta-2)/3} c_j \rangle} \qquad (2.35)$$

where $\bar{n}$ is the mean number per cell and the averages are as above. The factor $\langle c_i^{(\delta-2)/3} c_j \rangle$ is used as a correction for the difference in the angular covariance function at different depths, but is based on the assumption that the 'extra' galaxies seen on deeper plates are uncorrelated with the galaxies on the less deep plates, which is only true if all galaxies have the same absolute magnitude and is clearly not valid in practice, though the extent to which this effects the estimate is not clear. Groth and Peebles estimate it to be of the order of 15%, in the sense of making the estimates of w too high, when the cells i and j are on different plates. Note also that it depends on the assumed form $w(\theta) \propto \theta^{-\delta}$ and on the choice of δ (Groth and Peebles use 0·75).

In addition Groth and Peebles have analysed the counts in four separate zones in order to qualitatively determine the errors which can be expected in their estimates of w. One zone is found to have estimates

which are systematically higher than those in the other zones and this zone is also found to have a large scale density gradient correlated with galactic longitude, possibly due to inadequacies of the cosecant model of galactic obscuration. A further correction was then made by removing large scale density variations by fitting a smooth function to them and multiplying the counts by the reciprocal of the smoothed density at each point (normalized to keep the total counts constant). This was found to reduce the estimates of w on all scales, to a certain extent, the effect being most noticeable where the covariance function was small, at $\theta \gtrsim 3^{\circ}$, where the form of $w(\theta)$ was considerably steepened, conforming more nearly to the shape found by Peebles and Hauser than did the unsmoothed estimates. At a distance corresponding to z^{*} for the Shane-Wirtanen catalogue the change of slope (or break) would be at a linear separation $\sim 9h^{-1}$ Mpc ($h = H_{\circ}/100$ km s^{-1} Mpc^{-1}). The shape of the $w(\theta)$ curve is considered further, shortly.

The Jagellonian catalogue consists of counts of galaxies in squares of side 3·75 arcmin on a $6^{\circ} \times 6^{\circ}$ plate, the density being approximately one galaxy per square. Peebles (1975) used the estimator

$$w\left(\frac{\theta_i + \theta_s}{2}\right) = \frac{\langle n_k n_j \rangle}{\langle n_k \rangle \langle n_j \rangle} - 1 \qquad (2.36)$$

for the angular covariance function, where the averages are defined as in equation (2.34).

In each of the four surveys, it was found that a power law of index -0·8 was a reasonable fit to the data, though in the case of the Shane-Wirtanen catalogue the $w(\theta)$ estimates drop systematically below this form at large θ ($\gtrsim 3^\circ$) and there is a hint of similar behaviour for $\theta \gtrsim 10^\circ$ in the Zwicky catalogue limited at $15^m.0$. If the angular covariance function is written

$$w(\theta) = A\,\theta^{-0.8} \qquad (2.37)$$

with θ in degrees then for the various surveys we have

$$A_Z = 0.70 \qquad (2.38)$$

for the Zwicky catalogue limited at $15^m.0$ (Peebles 1974a, Peebles 1975 variously give amplitudes of 0·69, 0·7, 0·72; I henceforth take 0·70 as the canonical value),

$$A_{Z'} = 2.8 \qquad (2.39)$$

for the Zwicky catalogue limited at $13^m.0$ (taken from figure 1, Peebles (1974a), by eye estimate of the best fit)

$$A_{SW} = 0.068 \qquad (2.40)$$

for the Shane-Wirtanen catalogue (Groth and Peebles 1977: the earlier estimate by Peebles and Hauser 1974

and Peebles 1974a, also shown in Peebles 1975, gave $A_{SW} = 0{\cdot}08$) and

$$A_{Jag} = 0{\cdot}018 \qquad (2.41)$$

for the Jagellonian catalogue (Peebles 1975).

The amplitudes may be compared using the equations of section 2.2, in particular, using the simple 'scaling law' given by equation (2.28) for a shallow, magnitude limited sample

$$A \propto \mathcal{N}^{-0.6} \qquad (2.42)$$

assuming $\delta = 0{\cdot}8$

This should hold at both depths considered in the Zwicky analysis and should be a reasonable approximation in the case of the Shane-Wirtanen catalogue, but may be seriously in error for the Jagellonian field, as this is much deeper and is unlikely to be strictly magnitude limited, though for completeness the Jagellonian catalogue is included in table 2.1 which summarises the expected and observed scaling ratios for the samples considered in this section, under the assumption that $w(\theta)$ varies as a power law of index $-0{\cdot}8$.

Groth and Peebles (1977) have considered cosmological corrections due to redshifts and k-corrections and find that the agreement between the deeper samples and the Zwicky catalogue can be improved. Their corrected 'scaling law' based on the simple law

Table 2.1

SURVEY	$\mathcal{N}$ (per square degree)	A	$\left(\frac{\mathcal{N}}{\mathcal{N}_z}\right)^{-0.6} A_z$	$\frac{A}{A_z}\left(\frac{\mathcal{N}}{\mathcal{N}_z}\right)^{0.6}$
Z′	$3\cdot9 \times 10^{-2}$	$2\cdot8$	$3\cdot6$	$0\cdot78$
Z	$6\cdot2 \times 10^{-1}$	$7\cdot0 \times 10^{-1}$	$7\cdot0 \times 10^{-1}$	$1\cdot00$
SW	$5\cdot4 \times 10^{1}$	$6\cdot8 \times 10^{-2}$	$4\cdot8 \times 10^{-2}$	$1\cdot42$
Jag	$3\cdot3 \times 10^{2}$	$1\cdot8 \times 10^{-2}$	$1\cdot6 \times 10^{-2}$	$1\cdot12$

NOTE: Peebles and Hauser (1974) quoted a density 20% lower than that given by Groth and Peebles, this would increase the predicted amplitude in column four by about 12% to $5\cdot4 \times 10^{-2}$ for the Shane-Wirtanen catalogue. Their earlier estimate of A was about 15% higher than that of Groth and Peebles.

of equation (2.27) is

$$A \propto (y\, D^{*}_{eff})^{-1} (x\, D^{*}_{eff})^{-\delta} \qquad (2.43)$$

where D^{*}_{eff} is obtained from the sample density $\mathcal{N}$ and x and y are the correction factors, calculated for the model considered (i.e. luminosity function - $\Psi(M)$ is the number of galaxies per Mpc brighter than absolute magnitude M - k-corrections and cosmological parameters). Their results, assuming $\delta = 0{\cdot}75$, are presented in table 2.2, where

$$A^{S}_{Z} = A_{Z} (y\, D^{*}/ y_{z}\, D^{*}_{z})^{-1} (x\, D^{*}/ x_{z}\, D^{*}_{z})^{-\delta} \qquad (2.44)$$

is the amplitude found for the Zwicky catalogue scaled with depth according to equation (2.43). The particular model used for the calculations quoted in table 2.2 is Groth and Peebles' "standard model" i.e. zero cosmological constant pressure free universe, with an unevolving (proper) spatial covariance function ($\gamma = 3$ in equation 2.31, see section 2.3); a magnitude limited survey; k-corrections given by $k(z) = 3z$; an Abell (integral) luminosity function (Abell 1962),

$$\left.\begin{array}{lcll} \Psi(M_{B}) & \propto & \mathrm{dex}\left[\beta(M_{B} - M^{*})\right] & M_{B} > M^{*} \\ \Psi(M_{B}) & \propto & \mathrm{dex}\left[\alpha(M_{B} - M^{*})\right] & M^{*} > M_{B} > M_{o} \\ \Psi(M_{B}) & = & 0 & M_{o} > M_{B} \end{array}\right\} \qquad (2.45)$$

Table 2.2

SURVEY	hD^{*}_{eff} (Mpc)	A	x	y	A^{S}_{Z}	A/A^{S}_{Z}
Z	47 2	$7\cdot0 \times 10^{-1}$	1·000	1·000	$7\cdot0 \times 10^{-1}$	1·00
SW	209	$6\cdot8 \times 10^{-2}$	0·867	0·912	$6\cdot3 \times 10^{-2}$	1·08
Jag	383	$1\cdot8 \times 10^{-2}$	0·732	0·887	$2\cdot6 \times 10^{-2}$	0·72

with $\alpha = 0{\cdot}75$, $\beta = 0{\cdot}25$, $M^* = -18{\cdot}6 + 5 \log h$, $M_o = -21{\cdot}3 + 5 \log h$ (where $h = H_o/100$ km s^{-1} Mpc^{-1}); no galaxy luminosity evolution.

Using an extreme model with no galaxies fainter than M^*, Groth and Peebles found that the discrepancy between the expected and observed amplitudes for the Jagellonian catalogue could be reduced. The question of scaling very deep surveys which are not necessarily magnitude limit will be considered in detail in Chapter 3.

The particular form of the corrections used in equation (2.44), that is, the use of two factors x and y, is due to the fit made by Groth and Peebles to their data for the Shane-Wirtanen catalogue. As the $w(\theta)$ estimates for $\theta \gtrsim 2^\circ.5$ drop systematically below the $\theta^{-0.75}$ form which is found at small angles, they adopted a bilinear fit to the log w - log θ curve, with slopes -0·75 and -1·75. When scaled between different depths D_1^* and D_2^* the factor $x_2\ D_2^*/x_1\ D_1^*$ determines the shift in θ of the 'break' point, that is, the intersection of the two straight line portions of $w(\theta)$, while $y_2\ D_2^*/y_1\ D_1^*$ determines the change in amplitude of $w(\theta)$ at the break point (see figure 2.2).

The significance of the break is hard to judge. It is possible that it is an artefact of the method of analysis since it is greatly accentuated when the data is filtered and smoothed, but Groth and Peebles consider it to be an intrinsic property of the distribution for the following reasons: (i) It appears in the estimates

Figure 2.2

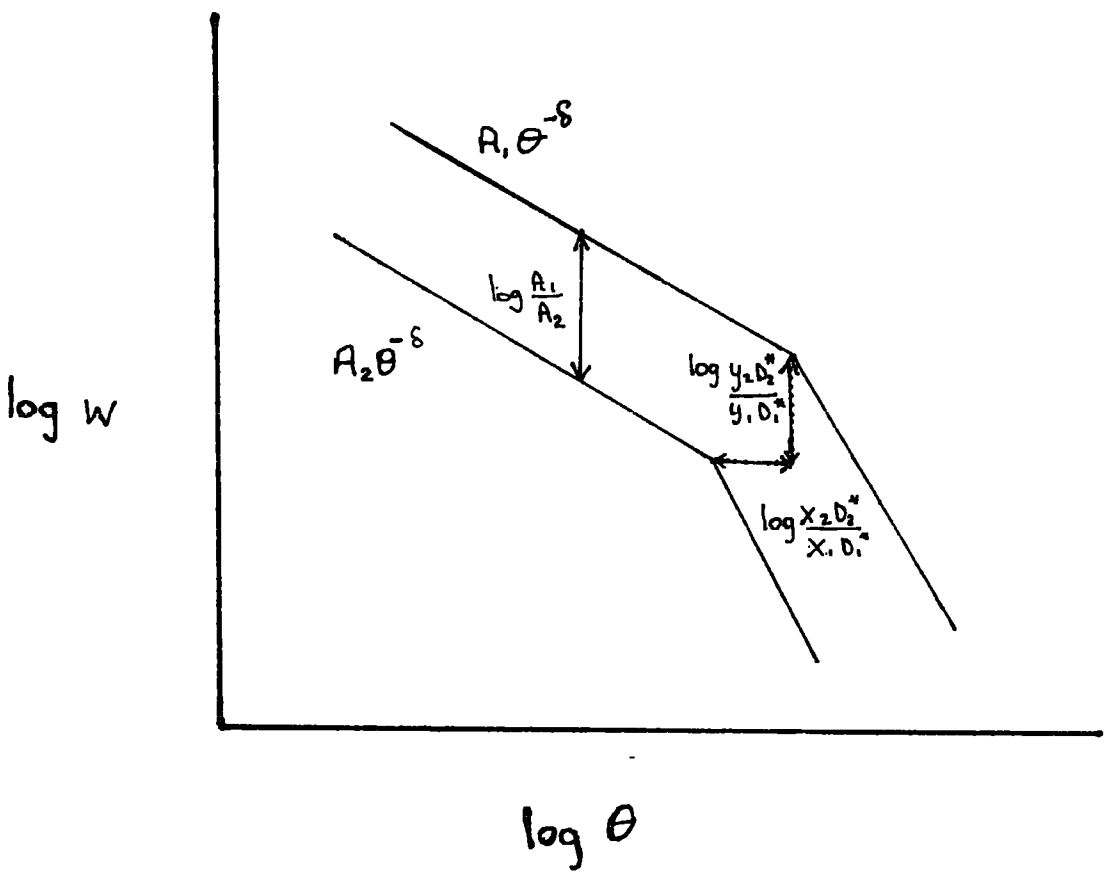

Groth and Peebles (1977) 'corrected' scaling law.

Note that

$$W_1\left(\frac{\theta x_2 D_2^*}{x_1 D_1^*}\right) = W_2(\theta)\frac{y_2 D_2^*}{y_1 D_1^*}$$

i.e. $$\frac{A_1}{A_2} = \left(\frac{x_1 D_1^*}{x_2 D_2^*}\right)^{-\delta}\left(\frac{y_1 D_1^*}{y_2 D_2^*}\right)^{-1}$$

of the covariance function in all four sub areas. (ii) The estimate of $w(\theta)$ for $\theta = 10^{\circ}$, for example, would need to be raised by more than five times the internal standard deviation over the four areas in order to fall on the extrapolated $\theta^{-0.75}$ power law. (iii) There is no evidence for structure on very large scales which could effect the small scale correlations, and (iv) the errors which would be required in order to maintain the power law on all scales are much larger than those estimated by considering the cell counts and their averages.

2.5 ESTIMATION OF THE SPATIAL COVARIANCE FUNCTION

From equations (2.21) to (2.25) it is immediate that if $w(\theta) = A\theta^{-\delta}$ then the spatial covariance function $\xi(s)$ is given by

$$\xi(s) = Bs^{-\gamma} \tag{2.46}$$

with $\gamma = \delta + 1$

and $$B = \frac{A\,\Gamma\left(\frac{\gamma}{2}\right)}{\sqrt{\pi}\,\Gamma\left(\frac{\gamma-1}{2}\right) S} \tag{2.47}$$

S being given by equation (2.26) for any given survey, via the selection function $\phi(z)$.

Using the approximation

$$S = (D^*)^{-\gamma} \frac{\int_0^\infty \phi^2(a)\, a^{5-\gamma}\, da}{\left(\int_0^\infty \phi(a)\, a^2\, da\right)^2} \qquad (2.48)$$

from equation (2.27), together with an Abell integral luminosity function (equation 2.45) to define ϕ through

$$\phi(a) = \Phi(M^* - 5 \log a) \qquad (2.49)$$

($\Phi(M) = \Psi(M)/\Psi(\infty)$ is the fraction of galaxies brighter than M). Peebles and Hauser (1974) obtained from their estimates of A, γ for the Shane-Wirtanen and Zwicky catalogues

$$B = 20\, h^{-1.8} \qquad (2.50)$$

where

$$h = H_o / 100 \text{ km s}^{-1} \text{Mpc}^{-1}$$

with a possible error of a factor of 2 due to the uncertainty in the luminosity function. The power law form was taken to hold over the range $0{\cdot}03 h^{-1}$ to $30\, h^{-1}$ Mpc. With their new estimates of the amplitude of $w(\theta)$ for the Shane-Wirtanen catalogue and using the corrected form of the selection function to take into account redshift and k-corrections

$$\phi(z) = \Phi(m_{lim} - 25 - 5 \log D_L(z) - k(z)) \qquad (2.51)$$

where $D_L(z)$ is the luminosity distance in Mpc at

redshift z and m_{lim} is the limiting magnitude of the survey, with the "standard model" luminosity function of equation (2.45), Groth and Peebles obtained

$$B = 15\, h^{-\gamma}$$

with $\gamma = 1.77$, for the range of separations $0.05\, h^{-1}$ to $9\, h^{-1}$ Mpc.

2.6 INVERSION OF LIMBER'S FORMULA

Rather than assuming a pure power law form for w and hence ξ, it is possible to analytically invert the relationship between w and ξ, which may be useful under certain conditions if the power law model is found to be inadequate, even though the inversion process, as defined by Fall and Tremaine (1977) is found to be very unstable, in that small changes in w can cause large variations in $\xi(w)$.

Equations (2.19) and (2.20) may be rewritten in the case of shallow surveys as

$$w(\theta) = \int_0^\infty r^4\, \Phi(r)\, L(r\theta)\, dr$$

where

$$L(v) = 2v \int_0^1 \frac{\xi(v/u)du}{u^2 (1 - u^2)^{1/2}}$$

and

$$\Phi(r) = \frac{\phi^2(r)}{\left(\int_0^\infty r^2 \phi(r)\, dr\right)^2}$$

Now using the Mellin transform (see e.g. Titchmarsh 1948)

$$\mathcal{M}[f] \equiv \tilde{f}(s) \equiv \int_0^\infty x^{s-1} f(x)\, dx$$

which has the properties

$$\mathcal{M}\left[\int_0^\infty x^p y^q f(xy)\, g(y)\, dy\right] = \tilde{f}(p+s)\,\tilde{g}(q-p+1-s)$$

and

$$\mathcal{M}\left[\int_0^\infty x^p y^q f(x/y)\, g(y)\, dy\right] = \tilde{f}(p+s)\,\tilde{g}(q+p+1+s)$$

we have

$$\tilde{w}(s) = \tilde{L}(s)\,\tilde{\Phi}(5-s)$$

$$\tilde{L}(s) = \tilde{b}(s)\,\tilde{\xi}(s+1)$$

where

$$b(x) = 2(1-x^2)^{1/2} \qquad 0 < x < 1$$

$$= 0 \qquad \text{otherwise}$$

Using the further property

$$\tilde{b}(s-1) = 2\pi/(s-1)\,\tilde{b}(s)$$

it follows that

$$\tilde{\xi}(s) = (s-1)\,\tilde{b}(s)\,\tilde{P}(s)\,\tilde{w}(s-1)$$

where

$$\tilde{P}(s) = \left[2\pi \tilde{\Phi}(6 - s)\right]^{-1}$$

so using the inversion formula for the Mellin transform

$$\xi(a) = -2 \frac{d}{dr} \int_0^\infty dx\, P(x) \int_0^1 dy\, \frac{w(a/xy)}{(1 - y^2)^{1/2}}$$

which is the result obtained by Fall and Tremaine. Using again the Abell integral luminosity function, Fall and Tremaine demonstrated the instability of the inversion to features in the form of $w(\theta)$, and concluded that significant features in ξ could be missed due to the difficulty in distinguishing real features from noise. Despite this, they were confident that from the Shane-Wirtanen data the behaviour of ξ at separations less than about 10 h^{-1} Mpc could be well fitted by a power law of index $\sim -1{\cdot}7$, though they considered that the behaviour of the angular covariance function beyond the break at $\sim 2^\circ{\cdot}5$ might not reflect the true form of ξ at large separations.

2.7 THE ANGULAR COVARIANCE FUNCTION FOR DIFFERENT MORPHOLOGICAL TYPES

It has been claimed by several observers that the central regions of some rich clusters and some compact smaller clusters are dominated by elliptical and

lenticular galaxies (Gunn and Gott 1972, Oemler 1974). It might then be expected that such features will be reflected in the covariance function for the different morphological types.

The Uppsala catalogue (Nilson 1973) contains identifications by morphological type for about 2000 galaxies north of $b = 40^{\circ}$ (it actually covers a considerably larger area, but only the north polar region is relevant here) and is complete to photographic magnitude 14.5.

Geller and Davis (1976) have used this data to determine the angular covariance function for spiral, elliptical and lenticular galaxies separately, as well as the overall covariance function.

Using all the galaxies they obtained

$$A_N = 1{\cdot}00 \quad , \quad \gamma = 1{\cdot}7$$

in good agreement with the results for the Zwicky catalogue obtained by Peebles and Hauser. When a subset of the Nilson catalogue, such that all galaxies within 14° of the centre of the Virgo cluster or within 3° of the centre of the Coma cluster were removed, was analysed the slope was steepened slightly and the amplitude was reduced by 25%.

The single type correlations were found to have

$\gamma = 1{\cdot}7$ and $A = 0{\cdot}69$ for spirals

$\gamma = 1{\cdot}7$ and $A = 3{\cdot}2$ for lenticulars

and $\gamma = 2{\cdot}1$ and $A = 2{\cdot}8$ for ellipticals.

In the case of spiral galaxies, the results for the restricted area were the same as those for the full catalogue, but for the other two types the amplitudes for the smaller area were considerably lower and the slopes steeper. It should be noted, though, that the numbers of lenticulars and ellipticals are very small, only 200 or 300, and hence the angular covariance function estimates are rather uncertain. Another facet of the large fraction of spirals in the sample is that the slope for the spiral-spiral correlation is the same as that for the overall-function, though it is seen that the amplitude is lower for the spirals. In the smaller area the amplitudes for the spirals and the whole distribution are almost equal, which indicates that the major difference between the samples is the presence of a number of highly correlated E and SO galaxies in the central regions of Virgo and Coma.

Using a cross-correlation function w_{ab} defined such that

$$\mathcal{N}_a \mathcal{N}_b [1 + w_{ab}(\theta)] \delta\Omega_a \delta\Omega_b$$

is the probability of finding galaxies of type a in a solid angle $\delta\Omega_a$ and type b in $\delta\Omega_b$, where $\delta\Omega_a$, $\delta\Omega_b$ are separated by an angle θ and $\mathcal{N}_a$, $\mathcal{N}_b$ are the densities of galaxies of types a, b, Geller and Davis obtained the cross-correlations between elliptical, lenticular, spiral and all galaxies. Note that if w_a, w_b

are the individual covariance functions then the total covariance function w_{a+b} is such that the probability of finding objects in areas $\delta\Omega_1, \delta\Omega_2$ is

$$(N_a + N_b)^2 (1 + w_{a+b}) \delta\Omega_1 \delta\Omega_2 = N_a^2 (1 + w_a) \delta\Omega_1 \delta\Omega_2 + N_b^2 (1 + w_b) \delta\Omega_1 \delta\Omega_2 + 2 N_a N_b (1 + w_{ab}) \delta\Omega_1 \delta\Omega_2$$

i.e.
$$w_{a+b} = \left(\frac{N_a}{N_a + N_b}\right)^2 w_a + \left(\frac{N_b}{N_a + N_b}\right)^2 w_b + \frac{2 N_a N_b}{(N_a + N_b)^2} w_{ab} \qquad (2.52)$$

They found that there were relatively twice as many 'excess' elliptical or lenticular galaxies near a randomly chosen galaxy, as there were spirals, and that the correlations between E and SO galaxies were twice as high as those between E and S or SO and S galaxies.

For the region excluding Virgo and Coma the first of these effects was only marginal for SO galaxies and was non-existent for ellipticals, the latter effect was still present though the spiral lenticular correlation was relatively higher, nearer to the elliptical lenticular correlation.

2.8 FIELD GALAXIES

Turner and Gott (1975) studied the distribution on the sky of Zwicky catalogue galaxies brighter than $14^{m}.0$, and claimed that there was evidence for two populations, associated galaxies and single galaxies, distinguished by the presence or absence of a neighbour galaxy less than $0^{\circ}.75$ degrees away. The covariance function of the 623 associated galaxies followed the expected power law form with a rather high amplitude ~ 3 (c f. Section 2.4) but the 465 single galaxies possessed a roughly constant (and positive) covariance on all scales from $45'$ to $\sim 15^{\circ}$. When the sample was restricted to a 'western' subregion, avoiding a noticeably deficient area of the whole sample, the single galaxy covariance function was essentially zero on these scales, corresponding to a completely homogeneous distribution.

However Fall *et al* (1976) point out that the flatness of w for the singles is almost certainly a necessary mathematical result of the selection criteria, in particular the choice of $45'$ as the angular scale determining singles. They conclude that the singles population defined by Turner and Gott cannot necessarily be regarded as a true field component of the galaxy population and that a similar separation could have been achieved given any underlying form of galaxy clustering with no preferred scale. Soniera and Peebles

(1977) also concluded that there was no distinct population of field galaxies.

2.9 CORRELATIONS OF CLUSTERS OF GALAXIES

Hauser and Peebles (1973) analysed the distribution of 1396 clusters in the Abell catalogue in regions of galactic latitude $|b^{II}| \geq 40^{\circ}$ covering 27% of the sky. The northern region was divided into three zones in latitude since the varying density suggested the presence of large scale obscuration. The (smaller) southern region gave a fourth zone.

For each zone w was estimated by counting the number, n, of other objects (whether in the same region or not) that appear in successive annuli of width $0^{\circ}.2$ centred on each cluster in the region in turn, and using

$$1 + w(\theta) = \frac{\bar{n}}{\Delta A(\theta) N_c} \qquad (2.53)$$

where $\Delta A(\theta)$ is the area of the annulus centred on separation θ and N_c is the density of clusters in the zone. This was repeated for three sets of clusters; those in Abell distance classes 1 to 4, 1 to 5 and 1 to 6, to obtain estimates of w to different depths.

They found positive values of w at small angles

in all the zones, evidence of clustering on scales of a few degrees. Integrating w - or alternatively using the power spectrum - they deduced superclusters of 2 or 3 members. The estimates of w for zone III, the lowest latitude zone, were noticeably higher than for the other regions, while the density was lower, implying that the catalogue was less deep there than in the other zones.

Using the 'scaling law'

$$w_2(\theta) = \frac{D_1}{D_2} w_1(\theta \frac{D_2}{D_1}) \qquad (2.54)$$

(c f. Peebles 1973, equation 69; the equivalent of equation 2.27 for a general w, which is simply obtained from equation 2.19 in the case of small z by using $\phi(r,D) = \phi(\frac{r\theta}{D\theta})$) with the distance class limits of Abell, they showed that the w estimates varied in the way expected for true clustering and were not merely due to varying obscuration or other such causes.

They introduced the analytic form

$$\bar{\xi}(r) = A \exp(-\lambda^2 r^2) \qquad (2.55)$$

for the spatial covariance function and found likely limits

$$30 \lesssim \lambda D_4 \lesssim 40$$

$$7 \lesssim A \lesssim 16$$

where D_6 is the limit of Abell's distance class 6, quoted as 638 h^{-1} Mpc ($h = H_o/100$ km s^{-1} Mpc^{-1}).

Peebles and Hauser (1974) refitted the data with a power law of index -1, while in a later paper, Seldner and Peebles (1977) assumed $w \propto \theta^{-0.8}$ as for the galaxy autocorrelation.

2.10 CROSS CORRELATION OF CLUSTER CENTRES AND INDIVIDUAL GALAXIES

The cross correlation function is defined such that

$$\delta P = \mathcal{N}_g(1 + w_{gc}(\theta))\,\delta\Omega$$

is the probability of finding a galaxy in the area $\delta\Omega$ distance θ from a cluster centre. This is, of course, equivalent to the definition given in section 2.7. Note that necessarily, $w_{gc} = w_{cg}$.

Peebles (1974b) used the galaxies in the Shane-Wirtanen catalogue along with the cluster centres obtained from Abell's catalogue. They used the estimate

$$w_{gc}(\theta) = \frac{\langle n(\theta)\rangle}{\langle n\rangle} - 1 \qquad (2.56)$$

where $\langle n\rangle$ is the average number of galaxies in a $1^\circ \times 1^\circ$ square of the Shane-Wirtanen catalogue and $\langle n(\theta)\rangle$ is the average number in the squares which have centres

distance $\theta - \Delta\theta/2$ to $\theta + \Delta\theta/2$ from a cluster centre where $\Delta\theta$ is some suitable bin size (squares which are the same distance from more than one cluster are counted with the appropriate multiplicity).

The cross correlation was calculated for four zones separately, the zones being delineated by galactic latitude, as in the analysis of the Abell catalogue discussed in section 2.9 above. In general, positive correlations were found on small scales, i.e. scales up to about 6°. The results for zone C the lowest latitude zone, where there is a low density of clusters, were substantially lower than for the other three zones, but taking into account the uncertainties Peebles considered it appropriate to use the mean over all four zones.

The clusters were further divided into Abell's richness classes 1, 2 and ≥ 3 and distance classes 3 to 6. Results for richness classes 1 and 2 were similar for D = 3, 4 and 5, while those for R $\geq$ 3 were lower in each case. For distance class 6 there was no evidence of correlations for any of the richness classes.

For all the subdivisions there existed a large scale (6° to 10°) correlation but whether this was genuine or an artefact of, for example, galactic obscuration, causing a density variation common to both clusters and individual galaxies was unclear.

Taking superclusters to contain 2 clusters as

before, they estimated that around 12% of galaxies were correlated with rich clusters, those in distance class 3 containing about 450 visible members each, reducing to 70 for clusters in distance class 5. It was noted that this was some 2 to 5 times as many as would be visible in a cluster like the Coma cluster situated at the appropriate distances; the correlations were also over much greater linear scales than the diameters normally assigned to such clusters.

A power law covariance function of index -0·7 to -1·0 (giving a spatial covariance function $\xi(r) \propto r^{-1.7}$ or $r^{-2.0}$) was found to fit the data for R = 1 quite well and to scale correctly between the different distance classes. This spatial covariance function had the same form as found by Peebles and Hauser (1974) for galaxy-galaxy correlations, but with a higher amplitude (by a factor ~ 4). The cluster-cluster correlation of Hauser and Peebles (1973) refitted by Peebles and Hauser had a higher amplitude still (by a factor ~ 2·5).

This was explained as being due to the fact that the position of the cluster galaxies (excepting those tightly concentrated at the cluster centre) and the clusters within a supercluster are assigned according to a common statistical law. This requires about 25% of galaxies to be in rich clusters.

As mentioned above, the very rich clusters ($R \geq 3$) have lower correlations, implying that there are fewer

total numbers of galaxies around the clusters, or that the luminosity function depends on R.

The analysis was repeated by Seldner and Peebles (1977a) using the 10′ by 10′ cells for the Shane-Wirtanen catalogue (Seldner et al 1977). The cross covariance function w_{gc} was estimated in exactly the same way as before (equation 2.56) but now with resolution 2′.5. Again all four zones gave comparable results and the average w_{gc} was used subsequently. The results were considered to be consistent with the previous ones, though, with the better resolution, correlations were evident for the clusters of distance class 6 (note however that an entirely different form for w_{gc} was obtained).

A single power law model for w was considered unacceptable and the empirical form

$$w_{gc} = A\,\theta^{-\beta} + B\,\theta^{-\gamma} \qquad (2.57)$$

was used. Requiring β, γ to be the same for all R and D the best fit was found to be

$$\beta = 1{\cdot}4 \quad , \quad \gamma = 0{\cdot}2$$

At small θ, $\theta^{-1.4}$ dominates so this was taken as the 'intrinsic' density run around a cluster (i.e. density $\propto r^{-2.4}$). Assuming the cluster-cluster correlation to be of the form $\theta^{-0.8}$ like the galaxy-galaxy correlation (this form was not used when the Abell catalogue was discussed previously, but it is a reasonable fit) then the

contribution to w_{gc} by neighbouring clusters should vary as $\theta^{-\gamma}$ with $\gamma = 0{\cdot}8 + 1{\cdot}4 - 2 = 0{\cdot}2$, in agreement with the value found above.

The density run, projected on the sky, for distance class D, richness class R, is given by

$$\begin{aligned} \mathcal{N}\sigma_{DR}(\theta) &= \mathcal{N} A_{DR}\, \theta^{-1.4} && \theta \le \theta_D \\ &= 0 && \theta > \theta_D \end{aligned} \qquad (2.58)$$

where the amplitude A_{DR} depends on distance and richness but the cut-off θ_D is presumed to depend only on distance. If it is chosen such that $\theta_3 = 5^\circ$ (i.e. $\theta_3 D_3 \simeq 15\ h^{-1}$ Mpc) then $\sim 8\%$ of galaxies are in Abell clusters, though this is very sensitive to θ_D, whereas other fits are not.

Note that Peebles (1974a) used a model with density fall-off $r^{-2.4}$ with randomly distributed cluster centres in a model for explaining the galaxy covariance function $w(\theta) \propto \theta^{-0.8}$.

2.11 USES OF THE CROSS CORRELATION

If it is assumed that the spatial correlation functions are fixed time independent functions in all parts of the universe, then by comparing the scaled results from different depths, the luminosity function

which makes them most nearly in agreement might be sought. (This is of course the opposite view to that taken elsewhere in this thesis, where the correlations at different depths are compared assuming that the luminosity function is known and fixed).

In section 2.10 the analysis by Seldner and Peebles (1977a) of the cross-correlation between Abell cluster centres and individual Shane-Wirtanen galaxies was discussed. Their results were consistent with a density run in the Abell cluster

$$n(r) = \langle n \rangle E_R r^{-2.4}$$

where E_R depends on the richness class R. Then for the magnitude limited Shane-Wirtanen galaxies, and ignoring cosmological corrections, in analogy with Limber's formula the surface density

$$\sigma_{DR} = A_{DR} \theta^{-1.4}$$

with

$$A_{DR} = E_R \frac{\int_{-\infty}^{\infty} (1 + x^2)^{-1.2} dx}{\int_0^{\infty} r^2 \phi(r)\, dr} \quad \frac{\int_{D_a}^{D_b} r^{2.6} \phi(r)\, dr}{\frac{1}{3}(D_b^3 - D_a^3)} \qquad (2.59)$$

where the D_i are the appropriate distance class limits and

$$\phi(r) = \Phi(m_{lim} - 25 - 5 \log r - k(r))$$

(c f. equations 2.21 to 2.26 and 2.51).

By using their estimates of A_{DR} for all (D,R) values they attempted to find the luminosity function which gave the best results. In particular, using richness class 1

$$A_{41}/A_{31} = 0{\cdot}73$$

$$A_{51}/A_{31} = 0{\cdot}14$$

$$A_{61}/A_{31} = 0{\cdot}020$$

The Abell luminosity function (equation 2.45) with $\alpha = 0{\cdot}8$, $\beta = 0{\cdot}1$, $M^* = -18{\cdot}3 - 5 \log h$ was found to be the most satisfactory but Abell's parameters were almost as good. The broader Schechter Function (Schechter 1976) was not as good a fit, as A_{41}/A_{31} could not be matched without making A_{61}/A_{31} too large. Using their best function

$$n(r) = 165\, F_R \langle n \rangle\, (hr)^{-2.4} \qquad hr \lesssim 15 \text{ Mpc} \qquad (2.60)$$

where F_R depends on richness R and is unity for R = 1. With Abell's parameters the amplitude is 20% higher.

CHAPTER THREE

THE DATA

'Objectively existing truth is selected by observations out of many subjective proposals'

Ya. B. Zeldovich.

3.1 U K S T U PLATES

All the new data which is considered in this thesis is from the UK Schmidt Telescope Unit's 48" Schmidt at Siding Spring, Australia. Details of the telescope, which is of classical Schmidt configuration, are given in Table 3.1.

The plates which have been used are non-survey, i.e. not part of the ESO Southern Hemisphere Sky Survey and of varying qualities. Two colours have been used, henceforth referred to as J and R. The J plates are obtained using Nitrogen sensitized IIIaJ Kodak emulsion with Schott glass GG395 filter, while the R plates were taken with Kodak 098 emulsion and a Schott glass RG630 filter.

Details of the plates used are given in Table 3.2. The field number given is the ESO sky survey field which the plate covers. The exception is plate J1921 which is centred on the South Galactic Pole and is not a survey field. Plate J149 is imperfect as it was taken during commissioning of the telescope, while plate J1921 was taken during a period of very poor atmospheric conditions.

3.2 COSMOS

The COSMOS (for CO-ordinate, Size, Magnitude, Orientation and Shape) machine at the Royal Observatory

Table 3.1

UK 48" Schmidt Telescope Details

Mirror Diameter	1·83m
Aper ture	1·24m
Focal Length	3·07m
Radius of Curvature of Focal Plane	3·07m
Unvignetted Field Radius	$2^{\circ}.73$
Plate Scale	$67''.1$ per mm - 14·9 μm per arc sec
Plate Size	356mm x 356mm (or 160 x 160)
Plate Thickness	1mm

Table 3.2

Plate Details

Plate No.	149	1049	1920	1921
Colour	J	R	J	J
Exposure (min)	120	60	60	60
Plate Centre R.A.	02h 4m	02h 4m	01h 09m	00h 53m
Dec.	-30° 00′	-30° 00′	-30° 00′	-28° 03′
Date Taken	3.9.73	8.12.74	25.11.75	25.11.75
Grade	Imperfect	Ungraded	B	BS2
Field No.	416	416	412	SGP

Note: BS2 indicates that the plate is of B2 grade due to poor seeing.

Edinburgh is an automatic plate measuring machine developed from the photodensitometer type machine GALAXY (Pratt et al 1975).

In its Coarse Mode form of operation COSMOS measures a transmission value for every 8 μm x 8 μm square of the area processed. This is done by measuring the intensity of light transmitted through the plate from a beam of diameter 25 μm (in the configuration current at the time of measurement of the plates considered here). This is illustrated schematically in figure 3.1. The transmission is then translated to a scale 0 to 127; 0 representing black, 127 for clear plate.

When the transmission has been measured for every 8 μm square cell in the required area, the data is processed by the pattern analyser so that all contiguous squares with transmission below a given threshold level are joined to form an image. The threshold is determined at each point from the run of transmission levels in nearby cells, as shown in figure 3.2. Images are processed on a typical Schmidt plate at a rate of 10^6 per hour.

The data on the images is then output in the form indicated in Table 3.3.

Figure 3.1

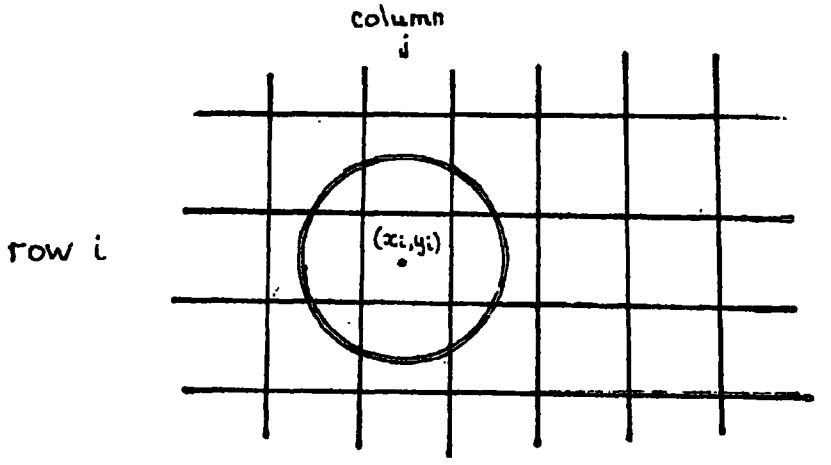

The COSMOS spot : If the amount of light transmitted through the plate, when the spot is in the position shown, centred on (x_i, y_i), is L in some units, then

$$T_{ij} = L$$

is the transmission recorded for square (i,j).

Figure 3.2

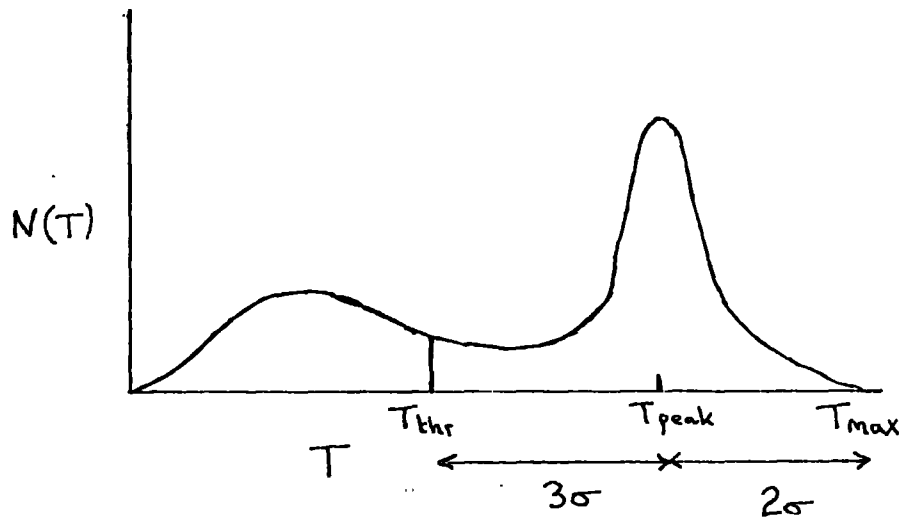

The COSMOS threshold : If $N(T)$ is the fraction of some fixed number of preceeding cells for which the transmission is T, then T_{thr} as shown in the diagram is the threshold transmission for the cell in question. The sky is assumed to produce a Gaussian like distribution at large T, and $T_{max} - T_{peak}$ determines its 'width' 2σ. The threshold can then be chosen at a suitable signal to noise ratio, usually 3. The hump at smaller T is due to images. Note that T_{peak} and σ vary across the plate, so T_{thr} varies accordingly. This is known as background following.

Table 3.3

COSMOS data output for each image

1	X co-ordinate of centroid
2	Y co-ordinate of centroid
3	Minimum X co-ordinate
4	Maximum X co-ordinate
5	Minimum Y co-ordinate
6	Maximum Y co-ordinate
7	Area
8	Minimum Transmission value
9	Threshold Transmission Value
10	Code (see section 3.3)

All positions are quoted to 0·1 μm, the area is quantised in 8 μm square increments and the transmissions are quantised in unit steps on the 0-127 scale. Code indicates the type of the image and is entered subsequently to the other values following further processing.

3.3 STAR/GALAXY SEPARATION

In order to be of any astronomical use, it is obvious that images must be sorted into (at least) galaxy and star categories. Experiments with various parameters by MacGillivray (1975) showed that the best discrimination was through the relationship between area and minimum transmission (henceforth referred to for convenience as TMIN).

Since a star should have a Gaussian profile at the photographic plate due to both scattering in the atmosphere (seeing) and scattering in the emulsion, then for a given threshold the area of the image is a function only of central intensity and the (fixed) width of the Gaussian profile (this may not be true for very small images when the emulsion thickness is comparable with the size). In the case of large images the area also includes diffraction spikes, but their area also depends only on brightness. Hence stellar images fall on a well defined line in the TMIN v AREA diagram. Galaxies, as extended objects rather than point sources, have greater areas for the same central intensity and hence fall in the region to the right of the star line (figure 3.3). The accuracy of this method of discrimination was tested by MacGillivray *et al* (1976a) who claimed - by cross comparison between COSMOS classification and visual identification - that about 95% of galaxy and

Figure 3.3

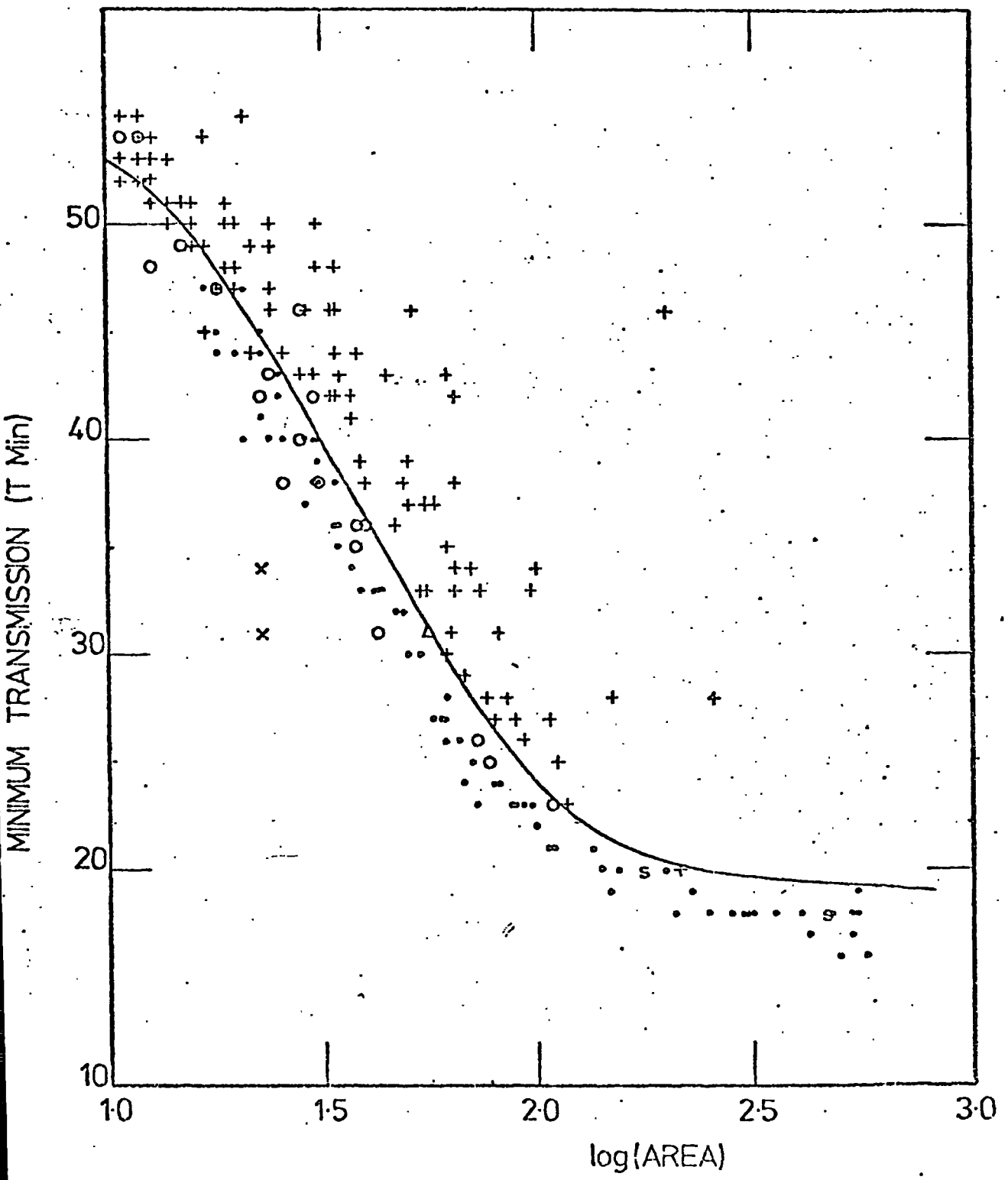

Plot of TMIN against AREA for stars (·), galaxies (+) and plate flaws and other errors (o, x, s). The solid curve denotes the discriminatory line between stars and galaxies. (From MacGillivray et al 1976a)

star images larger than a limit of 10 area increments ($640\,\mu m^2$) were correctly classified by COSMOS, the uncertainty increasing with decreasing size as the image size approached the seeing disc. All star/galaxy separation is performed to some such limit, usually 10 or 15 area increments, smaller images being left unclassified.

Since the background varies over the plate due to vignetting near the plate edges and particularly in the case of IIIaJ plates, emulsion variations, both in thickness and sensitivity, a different discriminatory curve is required for each background, or equivalently threshold, level. This has subsequently been found to cause technical problems when large areas of plate with rapidly varying thresholds are processed.

The type of image - galaxy, star or other - is entered into the COSMOS data tapes by a suitable code number entered into the parameter called CODE in table 3.3.

3.4 LARGE IMAGES

Figures 3.4 and 3.5 show maps of the images detected by COSMOS on measured regions of approximately 12cm x 12cm on the Schmidt plates J149 and R1049 which are of the same area of the sky but in different colours. The measured areas are also very nearly coincident and some bright objects can be readily identified in each diagram.

Figure 3.4

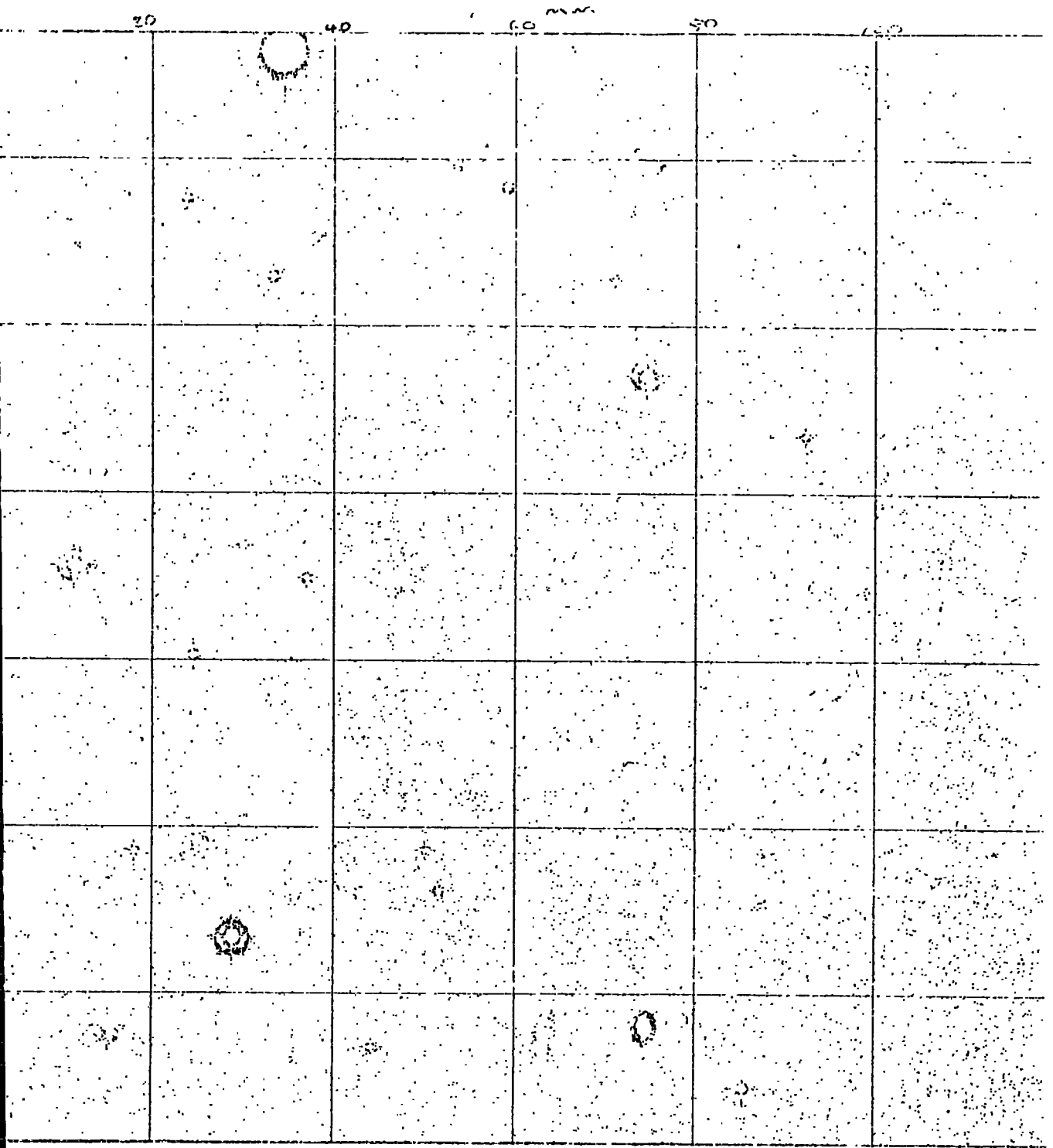

Map of images detected by COSMOS on part of plate R1049.

Figure 3.5

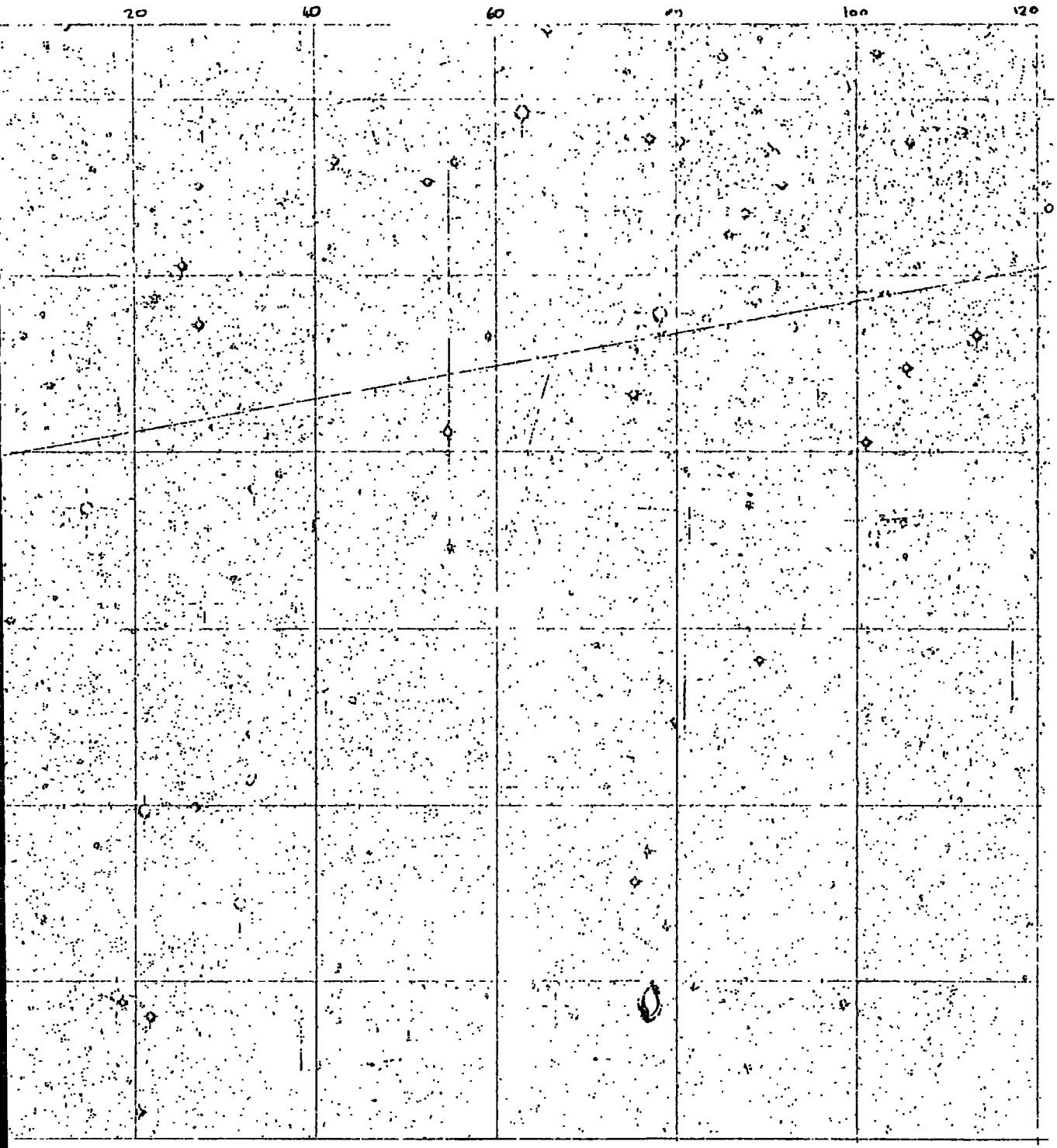

Map of images measured by COSMOS on part of Plate J149.

The long lines seen on the J plate are satellite trails and are not found to be a serious problem as they are broken up into a series of very thin images and are discarded during star/galaxy separations because of their small areas.

The images of bright stars and galaxies, for example those at co-ordinates approximately (27,27) and 75,15) on figure 3.4, are somewhat more awkward however since they tend to be broken up into several extended images. This is particularly the case with bright stars with prominent diffraction spikes, such as the one at co-ordinates approximately (63,118) on figure 3.5.

As these images would seriously bias any estimates of clustering of galaxies on the plate, they are removed from the data by introducing rectangular 'holes', that is areas where any images present are rejected from the final data. Fortunately these images occupy only a small fraction of the measured areas. In no case was more than 1·5% of the initial measured area removed.

3.5 IMAGE DENSITY

As mentioned in section 3.2, the threshold for image detection varies continuously over the plate due to the emulsion. As the threshold depends not only on the background but also on the noise which also

varies, the threshold at different parts of the plate may be at different isophotal intensities. It follows that the density of images recorded will vary over the plate, imposing large scale 'clustering' on to the true distribution. Also due to the different profiles the densities of stellar and galaxian images will vary differently with threshold.

The area in the measured region which has a particular threshold may be obtained from the COSMOS output and the variations in threshold may be mapped out; as illustrated in figures 3.6 and 3.8, for the measured areas of plates R1049 and J149 respectively. The corresponding variations in the star and galaxy densities are shown in figures 3.7 and 3.9. Clearly for plate R1049, the variations in threshold are small and the differences in densities are sufficiently small to be accounted for by the true variations from point to point. However, for plate J149 the emulsion non-uniformities give rise to a large range of threshold values and there is an obvious correlation between threshold and number density, with the latter changing by a factor of around 2 from one extreme to the other. It may also be noted from figure 3.8 that the threshold variation is approximately monotonic from left to right and this is mimicked by the density distribution.

Here it is clear that plate effects grossly distort the distribution of images recorded. If this is

Figure 3.6

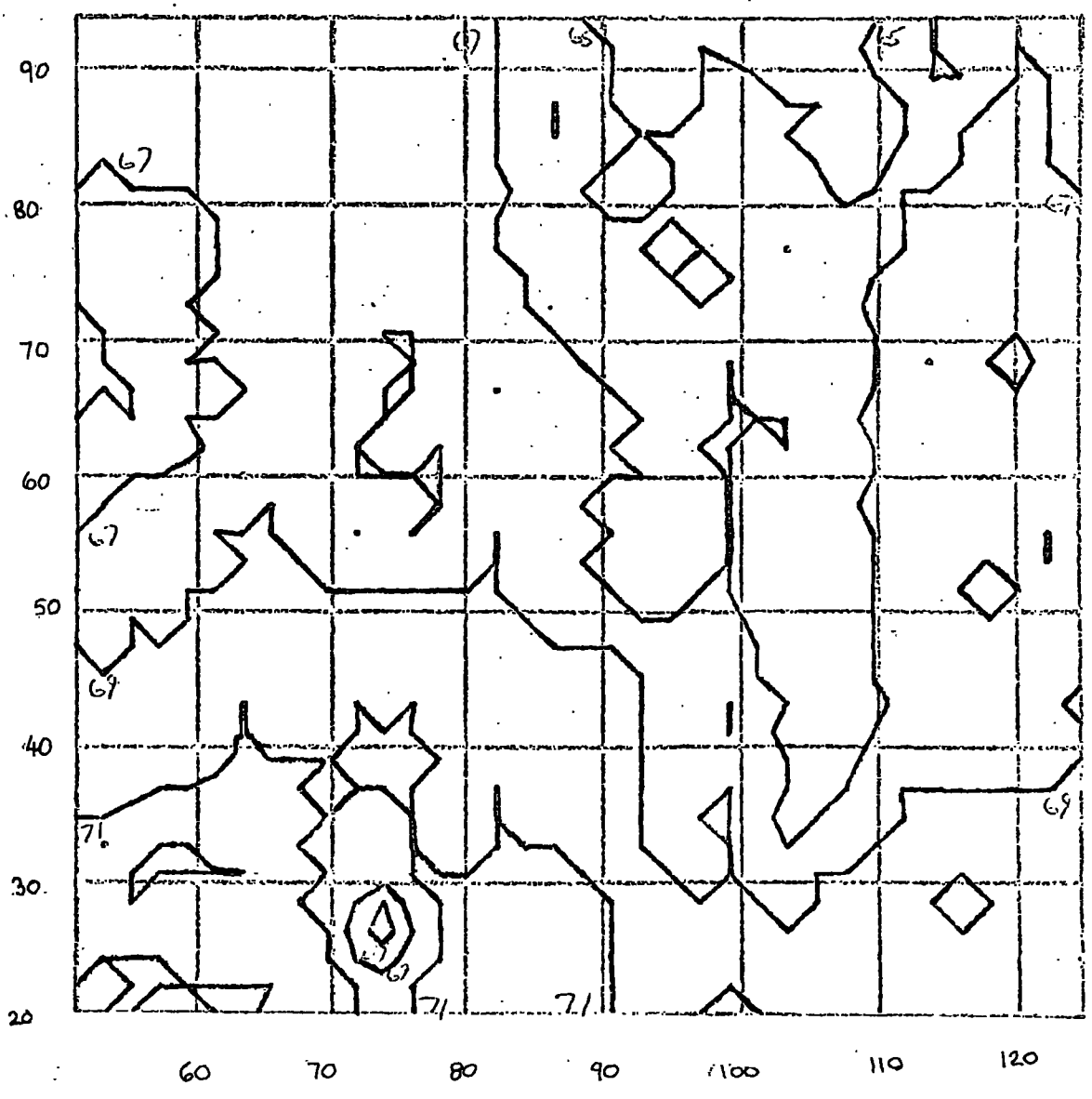

Contour map of the COSMOS thresholds on the measured area of plate R1049.

Figure 3.7

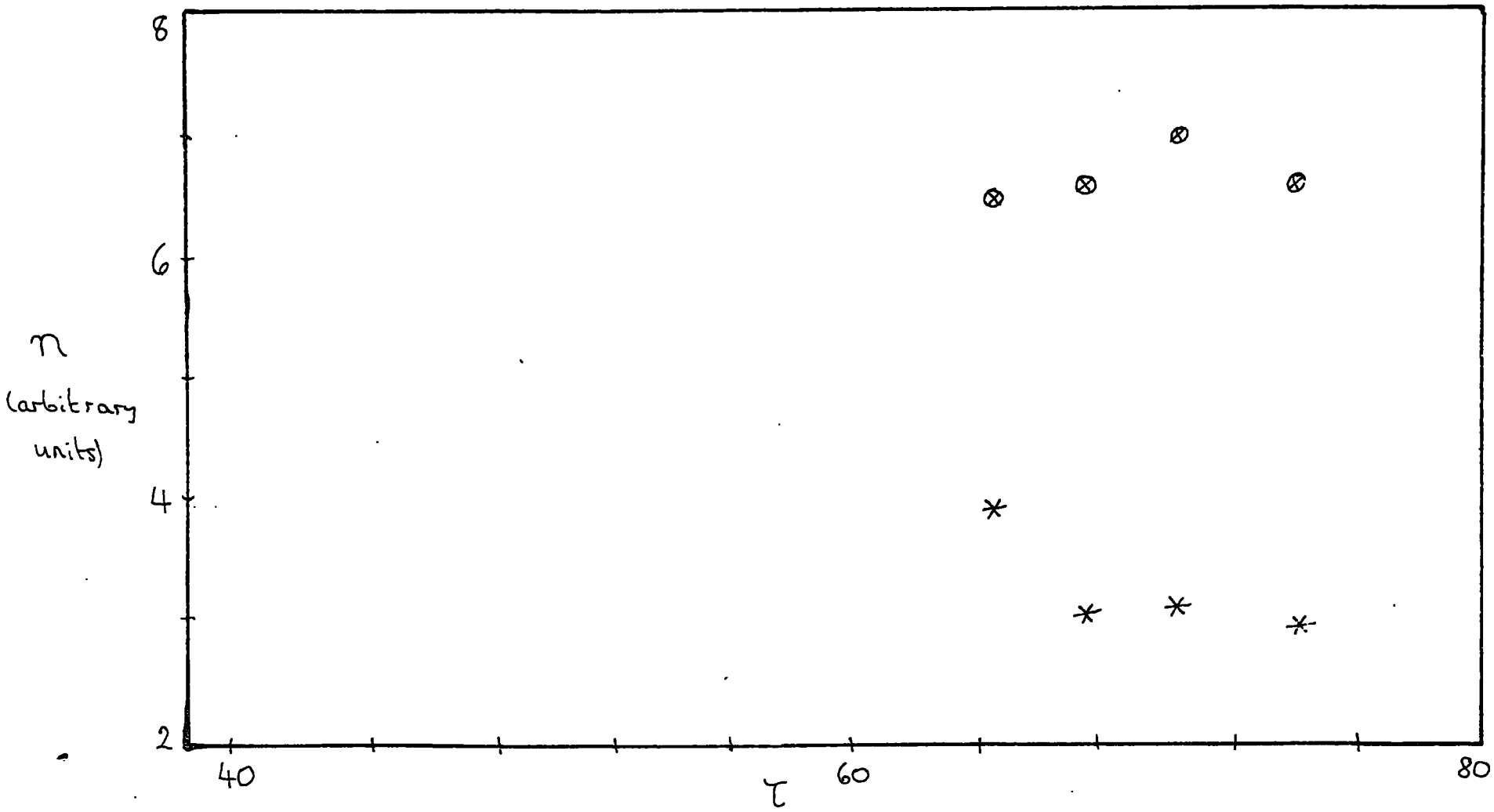

Variation of Galaxy (⊗) and star (*) density n with threshold τ, plate R1049.

Figure 3.8

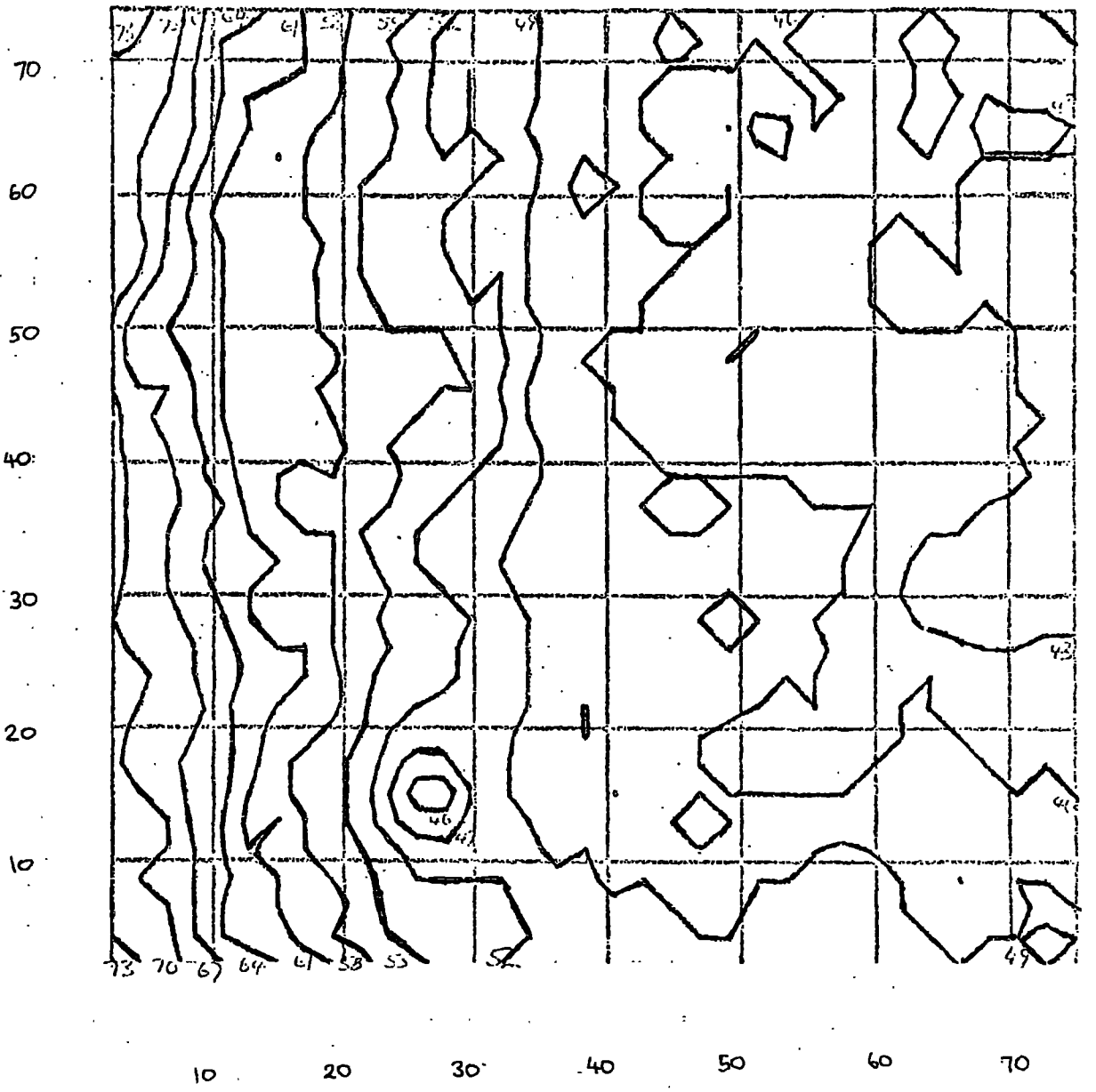

Contour map of the COSMOS thresholds on the measured area of plate J149.

Figure 3.9

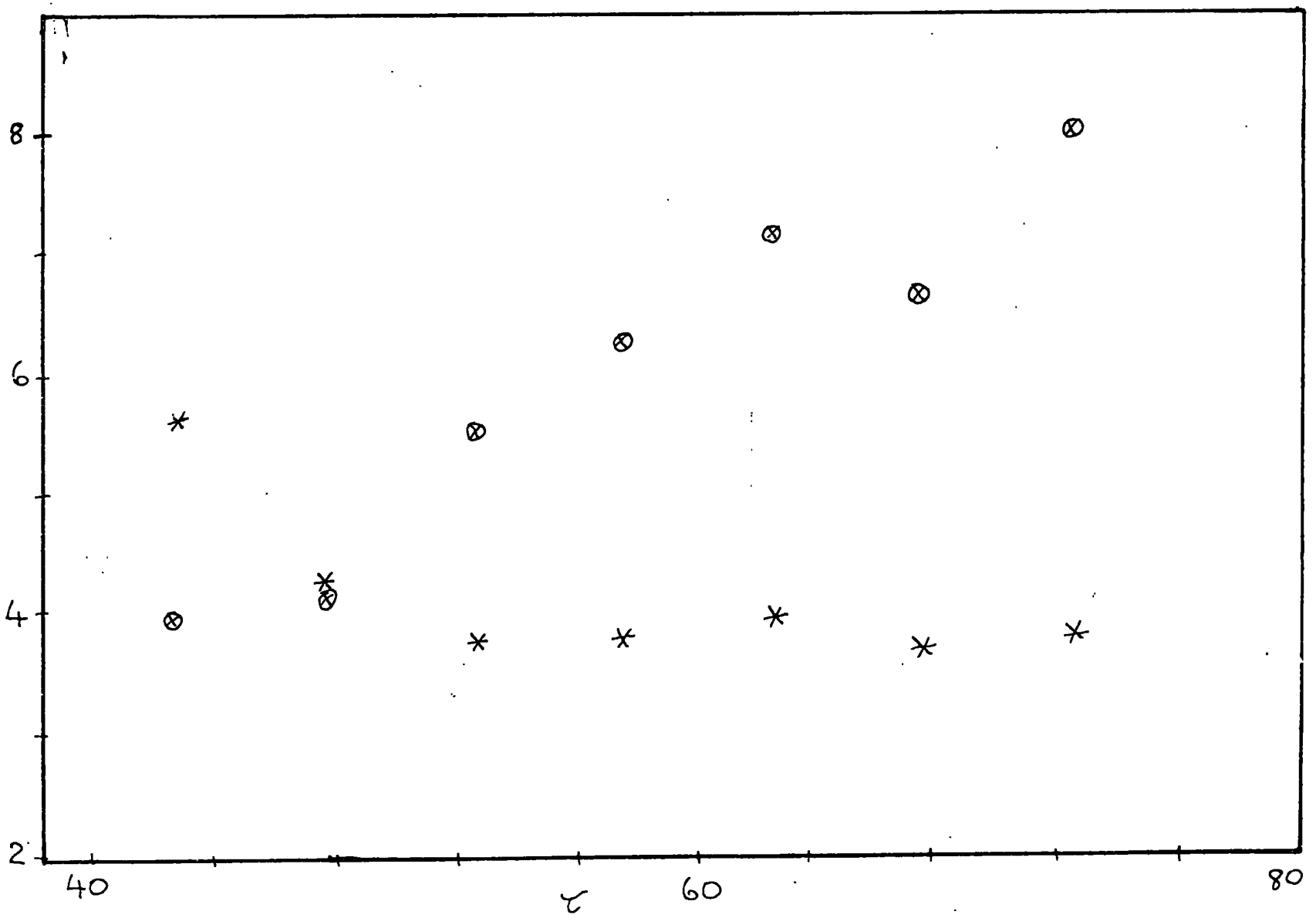

Variation of Galaxy (⊗) and Star (*) density n with threshold τ, plate J149.

the case, then to obtain a good estimate of the true clustering the data must be 'filtered' to remove these gross effects. This is discussed in the appropriate section in chapter 4.

Figures 3.10 and 3.11 illustrate another problem which can occur. Initially a large area about $5^{\circ} \times 5^{\circ}$ of plate J1920 was measured. Figure 3.12 shows the distribution of thresholds over this area and it may be seen that there are very wide variations and, at some points, very rapid variations.

When star/galaxy separation was attempted on this large region the computer algorithms were unable to cope with such variations and the output ratio of star images to galaxy images fluctuated wildly from one threshold to the next.

Consequently star/galaxy separation was only performed on smaller areas with less acute background variations, until improvements were made to the COSMOS background following programmes.

3.6 INTENSITY CALIBRATION

Measurement by COSMOS of the step wedge on a plate allows a calibration of the TMIN scale to be made. It is found (Zealey 1976) that a good fit to the observed relationship between intensity and transmission is the

Figure 3.10

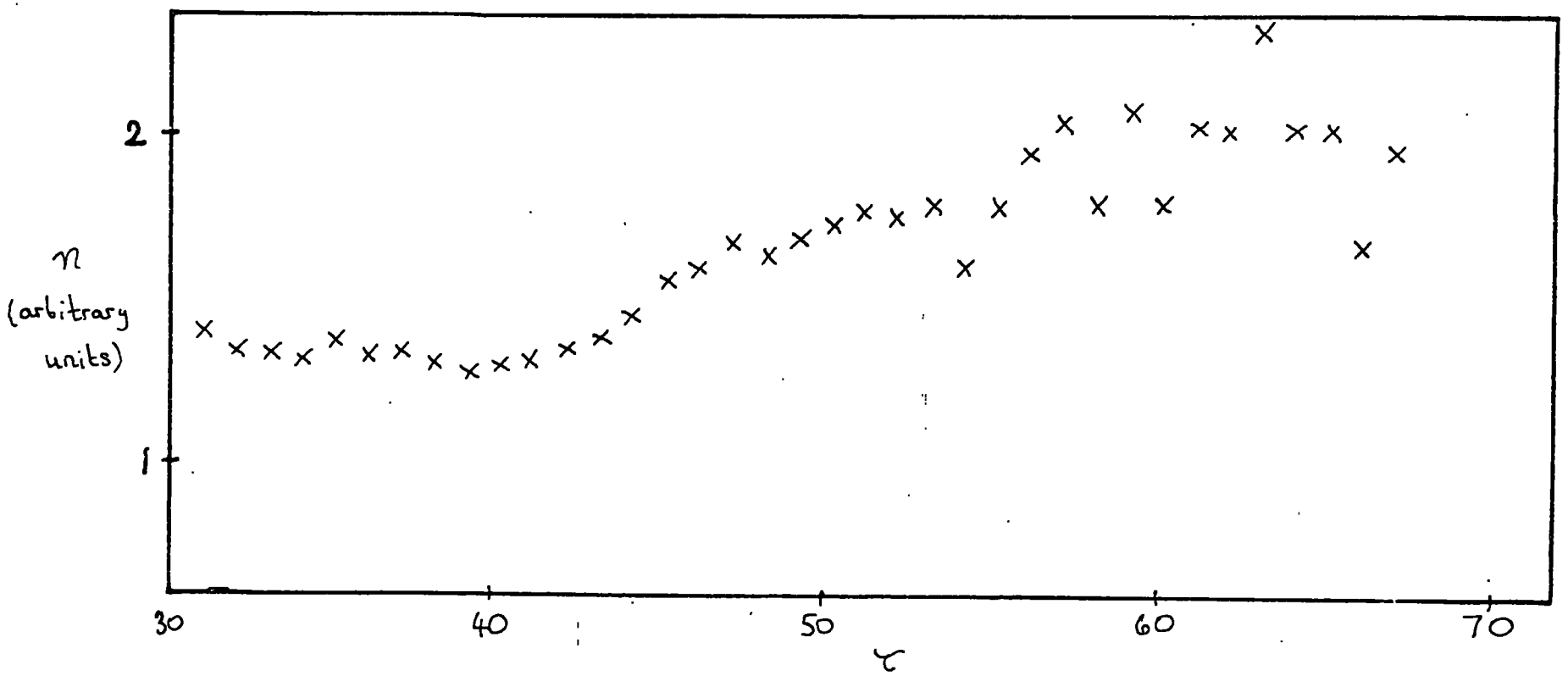

Variation of image density n with threshold τ for initial measurement of plate J1920.

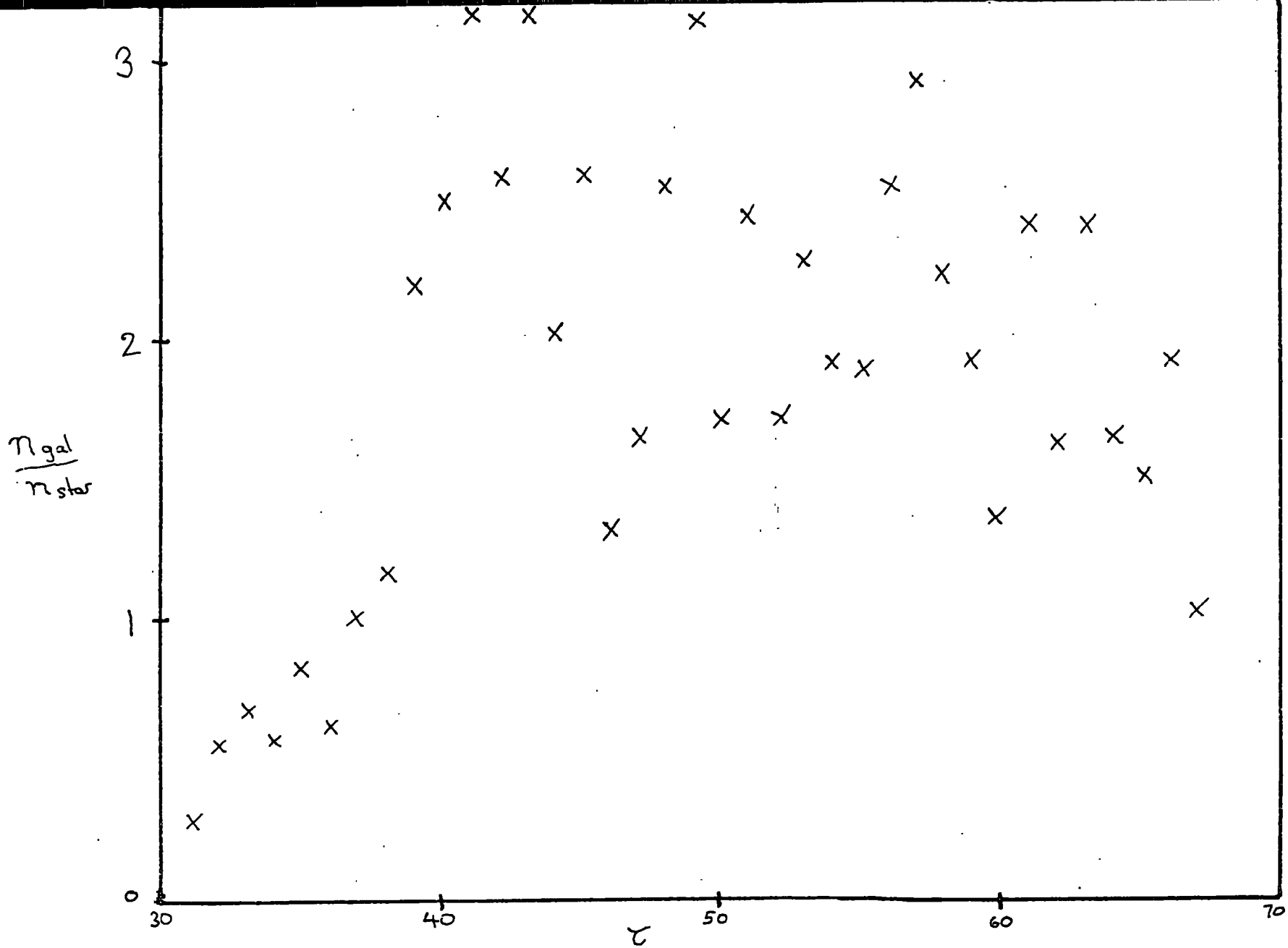

Plot of galaxy density/star density versus threshold for initial measurement of plate J1920

Figure 3.12

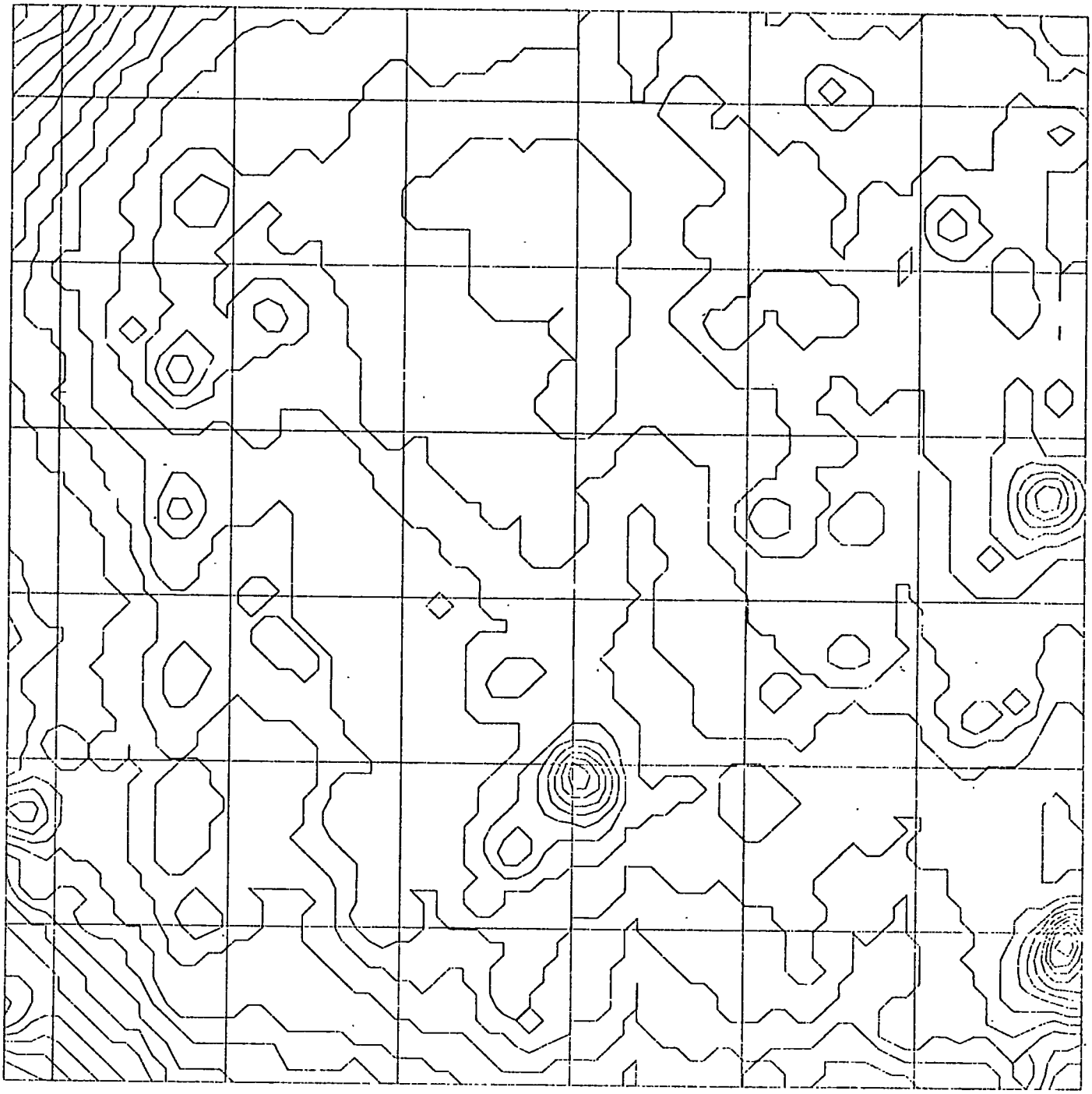

Contour map of threshold variations on plate J1920

usual Baker form (Baker 1949)

$$I = I_o\left(\frac{T_o}{T} - 1\right)^{\gamma} \qquad (3.1)$$

where I_o, T_o and γ are constants, T_o and γ being obtained from the wedge calibration.

Since we are generally interested in the brightness above the sky background it is useful to put $T = T_{peak}$ (corresponding to the sky level) and $T = T_{thr}$ in equation (3.1). Then

$$I_{sky} = I_o\left(\frac{T_o}{T_{peak}} - 1\right)^{\gamma} \qquad (3.2)$$

and

$$I_{thr} = I_o\left(\frac{T_o}{T_{thr}} - 1\right)^{\gamma} \qquad (3.3)$$

Now for an arbitrary transmission $T < T_{thr}$

$$I = I_{sky}\left(\frac{T_o}{T_{peak}} - 1\right)^{\gamma}\left(\frac{T_o}{T} - 1\right)^{-\gamma} \qquad (3.4)$$

Thus the intrinsic intensity of the object

$$I_{int} = I_{sky}\left[\frac{\left(\frac{T_o}{T} - 1\right)^{\gamma}}{\left(\frac{T_o}{T_{peak}} - 1\right)^{\gamma}} - 1\right] \qquad (3.5)$$

Taking the specific case of plate J1920, which obeys equation (3.1) with $T_o = 676$, $\gamma = 0{\cdot}533$, then for a typical threshold transmission (in the region selected for star/galaxy separation) of 43, and corresponding T_{peak} of 55

$$I_{thr} \approx 1{\cdot}16\ I_{sky}$$

i.e. images can be detected if they are about 16% above the sky background.

If we assume that the sky brightness at Siding Spring is approximately 23·0 J magnitudes per square arc second (though this is in some doubt) then this gives

$$\mu_{thr} \approx \mu_{sky} + 2 \approx 25$$

This gives an indication of the depth to which the COSMOS measured output can reach.

CHAPTER FOUR

THE ANGULAR COVARIANCE FUNCTION FROM DEEP SCHMIDT PLATES

'Perhaps if we can see how to measure the galaxy distribution in the right way it will prove to be the 'Rosetta Stone' by which we learn the underlying significance of the clustering of matter'.

P. J. E. Peebles.

4.1 ESTIMATION OF $w(\theta)$

Since the Schmidt plates are only $6^{\circ} \times 6^{\circ}$ in extent and the areas measured by COSMOS are considerably smaller again, plane geometry is used in this analysis with no need for corrections due to the curvature of the sky.

An estimator of the angular covariance function is

$$w(\theta) = \frac{N_o(\theta_{k-1}, \theta_k)}{N_e(\theta_{k-1}, \theta_k)} - 1 \qquad (4.1)$$

where $N_o(\theta_{k-1}, \theta_k)$ is the mean number of galaxies observed at a distance between θ_{k-1} and θ_k from a randomly chosen galaxy, $N_e(\theta_{k-1}, \theta_k)$ is the number that would be expected between θ_{k-1} and θ_k in a randomly distributed sample of the same density, and $\theta_{k-1} < \theta < \theta_k$.

Providing the chosen galaxy is not less than θ_k from the edges of the measured region, then the area of the annulus between limits θ_{k-1} and θ_k is

$$\Delta\Omega = \pi(\theta_k^2 - \theta_{k-1}^2) \qquad (4.2)$$

so

$$N_e(\theta_{k-1}, \theta_k) = \mathcal{N}\pi(\theta_k^2 - \theta_{k-1}^2) \qquad (4.3)$$

where $\mathcal{N}$ is the mean density per unit solid angle. Now if there are $N_c(\theta_k)$ such galaxies further than θ_k from the edges of the region, and there is a total number $N_T(\theta_{k-1}, \theta_k)$ galaxies between θ_{k-1} and θ_k away from them,

then

$$N_e(\theta_{k-1},\theta_k) = \frac{N_T(\theta_{k-1},\theta_k)}{N_c(\theta_k)} \qquad (4.4)$$

so

$$w(\theta) = \frac{N_T(\theta_{k-1},\theta_k)}{N_c(\theta_k)N\pi(\theta_k^2 - \theta_{k-1}^2)} - 1 \qquad (4.5)$$

However it is clear that for all the galaxies in the central area, further than θ_k from the edges, each separation between a pair of galaxies is counted twice, once with each galaxy as centre, so it is computationally convenient to use only half annuli centred on each galaxy (figure 4.1) in which case

$$w(\theta) = \frac{n(\theta_{k-1},\theta_k)}{n_c(\theta_k)N\frac{\pi}{2}(\theta_k^2 - \theta_{k-1}^2)} - 1 \qquad (4.6)$$

where $n(\theta_{k-1},\theta_k)$ is the total number of galaxies in half annuli centred on the $n_c(\theta_k)$ galaxies for which the half annuli lie completely in the measured region. Note that n_c is different from N_c because of the requirement that only the half annulus lies inside the area, rather than the whole annulus.

4.2 COMPUTATION OF $w(\theta)$

In computing the angular covariance function via

Figure 4.1

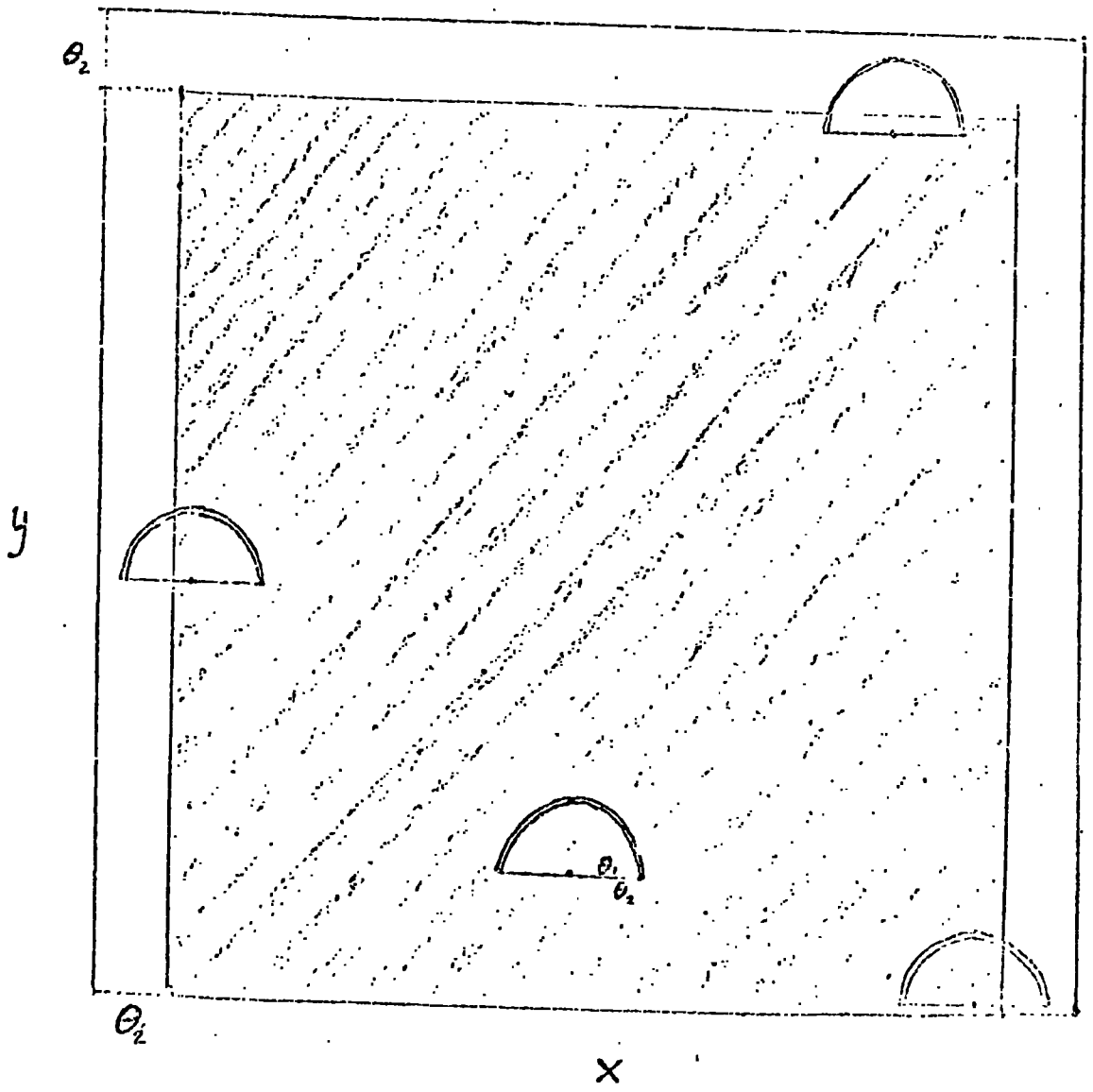

Galaxies used as centres: The annuli have interior and exterior radii θ_1, θ_2. All $n_c(\theta_2)$ galaxies which lie in the shaded area are used as centres for the half rings and the total number of galaxies inside the half rings is $n(\theta_1, \theta_2)$.

equation (4.6), it is apparent that the calculations depend principally on the evaluation of the separation between a large number of pairs of galaxies - a typical sample contains a total of around 10^7 possible pairs.

When the positions have been read in from the COSMOS data tape for a suitable set of images, e.g. those classified as galaxies and with areas above some limiting value, in an area bounded by the lines x = XMIN, x = XMAX, y = YMIN, y = YMAX, they are ordered in increasing y co-ordinates by a sorting routine. This gives

$$\left\{ (x_i, y_i) \; : \; y_{i+1} \geq y_i \; , \; i = 1, \ldots, N_G - 1 \right\}$$

where N_G is the number of galaxies in the sample. Then the position of the first galaxy in the ordering (x_1, y_1) is used as the first centre and so on through the order to (x_{N_G-1}, y_{N_G-1}) the last centre.

Consider in general the case where (x_i, y_i) is the centre galaxy. The positions of the subsequent images in the order

$$\left\{ (x_j, y_j) \; : \; j = i + 1, \ldots, N_G \right\}$$

are then taken and the square of the separation

$$\theta^2 = (x_j - x_i)^2 + (y_j - y_i)^2$$

is computed for each in turn, providing $|x_j - x_i| \leq \theta_{max}$, until the point in the sequence is reached where $y_j - y_i > \theta_{max}$, θ_{max} being the maximum separation for which $w(\theta)$ is to be estimated.

All values of $\theta^2 > \theta_{max}^2$ are thrown out and the remaining θ^2 values are put into equal length bins

$$((k-1)\theta_1^2 , k\theta_1^2) \qquad k = 1, \ldots , k_{max}$$

where $k_{max}\,\theta_1^2 = \theta_{max}^2$. Equal sized bins in θ^2 are chosen so that the expected number in each annulus (for a Poisson distribution),

$$\tfrac{1}{2}N\pi(\theta_k^2 - \theta_{k-1}^2)$$

in equation (4.6), will be constant.

Now if (x_i , y_i) is near to the edges of the area some of the annuli will not be complete, so define

$$\theta_{max}(i) = \text{Min}\left\{\text{XMAX} - x_i , x_i - \text{XMIN} , \text{YMAX} - y_i , \theta_{max}\right\}$$

then define an integer $k_{max}(i)$ so that

$$k_{max}(i)\,\theta_1^2 \leq \theta_{max}(i)^2 < (k_{max}(i) + 1)\,\theta_1^2$$

in which case only the first $k_{max}(i)$ half annuli are completely in the measured region.

In other words (x_i , y_i) is a centre galaxy for the first $k_{max}(i)$ values of θ and $n_c(\theta_k)$ in equation (4.6) is consequently incremented by one for all k, $k = 1, \cdots,$ $k_{max}(i)$. The separations which were in bins with $k > k_{max}(i)$ are discarded and $n(\theta_{k-1} , \theta_k)$ is incremented by the number of separations in the bin $\left((k-1)\,\theta_1^2 , k\theta_1^2\right)$ for each $k \leq k_{max}(i)$.

By proceeding in this way through all centre galaxies, $n(\theta_{k-1} , \theta_k)$ and $n_c(\theta_k)$ are obtained for the

sample and with

$$\mathcal{N} = N_a / \Omega \qquad (4.7)$$

where Ω = (XMAX-XMIN)×(YMAX-YMIN), $w(\theta)$ can be evaluated by equation (4.6). In practice θ is chosen to be the midpoint of the bin

$$\theta = \tfrac{1}{2}(\theta_{k-1} + \theta_k) \qquad (4.8)$$

though the value found is strictly the average over the range θ_{k-1} to θ_k. Assuming a form

$$w(\theta) = A\,\theta^{-0.8}$$

which, as shown below, is in reasonable agreement with the present results, the average w is

$$\begin{aligned}
\overline{w}_k &= \int_{\theta_{k-1}}^{\theta_k} A\pi\theta^{0.2}\,d\theta \;/\; \tfrac{1}{2}\pi\theta_1^2 \\
&= \frac{2A}{\theta_1^2}\left[\frac{\theta_k^{1.2} - \theta_{k-1}^{1.2}}{1.2}\right] \\
&= A\,\theta_1^{-0.8}\left[\frac{k^{0.6} - (k-1)^{0.6}}{0.6}\right] \\
&= A\,\theta_{mid}\; f(k) \qquad (4.9)
\end{aligned}$$

where $\theta_{mid} = \frac{1}{2}\left(\sqrt{k} + \sqrt{k-1}\right)\theta_1$ is the midpoint of the

interval and

$$f(k) = \left[\frac{\sqrt{k}^{1.2} - \sqrt{(k-1)}^{1.2}}{0.6}\right]\left[\frac{\sqrt{k} + \sqrt{(k-1)}}{2}\right]^{0.8}$$

$$= \frac{(k-1)}{0.6}\left[\left(1 + \frac{\sqrt{k} - \sqrt{(k-1)}}{\sqrt{(k-1)}}\right)^{1.2} - 1\right]$$

$$\left[1 + \frac{\sqrt{k} - \sqrt{(k-1)}}{2\sqrt{(k-1)}}\right]^{0.8}$$

$$= 2(k-1)\left[\frac{\sqrt{k} - \sqrt{(k-1)}}{\sqrt{(k-1)}} + o\left(\frac{\sqrt{k} - \sqrt{(k-1)}}{2\sqrt{(k-1)}}\right)^2\right]$$

$$\rightarrow 1 \quad \text{as} \quad k \rightarrow \infty$$

In fact $\bar{w}_k$ is almost exactly equal to $w(\theta_{mid})$ for all except the first bin, where $\bar{w}_1 = w(1{\cdot}056\ \theta_{mid})$, for example $\bar{w}_2 = w(1{\cdot}001\ \theta_{mid})$, so all estimates of w can be plotted at the midpoints of the bins with very little error.

4.3 EFFECTS OF HOLES

As mentioned in section 3.4, the removal of large images from the data introduces what may be described as holes in the galaxy field.

Let the total area of holes be H , w_a be the actual covariance function for the whole area if there

were no holes and w_c be the calculated covariance function for the recorded galaxies.

The calculated density

$$\mathcal{N}_c = N_G / \Omega \tag{4.10}$$

while the actual density

$$\mathcal{N}_a = N_G / (\Omega - H) \tag{4.11}$$

Then taking the same sample of galaxies as centres in each case (this assumes that recorded galaxies are a random selection of those that would actually be seen if the holes were not present)

$$\begin{aligned} 1 + w_c(\theta) &= \frac{n(\theta_{k-1}, \theta_k)}{n_c(\theta_k)\,\mathcal{N}_c\,\delta\Omega} \\ 1 + w_a(\theta) &= \frac{n(\theta_{k-1}, \theta_k) + \langle \delta H \rangle \mathcal{N}_a (1 + w_a(\theta)) n_c(\theta_k)}{n_c(\theta_k)\,\mathcal{N}_a\,\delta\Omega} \end{aligned} \tag{4.12}$$

since the galaxies which are missed in the counting of $n(\theta_{k-1}, \theta_k)$ are those in an area $\langle \delta H \rangle$, the mean area of the half annuli, area $\delta\Omega$, which lies in a hole.

$$\therefore\ 1 + w_a(\theta) = (1 + w_c(\theta))\left(\frac{\Omega - H}{\Omega}\right) + \left(\frac{\delta H}{\delta \Omega}\right)(1 + w_a(\theta)) \tag{4.13}$$

But

$$\frac{\langle \delta H \rangle}{\delta \Omega} = \frac{H}{\Omega} \tag{4.14}$$

provided the holes are randomly placed, so

$$w_a(\theta) = w_c(\theta) \qquad (4.15)$$

That is, to first order the correction in the calculation of the density cancels out with the missing counts in the rings, so the uncorrected w calculated by the method described above can be used as an unbiased estimate of the true angular covariance function for the field.

4.4 BINNED ANALYSIS OF THE ANGULAR COVARIANCE FUNCTION

The techniques described in section 4.2 do not, at large angular separations, use the whole of the available statistical information. This is due to the method of avoiding edge corrections, i.e. the use of only complete half annuli. Taking into account edge effects directly for every centre galaxy by the calculation of the fraction of each half annulus which lies inside the measured area, would be prohibitively time consuming computationally, but in the case of binned data, the problem is considerably eased.

If the data is binned into an $N_1 \times N_2$ array, such that n(i,j) is the number of galaxies in the cell (i,j) of the measured area then

$$\sum_{\theta_{k-1}}^{\theta_k} n(i,j)\, n(l,m)$$

(where the sum is over all the I_k pairs of cells whose centres are separated by a distance between θ_{k-1} and θ_k) is approximately equal to the number of galaxy pairs with separations between θ_{k-1} and θ_k.

Thus

$$w(\theta) = \frac{\sum_{\theta_{k-1}}^{\theta_k} n(i,j)\, n(1,m)}{I_k \mathcal{N}^2 \Delta A^2} - 1 \qquad (4.16)$$

where ΔA is the area of a single cell.

This estimate will not be as accurate for small θ as the one based on the true point positions, but improves as θ becomes much larger than the cell size. For very large separations it is more accurate than the former estimate because of the better utilization of the available information, and it allows an evaluation of $w(\theta)$ at very large θ to be made. Note that the accuracy (over and above the limitation brought about by the bins themselves) is best where I_k is largest.

4.5 THE RESULTS FOR PLATE R1049

The measured area on the plate is 73·728mm square, corresponding to 1·889 square degrees. It contains 4645 galaxies and 2106 stars above the area limit for discrimination of 960 μm^2. Below this there are a further

10042 small images which were not classified. This gives a galaxy number density of 2458 per square degree. A density contour map of the galaxy distribution is given in figure 4.2.

The angular covariance function for the 4630 completely defined galaxy images (the other 15 had at least one of the parameters missing) was evaluated by the techniques of section 4.2 in the ranges

$0 < \theta \leq 2000\,\mu m$ in bins with $\theta_1 = 200\,\mu m$

$2000 < \theta \leq 10000$ $\theta_1 = 1000$

$10000 < \theta \leq 30000$ $\theta_1 = 5000$

where as in section 4.2 the k th bin in any range is the interval $(\sqrt{k-1}\ \theta_1 , \sqrt{k}\ \theta_1]$. The results for the first of these ranges are shown in figure 4.3.

If the galaxies were randomly distributed over the measured area the expected number $n(\theta_{k-1} , \theta_k)$ in all the half annuli would be around 233 for all θ_k (it decreases slowly over the range of θ values because there are less centre galaxies for larger θ). The standard deviation would be about $\sqrt{233} \simeq 15$, so we would expect $w(\theta) = 0 \pm 0{\cdot}07$ for all θ in this range. It is clear that this is not consistent with the data presented in figure 4.3, where there are 15 values above 0·14, 39 above 0·07 and 7 below -0·07 (out of a total of 100).

Hence we may conclude that the galaxies are not randomly distributed. However, it is also clear from figure 4.3 that such fine binning will obscure any

Figure 4.2

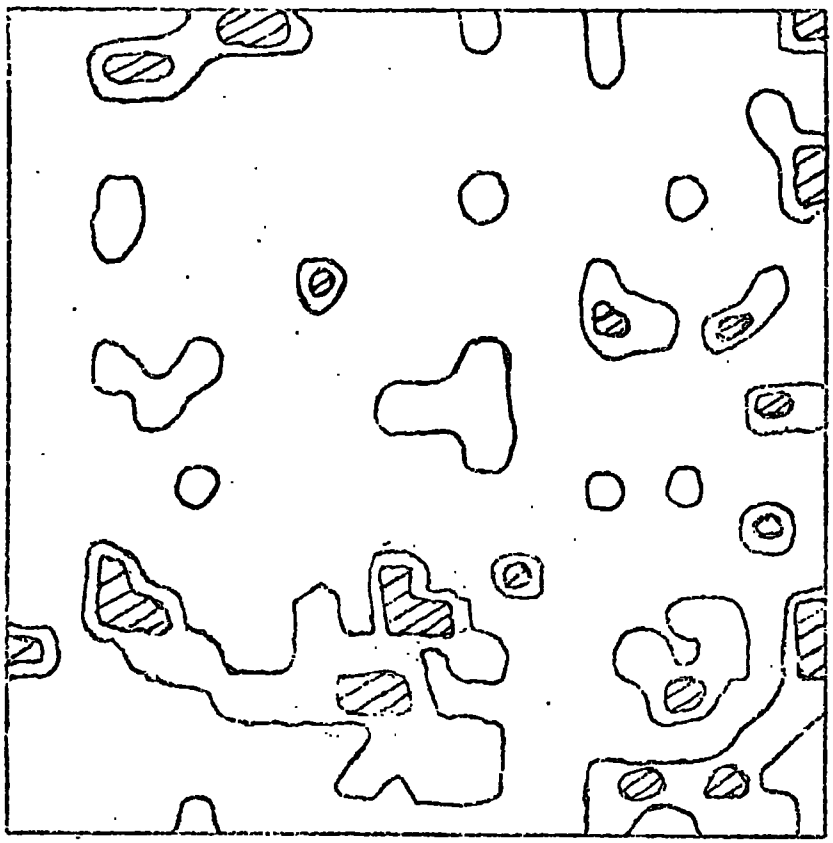

Galaxy number density contour map of the measured area of plate R1049.

Figure 4.3

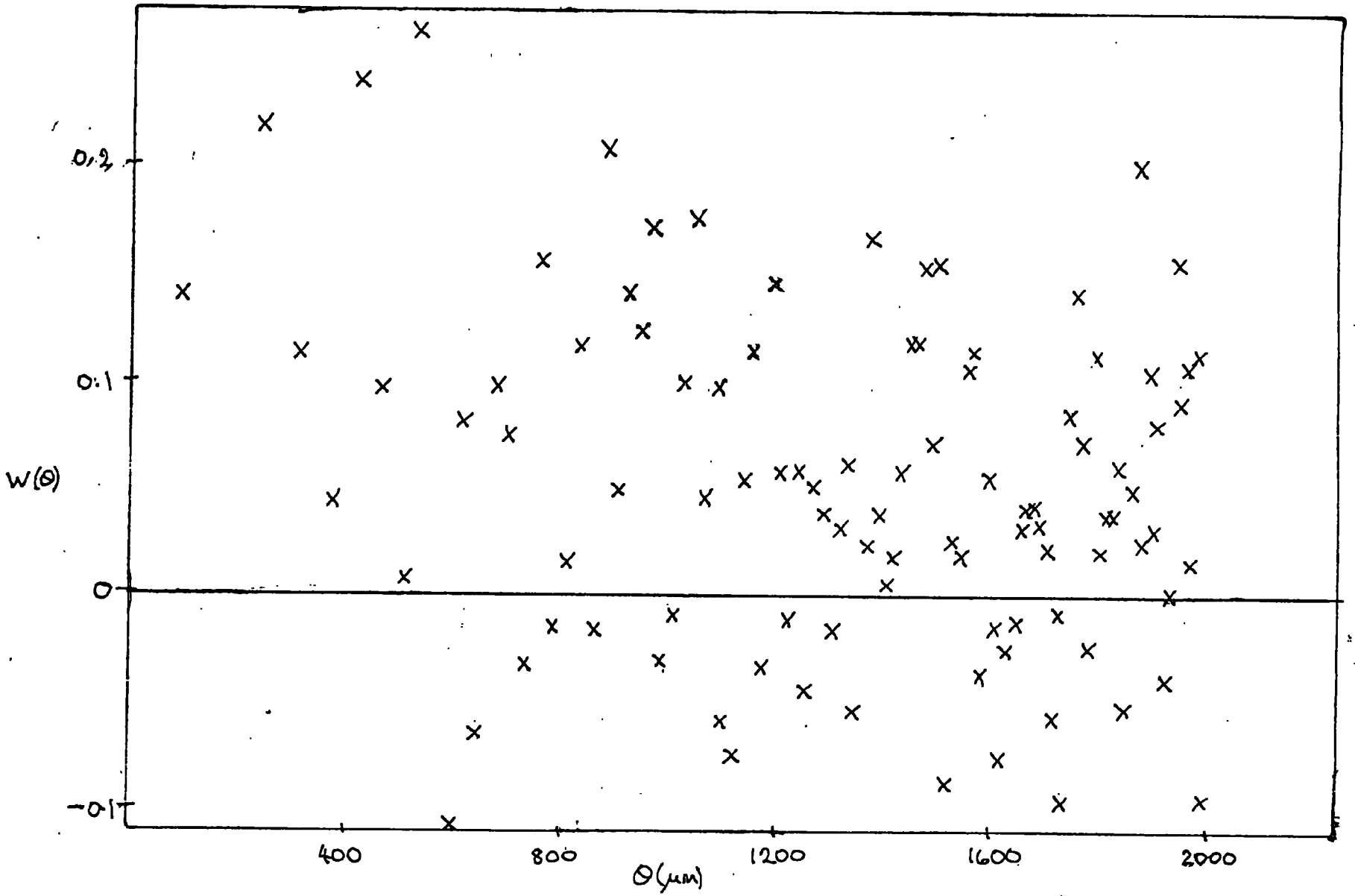

Angular covariance function w(θ) for the R sample with very fine binning.

structure that is present in the angular covariance function, because of the large random errors involved.

Thus it is necessary to smooth the results by averaging over adjacent bins; all subsequent results are presented with suitably larger bin widths. Figure 4.4 shows the results for plate R1049 in all the three ranges; for convenience the horizontal scale is contracted for the larger separations. The upper scale gives θ in angular measure.

Although the fluctuations are still fairly large in the range $0 < \theta \leq 2000\,\mu m$ (the error bars indicate a length 2σ, the standard deviation being calculated simply on the basis of Poisson statistics for the observed numbers of pairs $n(\theta_{k-1}, \theta_k)$ as the expected errors for any particular distribution are not known theoretically) the form of the angular covariance function can be clearly seen to be a decreasing function which falls fairly smoothly (allowing for the fluctuations) to zero at about $\theta = 7000\,\mu m$. There then exists a region of small negative values followed by more pronounced negative correlations. Although the error bar indicated for the largest range of separations is small, due to the large numbers of galaxies counted in the very wide bins, the points may not reflect the true form of w at large θ because the centres used are very few and may not give a representative sample of all possible pairs at these separations. The binned analysis (section 4.4) avoids these problems and the results for

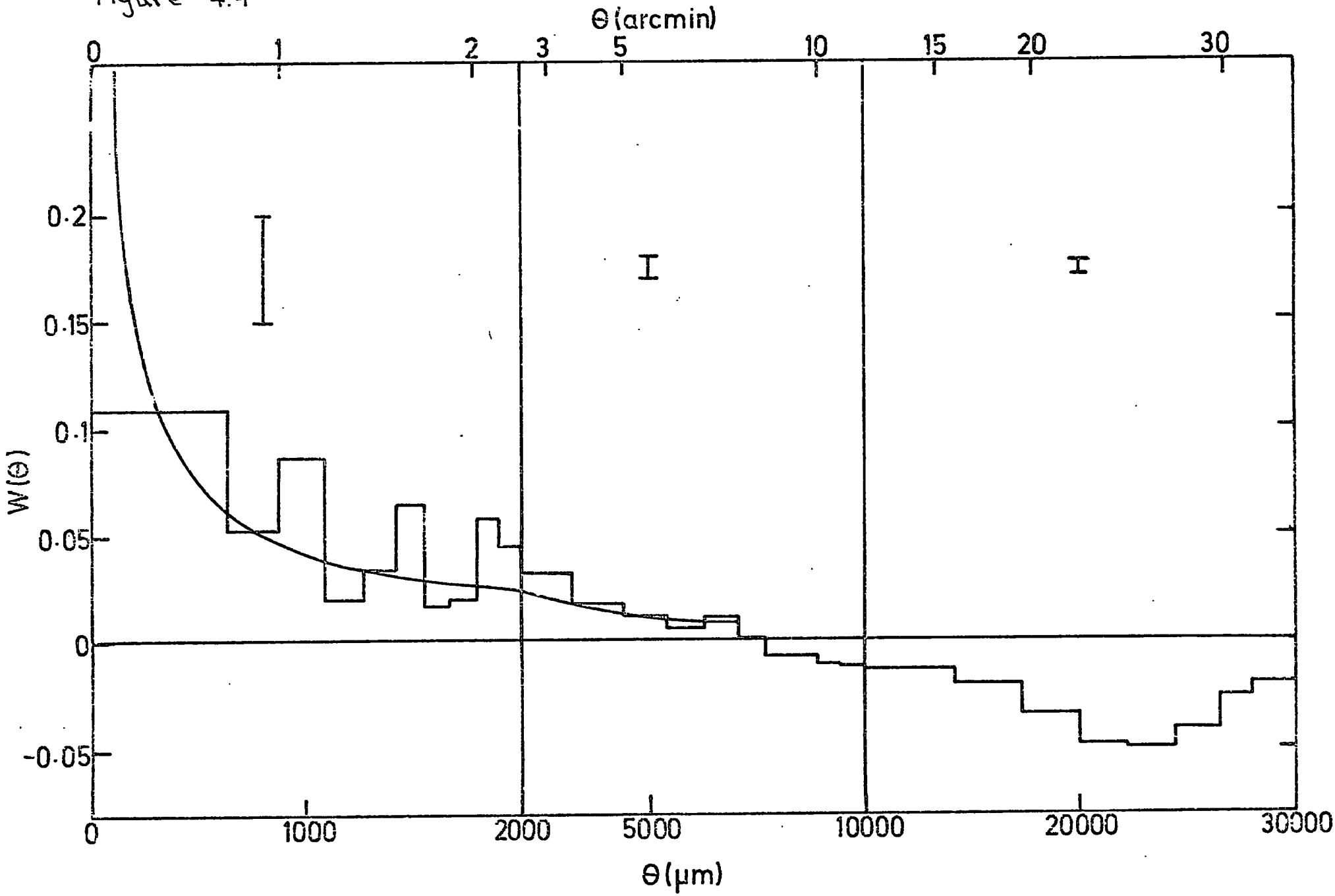

Angular covariance function w(θ) for R sample. Error bars indicate two nominal standard deviations. The smooth curve is a power law of index −0·8.

large θ obtained by this method are presented below.

In order to compare with previous results, it is obvious to try and fit a power law $\theta^{-\delta}$ to the results for $0 < \theta \lesssim 7000\mu m$. It is found that all powers in the range $0{\cdot}6 < \delta < 1{\cdot}0$ give tolerably good fits, the best fitting power depending somewhat on the range of θ for which the fit is made, but being approximately $-0{\cdot}8$ in agreement with previous determinations of the shape of $w(\theta)$. The smooth curve on figure 4.4 is a power law of index $-0{\cdot}8$.

In order to further study the form of the angular covariance function consider the cumulative function

$$E(\theta) = 2\pi \mathcal{N} \int_0^\theta w(a)\, a\, da \qquad (4.17)$$

which is the expected excess number of galaxies in a circle of radius θ centred on an arbitrary galaxy in the sample.

This is plotted for plate R1049 in figure 4.5, together with the straight line which shows the expected relationship assuming a power law of index $-0{\cdot}8$ for w (arbitrarily normalized). This is a good fit out to separations of about $4000\mu m$, the observed points subsequently falling below the predicted line, thus confirming the form

$$w(\theta) = A\,\theta^{-0{\cdot}8}$$

in the range $0 < \theta \lesssim 4000\mu m$ (about 5 arc min).

Figure 4.6 shows the log w - log θ plot for R1049, the straight line shown is the best fitting $-0{\cdot}8$

Figure 4.5

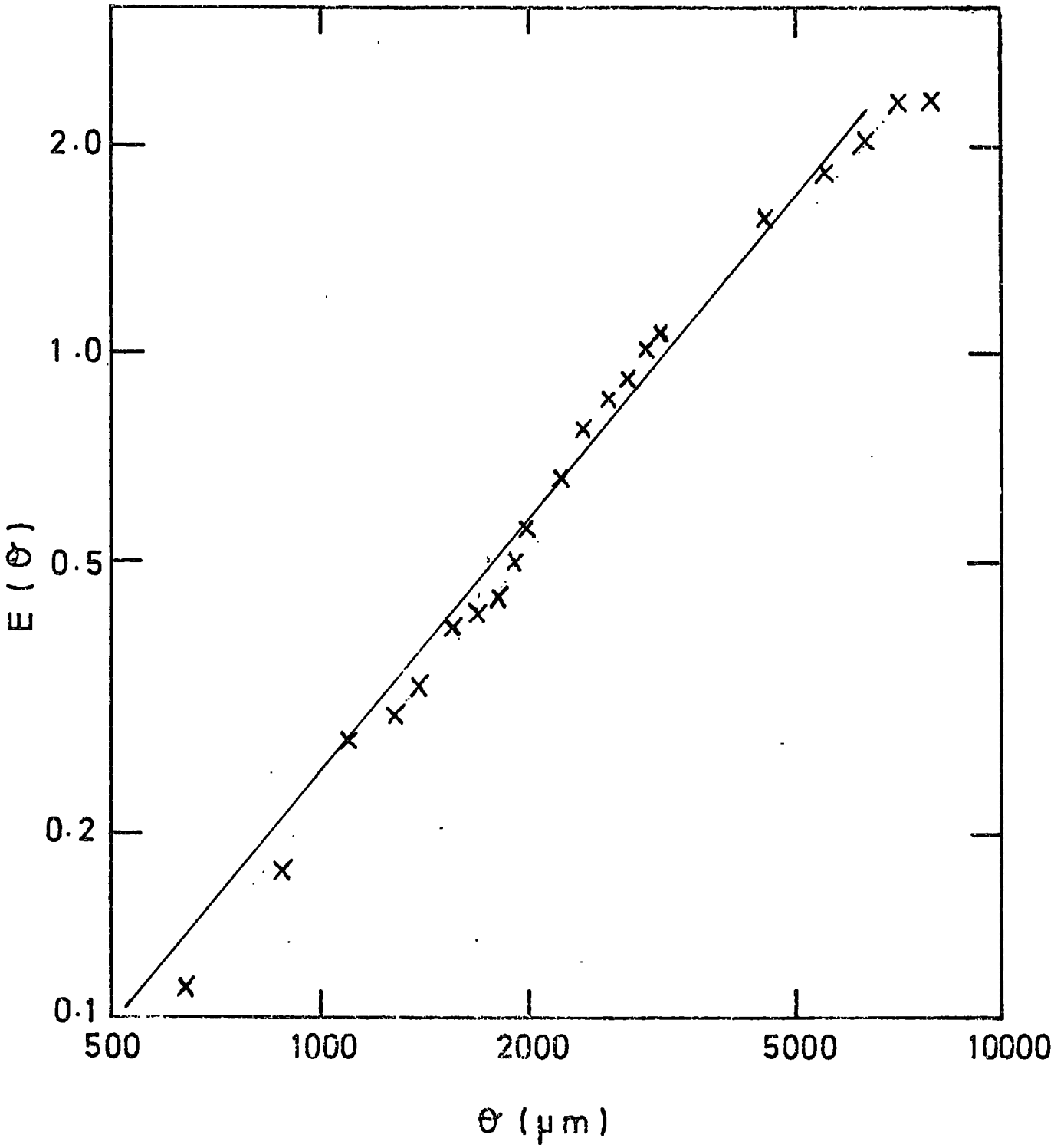

Cumulative function $E(\theta)$ for R sample. The straight line has a slope of 1.2

power law. Note that the fit is made, by a weighted least squares method, to the w - θ plot, not the log plot, over the range 0 to 4000 μm determined above.

The measured area was divided into four subregions and the calculation of w(θ) was made for each separately. The empirical standard deviation of each calculated w(θ) value is shown by the error bars in figure 4.6.

The best fit amplitude obtained, and henceforth used in all comparisons, is

$$A_R = (2{\cdot}21 \pm {\cdot}30) \times 10^{-3} \quad \text{for } \theta \text{ in degrees} \qquad (4.18)$$

In order to have a result more directly comparable with previous ones, a subset RS of the galaxies on R1049 has also been studied. This consists of all galaxies with angular diameters greater than 115 μm (the determination of angular diameters from the information available from COSMOS is dealt with in chapter 5). The subsample has a total of 606 galaxies in it, and has the same density - 335 per square degree - as the Jagellonian field mentioned previously in chapter 2.

Figure 4.7 shows the cumulative function E(θ) for this subset, again showing agreement with the expected relationship for a $\delta = 0{\cdot}8$ angular covariance function out to about 3000 μm while figure 4.8 shows the log w-log θ plot together with the best fitting power law of index -0·8 over the appropriate range. This has an amplitude

$$A_{RS} = (7{\cdot}8 \pm 1{\cdot}5) \times 10^{-3} \qquad (4.19)$$

Figure 4.6

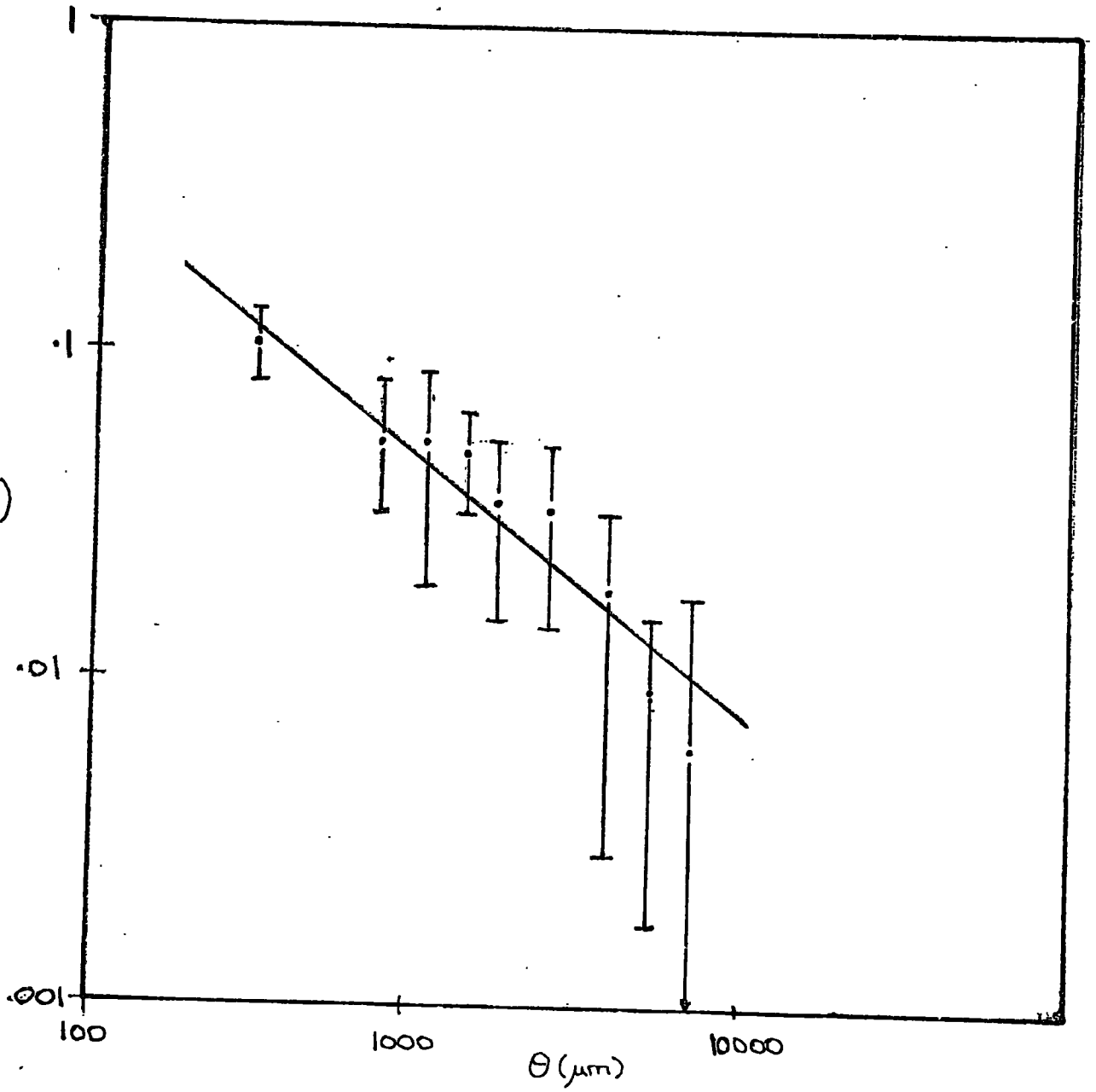

Log plot of $w(\theta)$. The straight line is the best fitting power law of index -0.8. Error bars indicate empirical s.d. found from four subregions of the R sample.

Figure 4.7

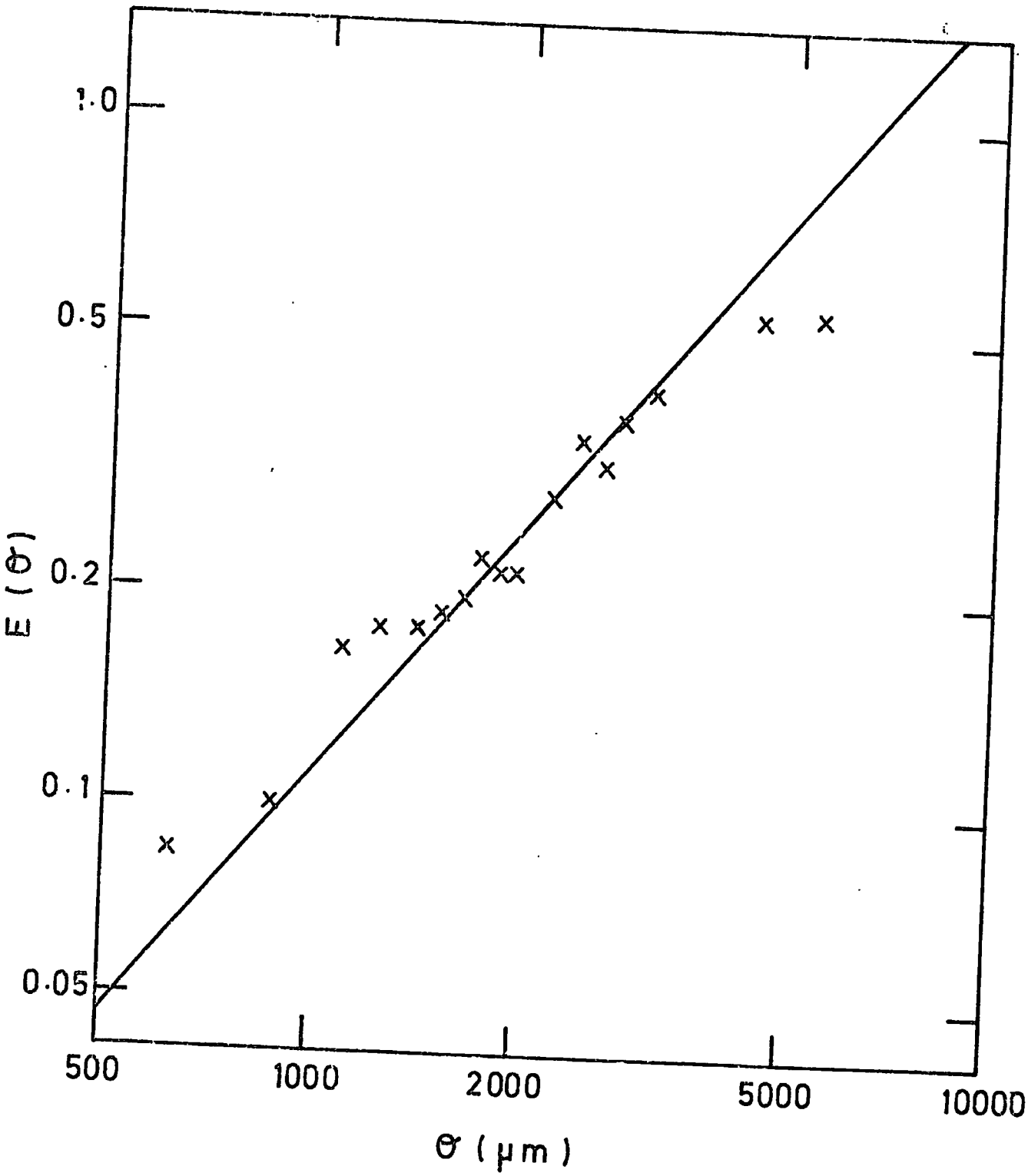

Cumulative function E(Θ) for RS sample. The straight line has a slope of 1.2.

Figure 4.8

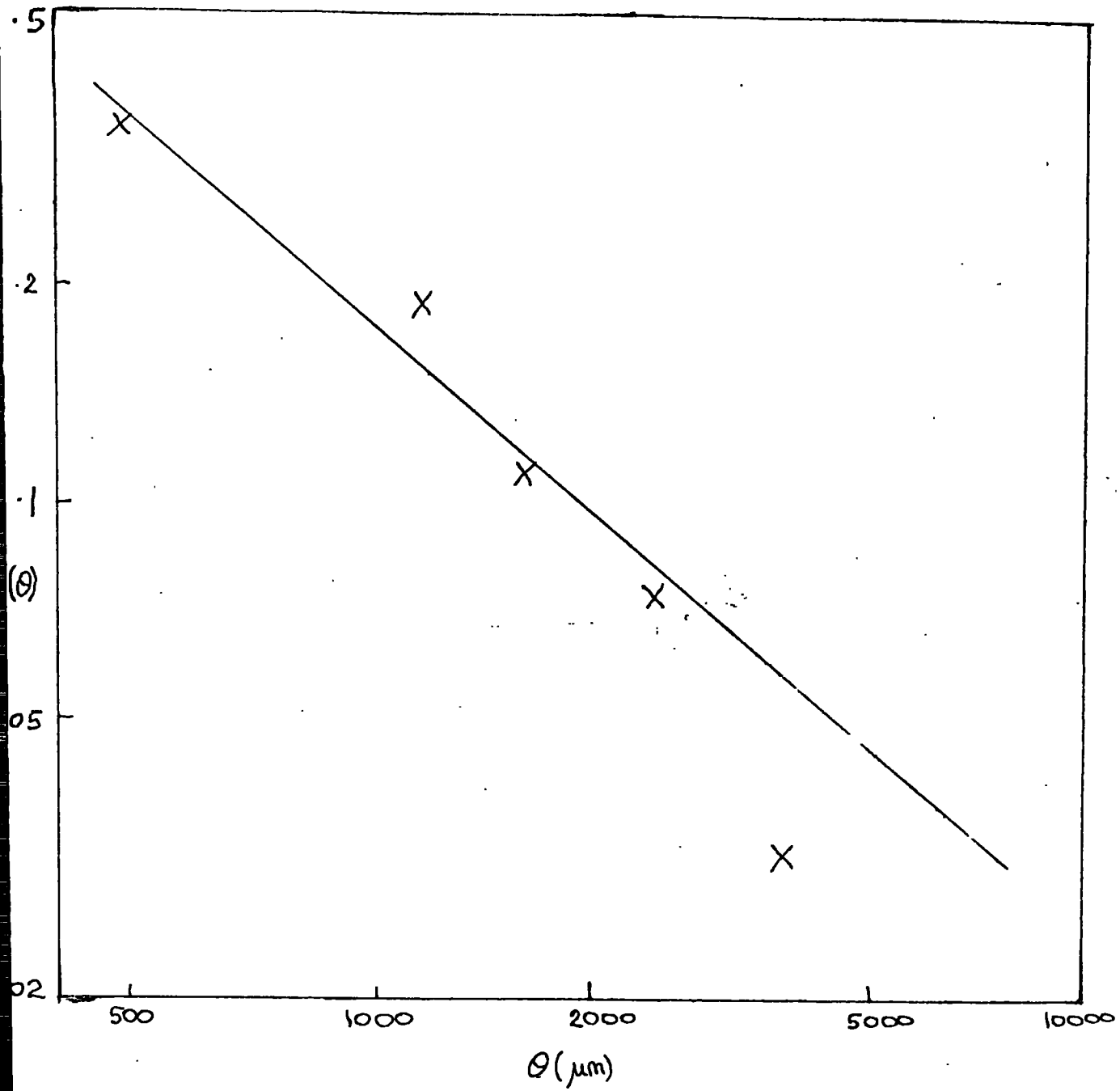

Log plot of $W(\theta)$ for the RS sample. The straight line has slope -0.8.

The binned analysis of the measured area of R1049, using bins of 1152 μm square, gives the results indicated in figure 4.9, where it can be seen that the behaviour at small θ follows closely that found in figure 4.4. At larger separations however this new more accurate representation shows that the angular covariance function is essentially zero beyond θ = 11000 μm implying no correlations on these scales. The reason for the inaccuracy of the former method at very large separations is the very prominent cluster near bottom centre of the measured region (see figure 4.2) which biases the choice of centre galaxies.

A smaller part of the measured area of plate R1049 was also considered, this being such that it had no 'holes' in it. The covariance function was found to be consistent with the overall $w(\theta)$ from the whole of the measured area, confirming the unimportance of 'holes'.

A covariance function for the images classified as stars was also computed for R1049. It was found to be consistent with $w(\theta) \equiv 0$ (figure 4.10), that is, the 'stars' may be taken to be randomly distributed over the plate. This suggests that these are all genuinely stars, correctly classified, but when a cross correlation was performed between 'stars' and 'galaxies' a positive correlation was found on small scales, suggesting that some 'stars' are really galaxies (if it is assumed that

Figure 4.9

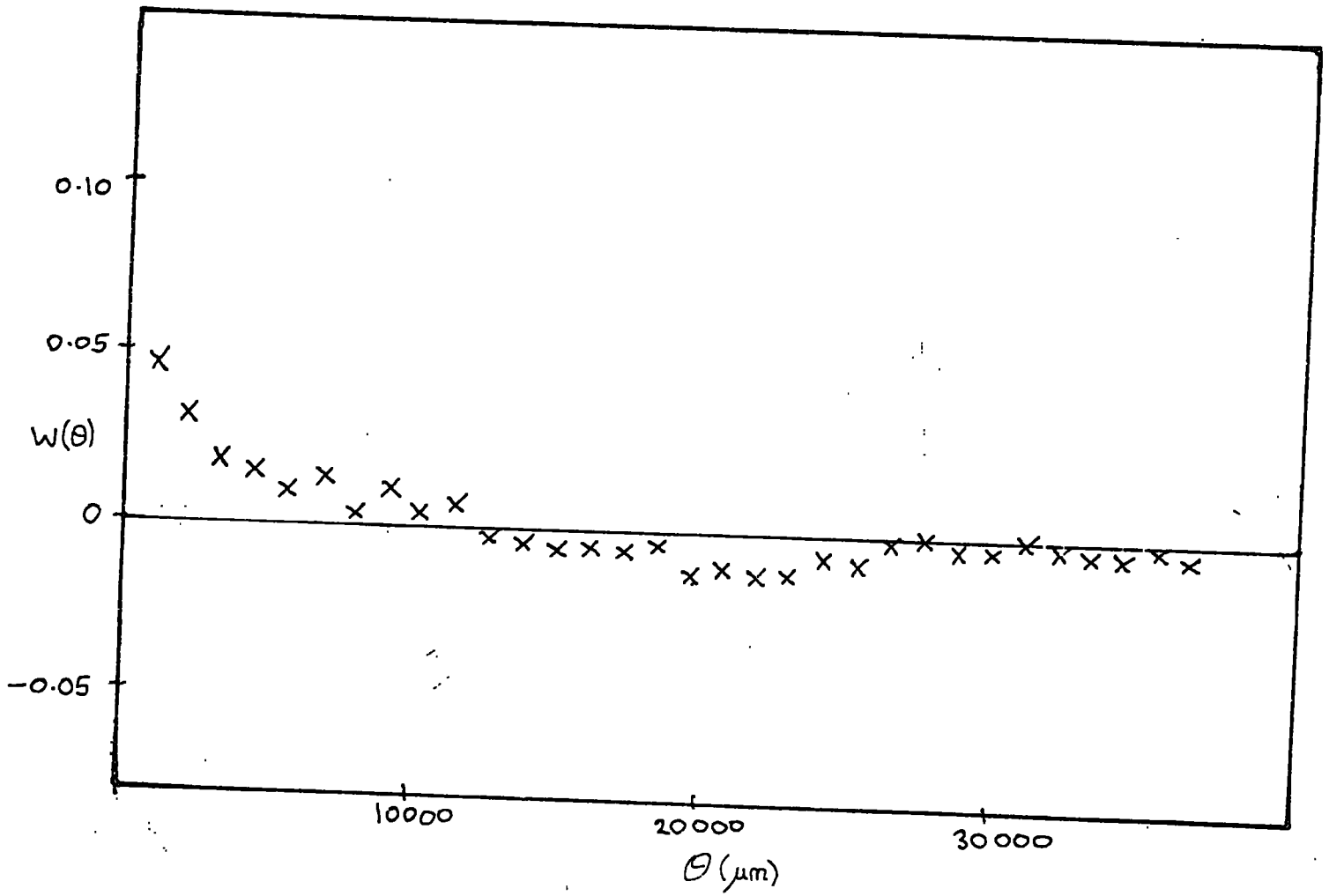

Angular covariance function $W(\theta)$ from binned analysis of R sample.

Figure 4.10

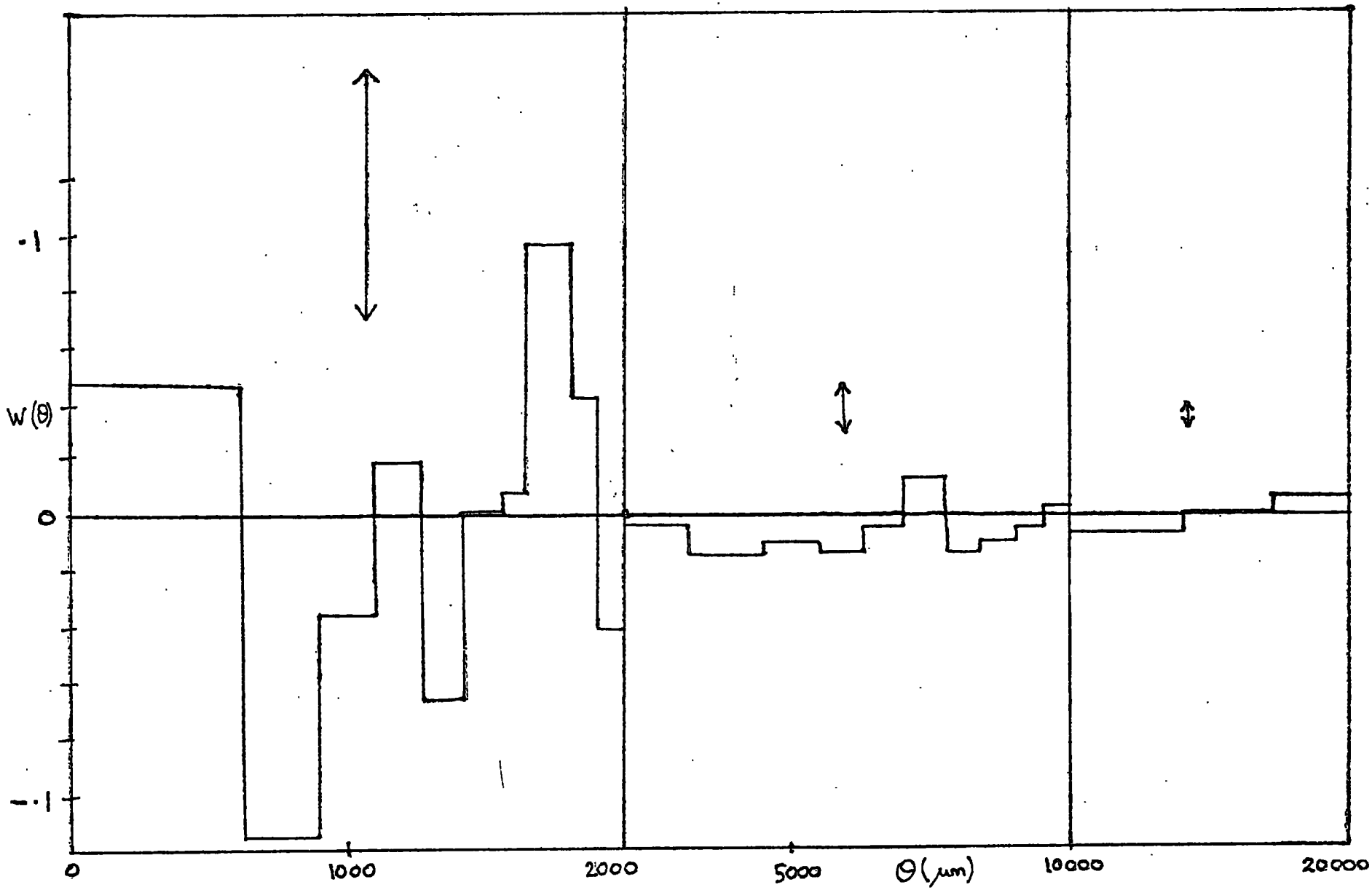

Angular covariance function for stars on measured area of plate R1049. Errors indicated are 2 s.d. (nominal).

the genuine stars are uncorrelated with each other and with the real galaxies). Assuming this, then from equation (2.52)

$$w_G = g^2 / G^2 \; w \qquad (4.20)$$

$$w_{G+S} = (g + s)^2 / (G + S)^2 \; w \qquad (4.21)$$

where w_G , w_{G+S} are the covariance functions calculated for the G 'galaxies' and G+S 'galaxies' and 'stars' and g, s are the numbers of real galaxies in G, S

$$\therefore \quad \frac{w_G}{w_{G+S}} = \frac{g^2 (G + S)^2}{G^2 (g + s)^2} \qquad (4.22)$$

Since w_G , w_{G+S} (figure 4.11), G and S are known this gives g/(g+s) and it is found to be approximately ·8, i.e. about 20% of galaxies may be lost into the star category.

Since stars are assumed uncorrelated the number of 'galaxies' which are really stars can not be calculated. If a significant number have been misclassified the amplitude of the true w could be higher than that calculated. If the above reasoning holds, then the near zero $w(\theta)$ for 'stars' must be due to the misclassified galaxies being randomly distributed (and therefore not a random selection of all galaxies).

Figure 4.11

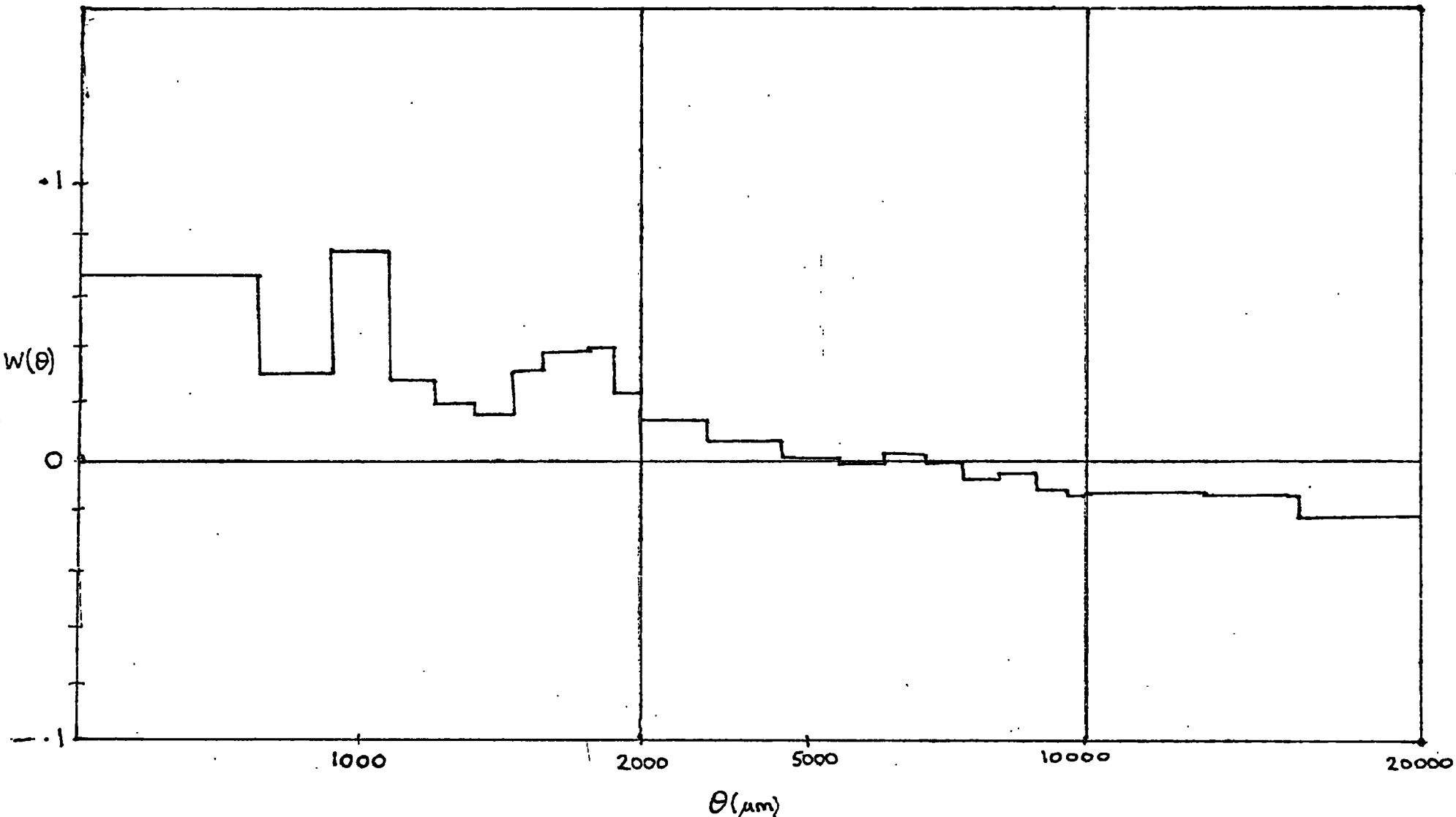

Angular covariance function for galaxies + stars on measured area of plate R1049.

4.6 THE RESULTS FOR PLATE J149

The COSMOS measured area on this plate is 72·704mm x 71·680mm, equivalent to 1·811 square degree, and contains 3371 images identified as galaxies and 2503 star images above the limiting area of 960 μm^2, plus a further 7592 small images. This gives a galaxy density of 1861 per square degree. The galaxy density contour map is given in figure 4.12.

The angular covariance function for the 3366 completely defined galaxy images was evaluated as for the red sample described above, and is shown in figure 4.13 as the dashed line.

However, as pointed out in section 3.3, plate J149 suffers from serious emulsion variations, leading to threshold correlated density variations.

To attempt to compensate for this artificial clustering, a correction factor for every point of the measured area is introduced.

Using figure 3.9, a smooth relationship between galaxy image density n and threshold transmission τ can be obtained. This can be put in the form

$$n(\tau)\, c(\tau) = \mathcal{N} \qquad (4.23)$$

where $c(\tau)$ is the correction factor for threshold τ, $n(\tau)$ is the average density for areas with threshold τ and $\mathcal{N}$ is the mean density over all the measured area, and

Figure 4.12

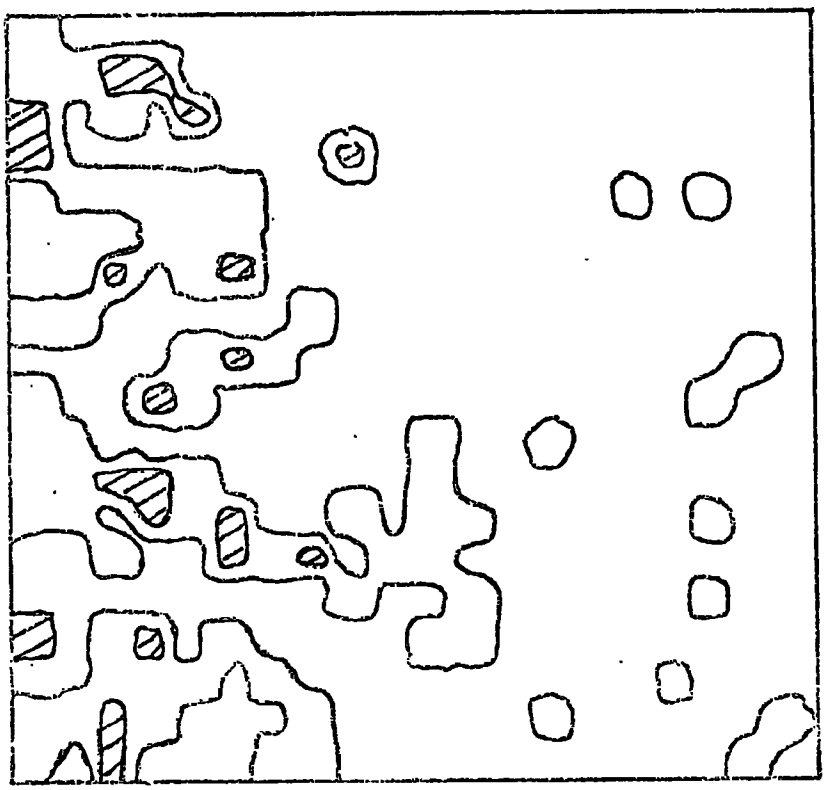

Galaxy number density contour map of the measured area of plate J149.

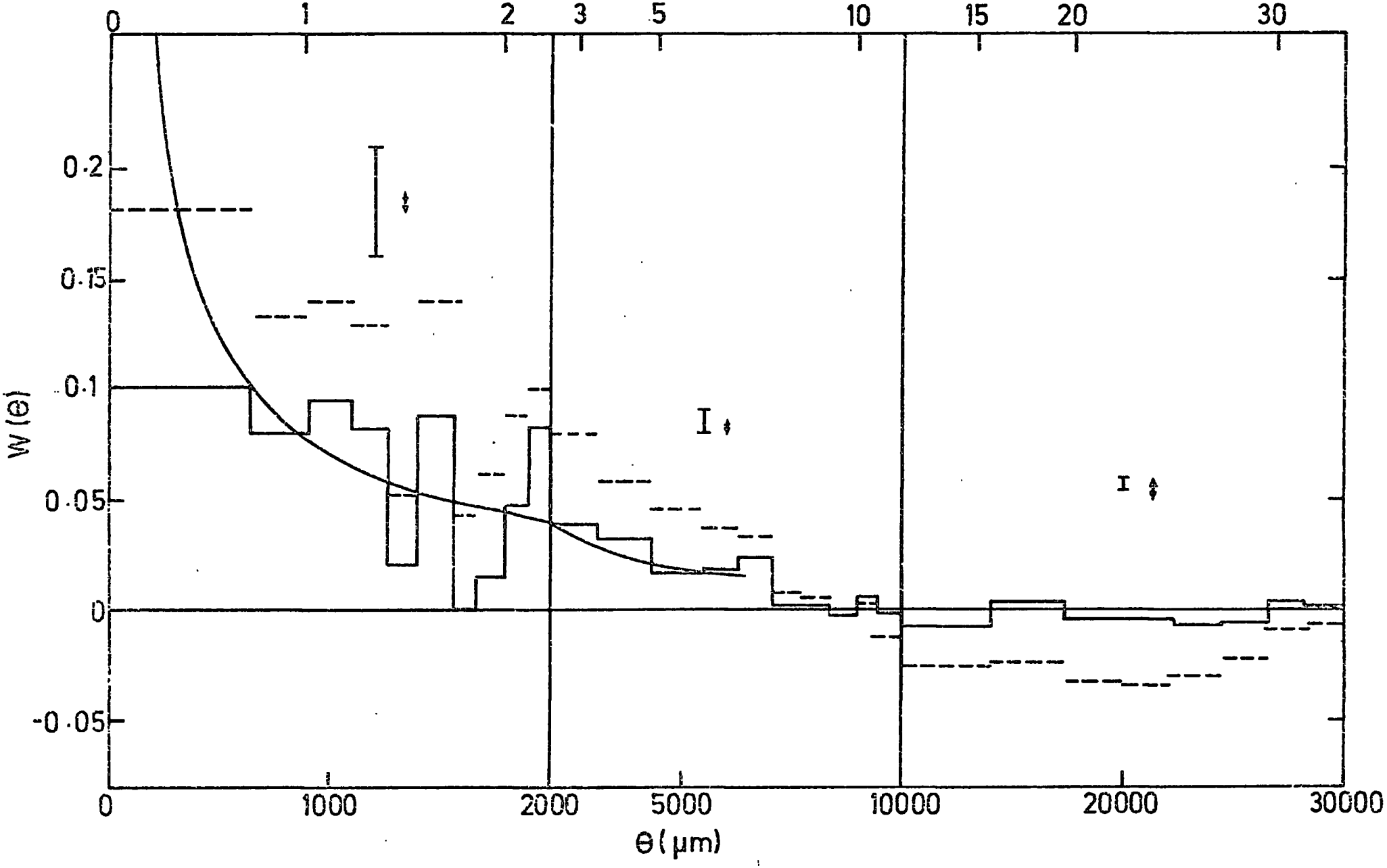

Angular covariance Function $w(\theta)$ for J sample ; unfiltered (dashed lines) and filtered (solid lines). Error bars indicate two nominal s.d., arrowhead errors indicate the difference made by a reasonable change to the filter. The smooth curve is a power law of index -0.8.

the fit

$$c(r) = 1/(0{\cdot}029r - 0{\cdot}529) \qquad (4.24)$$

was considered to be a good enough approximation.

To calculate the 'filtered' angular covariance function, equation (4.6) is replaced by

$$w(\theta) = \frac{\sum_{j \in J_k} \sum_{i \in I_j} c_i c_j}{\sum_{j \in J_k} c_j N \frac{\pi}{2}(\theta_k^2 - \theta_{k-1}^2)} - 1 \qquad (4.25)$$

where J_k is the set of all centre galaxies used previously for annuli of outside radius θ_k and I_j is the set of galaxies between θ_{k-1} and θ_k from the j th centre galaxy and c_i is the value of the correction factor $c(r)$ at the position of galaxy i. Clearly this reduces to equation (4.6) when $c_i = 1$, for all i.

This 'filtered' version of $w(\theta)$ is shown on figure 4.13 as the solid histogram. The smooth curve is again a power law of index -0·8. The arrowhead error bars indicate the difference that can be made by a 'reasonable' change in the slope of the fit to $n(r)$ (see fig.4.14). The straight error bars indicate two nominal standard deviations as before.

The general form of the function is as in the case of R1049, the figure 4.15 shows the cumulative function $E(\theta)$ to be in agreement with a power law angular covariance function with $\delta = 0{\cdot}8$ as before, out to about 7000 μm.

Figure 4.14

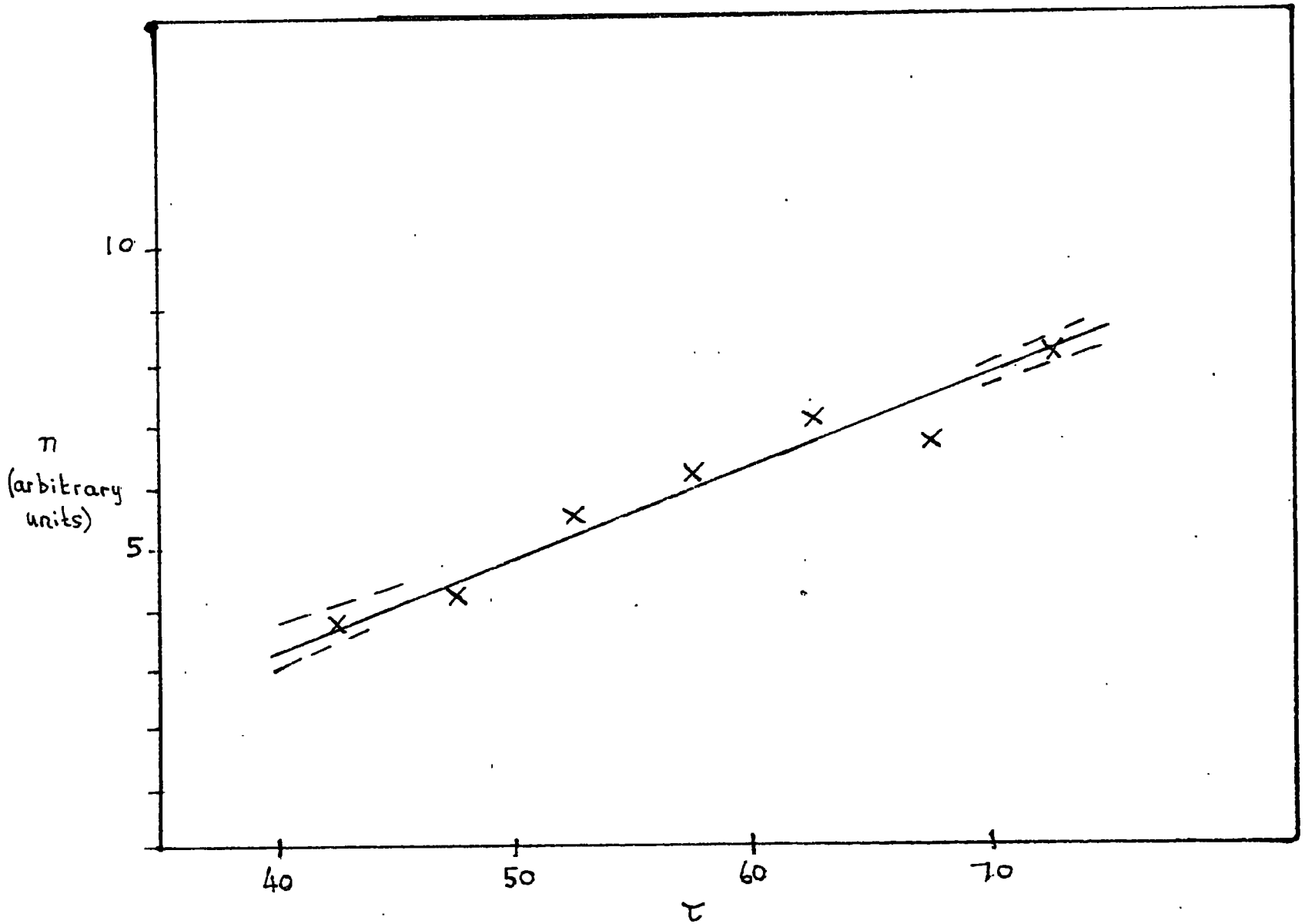

Correlation of threshold transmission τ with number density of galaxy images n, plate J149. The solid line shows the fit chosen. The dashed lines indicate the extreme fits.

Figure 4.15

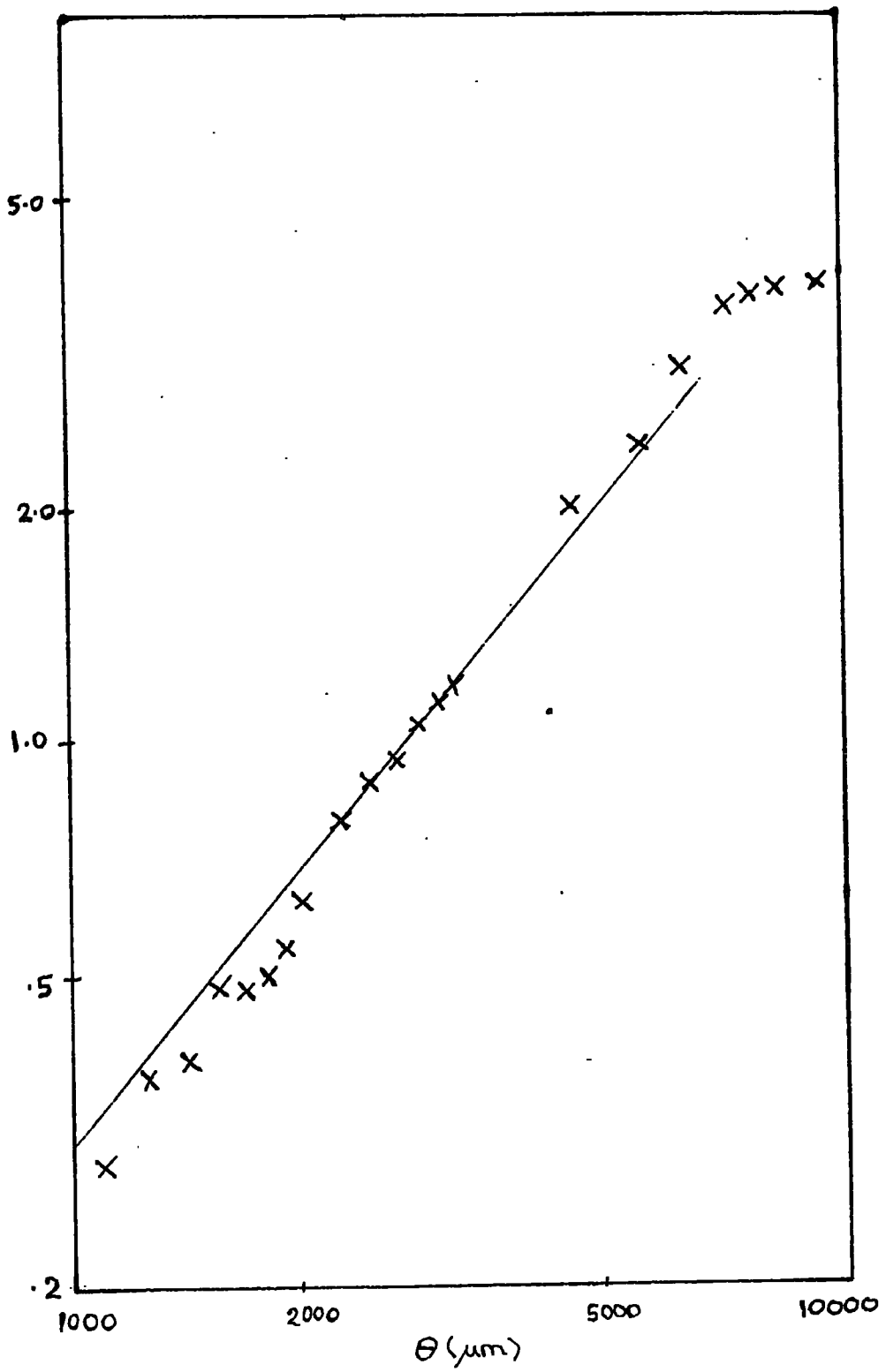

Cumulative function E(θ) for filtered J sample
The straight line has slope of 1·2.

The log w - log θ plot is given in figure 4.16, where the straight line is the best fit, obtained as before, which has an amplitude (for θ in degrees)

$$A_J = (2{\cdot}36 \pm 0{\cdot}41) \times 10^{-3} \qquad (4.26)$$

Figure 4.17 shows the filtered density contour map for the measured region and it can be seen that most of the major features are reproduced from figure 4.2, which is of nearly the same area of sky but in a different colour, which suggests that the filtering process has been successful and that only artificial clustering has been removed. Furthermore the 'filtered' covariance function for stars is near zero at all small separations, suggesting that any remaining large scale inhomogeneity does not effect w(θ) on small scales (since that is expected to be zero). It should be noted, though, that to obtain an actual covariance function for the stars a different filter should be used, calculated from the variation of star density with background, since this differs from the variation of galaxy density with background. For this reason a covariance function for the whole set of images and a cross-correlation between 'galaxies' and 'stars' are less useful than in the previous case, plate R1049, because of the difficulty of interpretation.

Note also from figure 4.13 the amplitude of w(θ) has been reduced by a factor of almost two by the 'filtering' process.

Figure 4.16

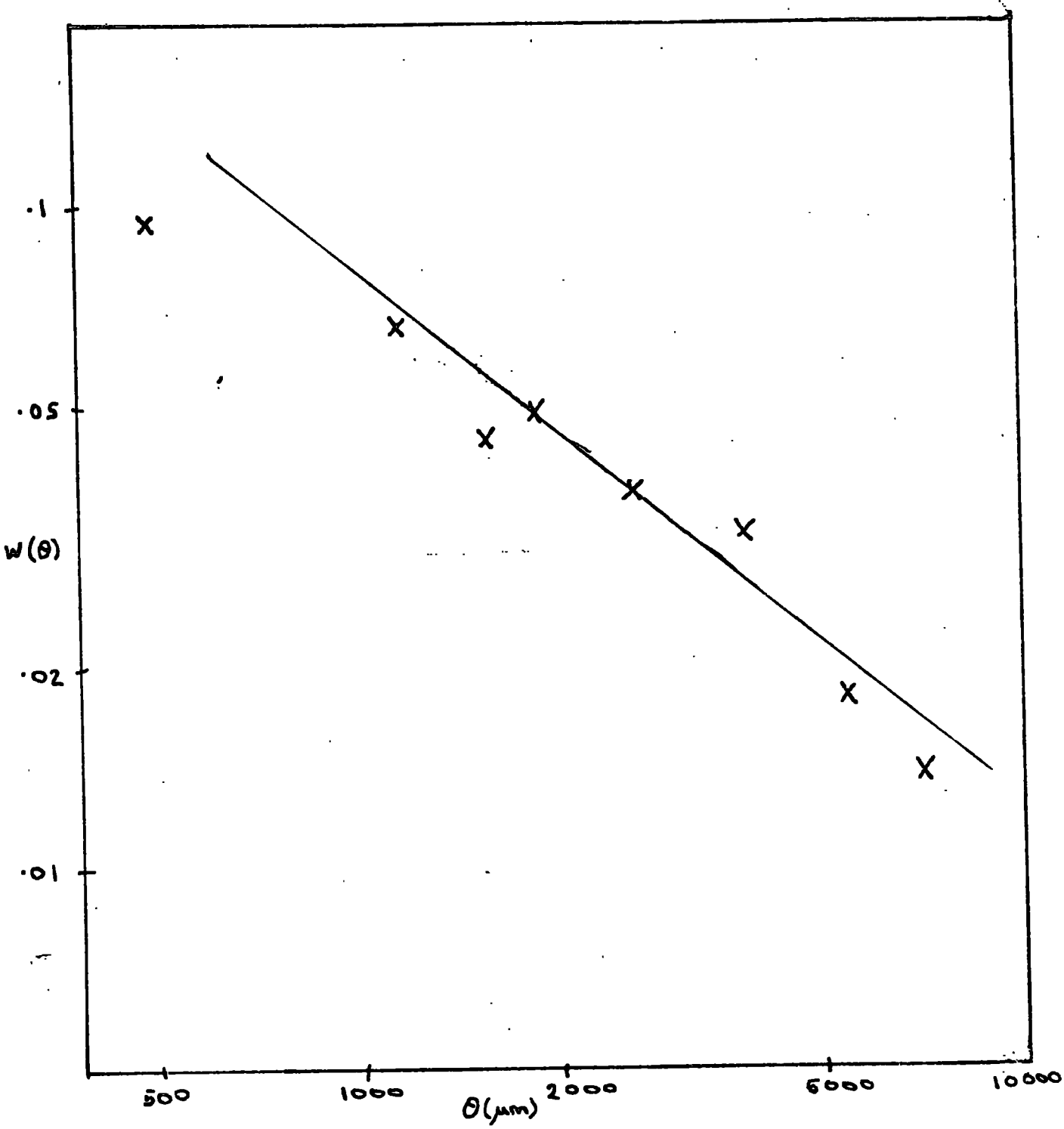

Log plot of $w(\theta)$, filtered J sample. Straight line has slope of -0.8.

Figure 4.17

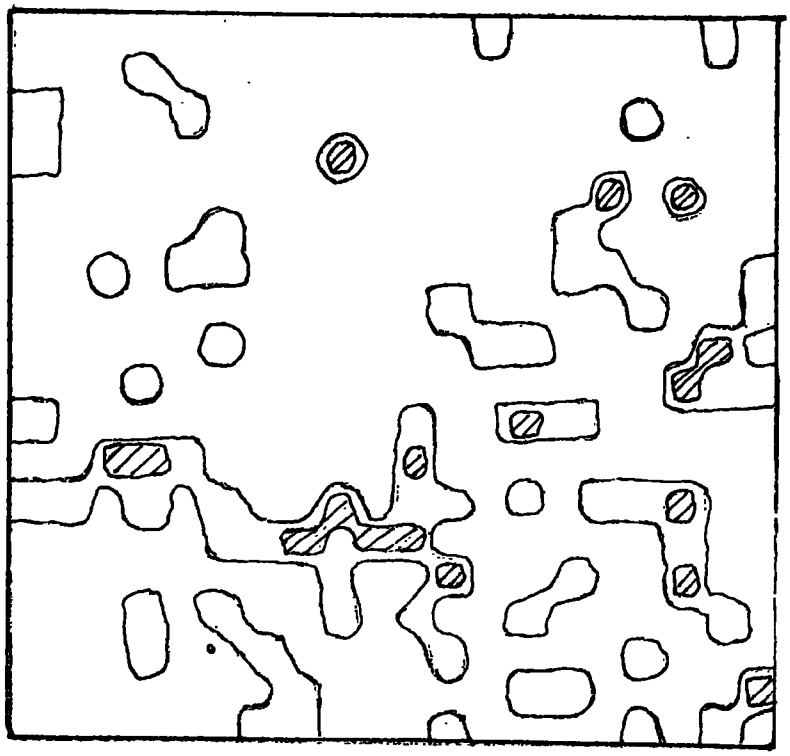

Filtered density contour map of galaxies in the measured area of plate J149.

This filtering process is unphysical in that galaxies are effectively counted c_i times, with c_i as defined previously, whatever their brightness. Thus on a densely populated region of the plate, bright (and presumably relatively nearby) galaxies are only counted as say '$\frac{1}{2}$ a galaxy' while a faint galaxy which would not even be recorded if it lay elsewhere on the plate is given just the same weight.

This implies that the contribution to w from relatively nearby clusters is diminished in these areas, while extra distant clusters are added in (relative to a smooth plate). However, on the areas with low density the nearby galaxies are still likely to be observed and their contribution will be exaggerated by the filtering, while the smaller (more distant) galaxies are not included in the sample so do not contribute.

Overall it is hoped that the filtered w will be similar to the 'real' w for a sample with the same number density per unit solid angle, since, at least on small scales, the result is more or less equivalent to averaging the covariance function for lots of small areas, each at a slightly different depth.

4.7 THE RESULT FOR AN EYE MEASURED SAMPLE OF GALAXIES ON PLATE J149

Prior to the COSMOS measurement of the region of plate J149 discussed in the previous section, another region of the plate was studied by eye, by Dodd, Morgan, Nandy, Reddish and Seddon (1975). They measured the positions of 3055 objects which they could identify as galaxies, in an area of 2 square degrees, the smallest galaxies recorded having angular diameters about 3·3 arc sec (50 μm). From the presence of stars claimed to be of 23rd magnitude, they inferred that the limiting isophote would be somewhat fainter than 24·2 magnitudes per square arc second.

Using their measurements of the positions a covariance function was calculated for this sample (Dodd *et al* 1976) but since the positions were quantised (due to the measuring accuracy of 254 μm) the basic equation (4.6) was modified to

$$w(\theta) = \frac{n(\theta_{k-1},\theta_k)}{n_c(\theta_k)\,\mathcal{N}\,\frac{\pi}{2}\,\Delta\Omega_k} - 1 \qquad (4.27)$$

where $\Delta\Omega_k$ is the total area of the 254 μm squares which have their centres in the half annulus between θ_{k-1} and θ_k from a given cell centre, (see figure 4.18).

The results are shown in figure 4.19, displayed in the same manner as for the previous two sections,

Figure 4.18

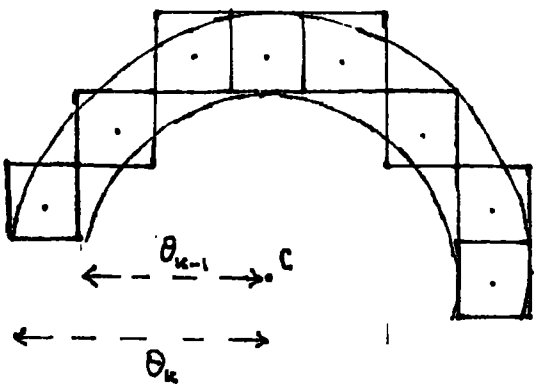

Quantization of area: The area in equation (4.27), $\Delta\Omega_k$, would in the case illustrated be 8 × the quantization square, i.e. $8 \times 254 \times 254\ \mu m^2$. In general, the number of squares can be calculated by finding the number of pairs of integers (x,y) such that

$$\theta_{k-1}^2 < 254^2(x^2+y^2) \leq \theta_k^2$$

and halving it.

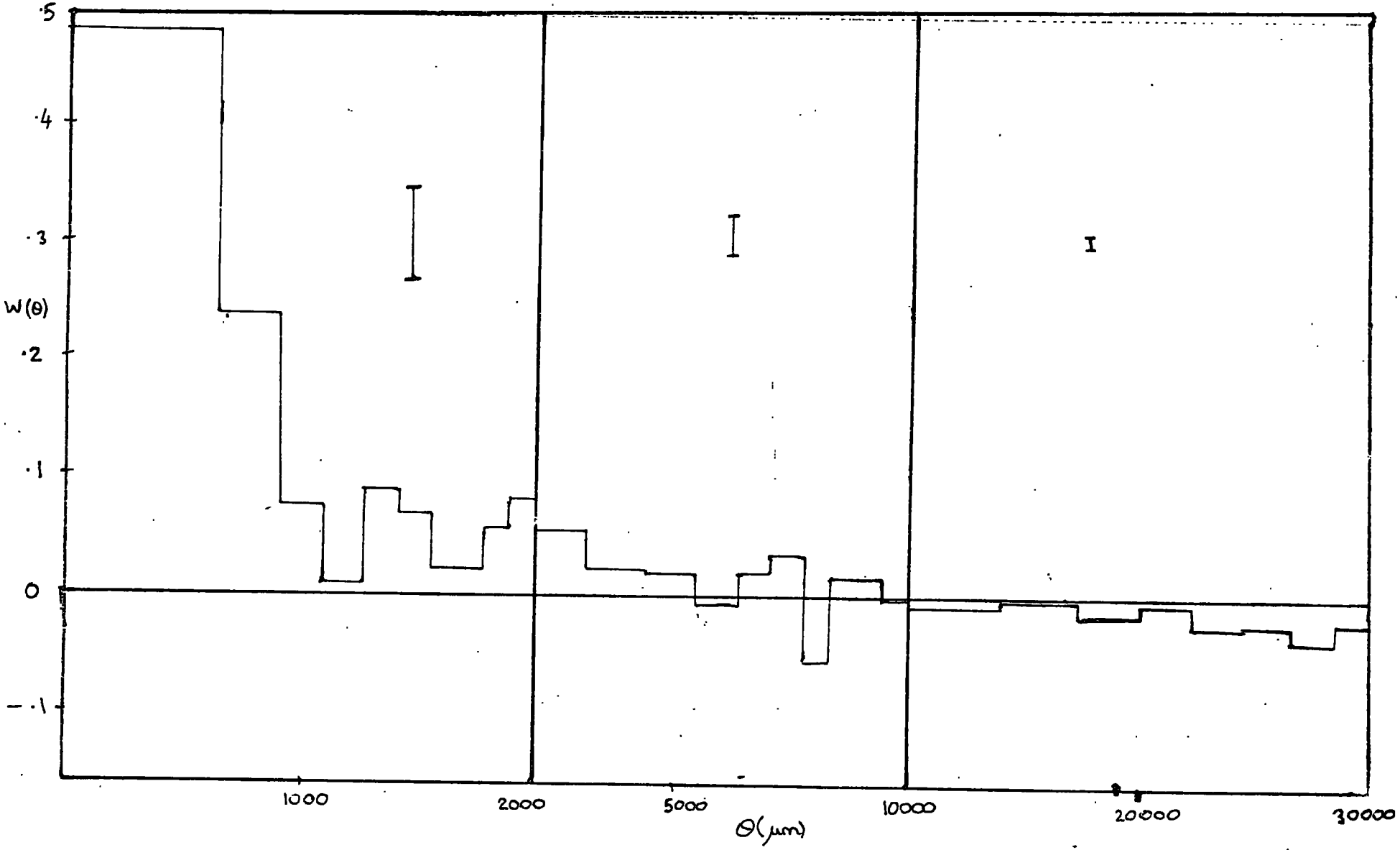

Angular Covariance function w(θ) for the D sample. Error bars indicate 2 nominal s.d.

again with a δ =0·8 power law superimposed.

Again using E(θ) (figure 4.20), a power law is seen to be a reasonable fit out to about 4000 μm, and the best fit amplitude (for δ =0·8 and θ in degrees, as always) is

$$A_D = (7{\cdot}0 \pm 0{\cdot}8) \times 10^{-3} \qquad (4.28)$$

This amplitude is much higher than A_J, even though the sample appears to be almost as deep, judging by the number density, and it can be conjectured that this may be due to a real fluctuation in the clustering, a difference between eye measurement and machine measurement or large scale variations because of the uneven emulsion and so forth, which can not be detected by the visual observer.

Further reference to this difference will be made in a later chapter.

4.8 THE RESULTS FOR PLATE J1920

As mentioned in chapter 3, the initial star/galaxy separation attempted for almost the whole area of the plate was unsuccessful due to the variations in threshold over this large region. However star/galaxy separation was performed successfully on a smaller area 81·920 x 119·808mm, (which corresponds to 3·41 square degrees)

Figure 4.20

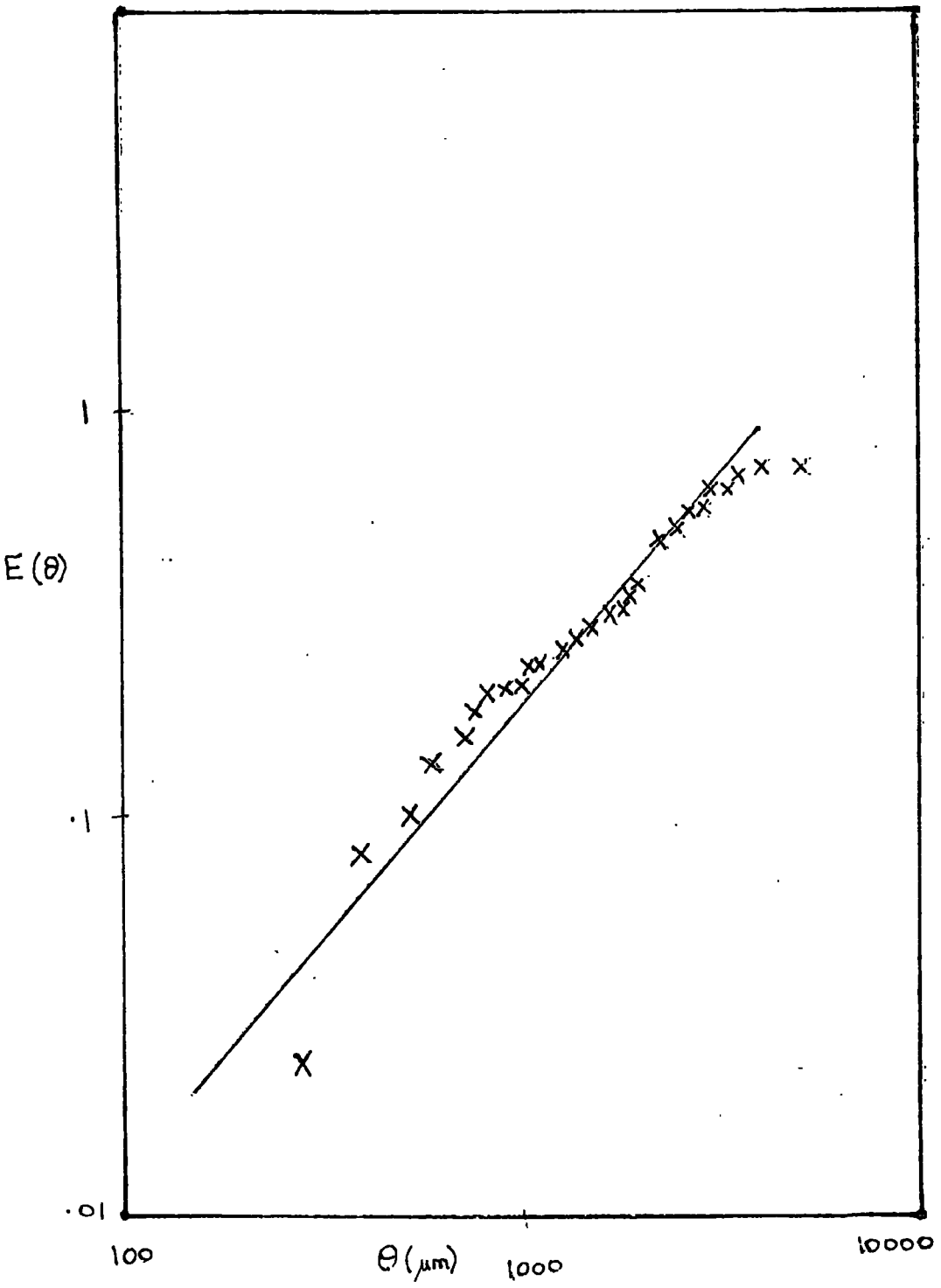

Cumulative function $E(\theta)$ for D sample.
The straight line has slope 1·2.

where threshold variations are small. Above an area limit for segregation of 640 μm^2, the area contains 6792 galaxies and 5755 stars. It may be noted that this gives a ratio of stars to galaxies of 0·85 very similar to the value 0·80 found for plate J149, which should be of a similar depth since its density of galaxies per square degree is almost the same as the 1991 per square degree found for J1920.

There is no evidence for any correlation between threshold and image density or any other large scale inhomogeneities, so no 'filtering' was deemed necessary and the angular covariance function was calculated via equation 4.6 in exactly the same way as for the measured region of R1049.

Plots of $w(\theta)$ and $E(\theta)$ are given as usual in figures 4.21 and 4.22. The best fit amplitude over the range $0 < \theta \leq 3000\mu m$ was found to be

$$A_{1920} = 3{\cdot}6 \times 10^{-3} \qquad (4.29)$$

Subsamples limited at 50 μm and 100 μm angular diameters were also considered, $w(\theta)$ and $E(\theta)$ being as shown in figures 4.23, 4.24, 4.25 and 4.26. Best fit amplitudes for these are

$$A_{1920/50} = 4{\cdot}5 \times 10^{-3} \quad \text{for the range } 0 < \theta \leq 3000\mu m \qquad (4.30)$$

$$A_{1920/100} = 10{\cdot}5 \times 10^{-3} \quad \text{for the range } 0 < \theta \leq 10000\mu m \qquad (4.31)$$

Figure 4.21

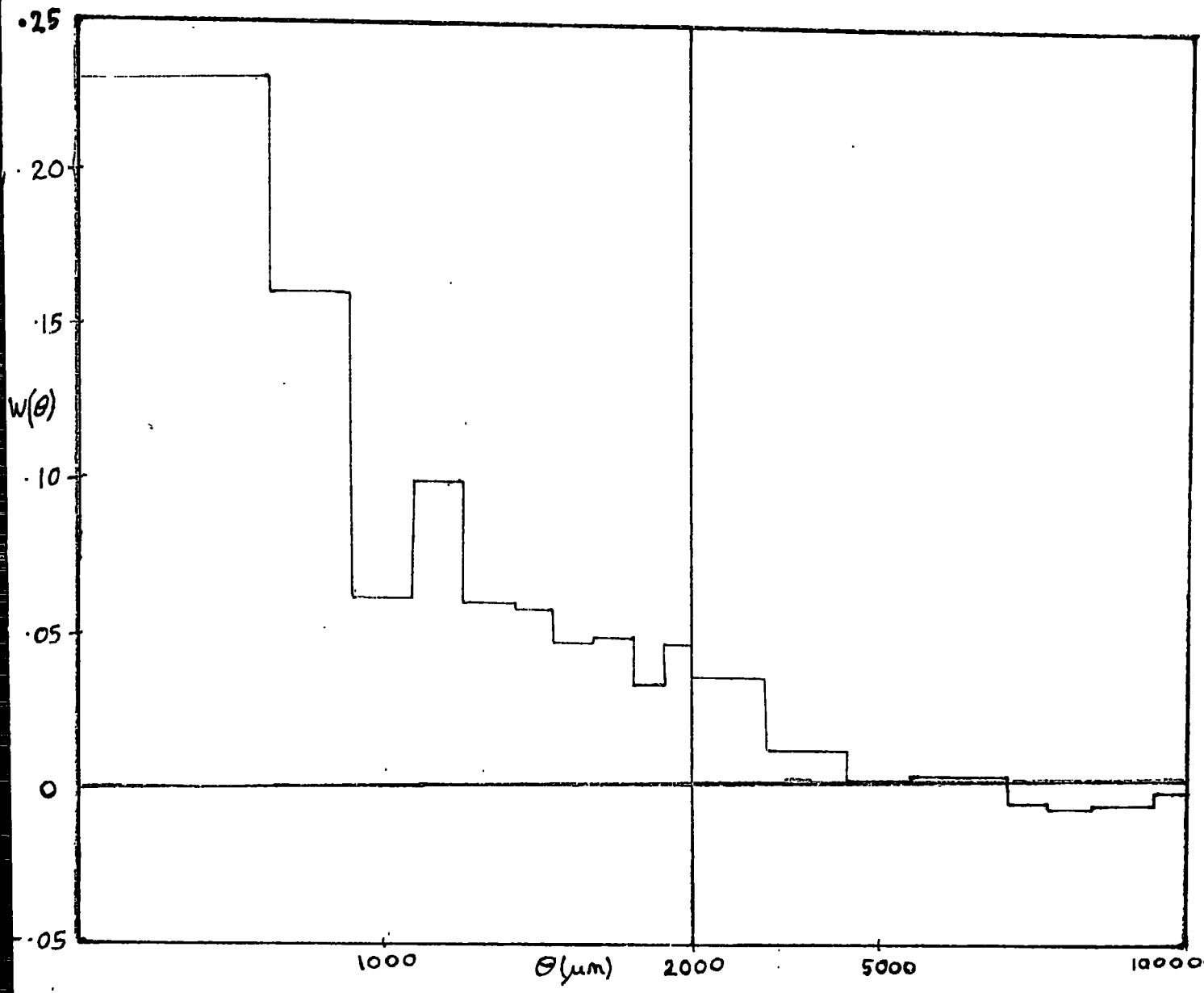

Angular covariance function $w(\theta)$ for 1920 sample.

Figure 4.22

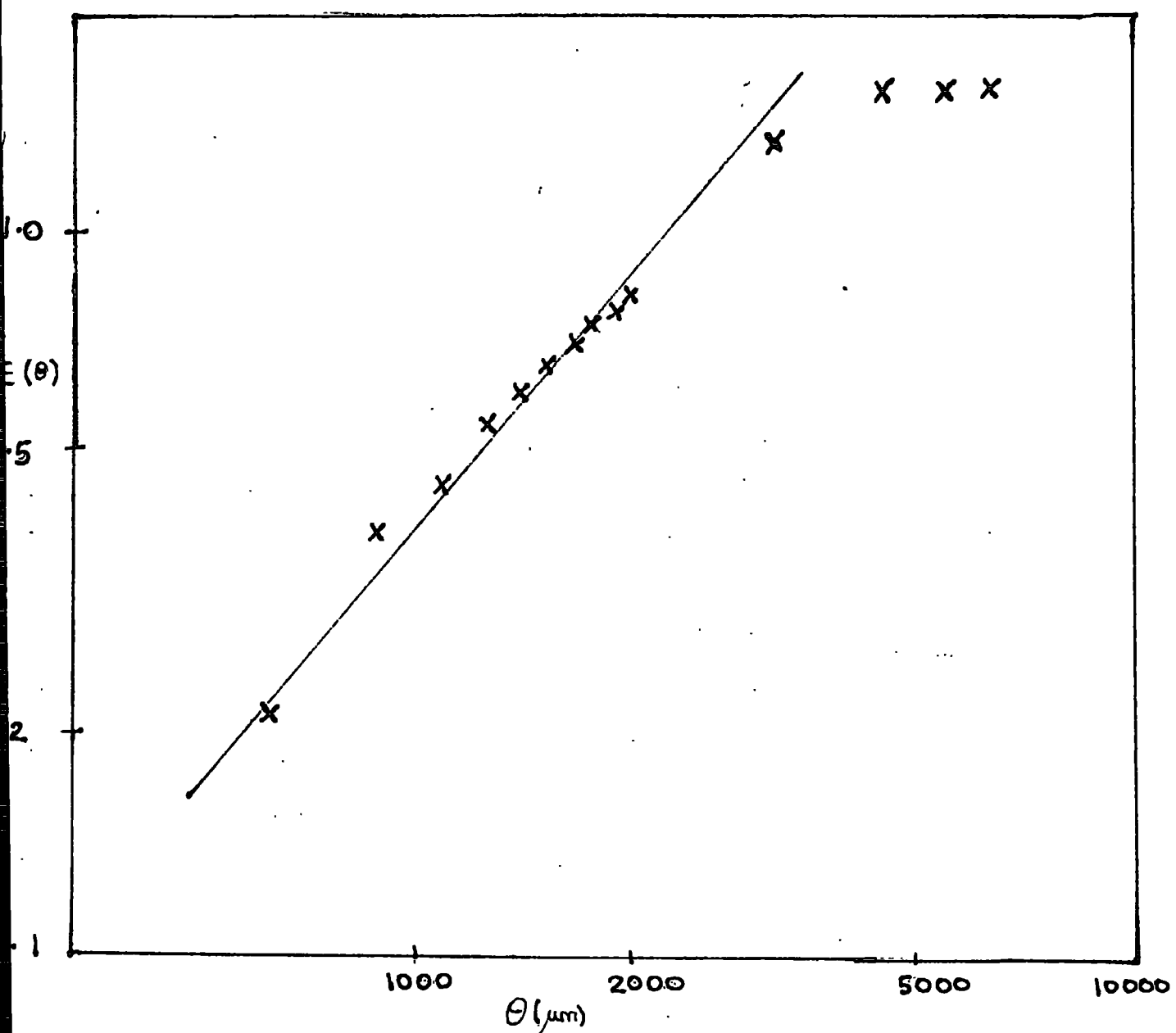

Cumulative function $E(\theta)$ for the 1920 sample.
The straight line has a slope of 1·2.

Figure 4.23

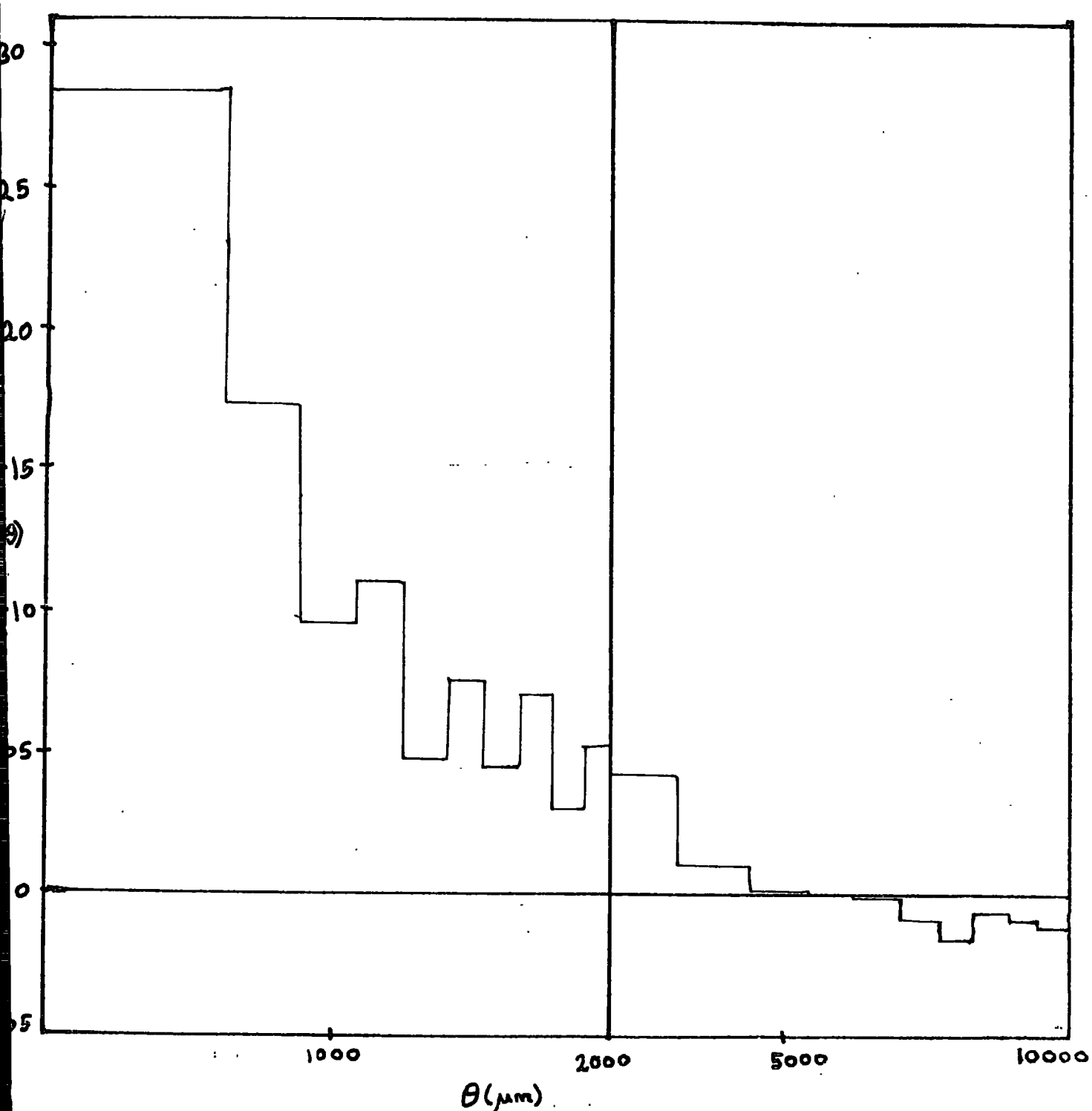

Angular covariance function W(θ) for 1920/50 sample.

Figure 4.24

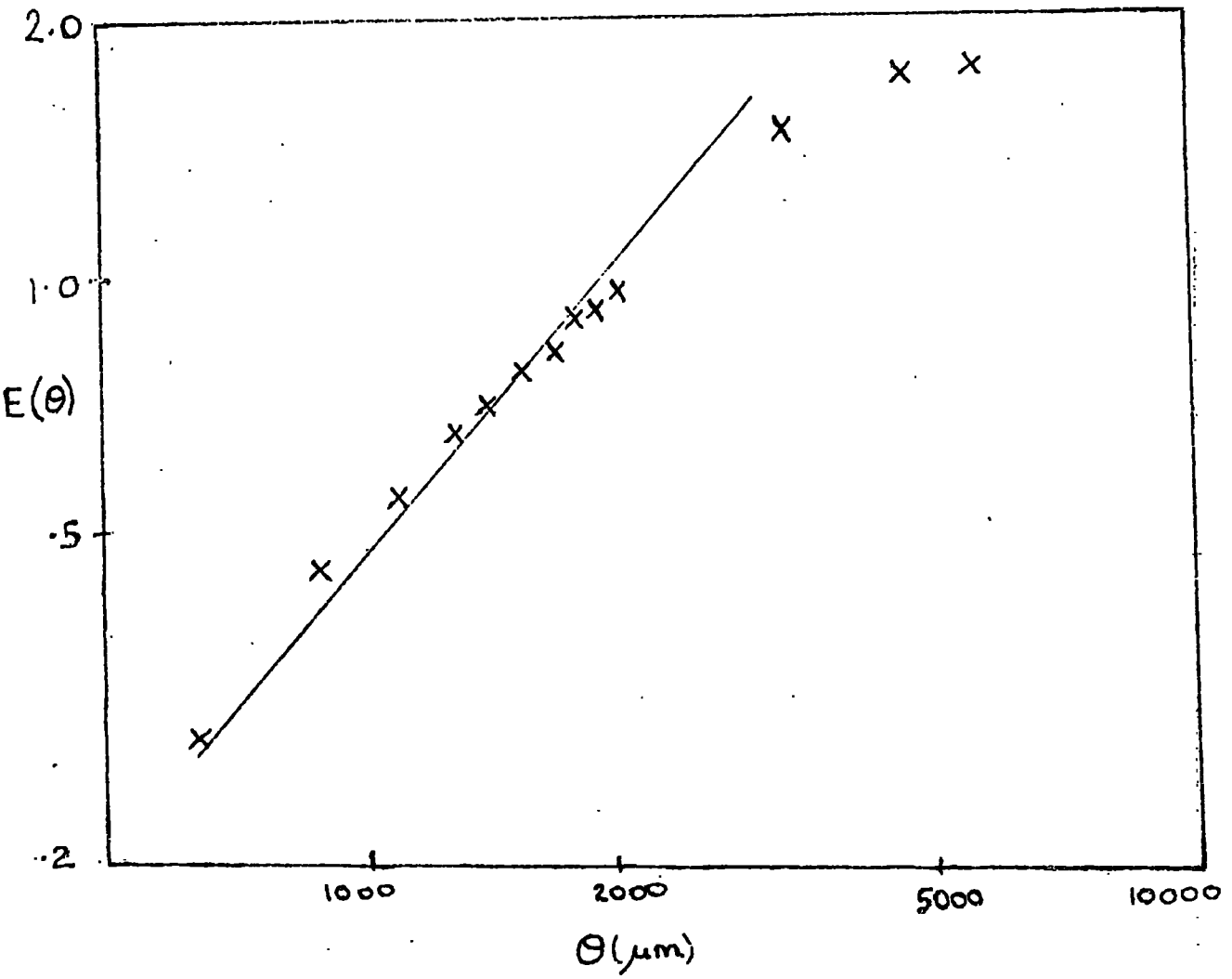

Cumulative function E(θ) for the 1920/50 sample. The straight line has a slope of 1·2.

Figure 4.25

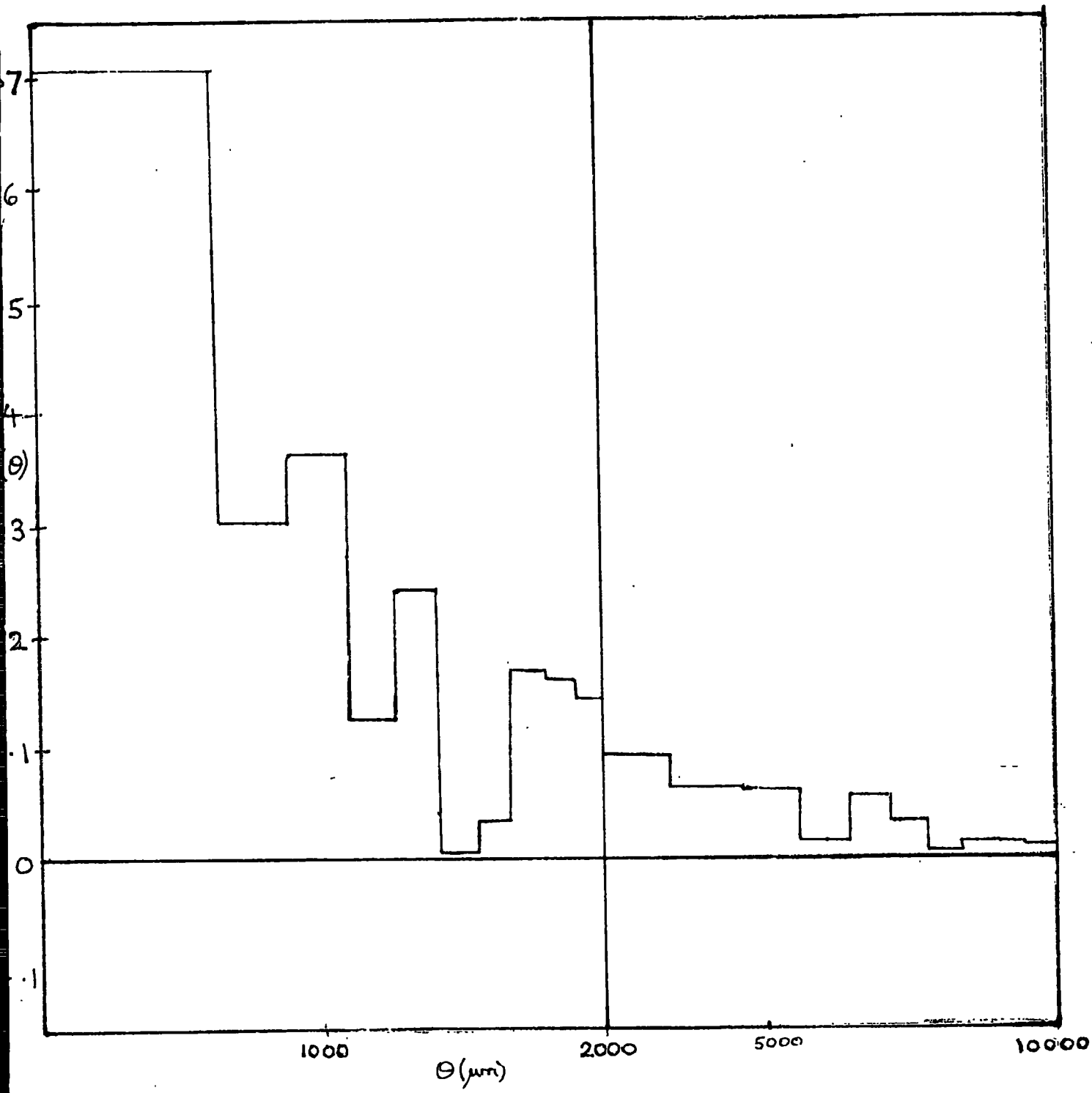

Angular covariance function $w(\theta)$ for 1920/100 sample.

Figure 4.26

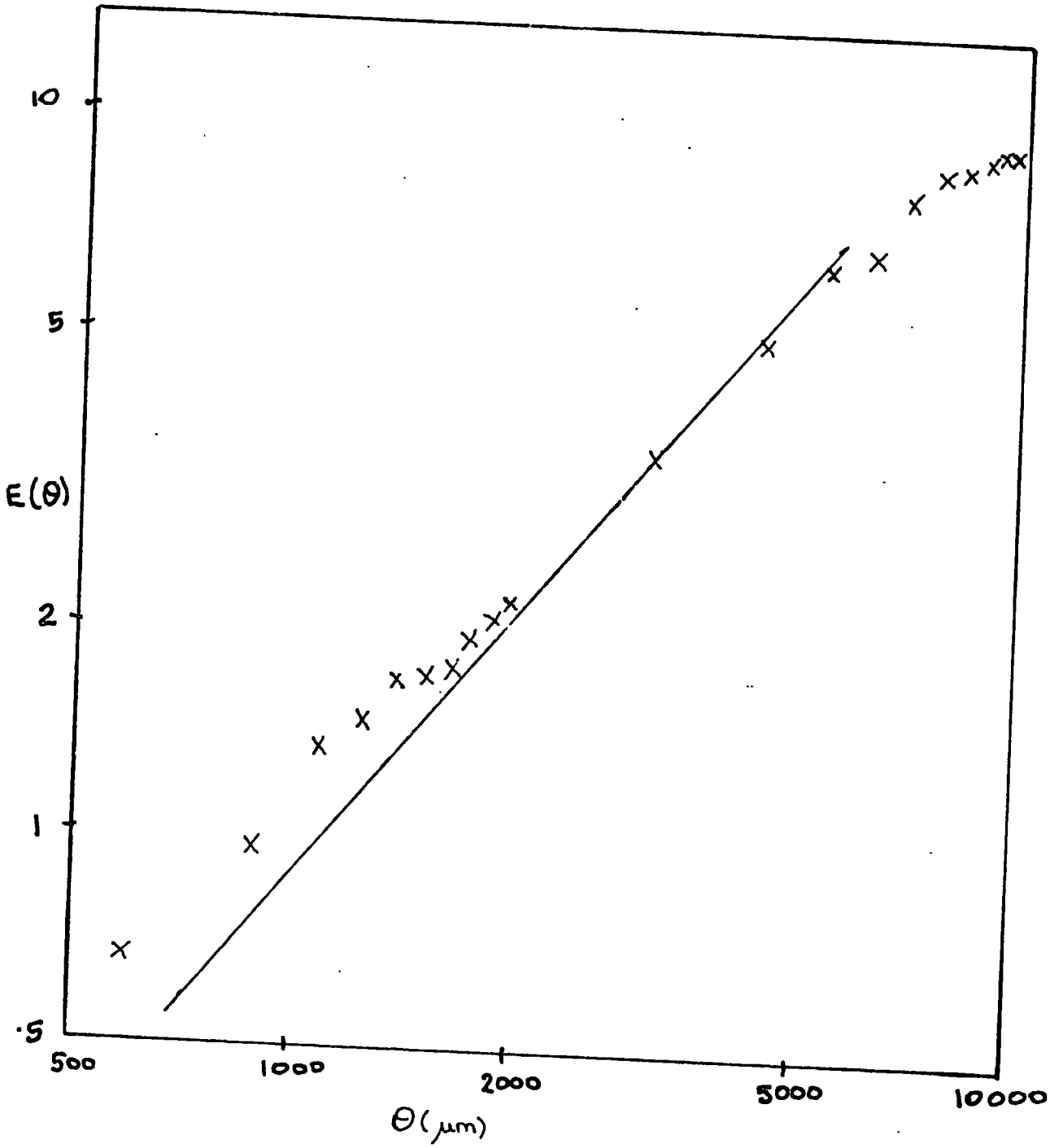

Cumulative Function E(θ) for the 1920/100 sample. The straight line has a slope of 1·2.

The galaxy number densities above these limits are 1622 and 469 per square degree respectively.

4.9 THE RESULTS FOR PLATE J1921

Plate J1921 was taken during a period of poor atmospheric conditions and consequently the seeing disc was very large. An area 122·880 μm square (5·249 square degrees) was measured by COSMOS, and down to a limit of 3840 μm^2, 4345 galaxies and 4485 stars were recorded. The large area limit for discrimination is a further consequence of the poor seeing, the smaller images being too blurred out to distinguish stars from galaxies. It also caused the plate to be much less deep than the others previously discussed, the density of the galaxies being only 828 per square degree.

Furthermore there are emulsion variations which cause the galaxy numbers to be correlated with thresholds and the plate requires 'filtering' in exactly the same manner as plate J149. Despite the problems the covariance function was calculated and both filtered (solid line) and unfiltered (dashed line) versions are shown in figure 4.27. The filtered $E(\theta)$ is given in figure 4.28.

The best fitting amplitude over the range $0 < \theta < 10000\ \mu m$ was

$$A_{1921} = 6{\cdot}1 \times 10^{-3} \qquad (4.32)$$

Figure 4.27

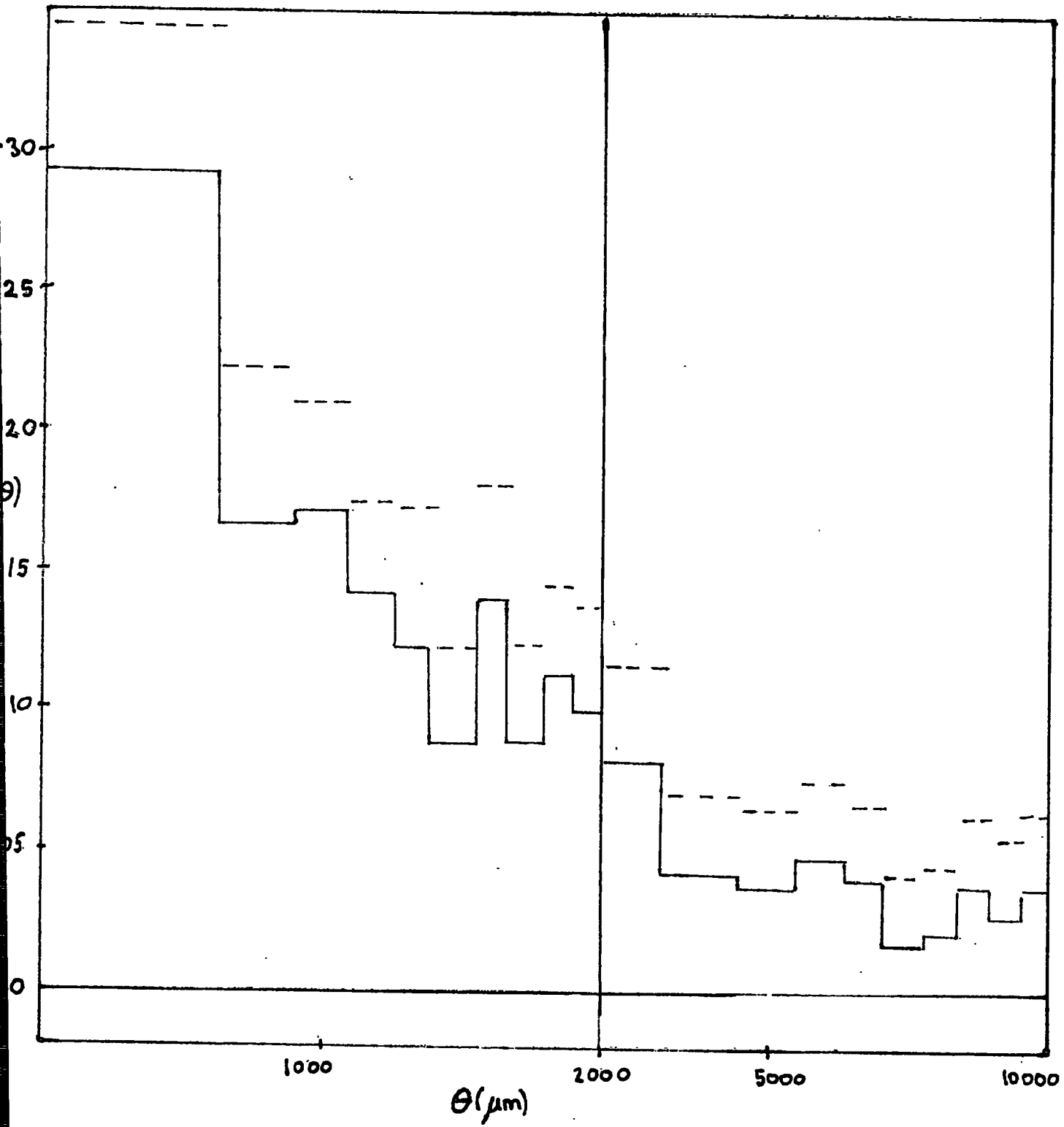

Angular Covariance function w(θ) For unfiltered (dashed lines) and filtered 1921 sample (solid lines).

Figure 4.28

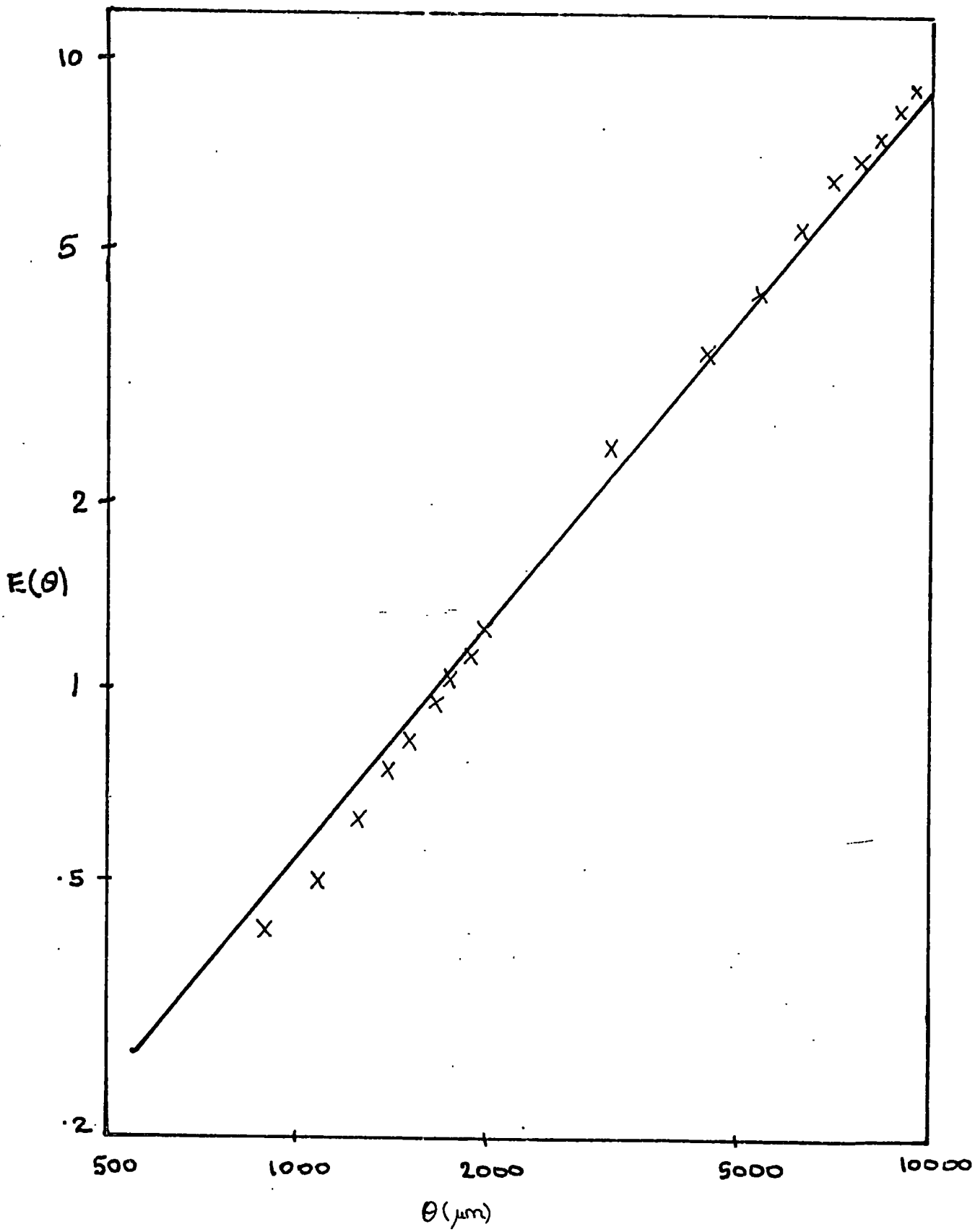

Cumulative Function E(θ) for the Filtered 1921 sample. The straight line has a slope of 1·2.

4.10 SUMMARY OF RESULTS

From the four available Schmidt plates four areas were measured by COSMOS and in addition a further area was measured by eye.

Two of the COSMOS measured areas - those on plates R1049 and J1920 suffer from no obvious defects and should be the most reliable samples, the latter being the best because of its much larger area.

The other two COSMOS measured regions suffer from severe emulsion problems and hence required the calculation of correction factors for every point of the plate in order to filter out unwanted large scale variations. Despite this the processing of the area of plate J149 seems to have been altogether satisfactory due to the good agreement between it and the measured area of R1049 which is in a different wavelength range but is nearly the same region of the sky. Plate J1921, however, is of poor quality and possibly, not too much weight should be attached to the results obtained from it.

In all the samples considered, the angular covariance function agrees with the form

$$w(\theta) = A\,\theta^{-\delta}$$

with δ approximately 0·8, verification of which is given

by the graphs of $E(\theta)$ which show that $E \propto \theta^{1-2}$ is a good fit in general (though E is of course merely an integral of w).

The number densities and best fitting amplitudes, assuming $\delta = 0{\cdot}8$ and θ in degrees, are summarised in table 4.1 for the samples considered above.

The comparison of these amplitudes with those obtained by other workers, (see chapter 2) via Limber's formula, equation (2.24), must be delayed until chapter 6 when the method of determining the selection function for such deep samples has been described.

There are at least two sources of error in the estimate of w used. Firstly, the mean density $\mathcal{N}$ has, necessarily, been calculated from the samples themselves. This may not reflect the true ensemble average $\langle \rho \rangle$. Such errors might be expected to be of the order $(1 + w)/\sqrt{N_G}$ where N_G is the number of galaxies in the sample and may be thought of as a 'zero error', since w is always small in the present samples, so that the error is approximately a constant, $(N_G)^{-1/2}$.

Secondly the edge-corrections applied (section 4.4) bias the estimates, as only the central galaxies are used as centres when θ is large. If the central region is not a 'fair sample' of the whole area then the estimates of $w(\theta)$ at large θ will be systematically in error, (as was the case for plate R1049, section 4.5). However, this will not effect w seriously at small θ and therefore will not cause an appreciable error in the calculated amplitudes.

Table 4.1

Sample	Number Density (per square degree)	Amplitude
R	2458	$2{\cdot}2 \times 10^{-3}$
RS	335	$7{\cdot}8 \times 10^{-3}$
J	1861	$2{\cdot}9 \times 10^{-3}$
D	1513	$7{\cdot}0 \times 10^{-3}$
1920	1991	$3{\cdot}6 \times 10^{-3}$
1920/50	1622	$4{\cdot}5 \times 10^{-3}$
1920/100	469	$1{\cdot}0 \times 10^{-2}$
1921	828	$6{\cdot}1 \times 10^{-3}$

The abbreviations for the samples are as in the text

R : plate R1049

RS : subset of R1049 with angular diameters >115μm

J : plate J149

D : eye measured sample, Dodd et al (1976)

1920 : plate J1920

1920/50 : subset of 1920 with angular diameters >50μm

1920/100 : subset of 1920 with angular diameters >100μm

1921 : plate J1921

CHAPTER FIVE

THE ANGULAR DIAMETER COUNTS OF GALAXIES

'A mathematical model of a class of
phenomena designates a set of
mathematically expressed assumptions
regarding a system of hypothetical
entities, designed with the hope that,
after an appropriate adjustment of
several intervening parameters,
the consequences of the assumptions
will agree with the observable
characteristics of the phenomena'.

Jerzy Neyman.

5.1 ANGULAR DIAMETER COUNTS AND THE DISTRIBUTION IN DISTANCE

The distribution in depth of the samples considered here can not be observed directly, the redshifts of the small faint images would be impossible to obtain, even if it were practicable to measure several thousand separate redshifts.

Since the apparent size of a galaxy will decrease as its distance increases, then if there were only one size and brightness of galaxy, the distribution of the galaxies in distance would be exactly reflected by the distribution of angular diameters of the galaxies.

Obviously this is far from realistic, in practice the angular diameter counts are the sum of the contributions from galaxies of all brightnesses and sizes, but nevertheless, the angular diameter counts and the distribution in distance are intimately related.

Given the actual galaxies that are present in some particular area of the sky, the two parameters which determine the distribution of angular diameters are the limiting isophote and the seeing, and these clearly also determine which galaxies are actually seen. If a prediction is made of the distribution, based on a model for the brightnesses and profiles of galaxies, for various isophotes and seeing, then the most likely isophote and seeing can be found by matching to the observed

angular diameters.

With these fixed, it is an easy matter to use the model again to predict the distribution in distance, in fact all that is required is the number of galaxies at each distance which have angular diameters above the cut-off for the sample being considered.

5.2 DETERMINATION OF ANGULAR DIAMETERS FROM COSMOS OUTPUT

Given the parameters listed in Table 3.3, in particular the minimum x and y co-ordinates and the area, it is possible, under the assumption that the image is elliptical to calculate the angular diameter.

Suppose the image has major and minor axes of length a and b respectively aligned along the x', y' directions, then

$$f \equiv \frac{x'^2}{a^2} + \frac{y'^2}{b^2} = 1 \qquad (5.1)$$

Let $P \equiv (x', y')$ be the point on the ellipse with a tangent parallel to the y-axis (see figure 5.1), then the angle ϕ between the normal at P (i.e. the x-axis) and the x'-axis is given by

$$\tan \phi = \frac{\partial f}{\partial y'} \Big/ \frac{\partial f}{\partial x'} = \frac{y' a^2}{x' b^2} \qquad (5.2)$$

Figure 5.1

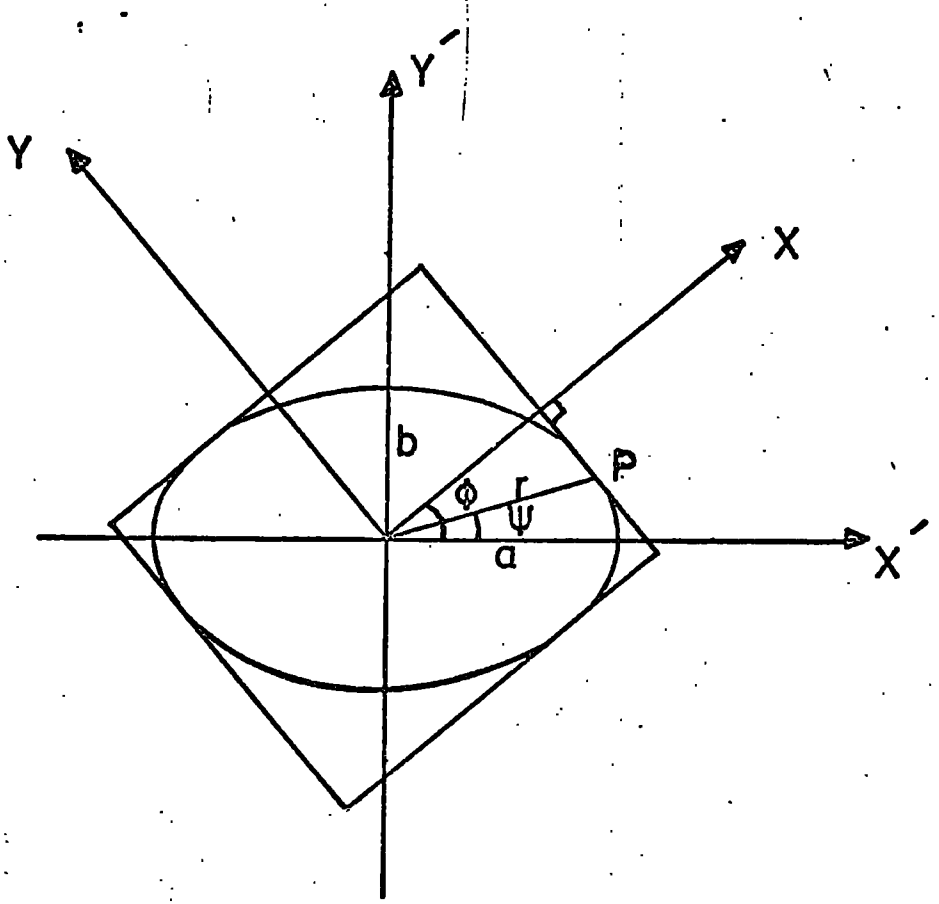

Calculation of angular diameter from x and y extents.

Now let ΔX , ΔY be the COSMOS values of the x and y extents of the image, so

$$\Delta X = 2 r \cos (\phi - \Psi)$$

where r is the distance from the centre to P and Ψ is the angle between the line joining the centre to P and the x′ direction. Then

$$\Delta X = 2 (x' \cos\phi + y' \sin\phi)$$

$$= 2 (a^2 \cos^2\phi + b^2 \sin^2\phi)^{1/2} \qquad (5.3)$$

and similarly

$$\Delta Y = 2 (a^2 \sin^2\phi + b^2 \cos^2\phi)^{1/2} \qquad (5.4)$$

Under the assumption of an elliptical image the COSMOS value of the area

$$A = \pi ab \qquad (5.5)$$

and using equations (5.3), (5.4) and (5.5)

$$\theta \equiv 2a = \left(Z + \frac{2A}{\pi}\right)^{1/2} + \left(Z - \frac{2A}{\pi}\right)^{1/2} \qquad (5.6)$$

where $$Z = \tfrac{1}{4}(\Delta X^2 + \Delta Y^2) \qquad (5.7)$$

Hence, provided $Z > 2A/\pi$, the angular diameter may be calculated directly from the COSMOS ΔX, ΔY and A. If $Z < 2A/\pi$ an elliptical image can not be fitted and the maximum of ΔX

and ΔY is used for θ. This is usually only necessary for very small images where the $8\mu m$ square quantization is important.

5.3 THE OBSERVED ANGULAR DIAMETER DISTRIBUTION

Using the formulae derived in the previous section the angular diameter of each galaxy above the area limit for detection can be obtained.

It is useful to use the function $f(\theta)$, defined to be the number of galaxies with log (angular diameter) in the range $\log \theta - \delta/2$ to $\log \theta + \delta/2$, where δ is a fixed logarithmic bin size, to describe the distribution of angular sizes.

Clearly $f(\theta) \propto \theta n(\theta)$ where $n(\theta)$ is the usual differential count, so for a homogeneous distribution in Euclidean space with no selection effects - and for the large θ end of the curve for any distribution - $f(\theta) \propto \theta^{-3}$ i.e. the log f - log θ plot will have a slope of -3.

A differential plot, either $f(\theta)$ or $n(\theta)$ is much more easily interpreted than the integral plots $N(>\theta)$ which have been used by some authors, as fluctuations in the differential counts, whether real or statistical in origin can give rise to a change in slope in the $N(>\theta)$ plot which may be interpreted as a local density enhancement. This was the interpretation put upon the

form of the integral plot for the eye measured region of plate J149 (see section 4.7) by Dodd et al (1975) but Ellis, Fong and Phillipps (1976) showed from the differential plot that there was no significant evidence for this feature.

The observed counts for the COSMOS measured plates R1049, J149, J1920 and J1921 are shown in figures 5.2, 5.3, 5.4 and 5.5 (in all cases a bin size $\delta = 0.5$ has been used, the counts also being normalized to those for 1 square degree).

5.4 PRINCIPLES OF THE PREDICTION OF ANGULAR DIAMETER COUNTS

Given the central brightness and the profile of the galaxy luminosity distribution, then for any given limiting isophote, it is, in the absence of seeing, a simple matter to determine the isophotal diameter of a galaxy, at any distance and check if it is greater than some value θ. For any particular galaxy type, the shape of the profile is fixed and if it is assumed that parameters of the profile and the central brightness are determined solely by the absolute magnitude of the galaxy, then for any given distance the faintest galaxy (in terms of absolute magnitude) which would have isophotal diameter greater than the value θ can simply be found. This faintest absolute magnitude M, then determines the contribution to the number counts

Figure 5.2

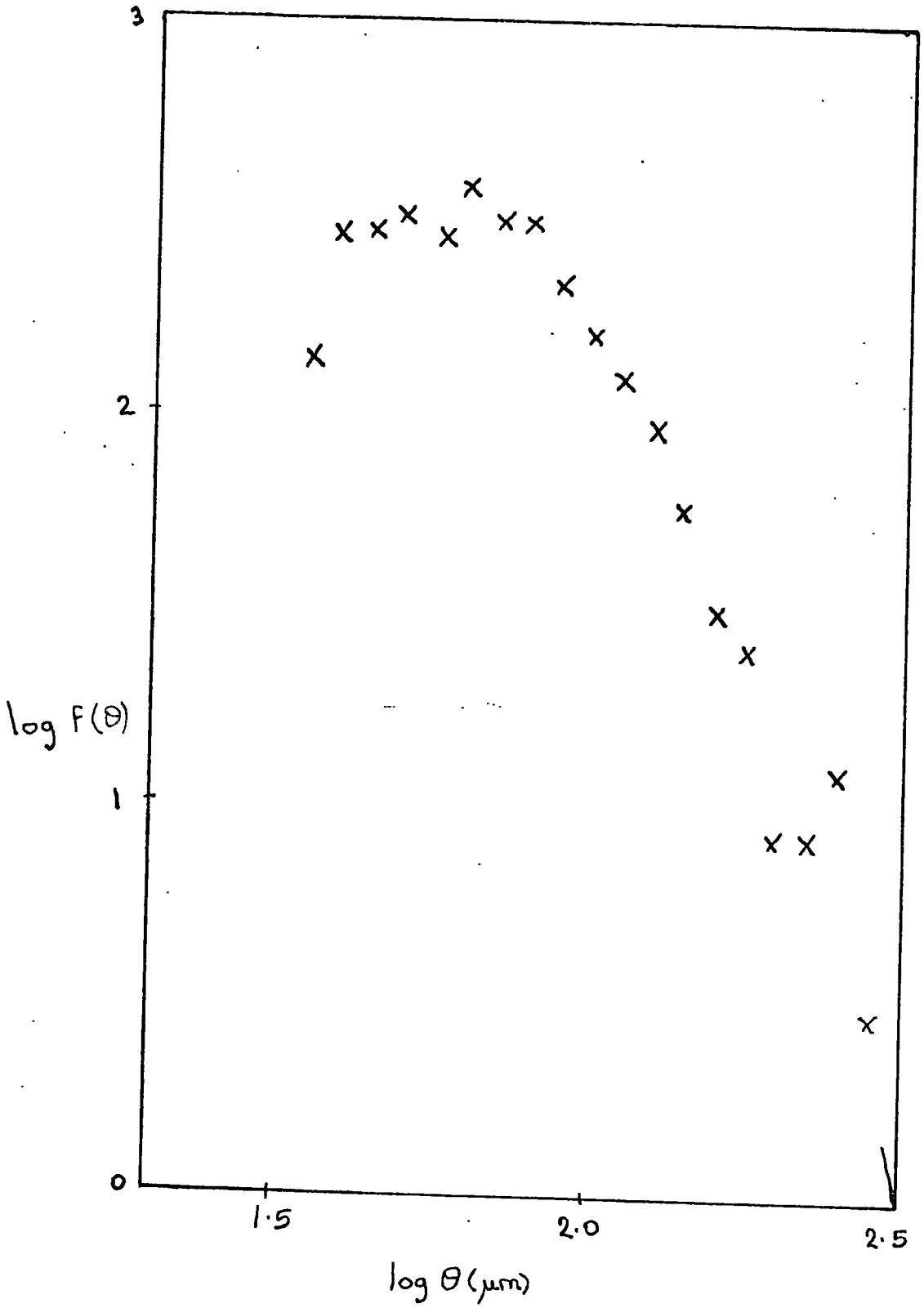

Differential number count F(θ) for R sample.

Figure 5.3

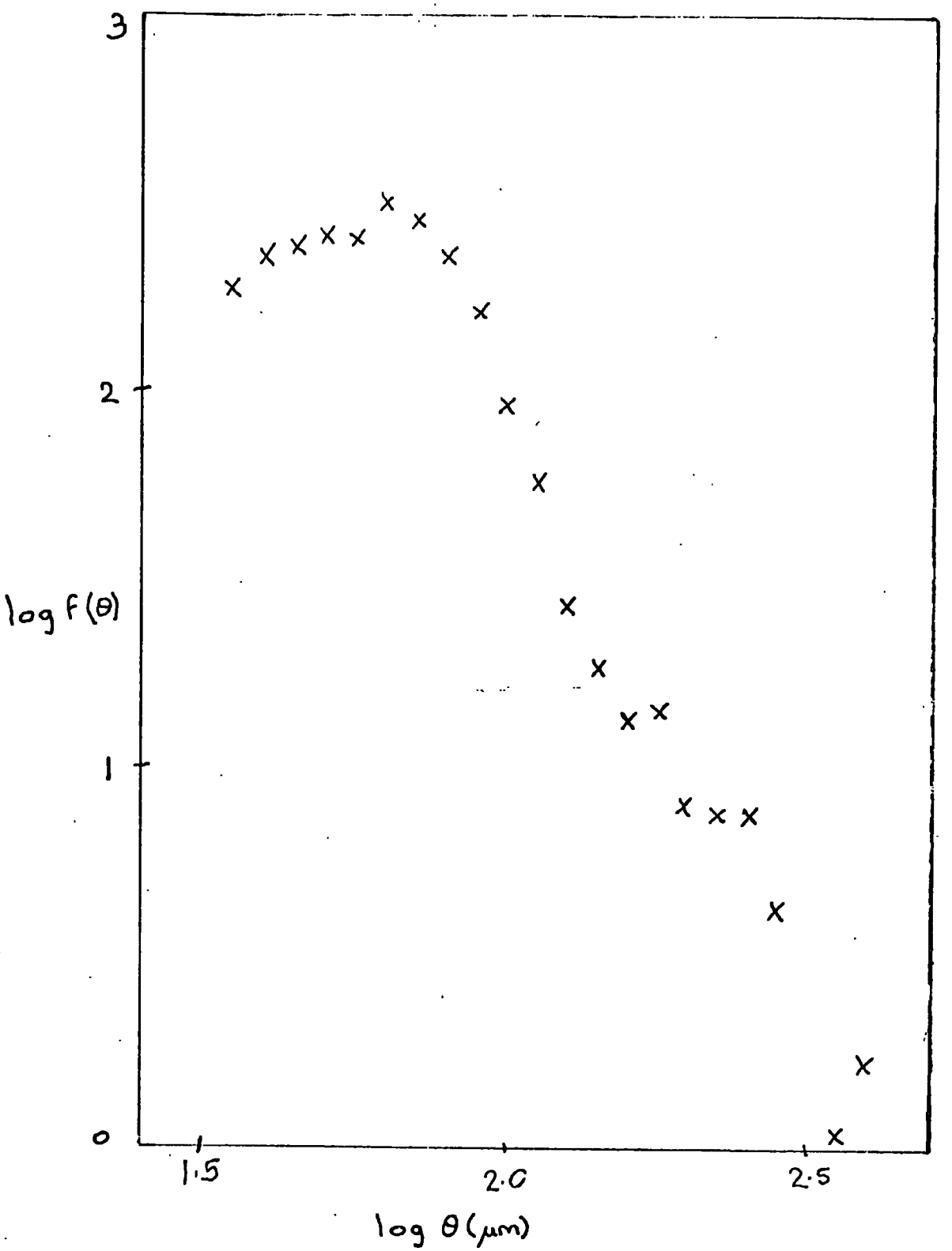

Differential number count f(Θ) for J sample.

Figure 5.4

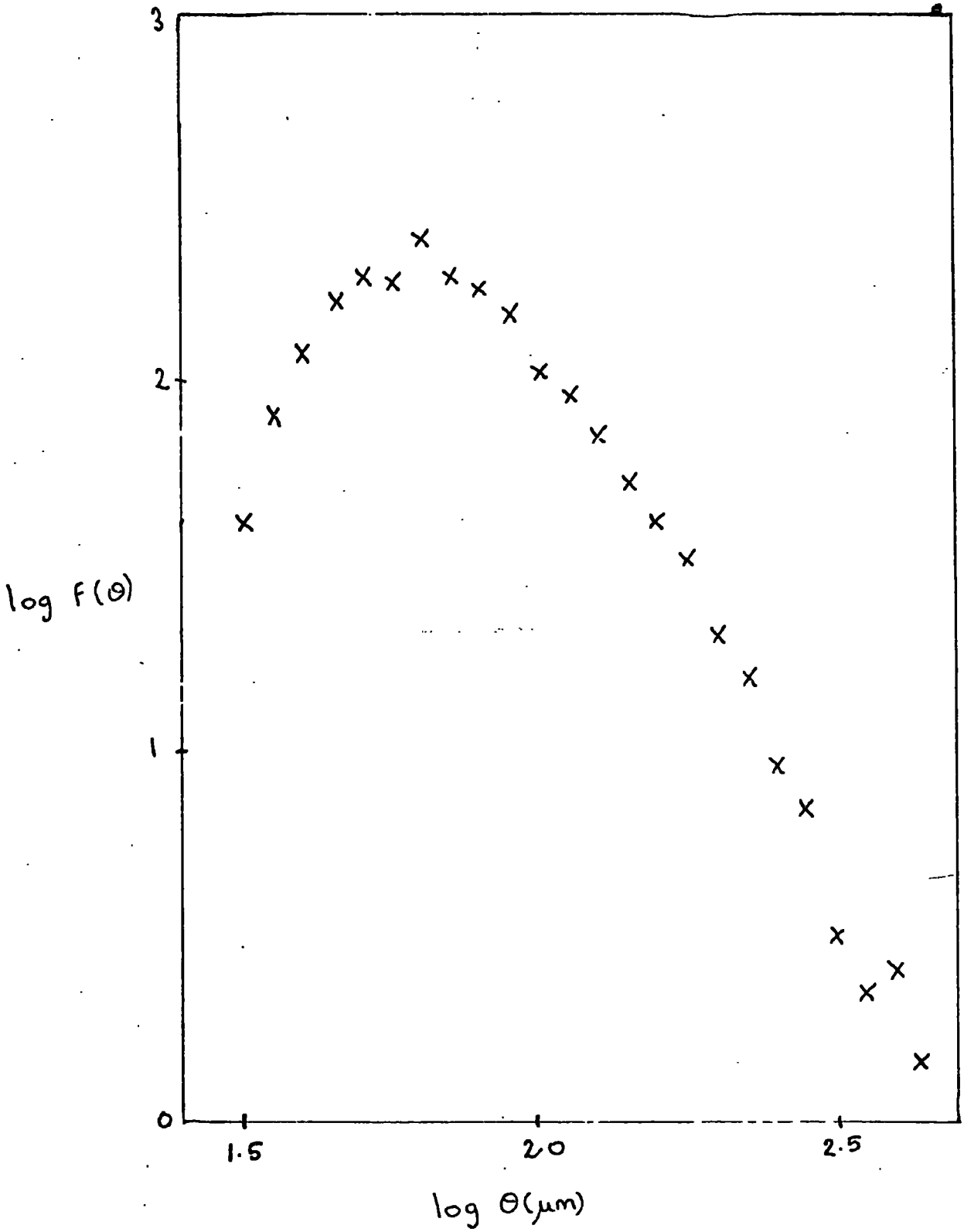

Differential number count f(θ) for 1920 sample.

Figure 5.5

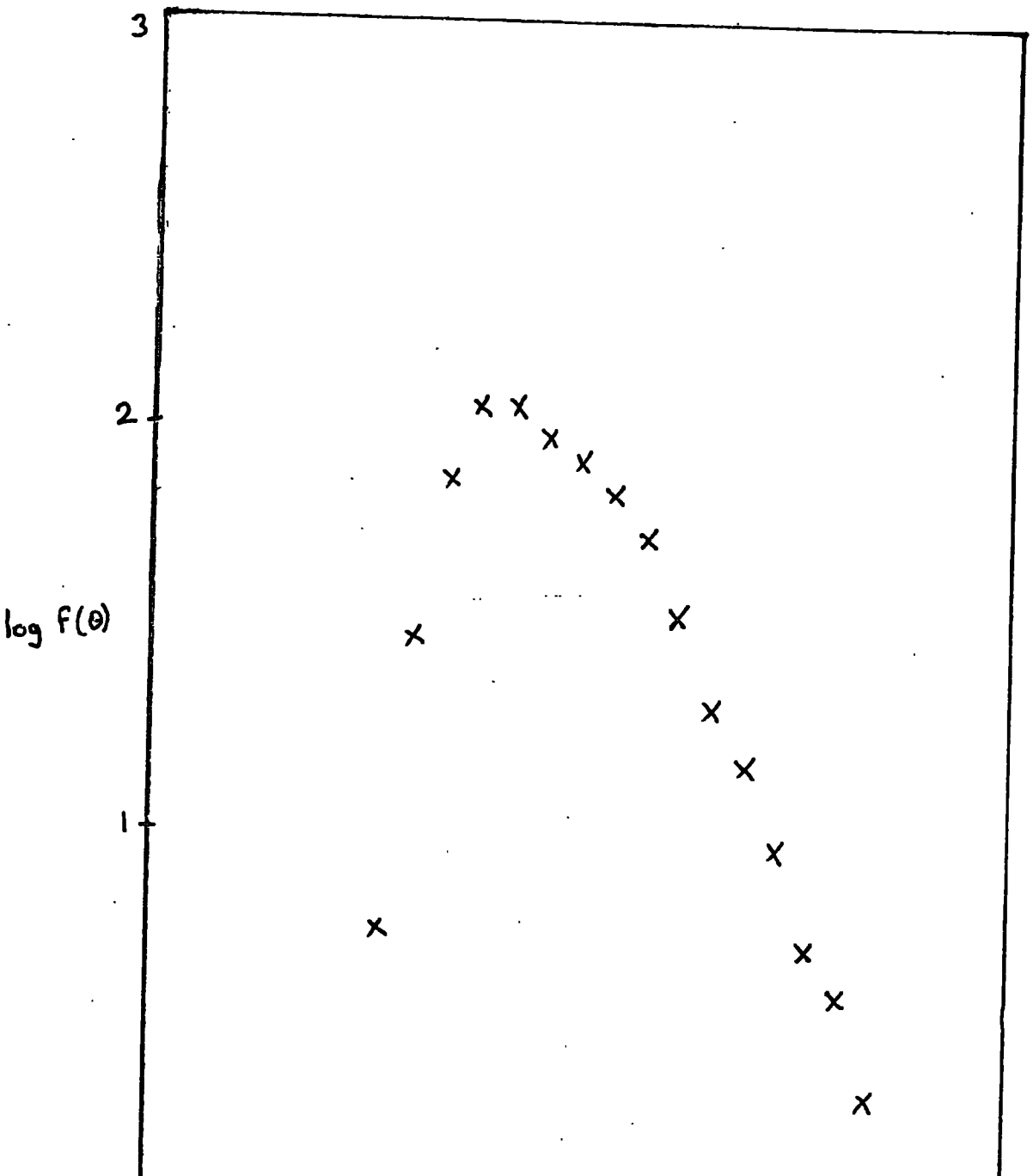

Differential number count F(θ) for 1921 sample.

from this type of galaxy, simply through the fraction of galaxies brighter than M.

When seeing needs to be taken into account, as is the case here, because of the very small images included in the sample, the calculation of the isophotal diameters is somewhat complicated as a convolved profile must be used, but in principle the same method still applies.

5.5 DETAILED MODEL AND PROCEDURE FOR CALCULATION OF ANGULAR DIAMETER COUNTS

Before any calculations can be made on the angular diameter counts, it is necessary to adopt a model for each type of galaxy.

Six different types of galaxy were used here, ellipticals, SO's, Sab's, Sbc's, Scd's and Sdm's in proportions similar to those estimated by Oemler from the data of Schechter (1976) and Christensen (1975) and given by Tinsley (1977). They are generally derived basically from de Vaucouleurs and de Vaucouleurs Reference catalogue (1964).

For the ellipticals a profile of the form (Abell and Mihalas 1966)

$$\begin{aligned} I(r) &= I_o\left(\frac{r}{a} + 1\right)^{-2} \qquad r \leq 21{\cdot}4\ a \\ &= 22{\cdot}4\ I_o\left(\frac{r}{a} + 1\right)^{-3} \qquad r > 21{\cdot}4\ a \end{aligned} \tag{5.8}$$

was used.

The radius parameter a, is apparently well correlated with absolute magnitude (Holmberg 1969) and Gudehus (1973) gives the relationship as

$$a = \text{dex}\,(-0{\cdot}167\, M_B - 6{\cdot}813) \qquad (5.9)$$

for a in Mpc. It follows, by integrating over the whole image that the central intensity, expressed in magnitudes, is

$$\mu_o = 0{\cdot}167\, M_B + 20{\cdot}93 \qquad (5.10)$$

Hence, knowing M, a and μ_o may be determined.

For all other types, an expo nential profile (Freeman 1970)

$$I(r) = I_o \exp(-r/a) \qquad (5.11)$$

was taken.

According to Freeman the central intensity of all spirals, that is the intensity of the disc extrapolated to the centre (not the actual central brightness as this may be different because of the nucleus), is constant, corresponding to $21^m{\cdot}65$ arc sec^{-2} in the blue. (This is supported by the work of Simkin 1975).

Again by integrating over the whole image this implies

$$a = \text{dex}\,(-0{\cdot}2\, M_B - 6{\cdot}386) \qquad (5.12)$$

with a in Mpc. So again M determines μ_o (this time a constant) and a. It should be noted that the profile does not take into account any nucleus or spiral arms which may be present, but the effects of these will be small in most cases and the seeing will tend to blur them into the disc. Recent photometry (e.g. Benedict 1976) has shown that the nuclei and arms usually contribute only a few per cent of the total luminosity, though some spirals like NGC4459 have very prominent nuclei (Liller 1960). Freeman noted two types of profiles, one in which the intensity rises above the exponential near the centre, the other where there is a region in which the intensity is lower than for the extrapolated exponential form. The existence of nuclear regions in SO galaxies (Van Houten 1961, Johnson 1961) has also been ignored. Although the bar appears prominent in barred galaxies there is actually little luminosity in the bar (de Vaucouleurs 1963) and this effect has also been neglected. Some dwarf irregulars have lower surface brightnesses, but even many of these appear to follow Freeman's law, and in any case they are too faint to be important except in the near neighbourhood of the Galaxy.

The observed profile for a galaxy at a redshift z, will then be

$$J(\Psi) = \frac{I(\Psi D_A)}{(1+z)^4\, 10^{0.4k(z)}} \qquad (5.13)$$

where D_A is the angular diameter distance. The factor $(1+z)^4$ arises from the change in surface brightness with redshift; the surface area subtended varies as D_A^{-2} while the intensity varies as $D_L^{-2} = D_A^{-2}(1+z)^{-4}$, D_L being the luminosity distance(see e.g. Weinberg 1972, e.q. 14.4.28 and appendix A). The factor $10^{0.4k(z)}$ is the change in intensity due to the k-correction, k(z), which is expressed in magnitudes.

These profiles must then be convolved with a two dimensional Gaussian seeing

$$G(\psi) = \exp(-\psi^2/2\sigma^2)/2\pi\sigma^{-2} \qquad (5.14)$$

where σ is the seeing parameter (see below). This gives

$$I(\psi) = \frac{I_o}{\sigma^2\pi(1+z)^4\,10^{0.4k(z)}}\left[\int_0^{21.4a/D_A}\int_0^{\pi}\left(1+\frac{r\,D_A}{a}\right)^{-2}\exp(-(r^2+\psi^2-2r\psi\cos\phi)/2\sigma^2)\,r\,dr\,d\phi\right.$$
$$\left.+\int_{21.4a/D_A}^{\infty}\int_0^{\pi}22.4\left(1+\frac{r\,D_A}{a}\right)^{-3}\exp(-(r^2+\psi^2-2r\psi\cos\phi)/2\sigma^2)\,r\,dr\,d\phi\right] \qquad (5.15)$$

This may be re-written

$$I(\psi) = \frac{I_o}{\pi(1+z)^4\,10^{0.4k(z)}}\left[\int_0^{21.4Y}\int_0^{\pi}\left(1+\frac{u}{Y}\right)^{-2}\exp(-(u^2+X^2-2uX\cos\phi)/2)\,u\,du\,d\phi\right.$$
$$\left.+\int_{21.4Y}^{\infty}\int_0^{\pi}22.4\left(1+\frac{u}{Y}\right)^{-3}\exp(-(u^2+X^2-2uX\cos\phi)/2)\,u\,du\,d\phi\right] \qquad (5.16)$$

or

$$I(X) = \frac{I_o}{(1+z)^4\, 10^{0.4k}}\, F_E(X,Y) \qquad (5.17)$$

where

$$X = \frac{\nu}{\sigma} \quad , \quad Y = \frac{a}{\sigma D_A} \qquad (5.18)$$

Similarly for spirals

$$I(\nu) = \frac{I_o}{\pi(1+z)^4\, 10^{0.4k(z)}} \int_0^{\infty}\int_0^{\pi} \exp(-u/Y)\, \exp(-(u^2 + X^2 - 2uX\cos\phi)/2)u\, du\, d\phi \qquad (5.19)$$

or

$$I(X) = \frac{I_o}{(1+z)^4\, 10^{0.4k}}\, F_S(X,Y) \qquad (5.20)$$

with X and Y as before.

It should be noted that these profiles assume that the galaxies are exactly face on to the observer. In all cases the calculations neglect the possible effects of inclination of the image, which are in any case very uncertain. Holmberg (1975) states that the effect of inclination on diameters is at most a few per cent and he neglects it in his work.

The seeing parameter σ in equation (5.14) defines the width of the Gaussian seeing, but is not the usual astronomical meaning of 'seeing'. This is normally taken to be the radius s which contains 90% of the light from a star, and is given by

$$s = 2{\cdot}146\ \sigma \qquad (5.21)$$

With these preliminaries, the calculation of $f(\theta)$ for a given seeing and limiting isophote may now be undertaken. Choose a particular value of ψ and consider first just one galaxy type, which has absolute magnitudes in the range $M^* - R$ to $M^* + R$. If the range of z over which galaxies will be visible is divided into a convenient number of equal bins Δz, the comoving volume corresponding to the i th bin is

$$\Delta V_i = D_A^2(z_i)\, c\, H_o^{-1}\, (1 + z_i)(2q_o z_i + 1)^{-1/2} \Delta z\, \Delta\Omega \qquad (5.22)$$

where $\Delta\Omega$ is the solid angle subtended, taken in all calculations to be one square degree, and z_i is taken to be the centre of the bin. Although ΔV_i strictly depends on q_o, the results are insensative to q_o and a value 0·02 was used (Shapiro 1971). Brown and Tinsley (1974) noted that number counts in general were not very dependent on q_o.

Now for this z_i, take the faintest galaxy of the type being considered, i.e. the faint end cut-off in the luminosity function, $M^* + R$. Given this magnitude, μ_o and a may be determined and

$$\mu(\psi) = \mu_o - 10 \log(1 + z_i) + k(z_i) - 2{\cdot}5 \log F(X,Y) \qquad (5.23)$$

calculated.

If $\mu(\psi) < \mu_{lim}$, the limiting isophote, then the galaxy is above the threshold an angle ψ from the centre of the image and hence has isophotal angular diameter greater than $2\psi = \theta$. If $\mu(\psi) > \mu_{lim}$, the galaxy is

smaller than θ, so the calculation is repeated for an absolute magnitude $M^{*} + R - \Delta M$, where ΔM is a small increment in magnitude, and so on up the luminosity function until a magnitude is reached for which $\mu(\psi)$ is less than μ_{lim}. Let this magnitude be M_i, then the number of galaxies larger than θ in the volume ΔV_i is

$$\Delta V_i \rho \Phi(M_i)$$

where ρ is the space density of the type of galaxy being considered and $\Phi(M_i)$ is the fraction of galaxies of this type brighter than M_i.

Summing over all the bins in z gives the total number of galaxies of this type with angular diameter greater than θ, and then summing over types gives the total number of galaxies larger than θ.

Repeating for various values of θ, the differential numbers can then be found and $f(\theta)$ calculated.

In the determination of $\mu(\psi)$ from equation (5.23), k-corrections are required for the different morphological types. These were taken from Pence (1976), quadratic fits to the data being considered sufficiently accurate.

As pointed out by Sandage (1961) the k-corrections for the R band are much smaller than for the B and V bands thus making the R band more suitable for observing very distant objects. This is borne out by the fact that the R plate used here, of only one hour exposure and not sky limited, has a density of galaxy images 30% higher

than the two hour exposure sky limited plate J149, (the J band is almost the same as the usual B band).

The energy fluxes used by Pence in the ultraviolet are in some doubt as they are from data collected by the OAO-2 satellite (Code et al 1972). This data is in conflict with that from the TD1 satellite (Carnochan et al 1975) also that from Skylab (Deharveng et al 1976), and Ellis, Fong and Phillipps (1977a) have noted that if the TD1 data is correct, the k-corrections for the U band will be small, making the U band suitable for observing very distant objects. The discrepancy however will not effect the k-corrections for the B (or J) band except at large redshifts $\gtrsim 0{\cdot}7$.

Also, to calculate $\Phi(M_i)$ a luminosity function is required, and that of Schechter (1976) was chosen. This has the differential form

$$N(M) = \rho\, F(M - M^*) \qquad M^* + R > M > M^* - R \qquad (5.24)$$

where ρ is the number density per Mpc^3, R defines the range of the luminosity function and the function F is given by

$$F(X) = \frac{0{\cdot}92}{\Gamma(1-\alpha,\beta)} \exp(-\exp(-0{\cdot}92\,X) + 0{\cdot}92\,(\alpha - 1)\,X) \qquad (5.25)$$

where Γ is an incomplete gamma function and α and β are parameters which vary between types. The values of ρ, α, β and M^* for each type used here are similar to those given

by Tinsley (1977) from Oemler's estimates. They are summarised along with the k-corrections and colours in table 5.1. Note that the function used is an overall luminosity function, no attempt has been made to use separate field and cluster luminosity functions (e.g. Icke 1973, Press and Schechter 1974, Oemler 1974, Turner and Gott 1976).

The B-R colours are required when $f(\theta)$ is calculated for the R plate, the luminosity function is simply translated by the value of B-R for each type and surface brightnesses are similarly shifted. The profiles are assumed to be the same in all colours (de Vaucouleurs 1961, Holmberg 1975) that is, there is no change in B-R across the galaxy. This appears to be supported by the work of Thuan and Oke (1976) and Benedict (1976), though Shapley (1972) states that spiral nuclei are redder than their discs, and Holmberg states that spiral arms are bluer.

A further effect which was taken into account in the calculations was luminosity evolution of the galaxies which could be extremely important for any analysis which depends on the distribution of redshifts in a sample (Tinsley 1976b). This is included in exactly the same way as the k-corrections, and the $k(z)$ in equations (5.13) and (5.23) may be considered as a composite of the actual k-corrections and the evolution. Three representative models, from a series derived by Tinsley (1977), were used, differing only in the redshift of the epoch of galaxy

Table 5.1

Properties of Galaxies (H_o = 50 kms^{-1}/Mpc)

Types	Luminosity Function Parameters				Colours
	ρ	α	β	M_B^*	B - R
E	0·0013	1·25	0·025	-20·90	1·85
Sab	0·0020	1·25	0·025	-21·00	1·65
Sbc	0·0020	1·25	0·025	-21·15	1·30
Scd	0·0025	2·00	0·025	-20·50	1·16
Sdm	0·0025	2·00	0·025	-20·55	1·05
S0	0·0027	1·25	0·025	-20·90	1·85

Types	Evolutionary Corrections $EC = Az + Bz^2$				k-corrections $K = Cz + Dz^2$			
	R		J		R		J	
	A	B	A	B	C	D	C	D
E	-1·46	-0·12	-1·89	- 1·02	1 09	1·28	5·00	-1·40
Sab	-3·98	1·42	-4·38	1·23	1·02	0·92	4·00	-1·50
Sbc	-3·50	1·67	-3·80	1·44	-0·03	1·23	3·20	-1·40
Scd	-3·18	1·15	-3·54	1·02	-0·21	1·11	3·00	-2·00
Sdm	-3·60	1·88	-3·59	1·61	-0·63	1·03	2·00	-1·50
S0	-1·46	-0·12	-1·89	-1·02	1·09	1·28	5·00	-1·40

Notes:
1. Luminosity function parameters from Tinsley (1977)
2. B-R colours computed by Tinsley (1977)
3. Luminosity evolution, EC, for a 'conservative' model by Tinsley (1976a)
4. k-corrections from Pence (1976).

formation; a conservative model with $z_f = 6{\cdot}2$, a liberal model with $z_f = 3{\cdot}5$ and a radical model with $z_f = 1{\cdot}6$ (Tinsley 1976a). The parameters for the conservative model are included in table 5.1. The models take into account both the evolution of total luminosity and of the shape of the spectrum, i.e. the colour indices. Smoothed (quadratic) fits have been taken, which should be good enough in the range of interest $z \leq 0{\cdot}7$.

5.6 RESULTS OF ANGULAR DIAMETER CALCULATIONS

Using the method of the previous section the effects on the number counts of the limiting isophote, seeing, luminosity evolution and the faint end cut-off of the luminosity function can be investigated.

Tinsley (1977) suggests $R = 4$ for the range of the luminosity function, giving a cut-off around $-17^{m}{\cdot}0$, but Christensen (1975) has presented evidence based on a few nearby galaxies, for the distribution increasing right up to $-14^{m}{\cdot}0$. The results of Arakelyan and Kalloglyan (1970) also indicates this. The effect of changing $R = 4$ to $R = 7$, i.e. the inclusion of a large number of faint galaxies, is illustrated in figure 5.6, for reasonable threshold and seeing values. It can be seen that the changes are small, and in fact the actual difference is likely to be less than that shown as the

Figure 5.6

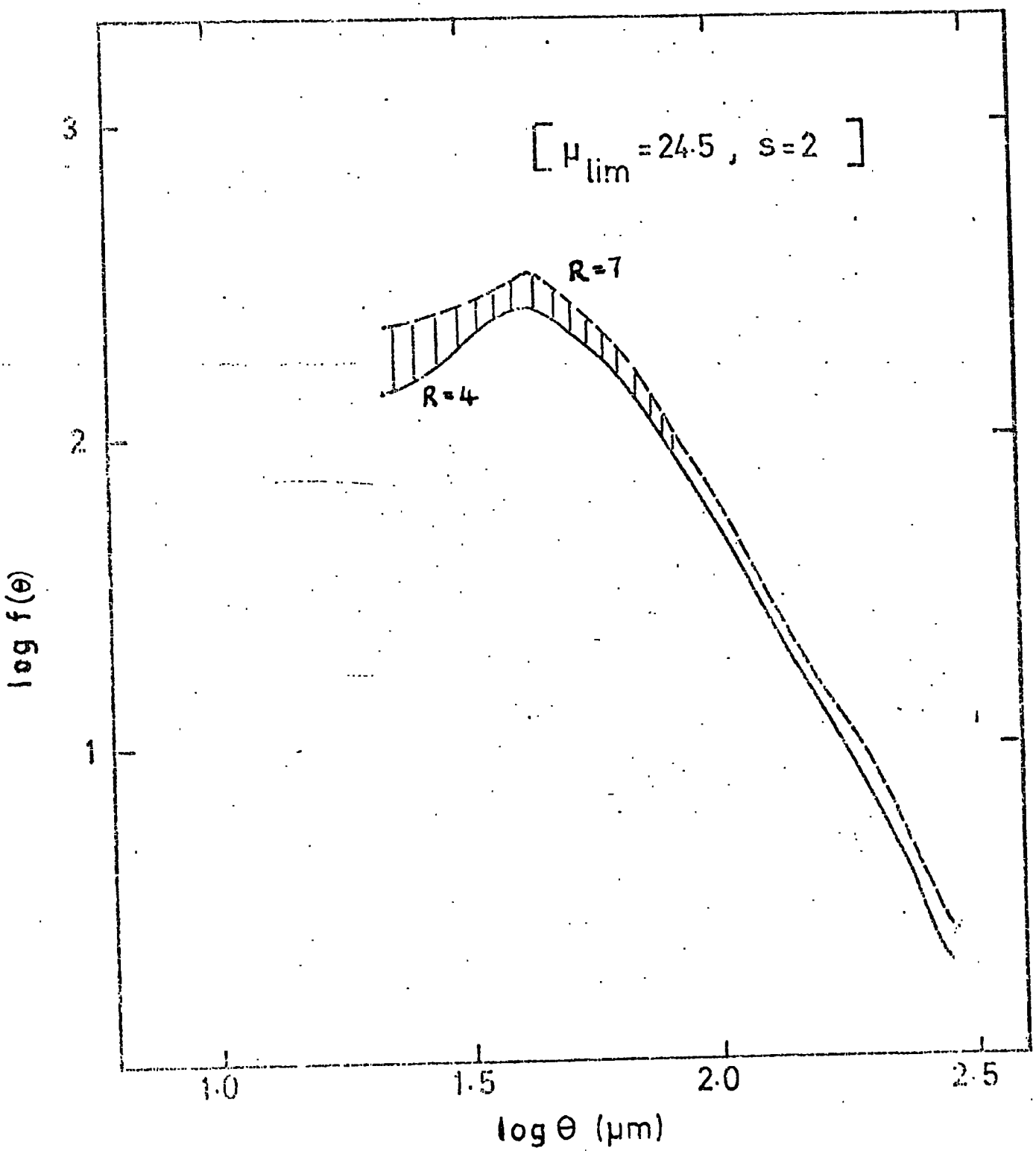

Expected differential number count $f(\theta)$ for J plate with μ_{lim} and s as shown and different luminosity function ranges as indicated

dwarf galaxies probably have lower surface brightnesses than the calculations assume (Abell 1977 private communication). For all subsequent calculations R will be assumed to be 4.

The effect of using the different models for the luminosity evolution are shown in figure 5.7, for a fixed threshold and seeing. The evolution brightens the distant galaxies, hence making their isophotal diameters larger. Also the more rapid the evolution, the greater is the increase in slope of the large θ end, due to the cancelling of the effect of k-corrections. The competition between the k-corrections and the evolution determines whether the apparent size drops off faster or slower than the inverse of the co-ordinate distance and thus whether the slope at large θ is above or below -3.

For illustration, figure 5.8 shows the combined k-corrections and evolutionary corrections for the cases of no evolution and conservative evolution.

Figure 5.9 shows the effect of altering the limiting isophote. Obviously the galaxies appear larger the lower the limit of detection and larger numbers are seen because less galaxies are lost completely below the threshold. Note that the slope for large θ and the point of turnaround (i.e. the maximum) are little affected by the change in isophote.

Figure 5.10 shows the effects of changing the seeing. The numbers at large θ are initially increased

Figure 5.7

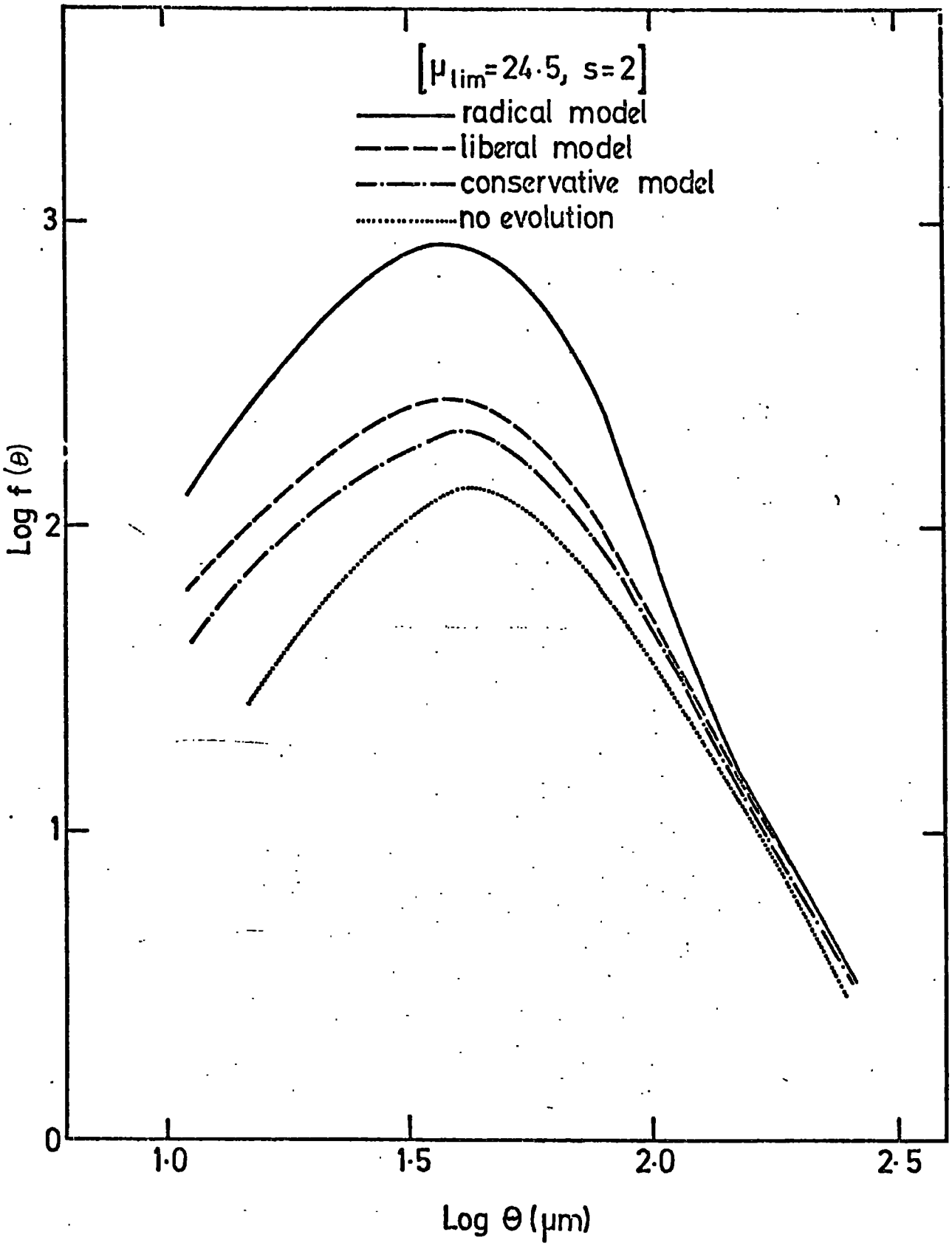

Expected differential count $f(\theta)$ for J plate with μ_{lim} and s as shown and various galaxy evolution models as indicated.

Figure 5.8

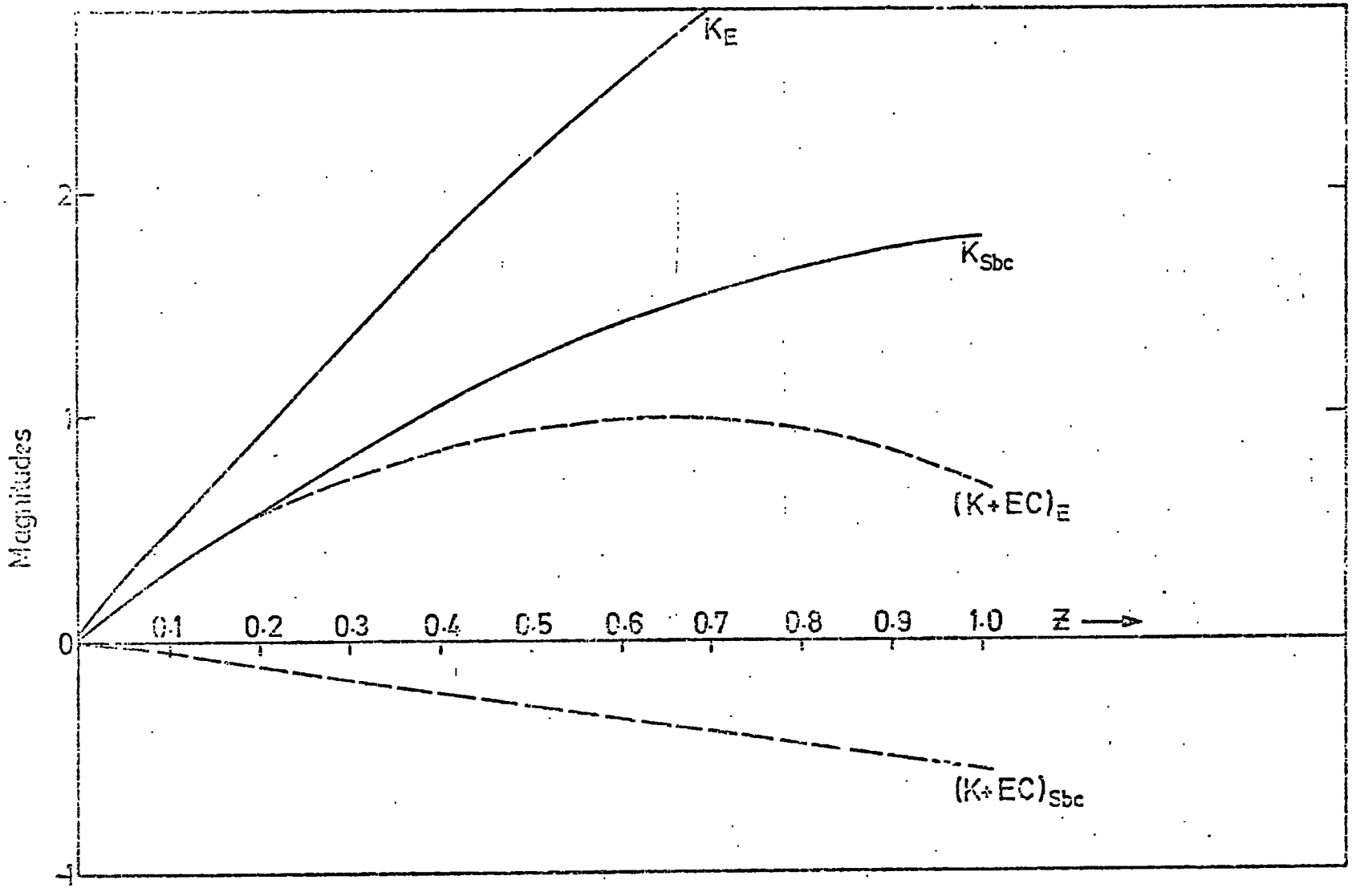

Evolutionary corrections and k-corrections for E and Sbc galaxies.

Figure 5.9

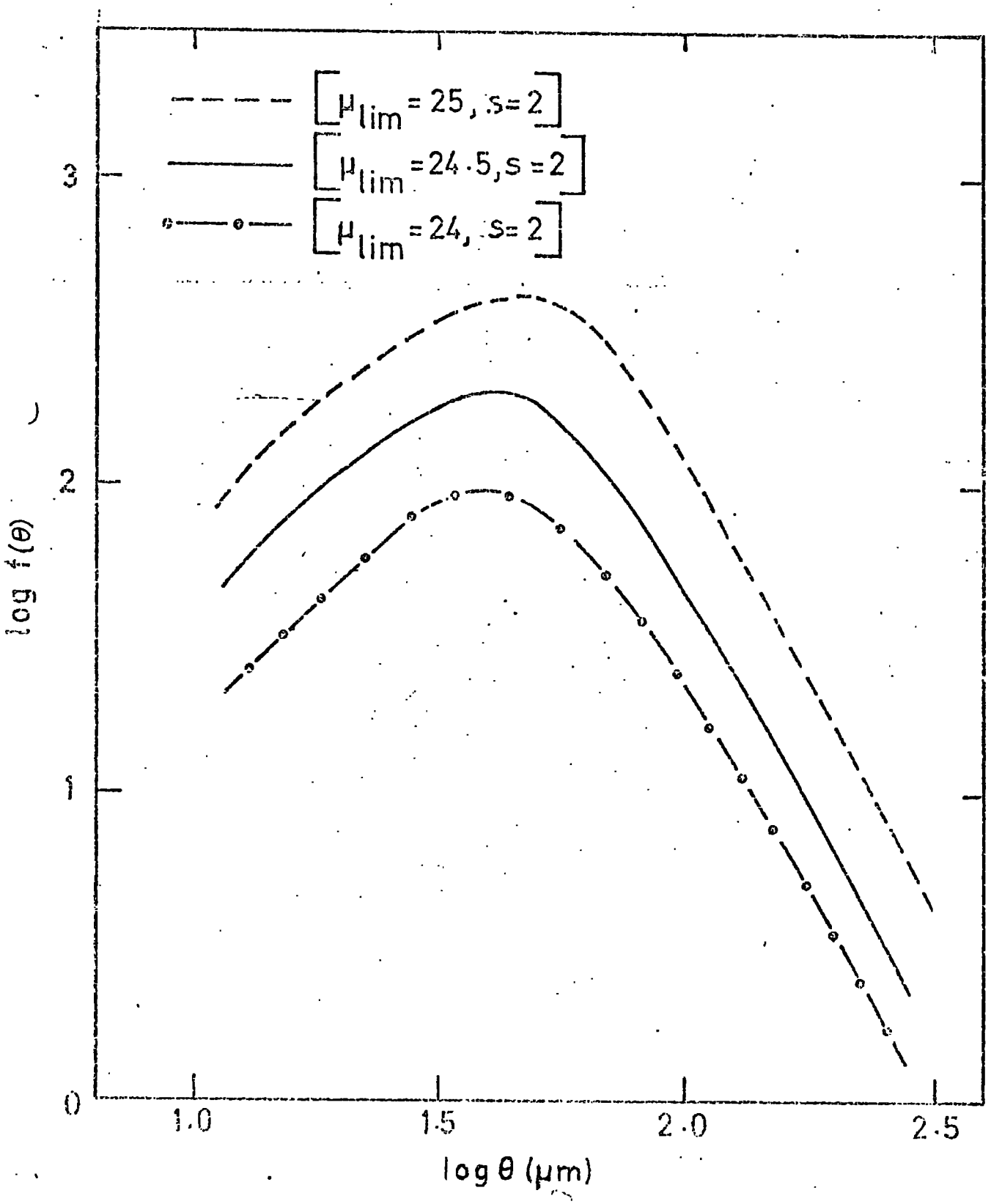

Expected differential count $f(\theta)$ for J plate with S as shown and various values of μ_{lim} as indicated.

Figure 5.10

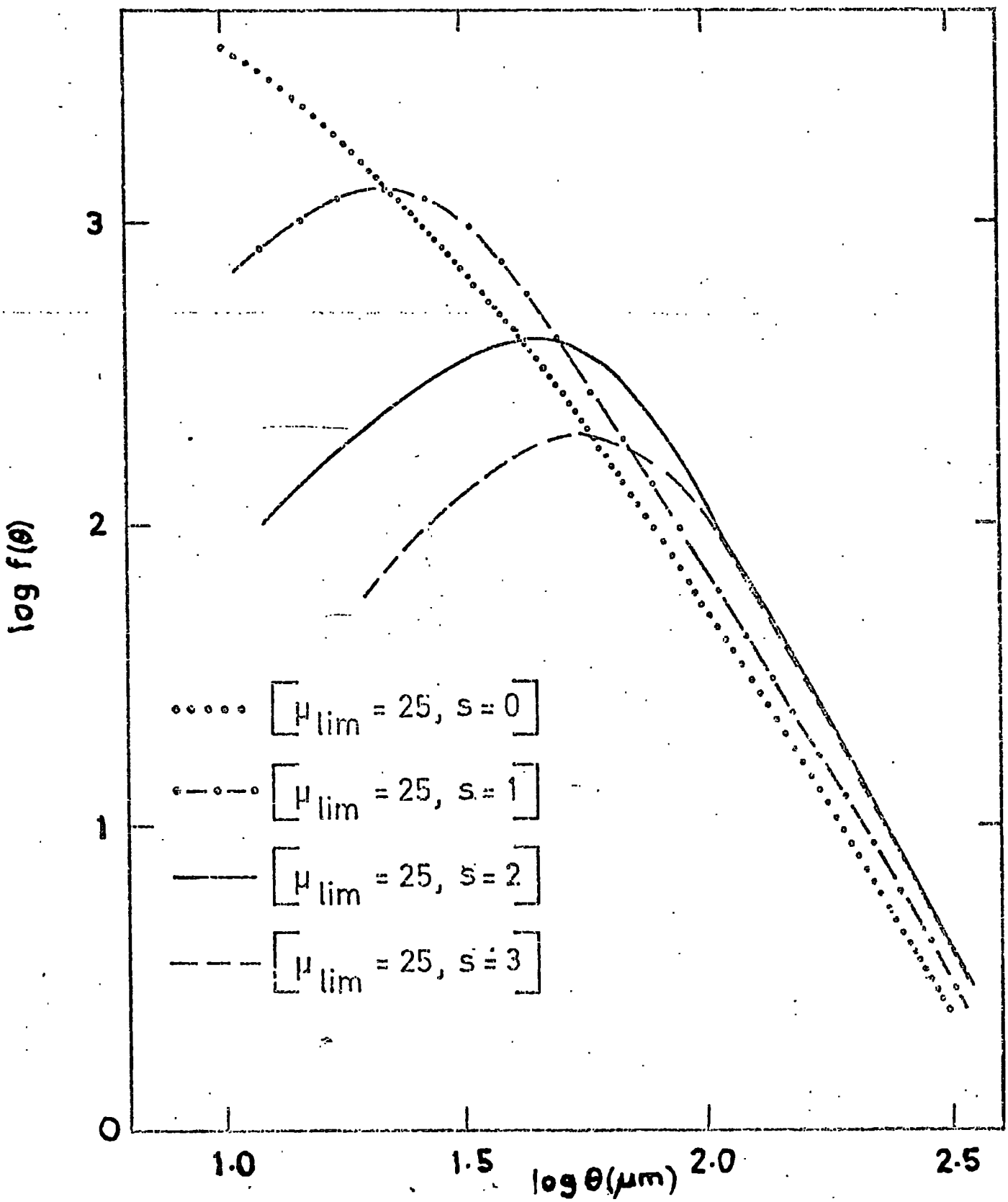

Expected differential count $F(\theta)$ for J plate with μ_{lim} as shown and various values of s as indicated.

as the seeing increases from zero due to the spreading out of the image, but for s $\gtrsim$ 2 arc sec the numbers tend to be constant. However the important change is in the turnround point which shifts very significantly towards larger θ as the seeing becomes larger, as more and more small images are lost due to being smeared out to low surface brightnesses.

Due to the qualitatively different effects caused by changing the luminosity evolution, seeing or limiting isophote, it is possible to find a best fit for all three parameters when matching to an observed distribution. This is illustrated in figure 5.11 where the solid curve shown superimposed on the observed distribution (filled circles) for R1049 is for conservative evolution, seeing of 2".5 and a limiting isophote of 23.0 R magnitudes per square arc second.

Fits to the observed data on plates J149 and J1920 have also been made and confirm that conservative evolution gives a good match. Values of $24^{m}.75$ per square arc second and 2".5 were taken to fit J149, $25^{m}.25$ per square arc second and 3".5 to fit J1920. In the case of J149, the fit was less good than for the others. This is almost certainly due to the threshold varying over the plate - figure 5.12 shows that the observations are bracketed by the expected results for $\mu_{lim} = 24^{m}.5$ and $\mu_{lim} = 25^{m}.0$ with the same seeing and conservative evolution; $\mu_{lim} = 24^{m}.75$ gives a reasonable compromise.

Figure 5.11

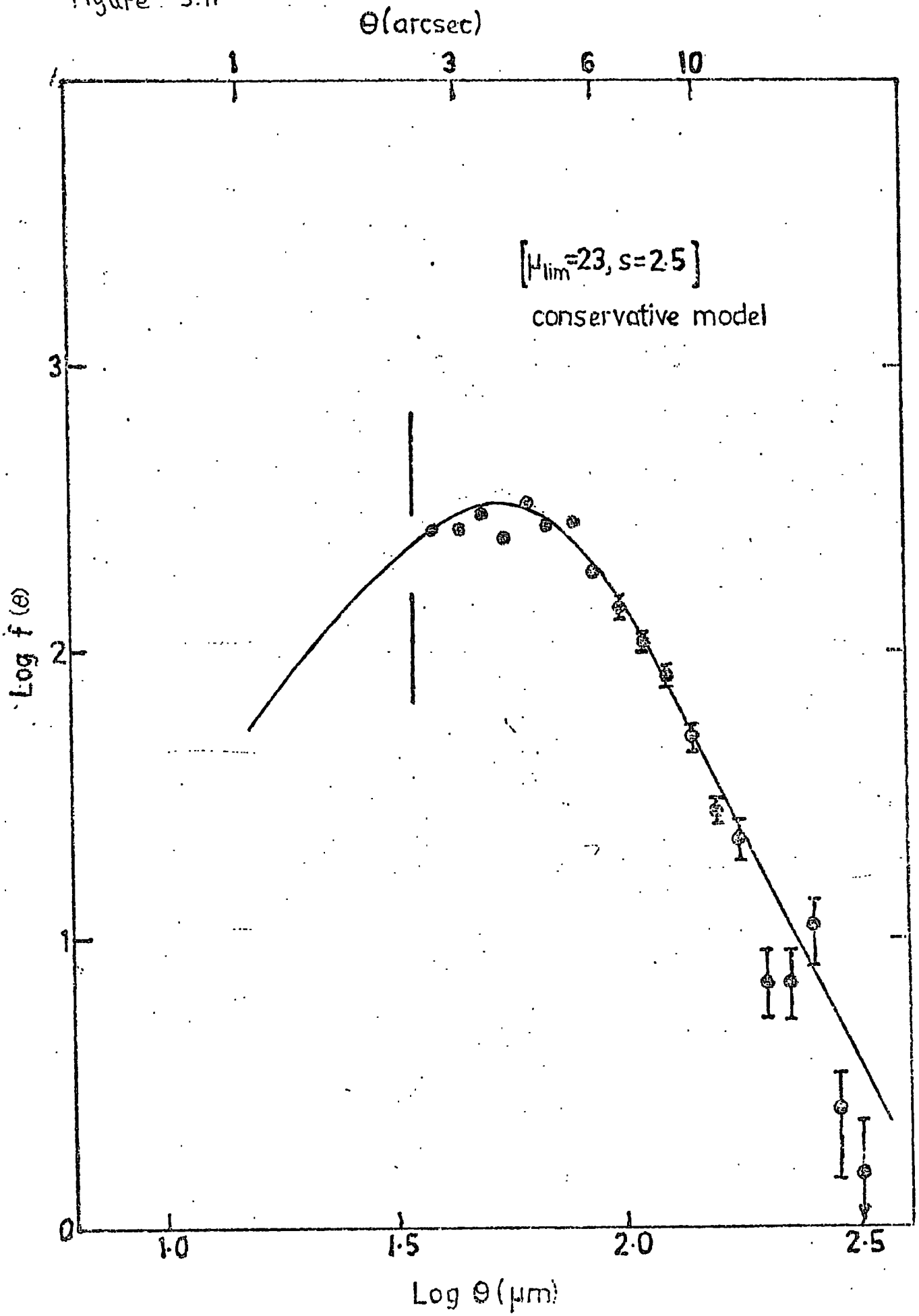

Comparison of the observed $f(\theta)$ for the R sample (•) and a predicted distribution (solid curve) for the parameters indicated.

Figure 5.12.

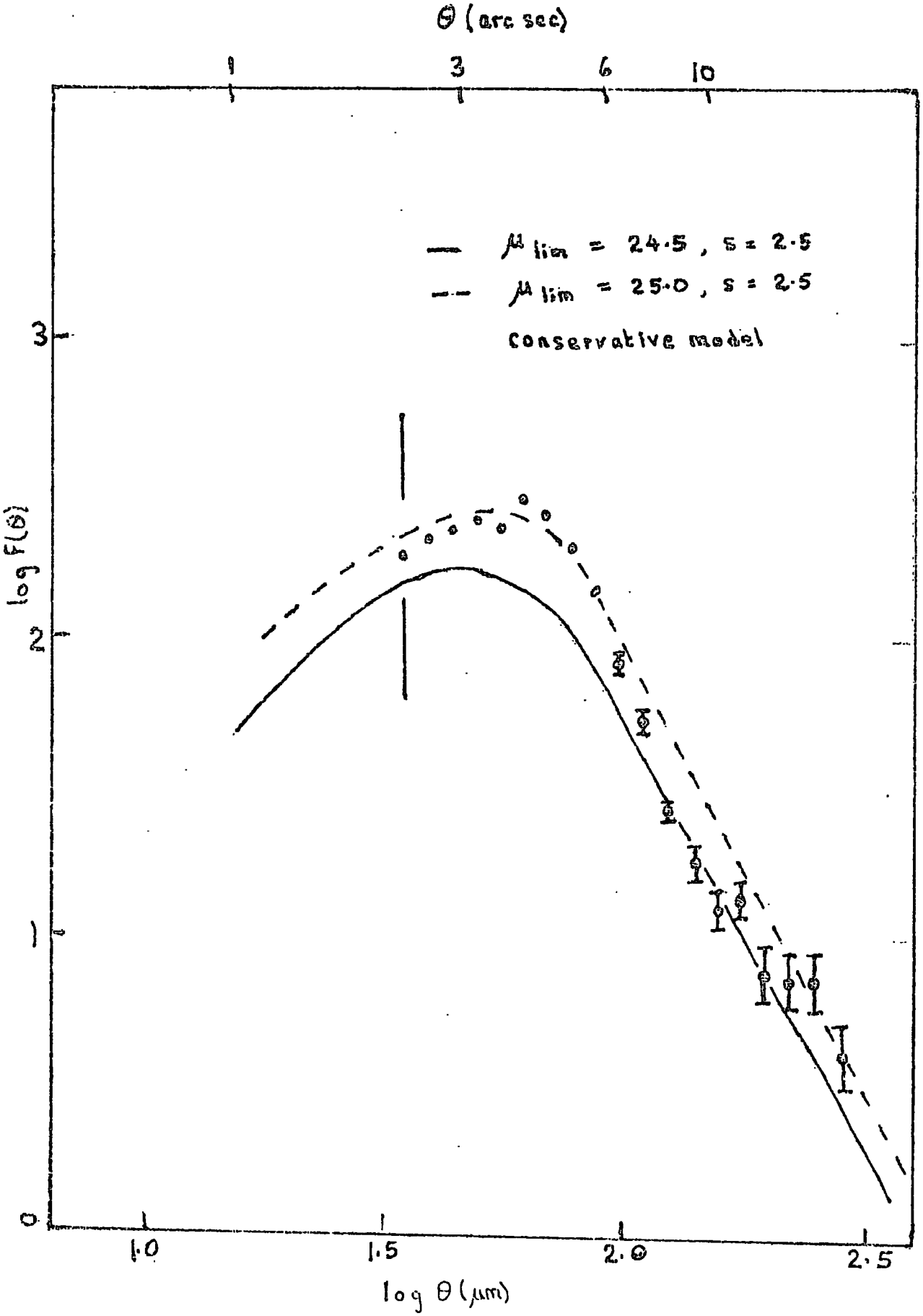

Comparison of the observed F(θ) for the J sample (o) and predicted distributions (curves) for the parameters indicated.

For plate J1921 the seeing was so bad that it could not be estimated directly by this method and the background is similarly uncertain, as extremely poor seeing could move the large θ part of the curve significantly to the right, i.e. to even larger θ. However the fit is probably consistent with a limiting isophote similar to that of J1920; that is ~ 25.25.

It should be remembered here that the seeing discussed in this section is an effective combination of atmospheric seeing and spread in the photographic emulsion, as mentioned earlier, and also of the detection process, since COSMOS surveys with a non-negligible spot size.

For the eye measured region of plate J149, it will be assumed that the selection function is the same as for the COSMOS measured area except that the diameter cut-off is at 3·3 arc sec. Thus we are able to quantify the parameters needed to calculate the distribution in depth of any sample and this calculation is described in the following chapter.

CHAPTER SIX

THE DISTRIBUTION IN DEPTH AND SCALING

'The four dimensional process of clustering is of course non-observable'.

Jerzy Neyman.

6.1 CALCULATION OF THE DISTRIBUTION IN DEPTH

As pointed out in section 5.1, given the actual galaxies which are present in some area of the sky, the determining factors as to which ones are visible in any particular sample are the limiting isophote and the seeing.

From the results of chapter 5, it can be assumed that these are now known from the angular diameter counts, so given the model of the galaxy population presented in section 5.5 the distribution in depth can be calculated.

Consider, for convenience, just one galaxy type, and divide the range of redshift in which galaxies are expected to be visible into a number of equal bins, which have corresponding comoving volumes ΔV_i (cf. section 5.5 equation 5.22) and for each bin in turn the number of galaxies larger than the cut-off for the sample being considered can be found.

The calculations to find the faintest absolute magnitude M_i which would give an image larger than the cut-off for the sample are made in exactly the same way as in the calculation of $f(\theta)$, and the number of galaxies in ΔV_i that will be included in the sample is given simply by

$$\Delta n(z_i) = \Phi(M_i)\Delta V_i \rho$$

where $\Phi(M_i)$ is the fraction of galaxies of the type considered which are brighter than M_i and ρ is the (constant) comoving density of that type of galaxy.

Summing over all types gives the total number of galaxies in ΔV_i, ΔN_i. Then the selection function $\phi(z_i)$, i.e. the fraction of galaxies at z_i included in the sample, is given by

$$\phi(z_i) = \frac{\Delta N_i}{\Delta V_i \rho_T}$$

where ρ_T is the total comoving density of galaxies.

The calculated $\phi(z)$ curves for the parameters found to fit plates R1049 and J149 are shown in figure 6.1 and 6.2. The great importance of seeing in the loss of galaxies below the threshold is seen clearly by comparing these with the curves shown in figure 6.3 for the case of no seeing.

Note that all galaxies are visible out to redshifts around 0·08 to 0·10 and $\phi(z)$ subsequently decreases monotonically. For the R plate galaxies are detected with an efficiency better than 10% out to a redshift $z = 0{\cdot}36$, corresponding to a luminosity distance of 2500 Mpc, in the $H_o = 50$ kms^{-1}/Mpc, $q_o = 0{\cdot}02$ model. For plate J149 10% of galaxies are detected out to $z = 0{\cdot}29$ ($D_L = 2000$ Mpc).

The distribution in depth may be further illustrated as the number of galaxies in each redshift range in a solid angle of 1 square degree

$$\Delta N_i = n(z_i)\Delta z = \phi(z_i)\Delta V_i \rho_T \qquad (6.1)$$

Figure 6.1

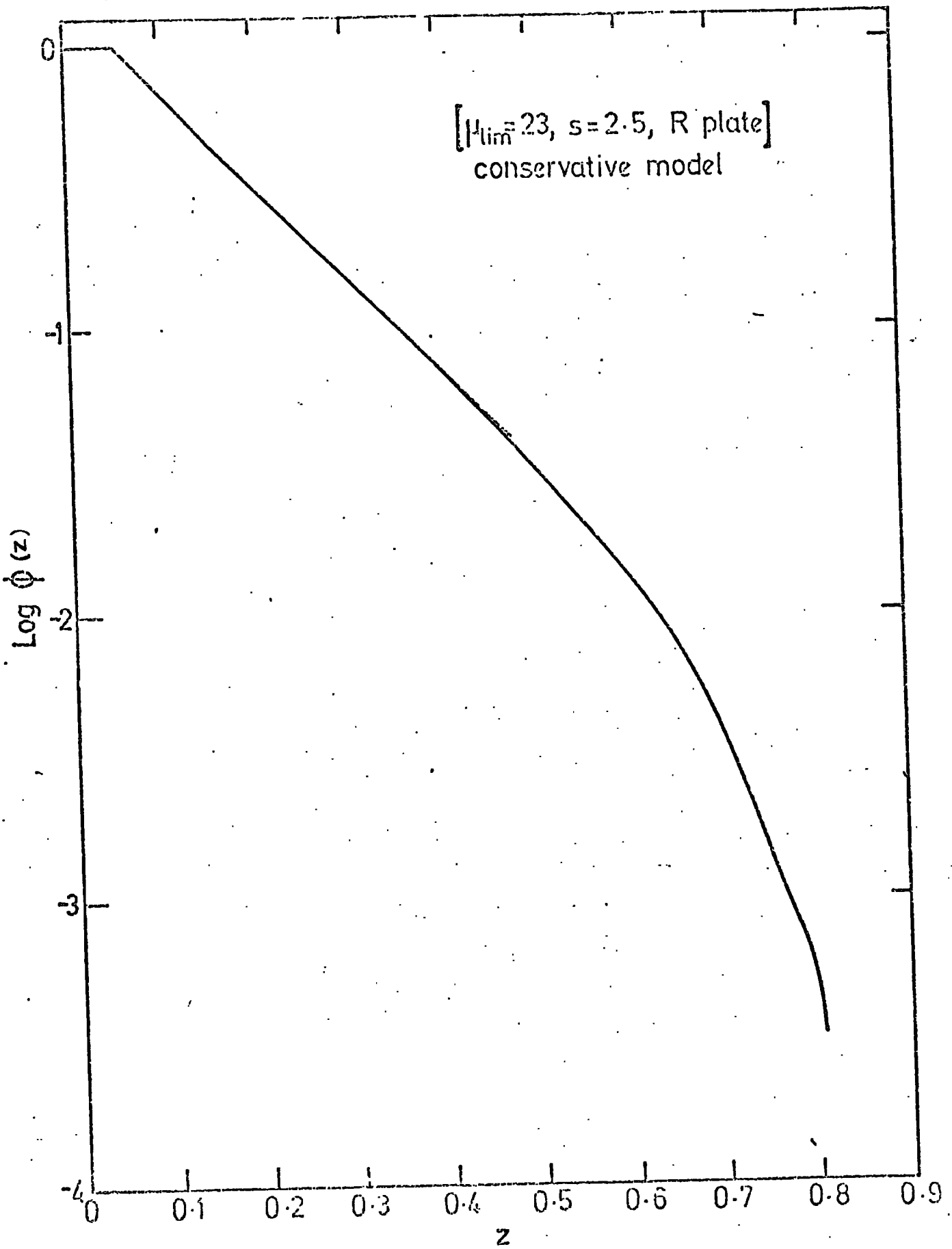

Selection function $\phi(z)$ for the parameters taken to match the R sample.

Figure 6.2

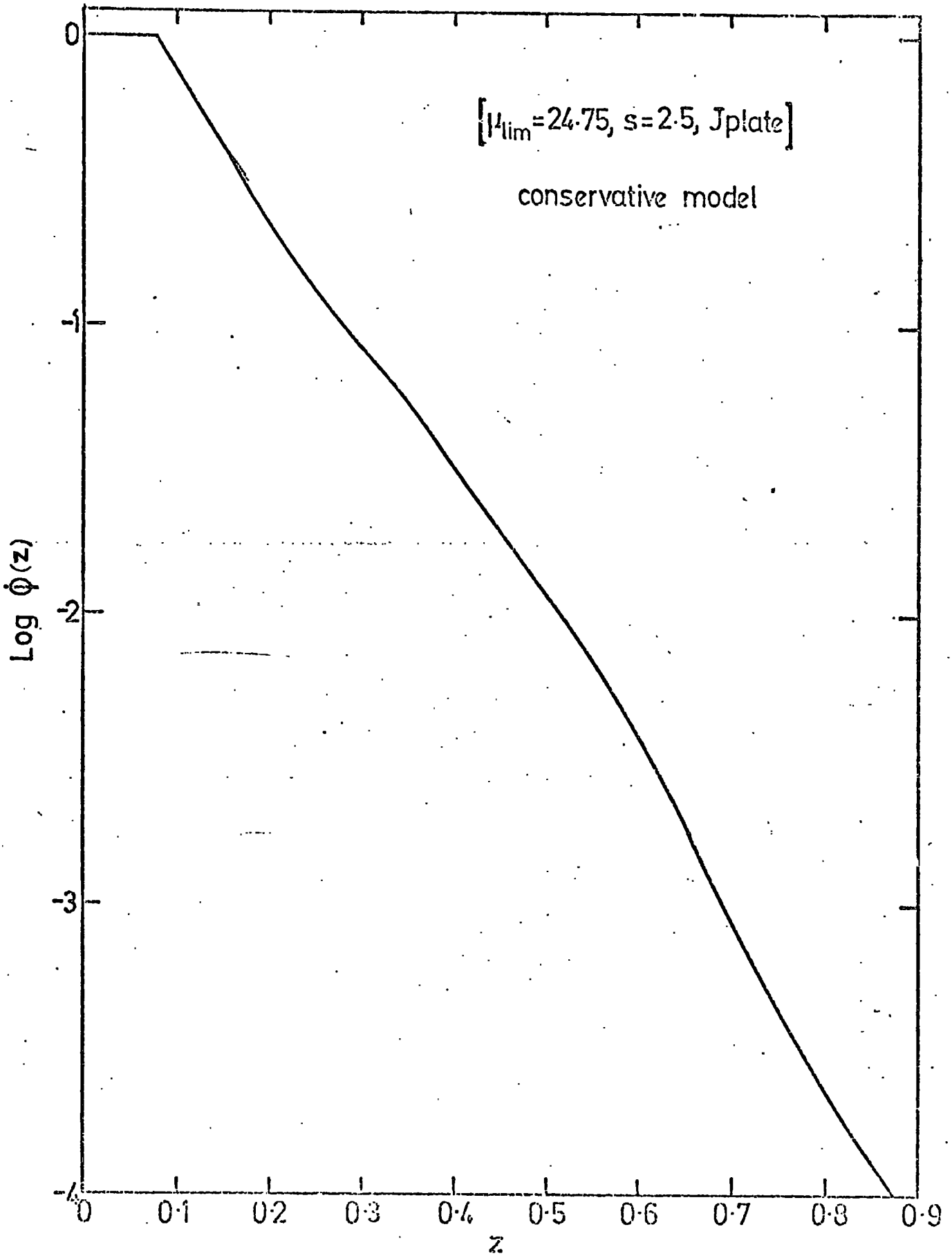

Selection function $\phi(z)$ for the parameters taken to match the J sample.

Figure 6.3

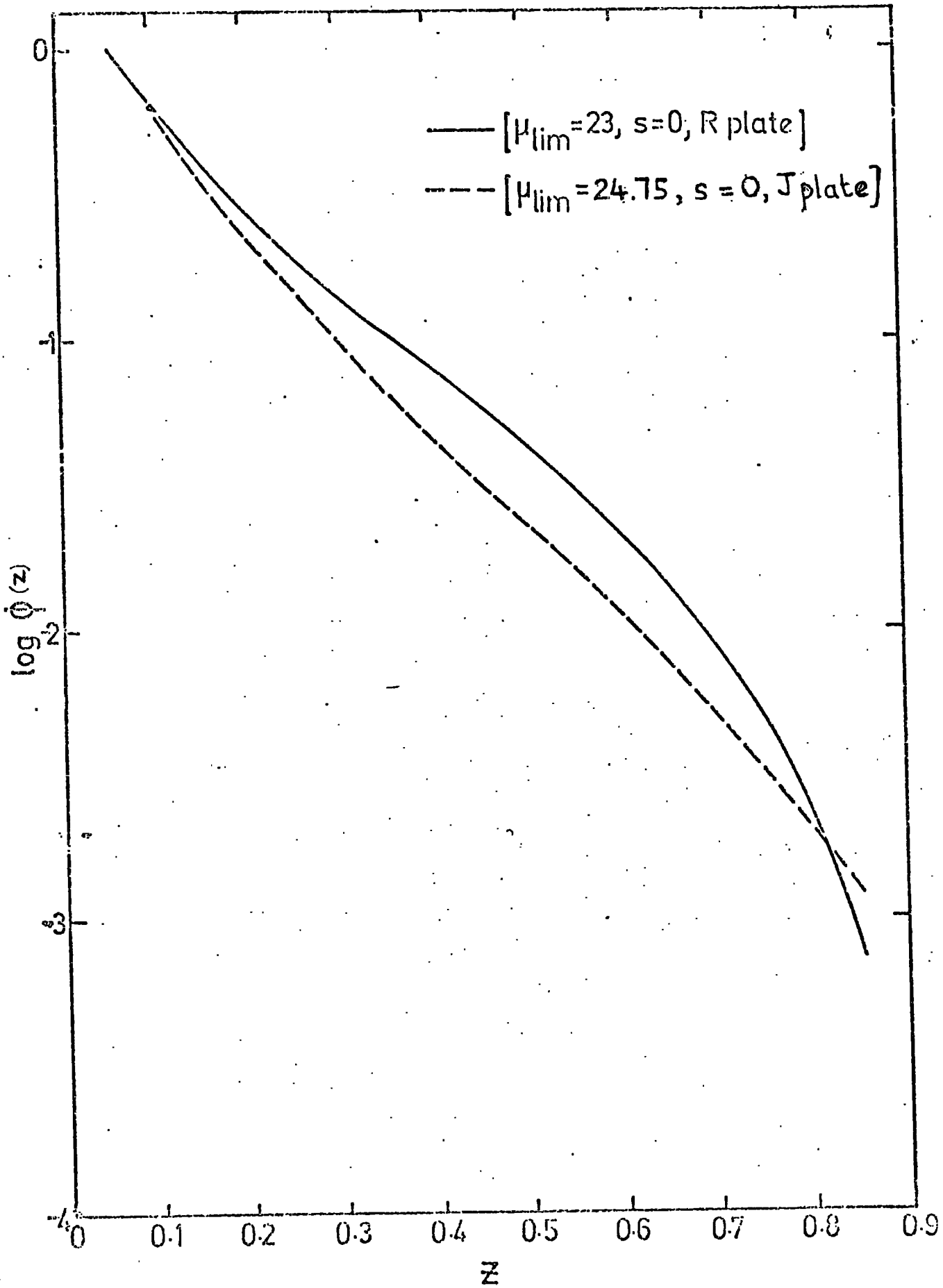

Selection functions for R and J samples for the case of no seeing.

where as before ΔV_i is the co-ordinate volume corresponding to the redshift range $z - \frac{1}{2}\Delta z$ to $z + \frac{1}{2}\Delta z$, and a solid angle of 1 square degree, and ρ_T is the total comoving density of galaxies. This is illustrated in figure 6.4 for the parameters derived for plate J149.

At each distance and for each type, there is a faintest absolute magnitude M_i which gives rise to a galaxy image large enough to be included in the sample. The apparent magnitude of this galaxy can be calculated from

$$m_i = M_i + 5 \log D_L(z_i) + 25 + k(z_i) + e(z_i)$$

(e being the evolutionary correction) and this corresponds to a 'faintest magnitude' for that particular galaxy type and distance. For any particular type the 'faintest magnitude' is initially constant but then falls monotonically with increasing z so there is a maximum redshift z_m for which galaxies with apparent magnitude m are included in the sample. This is illustrated for the J149 sample in table 6.1.

The number of galaxies of this type in the magnitude range (m, m + Δm) included in the sample is then simply

$$\sum_{z_i \leq z_m} N(m - 5 \log D_L(z_i) - 25 - k(z_i) - e(z_i))\, \Delta m\, \Delta V_i$$

while the total number of galaxies in this range (included

Figure 6.4

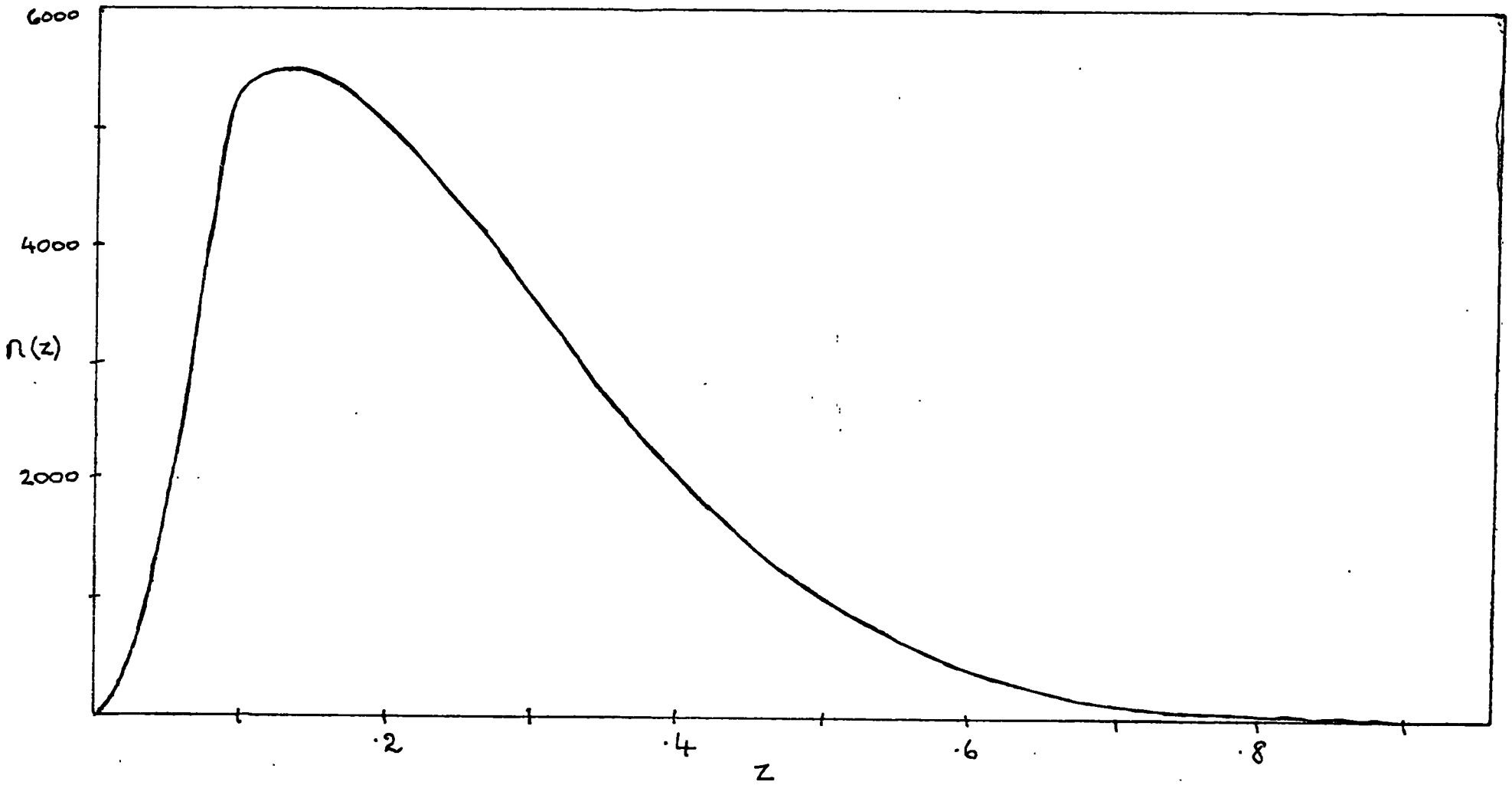

Differential distribution in depth $n(z)$ for the parameters used for the J sample.

Table 6.1

Variation of Limiting Apparent Magnitude with Redshift and Type

z	m_{lim} Ellipticals	Sab
·025		
·075	21·4	
·125	21·4	21·8
·175	21·3	21·6
·225	21·3	21·6
·275	21·3	21·5
·325	21·3	21·5
·375	21·2	21·4
·425	21·2	21·3
·475	21·1	21·3
·525	21·1	21·2
·575	21·0	21·1
·625	21·0	21·0
·675	21·0	20·9
·725	21·0	20·8
·775	21·0	20·7
·825	21·0	20·6
·875	21·0	20·4
·925	20·9	20·3
·975	20·9	20·2

in the sample or not) is

$$\sum_{i=1}^{\infty} N(m - 5 \log D_L(z_i) - 25 - k(z_i) - e(z_i)) \Delta m \Delta V_i$$

where N(M) is the differential luminosity function. Thus summing over all types, this gives the fraction $\phi(m)$ of galaxies of apparent magnitude m which is included in the given sample. This is shown in figure 6.5 for the R1049 and J149 samples. It is clear that these are far from magnitude limited; if they were then ϕ would be a step function.

Note that the behaviour of m_{lim} as a function of z is not always as in the above case. It can happen, for some area cut-offs, that m_{lim} actually rises as z increases, that is fainter galaxies (in terms of apparent magnitude) are visible at large distances. This is discussed further in section 7.6.

6.2 DISTRIBUTION IN DEPTH FOR DIFFERENT MORPHOLOGICAL TYPES

It is of interest to compare the distribution in z for the different morphological types, as this may be important if different types are differently correlated (Geller and Davis 1976).

Typical distributions are shown in figure 6.6 in the n(z) form so that the relative numbers of the

Figure 6.5

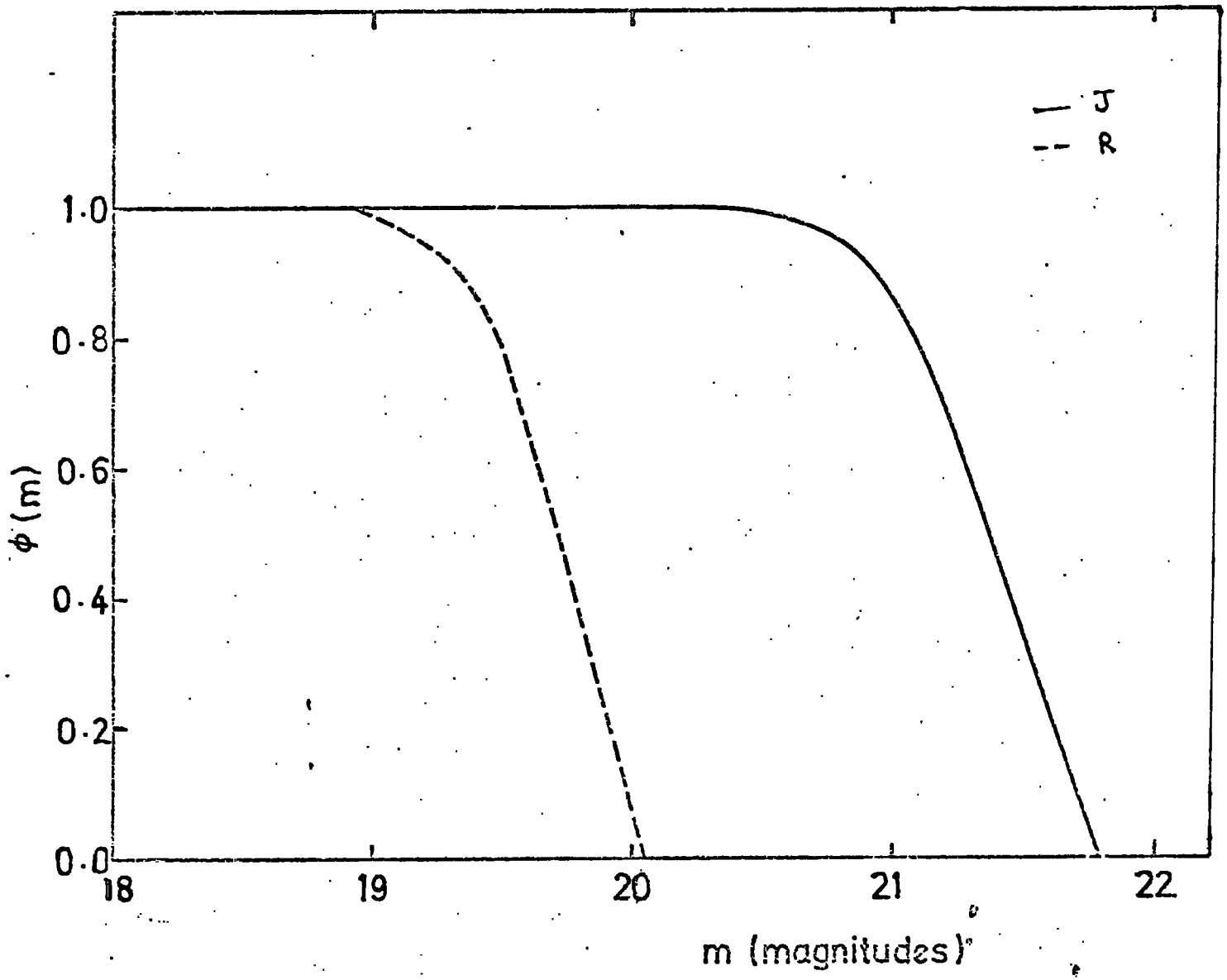

The fraction of galaxies of magnitude m included in the sample, for the models adopted for the J and R samples.

Figure 6.6

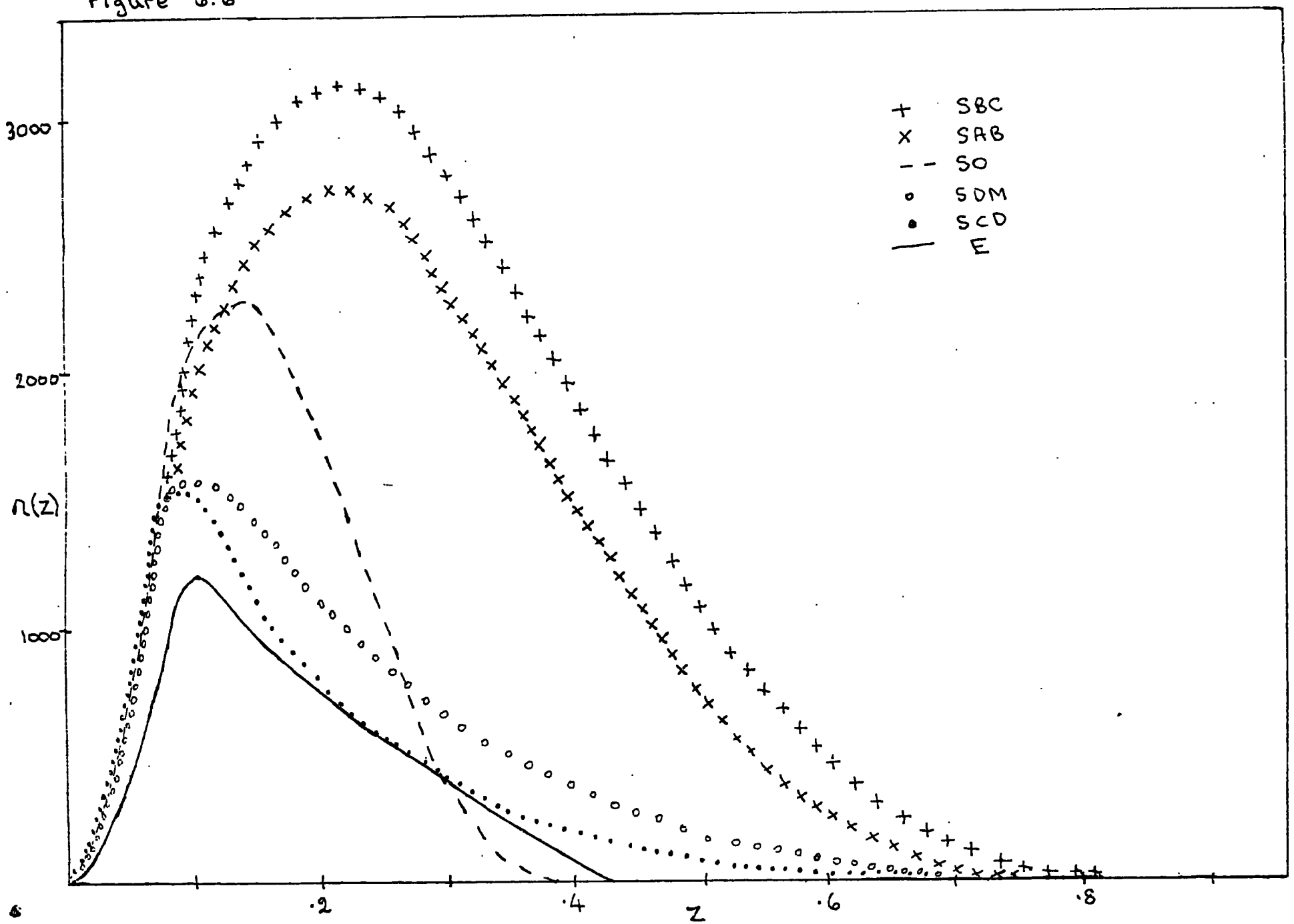

Differential distribution in depth n(z) for individual types of galaxies; with parameters as for J sample.

different types can be clearly seen. It is evident that the E and SO galaxies are rapidly lost, so that at the greatest depths i.e. $z \gtrsim 0{\cdot}4$ the visible galaxies are essentially all spirals, in particular the larger Sab and Sbc's.

It is also of interest at this point, to compare the corresponding angular diameter counts for the different types of galaxies. These are shown in figure 6.7. Obviously the main contribution is from Sab and Sbc galaxies, and it may be noted that the slopes at the large θ end vary slightly from type to type because of the different k-corrections and evolution.

Fortunately though, the slopes are all fairly similar and also the peak in the distribution is very nearly at the same value of θ for each type. This means that even if the relative numbers of the different types, used in the model, were quite seriously in error, the overall shape of the $f(\theta)$ distribution would be altered little.

6.3 SCALING

In section 2.2, it was shown that for a pure power law spatial covariance function, the angular covariance function is also a power law and the amplitude for any particular sample depends on its selection function

Figure 6.7

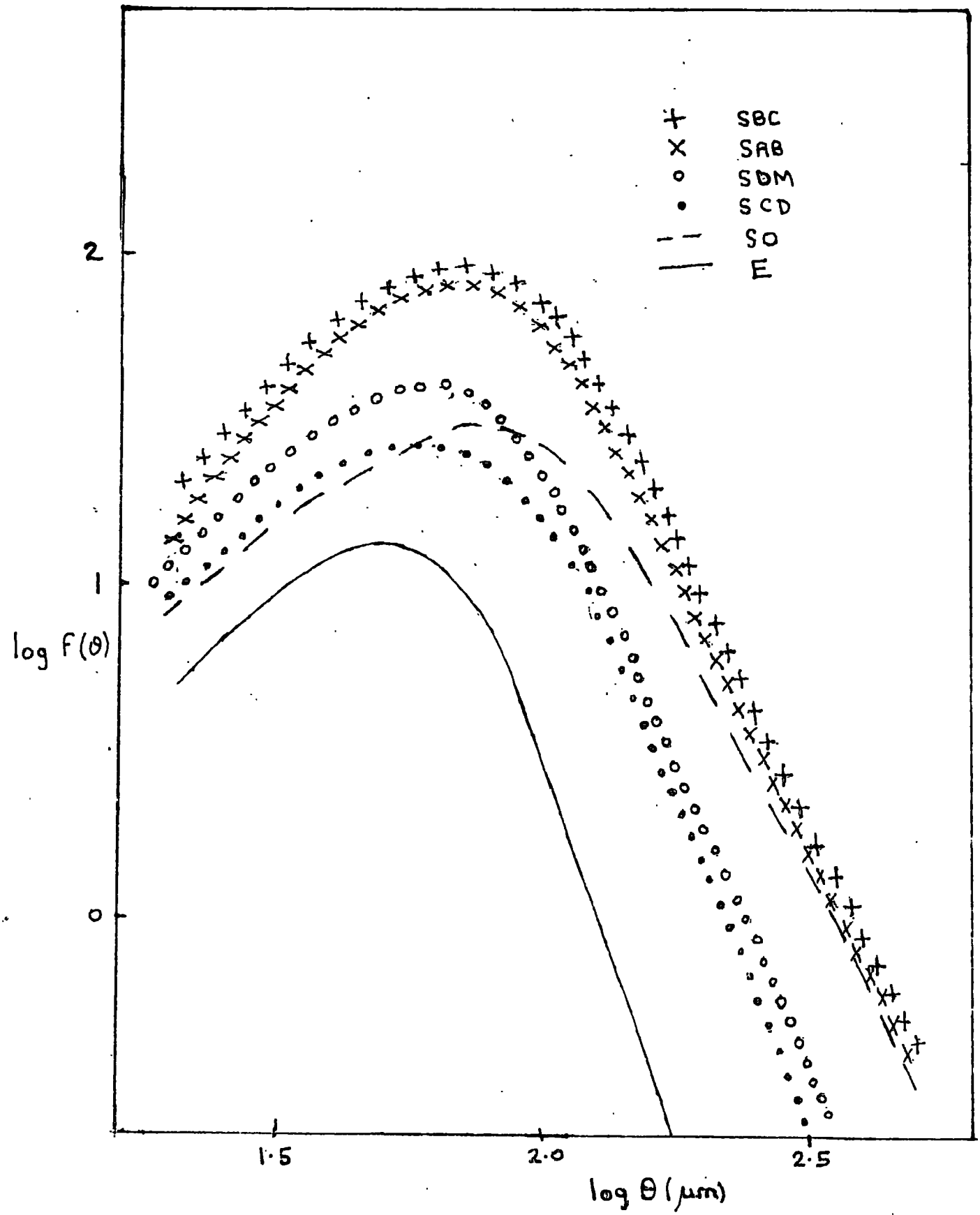

Differential angular diameter counts for individual galaxy types, with parameters as for J sample.

through the factor

$$S(\phi) \propto \frac{\int_0^\infty (1+z)^6 \, h(z) \, g(z) \, f^{4-\delta}(z) \, \phi^2(z) \, dz}{\left(\int_0^\infty (1+z)^3 \, g(z) \, f^2(z) \, \phi(z) \, dz \right)^2}$$

Now by the methods of chapter 5, ϕ can be determined for any deep sample like the ones under consideration here, which are not simply magnitude limited.

Clearly, ϕ can also be determined using the model of the galaxy distribution described in section 5.5 for a magnitude limited survey, by using

$$\phi(z) = \Phi(m_{lim} - 25 - 5 \log D_L(z) - k(z) - e(z)) \qquad (6.2)$$

where $\Phi(M)$ is the fraction of galaxies of the type considered which are brighter than M.

The natural point for comparison of the amplitudes found for the present deep samples with the amplitudes found for previous samples is the Zwicky catalogue limited at $15^m.0$, as was done in tables 2.1 and 2.2.

Taking $m_{lim} = 15 \cdot 0$ in equation (6.2) and using the same model for the galaxy luminosity function, k-corrections and evolution as in section 5.5, the selection function for the Zwicky sample was calculated. The calculated number per square degree was $0 \cdot 60$ in good agreement with the observed density $0 \cdot 62$ per square degree. This agreement lends support to the form and absolute scale of the luminosity function used in the

model. From the selection function the value of S appropriate for the Zwicky catalogue was then obtained, for three forms of $h(z)$; $(1+z)^{-\eta}$ with $\eta = 1{\cdot}8$, 3 and $4{\cdot}2$ (see equation (2.32)).

The values of S for the samples from plates R1049, J149, J1920 and J1921 were also calculated using the selection functions derived in the previous sections. In the case of J1921 a fairly arbitrary value of the seeing, $s = 5$, was chosen to give reasonable agreement with the total number of galaxies per square degree, assuming a limiting isophote of 25·25 magnitudes per square arc second.

The values of the amplitudes and the scaled Zwicky amplitudes, given by

$$A_z^S = \frac{S}{S_z} A_z \qquad (6.3)$$

where A_z and S_z are the amplitude and scaling factor for the Zwicky catalogue, are given in table 6.2 for all the samples considered here as well as the Shane-Wirtanen and Jagellonian samples, with selection criteria as described in the notes to the table.

The amplitude for the Shane-Wirtanen catalogue is seen to be too high by a significant amount for each of the values of the evolutionary parameter . Note that the non-evolving ($\eta = 3$) model gives exactly the

Table 6.2

Sample	A	A_z^S $\eta=1\cdot8$	$\eta=3\cdot0$	$\eta=4\cdot2$	A/A_z^S $\eta=1\cdot8$	$\eta=3\cdot0$	$\eta=4\cdot2$
Z	$7\cdot0\times10^{-1}$	$7\cdot0\times10^{-1}$	$7\cdot0\times10^{-1}$	$7\cdot0\times10^{-1}$	1·00	1·00	1·00
SW	$6\cdot8\times10^{-2}$	$5\cdot1\times10^{-2}$	$4\cdot8\times10^{-2}$	$4\cdot7\times10^{-2}$	1·33	1·42	1·45
Jag 1	$1\cdot8\times10^{-2}$	$2\cdot4\times10^{-2}$	$2\cdot2\times10^{-2}$	$2\cdot0\times10^{-2}$	0.75	0·82	0·90
Jag 2	$1\cdot8\times10^{-2}$	$1\cdot8\times10^{-2}$	$1\cdot7\times10^{-2}$	$1\cdot5\times10^{-2}$	1·00	1·07	1·20
R	$2\cdot2\times10^{-3}$	$6\cdot7\times10^{-3}$	$5\cdot3\times10^{-3}$	$4\cdot2\times10^{-3}$	0·33	0·42	0·52
RS	$7\cdot8\times10^{-3}$	$1\cdot5\times10^{-2}$	$1\cdot3\times10^{-2}$	$1\cdot1\times10^{-2}$	0·52	0·60	0·71
J	$2\cdot9\times10^{-3}$	$9\cdot0\times10^{-3}$	$7\cdot6\times10^{-3}$	$6\cdot4\times10^{-3}$	0·32	0·38	0·45
D	$7\cdot0\times10^{-3}$	$9\cdot7\times10^{-3}$	$8\cdot1\times10^{-3}$	$6\cdot9\times10^{-3}$	0·72	0·86	1·01
1920	$3\cdot6\times10^{-3}$	$8\cdot2\times10^{-3}$	$6\cdot9\times10^{-3}$	$5\cdot8\times10^{-3}$	0·44	0·52	0·62
1920/50	$4\cdot5\times10^{-3}$	$9\cdot2\times10^{-3}$	$7\cdot7\times10^{-3}$	$6\cdot6\times10^{-3}$	0·49	0·58	0·68
1920/100	$1\cdot0\times10^{-2}$	$1\cdot6\times10^{-2}$	$1\cdot4\times10^{-2}$	$1\cdot3\times10^{-2}$	0·62	0·71	0·80
1921	$6\cdot1\times10^{-3}$	$1\cdot3\times10^{-2}$	$1\cdot1\times10^{-2}$	$9\cdot4\times10^{-3}$	0·47	0·55	0·65

Z is the Zwicky catalogue with $m_{lim} = 15\cdot0$.

SW is the Shane-Wirtanen catalogue, assumed to be magnitude limited with $m_{lim} = 18\cdot5$ (to give the correct density).

Jag 1 is the Jagellonian field, taken to have a diameter limited selection function giving the correct density.

Jag 2 is the Jagellonian field, taken to be magnitude limited with $m_{lim} = 20\cdot0$ (to give the correct density).

All other samples are as in table 4.1 with selection criteria as indicated in chapter 5.

same predicted amplitude as the simple scaling law (table 2.1) showing that the more complicated models described in the last chapter do indeed reduce to the simple case for a relatively shallow survey. The discrepancy in this case may be due to the disparity between the various plates and the assorted correction factors producing a relatively large error in the final estimate of the amplitude. Of course, if the form of w does fall away from a perfect power law as claimed by Groth and Peebles (1977) for this sample (section 2.4), this discrepancy can be decreased (table 2.2).

The two (of many) possible selection functions considered for the Jagellonian field are probably fairly extreme cases, and the fact that their predicted amplitudes bracket the value expected from scaling the Zwicky amplitude may indicate that the true selection function for the sample could give very good agreement with the expected amplitude.

The R and J samples can be seen to have amplitudes much lower than expected for any of the η values, with a discrepancy of about a factor 2·5 in each case for $\eta = 3$. A value of η large enough to give reasonable agreement, would imply such a remarkably rapid collapse of the clusters as to be physically quite unrealistic.

The restricted RS sample also has a lower than expected amplitude, though it is not discrepant by quite as large a factor as the deeper R sample.

Although the true selection function for the Dodd *et al* eye-measured sample is not known it is noteworthy that the amplitude found is considerably higher than for the presumably similar J sample. Even though the selection function used for the calculations in table 6.2 may be quite inaccurate it is unlikely that the true selection function would give rise to a difference large enough to bring it into agreement with the J sample, unless the selection were not uniform across the plate. If that is the case, the data should have been 'filtered' before the covariance function was calculated, and as indicated by results for plates J149 and J1921 filtering can reduce the calculated amplitudes by a considerable factor. This is a serious possibility as the plate was measured by several observers over a considerable period of time, and uniformity would be difficult to achieve.

Alternatively the J sample may be contaminated by stars, as was pointed out earlier for the R sample (section 4.5) and this could decrease the amplitude from the 'true' value. A further complication may arise through random errors in the areas assigned to the images by COSMOS: for small images which only contain a few pixels, random errors could remove some galaxies which should be in the sample and replace them with fainter galaxies which have been accidentally increased in size. These fainter galaxies would, on average, be less correlated

than those that are lost - or equivalently the true selection function for the images counted is flatter but extends to deeper distances than the calculated one, hence decreasing the scaling factor.

This factor could, of course, be important in all the other surveys, not just the J sample, and may account for the greater discrepancy at very deep cuts (small areas) compared to less deep cuts (larger areas) as noted above for the R and RS samples, and again below for plate J1920.

Plate J1920, using all the galaxies, shows a discrepancy of a factor of about 2, for the $\eta = 3$ case, the amplitude being lower than expected for all the quoted values of η , as for R1049 and J149.

The two restricted samples also have lower amplitudes than expected, but it is of interest to note that the discrepancy decreases as the depth is reduced, repeating the behaviour found between the R and RS samples.

Plate J1921, although uncertain, gives similar results to plate J1920 cut back to the corresponding density, being discrepant by a factor around 2 from the expected value.

6.4 GENERAL SCALING FOR DIFFERENT TYPES OF SELECTION CRITERIA

The scaling factor S can be calculated by the methods of the previous sections for any type of selection criteria. The ones that are probably of most interest are (1) magnitude limited samples, (2) diameter (or area) limited samples for a given threshold and (3) threshold limited samples for a given limiting image size. The first class is obviously needed for shallow surveys where all magnitudes are know and have already been discussed in connection with the Zwicky catalogue. Different depths of survey are then merely those with different limiting magnitudes, e.g. the Zwicky catalogue limited at $13^{m}.0$ or $15^{m}.0$. The second is necessary for surveys similar to the ones used in this thesis, where machine measurements are used and identifications of objects are made above some limiting image area for a fixed (in perfect conditions) intensity threshold, which may be known or be estimated from other considerations (chapter 5). Different depths are obtained by using different area or diameter cut-offs as was the case for plate J1920, for instance, (see section 4.8). The third type may be applicable for different samples, i.e. plates to different depths, where the size limit of a detectable image is fixed (by the observer or measuring machine) but the intensity threshold at which the image is detectable varies with the emulsion, exposure etc.

Scaling factors for these types of selection function are illustrated in figure 6.8, plotted against the corresponding density of sample galaxies. Note that for a given density there may be a wide spread of possible values for S. The three lines are for the selection functions described in table 6.3.

Figure 6.8

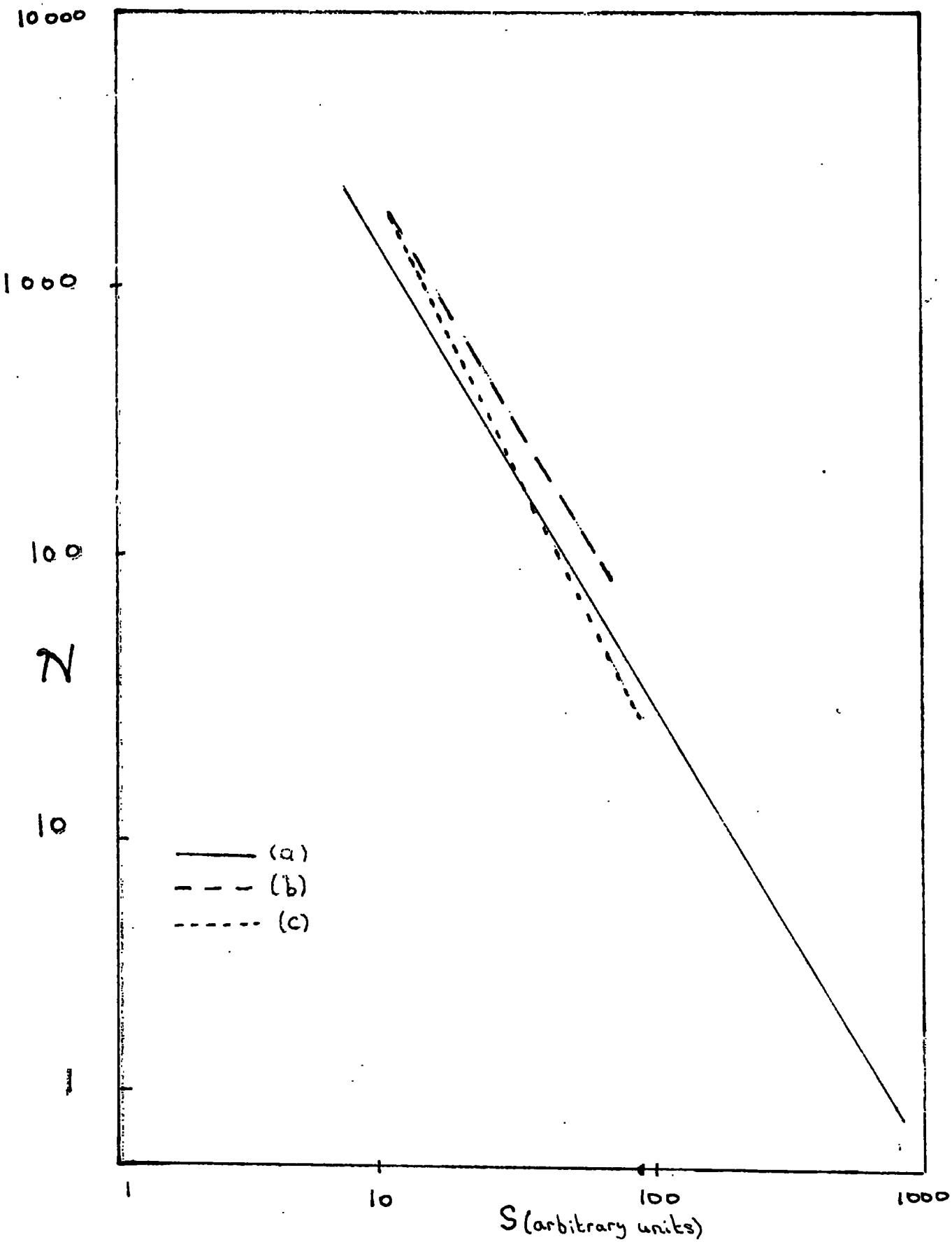

Variation of scaling factor S with number density $\mathcal{N}$ per square degree, for three types of selection function as in table 6.3., and $\eta = 3$.

Table 6.3 (a)

Magnitude limited, conservative evolution, $\delta = 0{\cdot}8, \eta = 3$

m_{lim} (blue)	$\mathcal{N}$ (per square degree)	S (arbitrary units)
14·5	·31	1295
15·0	·60	942
18·5	54	65
19·0	97	45
19·5	178	32
20·0	322	22
20·5	576	16·1
21·0	1021	11·4
21·5	1788	8·1

Table 6.3 (b)

Threshold limited, angular diameter $\geq 35\mu m$, conservative evolution, $\delta = 0{\cdot}8, \eta = 3$, $s = 2''.5$.

μ_{lim}(blue)	$\mathcal{N}$(per square degree)	S (arbitrary units)
23.0	78	69.7
23.5	219	37.3
23.75	354	28.7
24.75	1703	10.5

Table 6.3 (c)

Angular diameter limited, intensity threshold $24^{m}.75$ (blue), conservative evolution, $\delta = 0.8$, $\gamma = 3$, $s = 2''.5$.

$\log \theta_{lim}$ (μm)	$\mathcal{N}$ (per square degree)	S (arbitrary units)
2·10	131	35·5
2·00	256	25·7
1·95	352	21·8
1·85	626	16·8
1·75	992	13·6
1·65	1360	11·6
1·60	1536	11·0
1·55	1703	10·5

CHAPTER SEVEN

FURTHER ANALYSIS ON THE UKSTU PLATES

'The human plate reader is a noisy device, subject to large secular variations'.

C. Seeger.

7.1 ANGULAR DIAMETER OF STARS

The angular diameter distribution for stars may be computed in exactly the same way as for galaxies (section 5.3). This is shown in figure 7.1 for plate R1049. It is seen that there is a quite smooth distribution for $\theta \geq 55\mu m$ but that below that value there is a second peak near the lower limit for classification of $35\mu m$. This may be due to misclassification of some faint galaxies as stars, as was previously suspected from the cross correlation function and the covariance function for all objects (section 4.6).

The same feature appears, though less significantly, in the corresponding distribution for the plate J149 (which is of course, of nearly the same area of sky, so it may in fact reflect a real feature, e.g. a cluster of faint stars). This is shown in figure 7.2.

Figure 7.3 shows the distribution for another blue plate J1920 (J1921 was not considered due to the poorly known seeing). The secondary maximum at small θ is not seen in this example, and the distribution seems quite smooth.

7.2 MAGNITUDES OF STARS

It may be assumed that the profile of a star on a photographic plate is nearly Gaussian, or strictly a

Figure 7.1

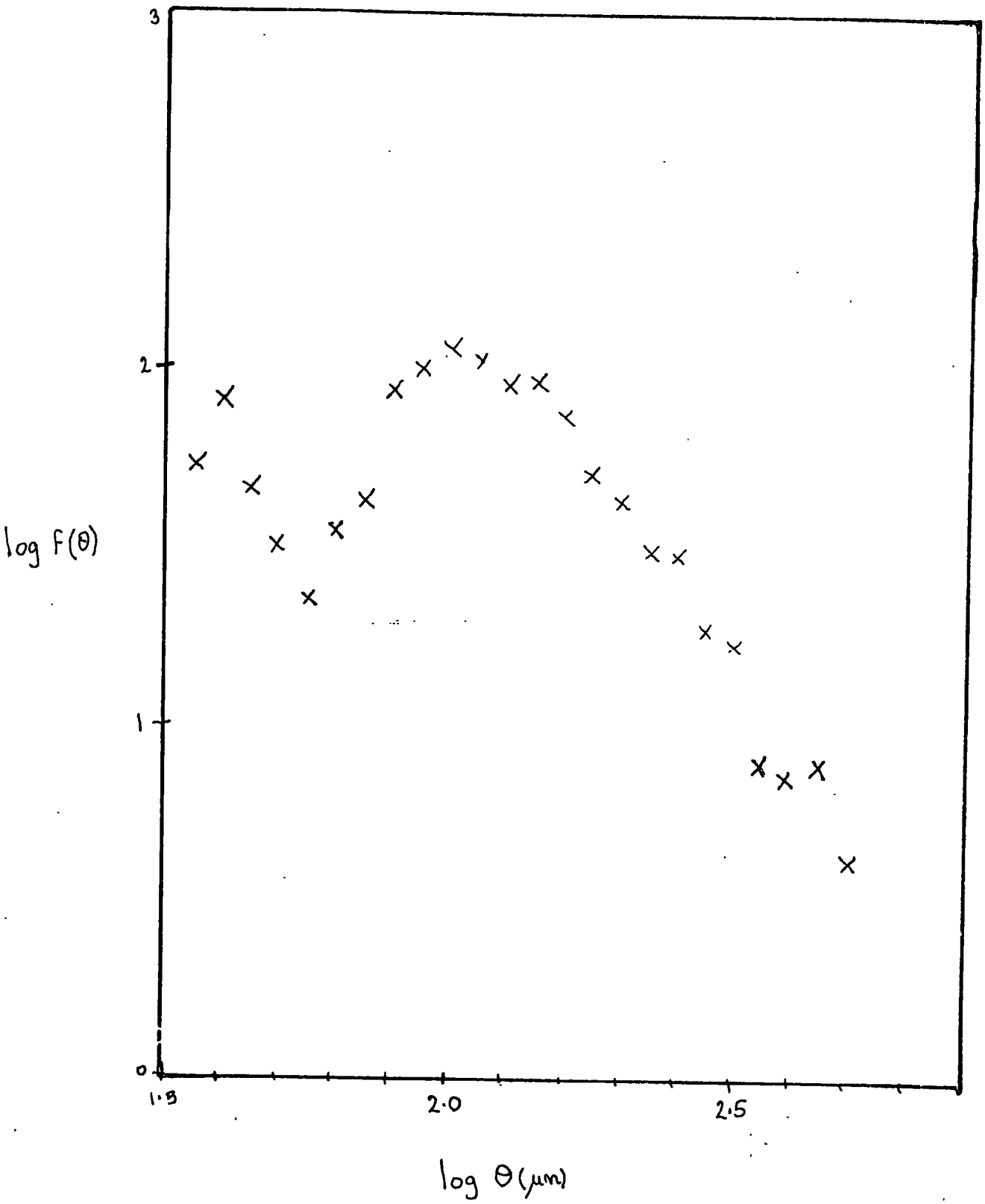

Plot of $F(\theta)$ for stars on measured area of plate R1049.

Figure 7.2

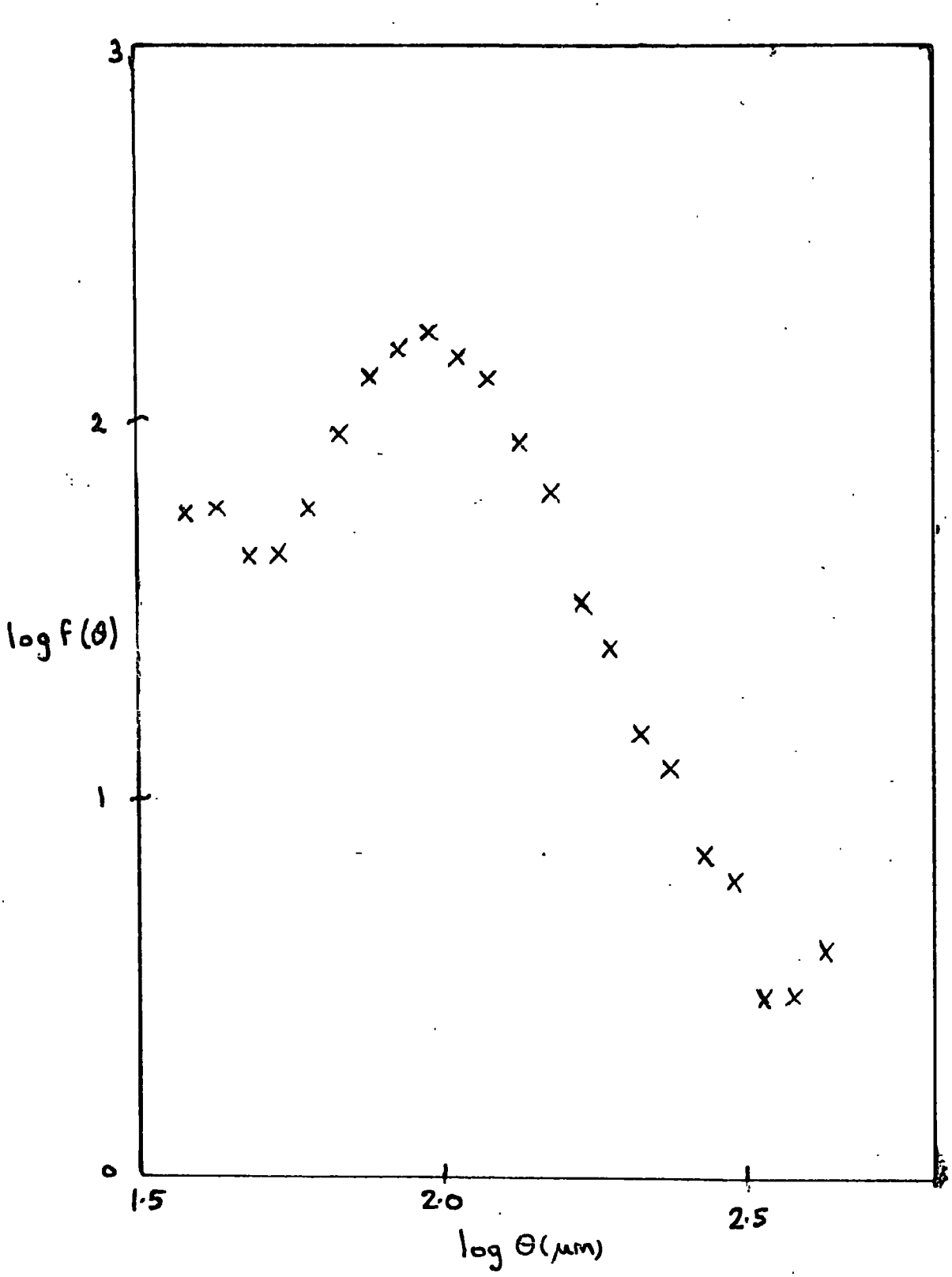

Plot of $f(\theta)$ for stars on the measured area of plate J149.

Figure 7.3

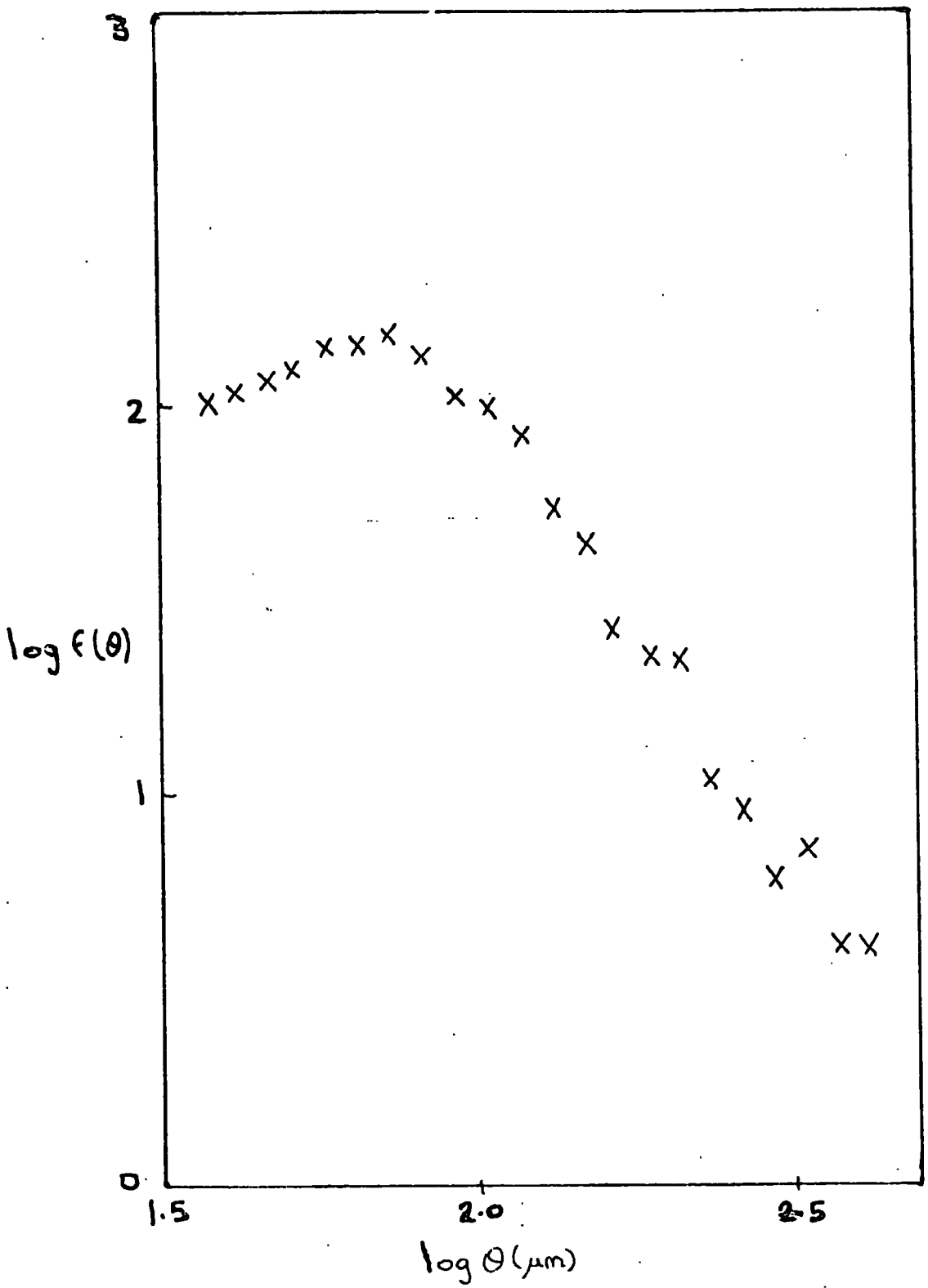

Plot of $f(\theta)$ for stars on the measured area of plate J1920.

product of several Gaussians due to atmospheric scattering, scattering in the telescope optics and scattering in the photographic emulsion, provided that the star is not too bright (or indeed, too faint).

In this case take the profile to be

$$I(r) = I_o \exp(-r^2 / 2\sigma^2) \qquad (7.1)$$

where I_o is the central intensity (per square arc sec) and σ is the seeing in seconds (see section 5.5, equation 5.21). Then the total intensity

$$I = I_o \int_0^\infty \exp(-r^2 / 2\sigma^2) \, d(r^2)$$

$$= 2\pi\sigma^2 I_o \qquad (7.2)$$

If the radius of the star (above the limiting isophote I_{thr}) is R then

$$I_o \exp(-R^2 / 2\sigma^2) = I_{thr}$$

$$\therefore \quad I = I_{thr} 2\pi\sigma^2 \exp(R^2 / 2\sigma^2)$$

or $$m = \mu_{lim} - 2{\cdot}5 \log_{10}\left[2\pi\sigma^2 \exp(R^2 / 2\sigma^2)\right]$$

$$\therefore \quad m = \mu_{lim} - 2{\cdot}5 \log_{10} (2\pi\sigma^2) - 2{\cdot}5 \log_{10} e \, . \, A/2\pi\sigma^2 \qquad (7.3)$$

where μ_{lim} is the limiting brightness expressed in magnitudes per arc

$\sec^2$, m is the integrated (to infinity) magnitude and A is the area of the stellar image in square arc seconds.

For a point image, i.e. R = 0

$$\bar{m}_* = \mu_{lim} - 2{\cdot}5 \log (2\pi\sigma^2) \qquad (7.4)$$

so this is clearly the ultimate magnitude limit for the plate. If the limit is set by stars of a given area A_{lim} then

$$m_{lim} = \mu_{lim} - 2{\cdot}5 \log(2\pi\sigma^2) - 2{\cdot}5 \log e \; A_{lim}/2\pi\sigma^2 \qquad (7.5)$$

For plate J149 using the values of μ_{lim}, σ and A_{lim} from sections 4.6 and 5.6, this becomes

$$m_{lim} \simeq 21{\cdot}9 \qquad (7.6)$$

while for J1920 we have

$$m_{lim} \simeq 22{\cdot}1 \qquad (7.7)$$

Note that this limit only applies to stars, the magnitude limit for galaxies was discussed in section 6.1. Remembering that the density of stars on each is quite similar, around 1700 per square degree on J1920, around 1400 on J149, this appears to be reasonable agreement on the depth of the plates, lending support to the respective σ and μ_{lim} values. However, the values quoted by Allen (1973) for the density of stars to various magnitude limits, give 1400 to 1800 for $m_{lim} = 21^m{\cdot}0$ at the North Galactic Pole. The counts only rise slowly around 21^m, though, and there may

be a difference from the NGP to the SGP or a small amount of absorption at the galactic latitude of the plates, so this apparent discrepancy may not be as serious as it appears. Note also that Dodd et al (1975) estimated the limiting stellar magnitude for their eye measurements on plate J149 to be $22^{m}.0$.

The distribution n(m) of the number of stars per square degree brighter than (blue) magnitude m is shown for J149 and J1920 in figures 7.4 and 7.5. For comparison figure 7.6 shows the distribution obtained from Allen. The shape of the curve for J1920 is quite similar, though there is some difference in amplitude, which could be removed if the limiting isophote were raised, though this may not be necessary for the reasons mentioned above. The curve for J149 is considerably shallower. This is unlikely to be a real effect and could be due to the effect of the varying thresholds across the plate. It could also be caused by an underestimation of the seeing.

7.3 CENTRAL SURFACE BRIGHTNESS OF GALAXIES

The measurements given by COSMOS (table 3.3) include the minimum transmission and threshold transmission and from these the relative central brightness, threshold brightness and sky brightness can be obtained, provided a

Figure 7.4

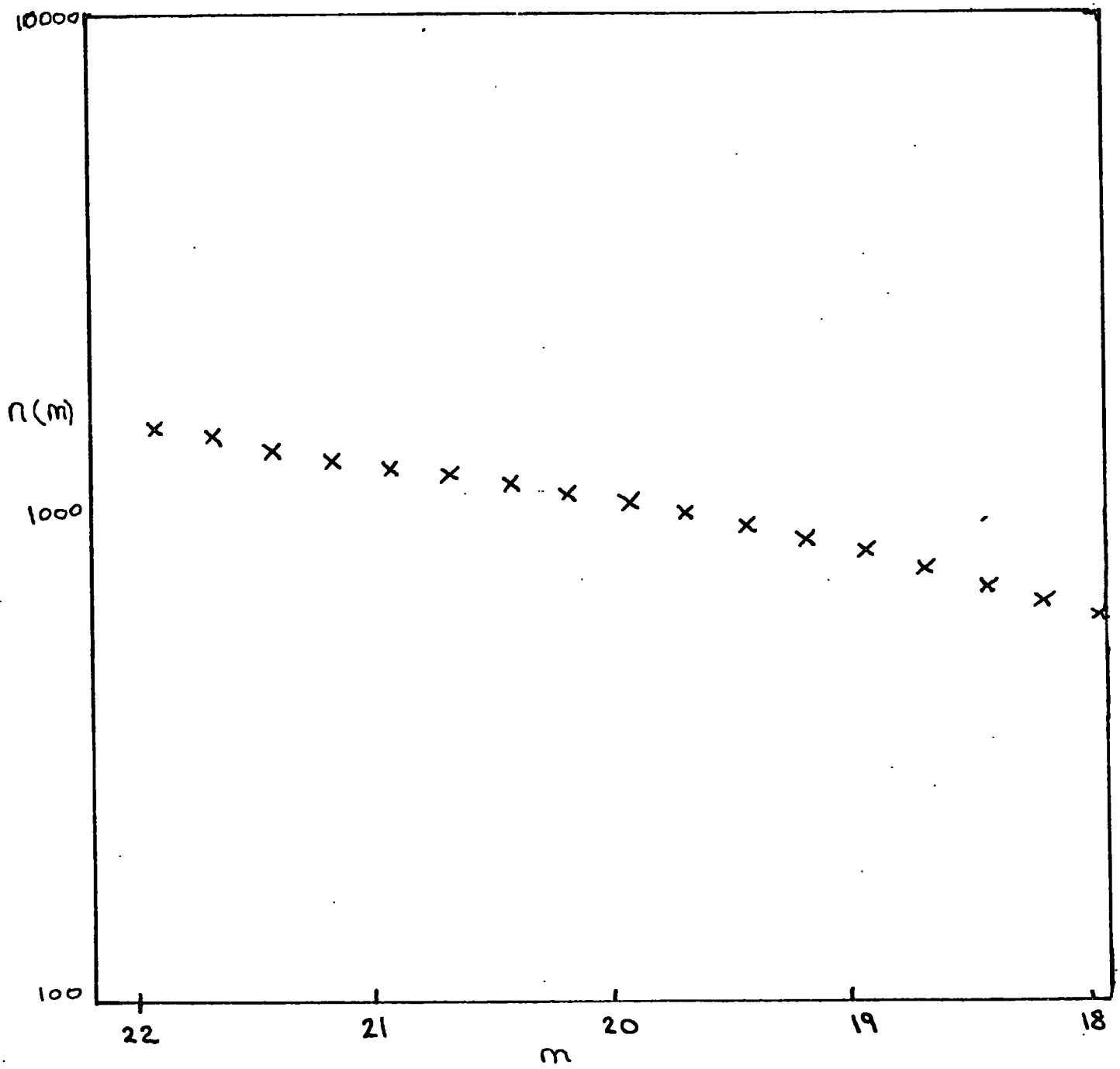

Distribution $n(m)$ of the number of stars per square degree brighter than magnitude m, for the measured area of plate J149.

Figure 7.5

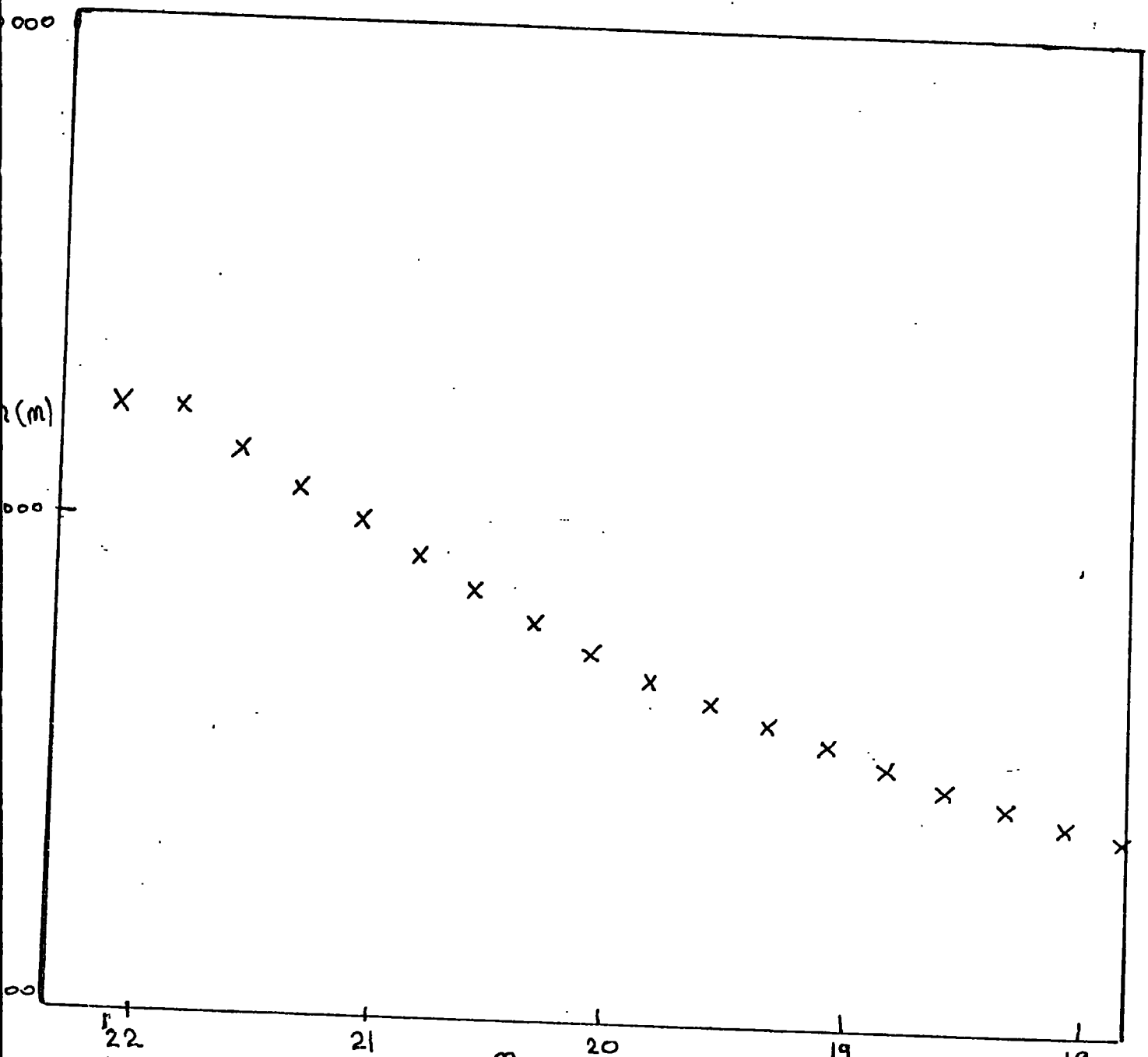

Distribution n(m) of the number of stars per square degree brighter than magnitude m, for the measured area of plate J1920.

Figure 7.6

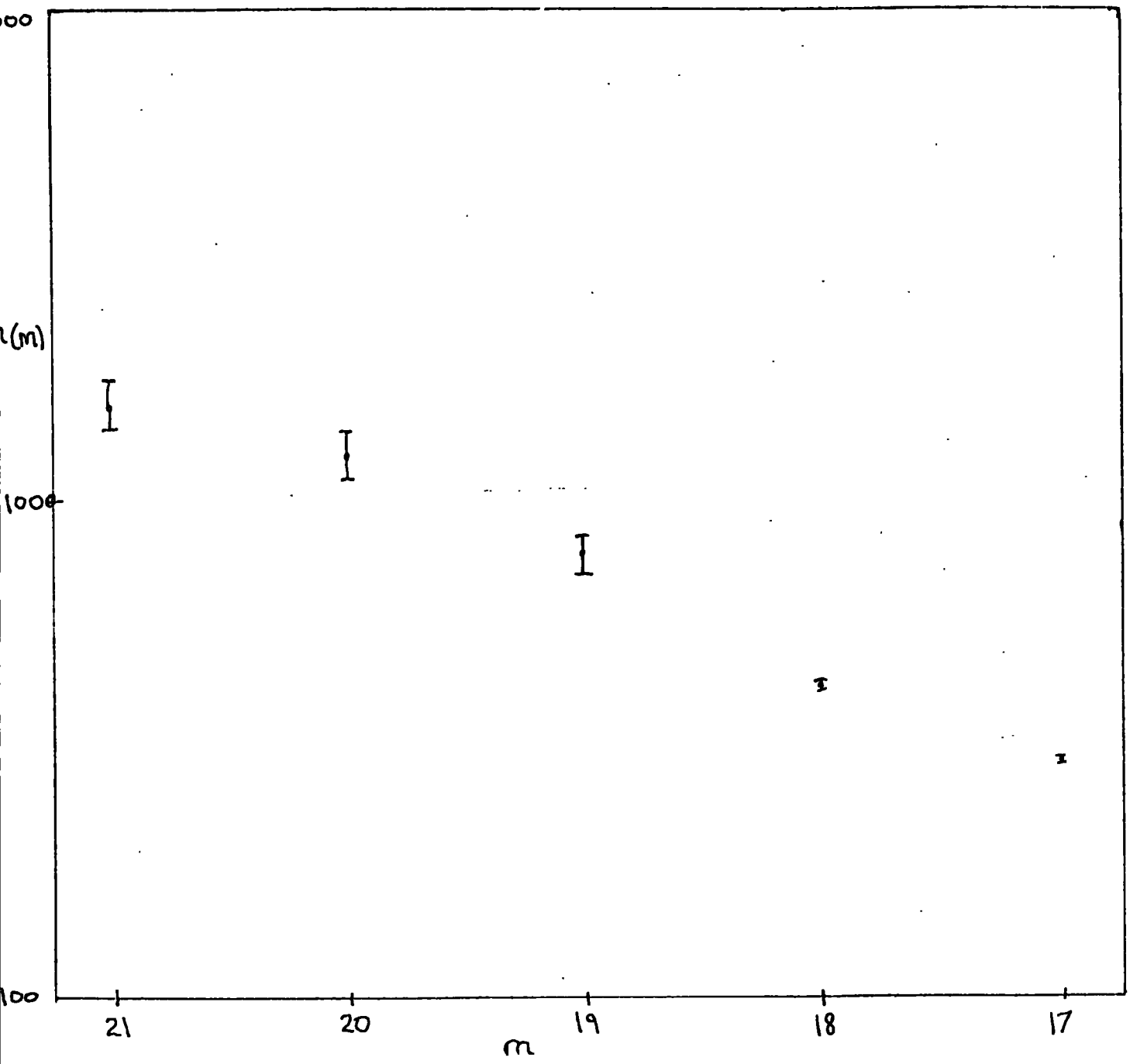

The distribution n(m) of the number of stars brighter than magnitude m, for the northern galactic pole area (from Allen 1973).

calibration is available (section 3.6). Hence assuming that the threshold μ_{lim} is known, the central brightness S_o can be obtained. Note that the calculation of S_o depends on the correct calibration of the plate and the correct sky subtraction (i.e. knowledge of the transmission which corresponds to the sky level) since from section 3.6

$$S_o = \mu_{lim} - 2{\cdot}5 \log \frac{I_{centre}}{I_{limit}}$$

$$= \mu_{lim} - 2{\cdot}5 \log \left[\frac{\left(\frac{T_o}{TMIN} - 1\right)^{\gamma} - \left(\frac{T_o}{T_{sky}} - 1\right)^{\gamma}}{\left(\frac{T_o}{T_{thr}} - 1\right)^{\gamma} - \left(\frac{T_o}{T_{sky}} - 1\right)^{\gamma}} \right] \quad (7.8)$$

or alternatively

$$S_o = \mu_{sky} - 2{\cdot}5 \log \left[\frac{\left(\frac{T_o}{TMIN} - 1\right)^{\gamma}}{\left(\frac{T_o}{T_{sky}} - 1\right)^{\gamma}} - 1 \right] \quad (7.9)$$

if the sky brightness μ_{sky} is known instead of the threshold. The distribution of S_o is shown for plate J1920 in figure 7.7 where $N(S_o)\ \Delta S$ is the number of galaxies with central brightness in the range $(S_o - \frac{1}{2}\Delta S,\ S_o + \frac{1}{2}\Delta S)$.

Figure 7.7

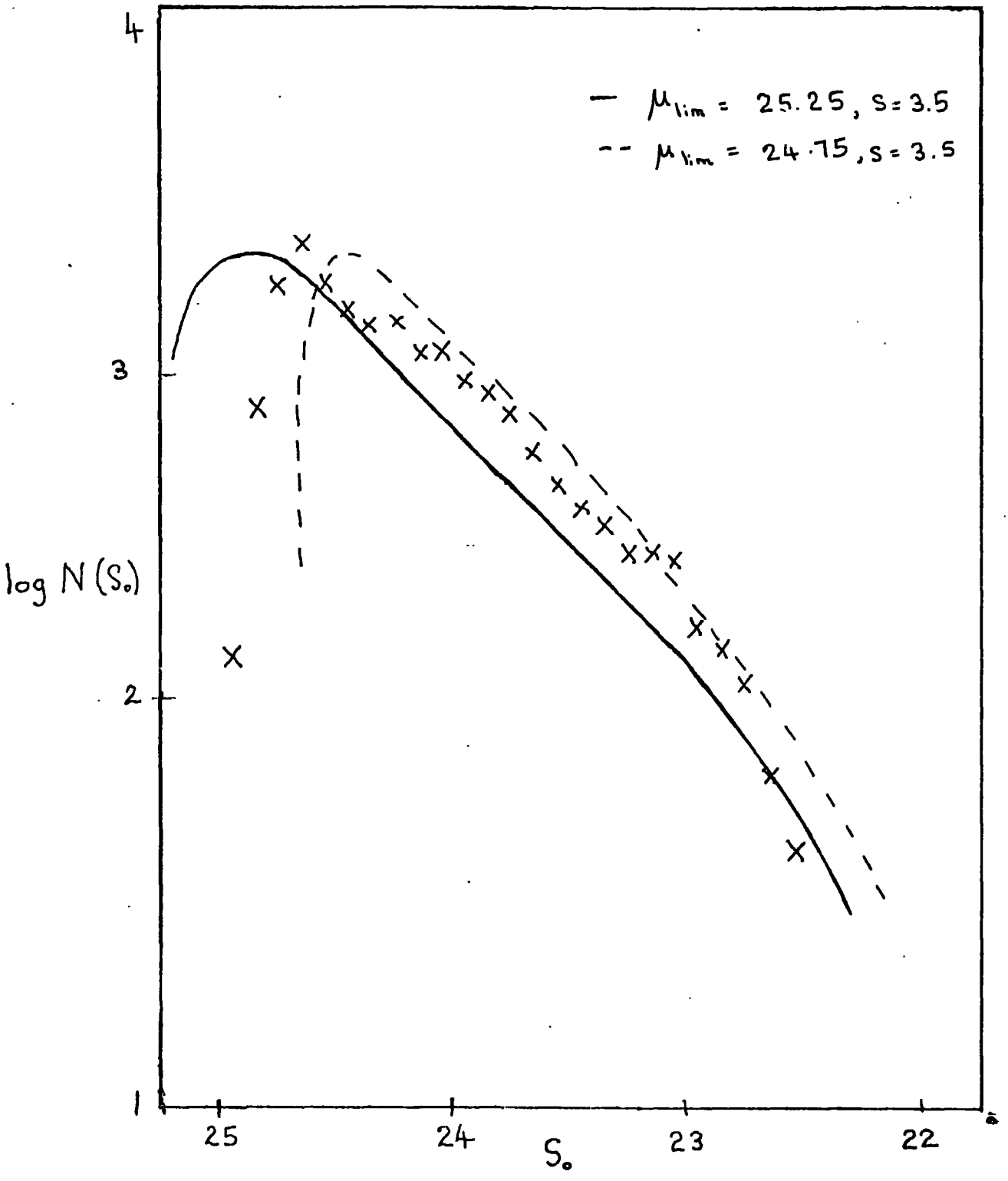

Distribution of the number of galaxies with observed central surface brightness S_0 magnitudes per square arc sec (crosses), compared with two expected distributions, for the 1920 sample.

The solid curve is the expected distribution for $\mu_{lim}=25^{m}.25$ per square degree, seeing of $3''.5$ and the model of the galaxy distribution used for the angular diameter calculations (section 5.5). It can be seen that there is good overall agreement of the shape of the curve but that the observed curve is slightly higher over most of its range. (This is accounted for by the fact that near the threshold the numbers observed are very low, making up for the excess at greater brightnesses - the total numbers obviously being the same, as this was one of the criteria for fixing the threshold and seeing. It appears therefore that some objects with S_o near the threshold may be lost, so the effective threshold - i.e. where detection is roughly complete - may be somewhat brighter. If a higher threshold, say $24^{m}.75$ is used, the expected distribution is higher for the values away from the threshold.(dotted curve in figure 7.7) although there are less objects in total).

This good agreement indicates that the model of the galaxy distribution used is self consistent, in as much as it gives reasonable results for quantities and distributions which were not used in the determination of the parameters of the model.

In particular, the wide spread of calculated S_o values is noteworthy in view of the fact that the majority of the galaxies (i.e. the spirals and lenticulars) were

given the same intrinsic central intensity, corresponding to $21^{m}.65$ per square arc second, according to Freeman's law. This is due in the main to the range of redshifts of galaxies in the sample (though the seeing also has an important effect by decreasing the central intensity more for smaller images).

Neglecting seeing, S_o depends on z through the diminution factor $(1 + z)^4$ and through the k-corrections and evolutionary corrections but not on the cosmological model. This was noted by Hubble and Tolman (1935) who proposed - in the absence of k-corrections and evolution - the use of plots of S_o against z to prove the expansion of the universe as opposed to the 'tired light' theory of redshifts. Gudehus (1975) proposed their use to determine evolutionary parameters. (In fact, Petrosian (1976) noted that what was generally measured was a mean brightness inside some isophote, and Tinsley (1977a) showed that such average brightnesses were dependent on the cosmological model as much as on the evolution). Although the central brightness measured by COSMOS is actually an integral over the central $\sim 12{\cdot}5\ \mu m$ of the image (and hence depends on the width of the galaxy profile), the measured S_o's for a sample with no seeing depend primarily on z. Hence (for a spiral) S_o gives an estimate of the redshift. The effect of seeing is discussed further in section 7.5.

The good agreement between the measured S_o distribution and that predicted is also a point in favour of Freeman's law, as opposed to Disney's view that is merely due to the selection criteria for the galaxies studied in

obtaining it (Disney 1976). Of course, a suitable spread of intrinsic S_o values could give rise to a similar observed distribution, but it seems unlikely that a wide spread of central intensities could lead to such a narrowly peaked observed curve.

Disney's point is that it seems a strange coincidence that the observed values of the central surface brightness of both spirals and giant ellipticals are just those that would give the maximum area on a sky survey print (in the model used in this thesis the ellipticals do not all have the same S_o but this does not invalidate the point since giants with roughly the same absolute magnitude are the best studied), and it may be interesting at this point to consider another such coincidence.

The simple formula

$$M + 5 \log \theta + 5 \log D = \text{constant} \qquad (7.10)$$

which is often cited to show that measuring angular diameters is essentially the same as measuring apparent magnitudes ($M + 5 \log D + \text{constant}$) (see e.g. Weinberg 1972, chapter 14) only occurs if S_o is constant or the profile is inverse square, which are assumed for spirals and ellipticals respectively.

For, in general, if

$$I(r) = I_o f(r/a) \ , \quad \text{(cf. equations 5.8 and 5.11)} \qquad (7.11)$$

then the total intensity

$$I \propto I_o a^2 \qquad (7.12)$$

or $$M = S_o - 5 \log a + \text{constant} \qquad (7.13)$$

and, for a small distance D

$$S_o - 2{\cdot}5 \log f(\theta D/a) = S_L \qquad (7.14)$$

where S_L is the limiting isophote and θ is the observed isophotal radius.

Hence

$$10^{0.2 S_o} f^{-1}(10^{0.4(S_o - S_L)}) = \theta D 10^{0.2M} \times \text{constant}$$

or, putting $0{\cdot}2(S_o - S_L) = \log y$

$$M + 5 \log \theta + 5 \log D + \text{constant} = 5 \log (y f^{-1}(y^2)) \qquad (7.15)$$

Thus (7.10) is only true if $yf^{-1}(y^2) = \text{constant}$
i.e. if $y = \text{constant}$ (i.e. $S_o = \text{constant}$; spirals)
or if $f^{-1}(y^2) = 1/y \Rightarrow f(y) = 1/y^2$ (i.e. $I(r) \propto r^{-2}$; ellipticals).
In other words has the assumed form of the profile, which must be used to find the extrapolated absolute magnitude, e.g. using equation (7.10), influenced the laws obtained relating the surface brightness and absolute magnitude?

7.4 INDIVIDUAL CLUSTERS OF GALAXIES

When the expected distribution of angular diameters was calculated (section 5.5) the total numbers expected at any θ were found by summing over volume elements at different redshifts. Hence the contribution from any

particular distance is simply obtained from the same calculation.

This gives the shape of the distribution for a single cluster at this distance, assuming that the ratios of each type of galaxy and the luminosity function are the same in clusters as in the overall distribution.

Figure 7.8 illustrates the shape of the cluster $f(\theta)$ for several values of redshift z, and the parameters used for the fit to the data from plate R1049.

Clearly the amplitude of the curves depends on the volume of the cluster and the density contrast relative to the mean space density of galaxies - or equivalently on the number of objects in the cluster.

Figure 7.9 shows how the addition of a large cluster at $z = \cdot 1$ can effect the $f(\theta)$ distribution. The distributions are for clusters of contrast factor 10 and 100 covering the whole area - i.e. for an area restricted to the apparent extent of the cluster, and with the thickness of one bin in z used in the calculations i.e. $\Delta z = \cdot 01$ or $30h^{-1}$ Mpc.

On plate R1049 there is an area of considerably higher density than the average. It is clearly difficult to interpret the difference between the two curves in figure 7.10 for the region of the 'cluster' and for an average region of the same area elsewhere on the plate, so a plot of the difference alone is given in figure 7.11 -

Figure 7.8

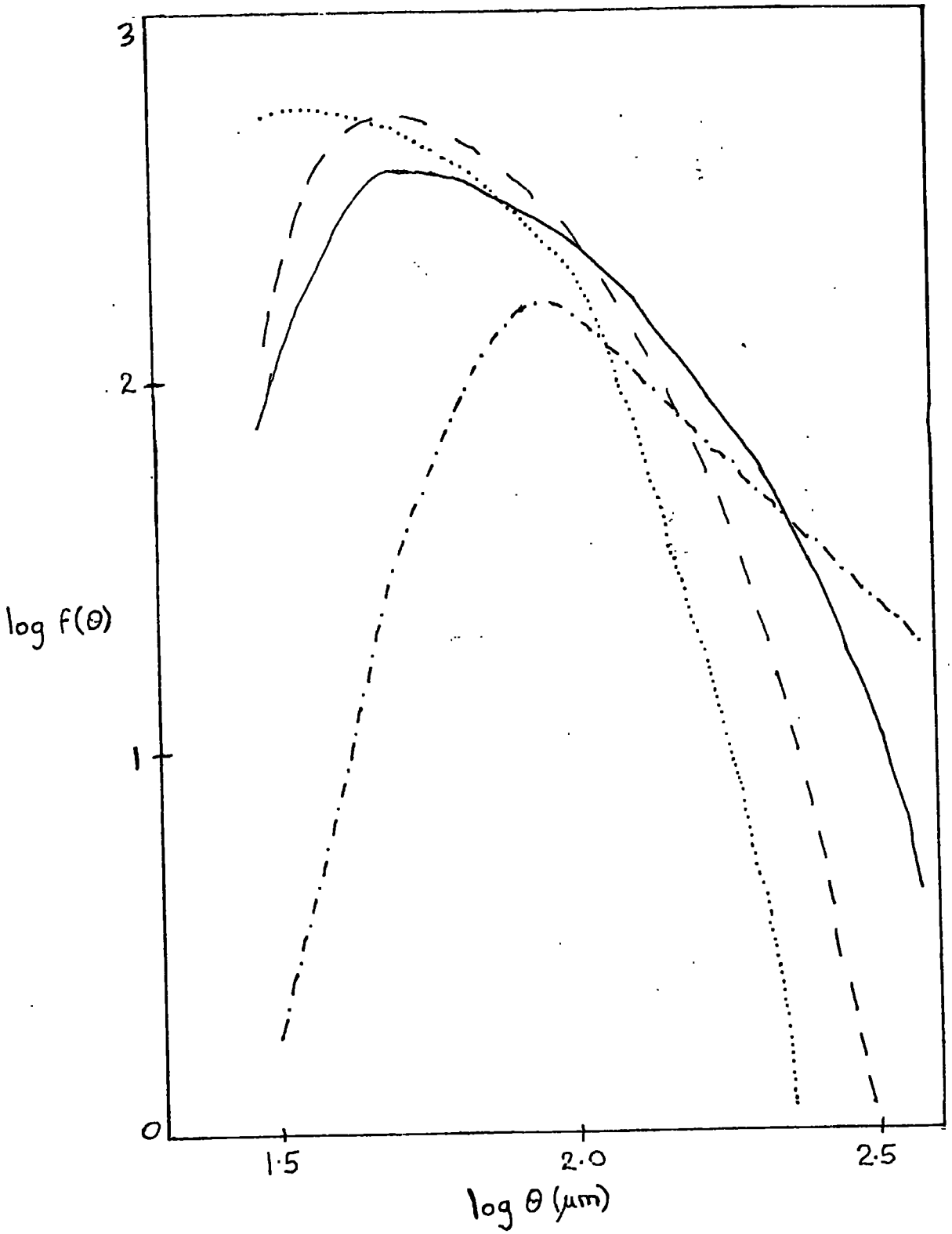

Distribution of angular diameters expected from clusters at redshift $z = \cdot 05$ (dot/dash curve), $z = \cdot 10$ (solid curve), $z = \cdot 15$ (dashed curve) and $z = \cdot 20$ (dotted curve). The vertical scale is arbitrary.

Figure 7.9

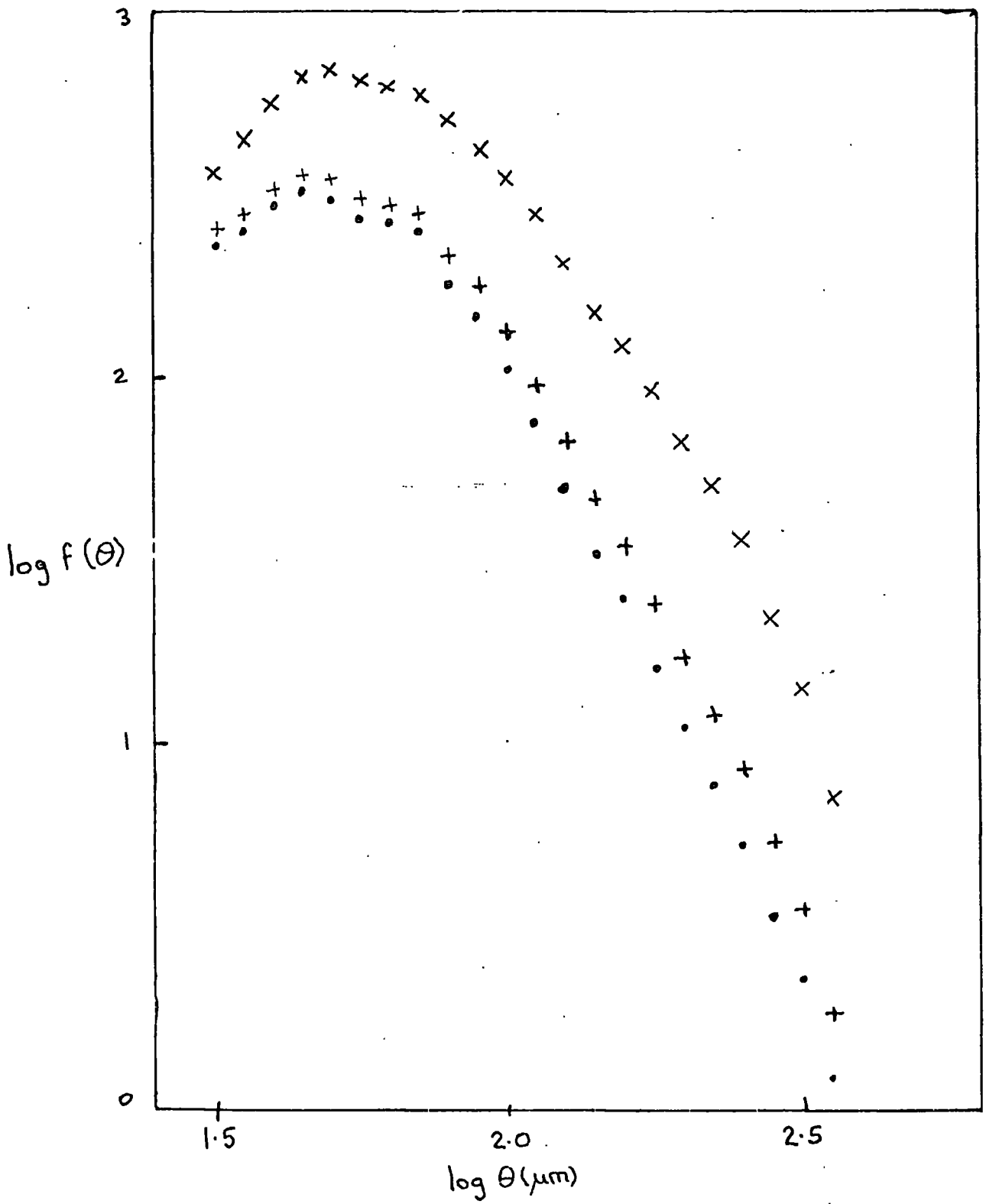

Differential angular diameter counts f(θ) for a mean distribution with the parameters for the R sample (·), and with the addition of small (+) and large (x) clusters at z = 0.1 (see text). The vertical scale is arbitrary.

Figure 7.10

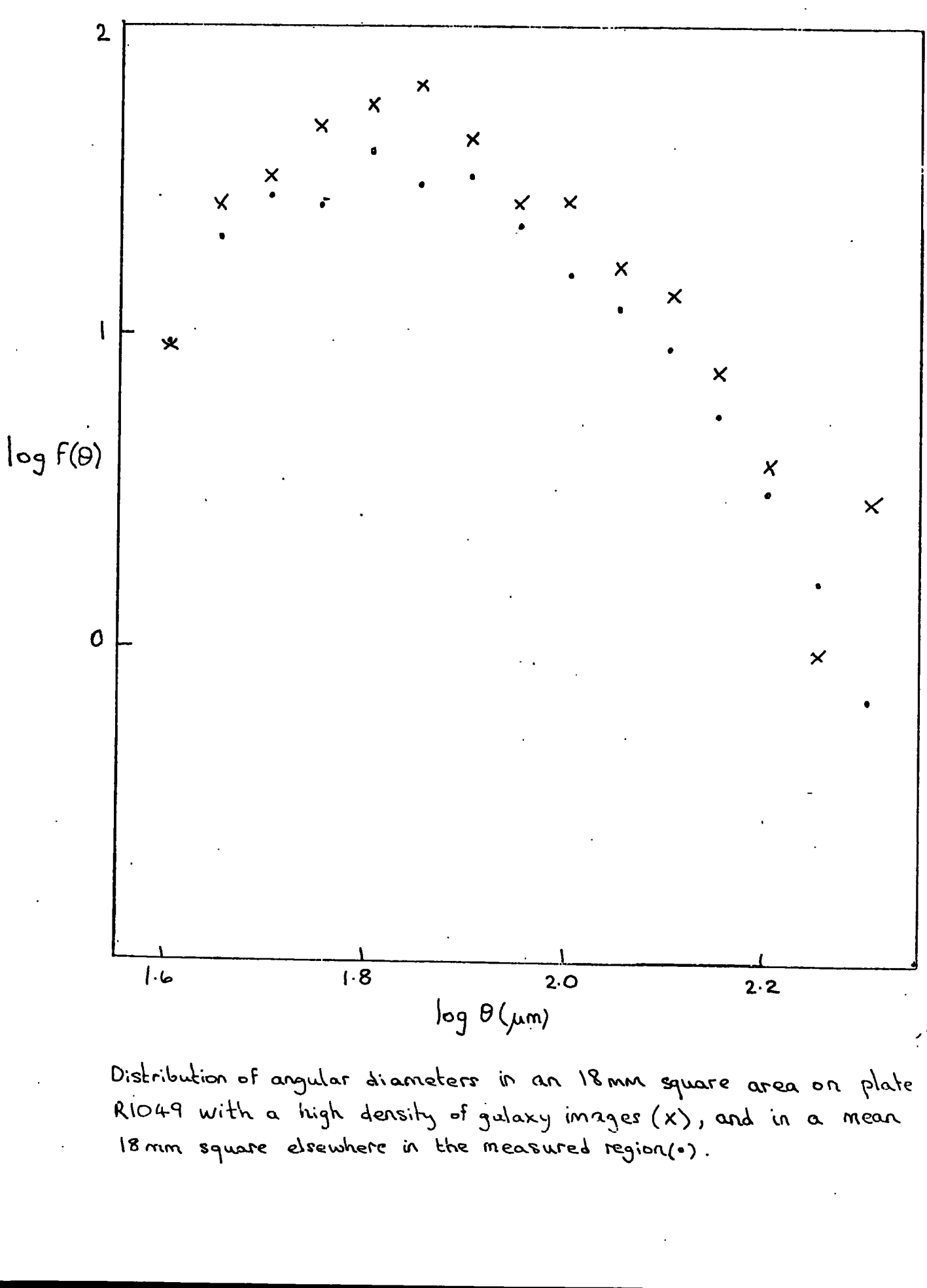

Distribution of angular diameters in an 18 mm square area on plate R1049 with a high density of galaxy images (x), and in a mean 18 mm square elsewhere in the measured region(•).

Figure 7.11

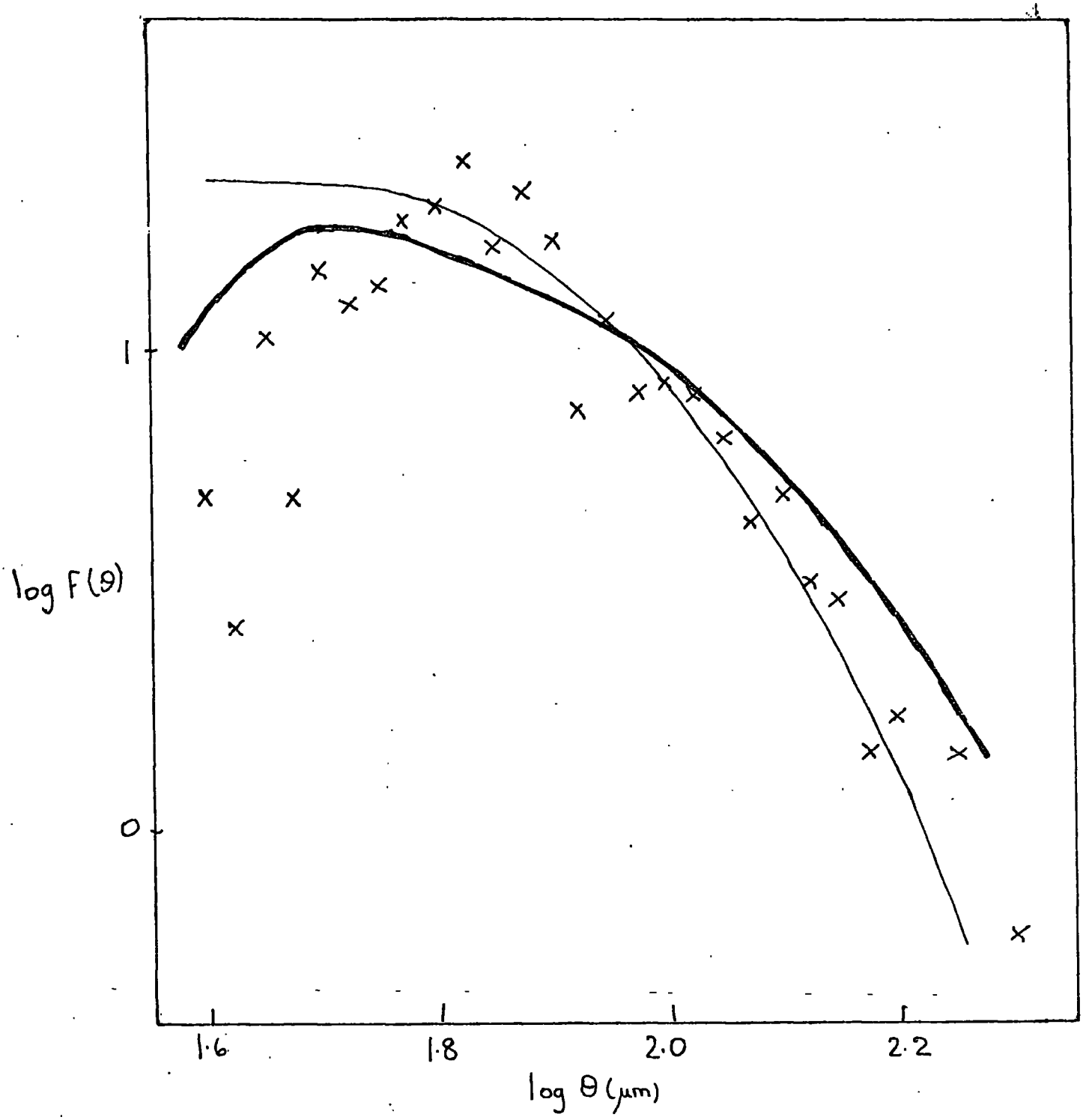

Distribution of angular diameter counts in the high density region in excess of the mean for the R sample (crosses) compared to the expected distributions for clusters at $z = .15$ (heavy line) and $z = .20$ (thin line), arbitrarily normalized.

this has been smoothed over adjacent bins because of the poor statistics. Superimposed on it are the curves for clusters at $z = \cdot 15$ and $z = \cdot 20$ arbitrarily normalized. It can be seen that there is rough agreement for the $z = \cdot 15$ case - the slope of the drop-off for $\log \theta \gtrsim 1 \cdot 8$ being similar in each case and this is the feature which probably best describes the different expected curves (see figure 7.8). It may be tentatively concluded therefore, that the cluster visible on the plate has a redshift of approximately 0·15. With better defined rich clusters, this method could be used with much more certainty, or alternatively for a cluster of known redshift the shape of the $f(\theta)$ curve could be used to check on the accuracy of the model used in the angular diameter determinations and/or the parameters μ_{11m}, σ of the best fit.

This method of distance estimation is analagous to that of Abell (1962) who used the apparent luminosity function, that is the distribution of apparent magnitudes, and similar to that of Press and Schechter (1976; also Turner and Gott 1976) though they used a maximum likelihood test on the brightest members, rather than the overall distribution, - this could possibly be imitated by using the largest few galaxies - and that of Sandage (1972, 1975, also Sandage and Hardy 1973) who used the brightest cluster galaxy as a standard candle.

It should be noted that these tests require the

members of the cluster to be known (so that the brightest can be measured etc.,) though generally it is assumed that all galaxies observed in some small area are cluster members, whereas the test described above merely subtracts a mean diameter distribution from the distribution for the cluster region.

7.5 JOINT DISTRIBUTION OF ANGULAR DIAMETER AND CENTRAL BRIGHTNESS

In the calculation of the angular diameter counts it is evident that given the distance (i.e. redshift) and absolute magnitude of a galaxy of any type, the angular diameter and central surface brightness can both be obtained. That is θ and S_o are functions of M and z for a given model and it follows that M and z are functions of θ and S_o for any particular type of galaxy (though not necessarily single valued functions). Theoretically, given the angular diameter and central intensity of a given type of galaxy, the redshift and absolute magnitude can be determined. This has to be done graphically since the simultaneous equations can not be solved analytically. Figure 7.12 shows the lines of S_o = constant and θ = constant on the (M,z) plane for ellipticals with model parameters appropriate for plate J1920. Unfortunately as can be seen these are

Figure 7.12

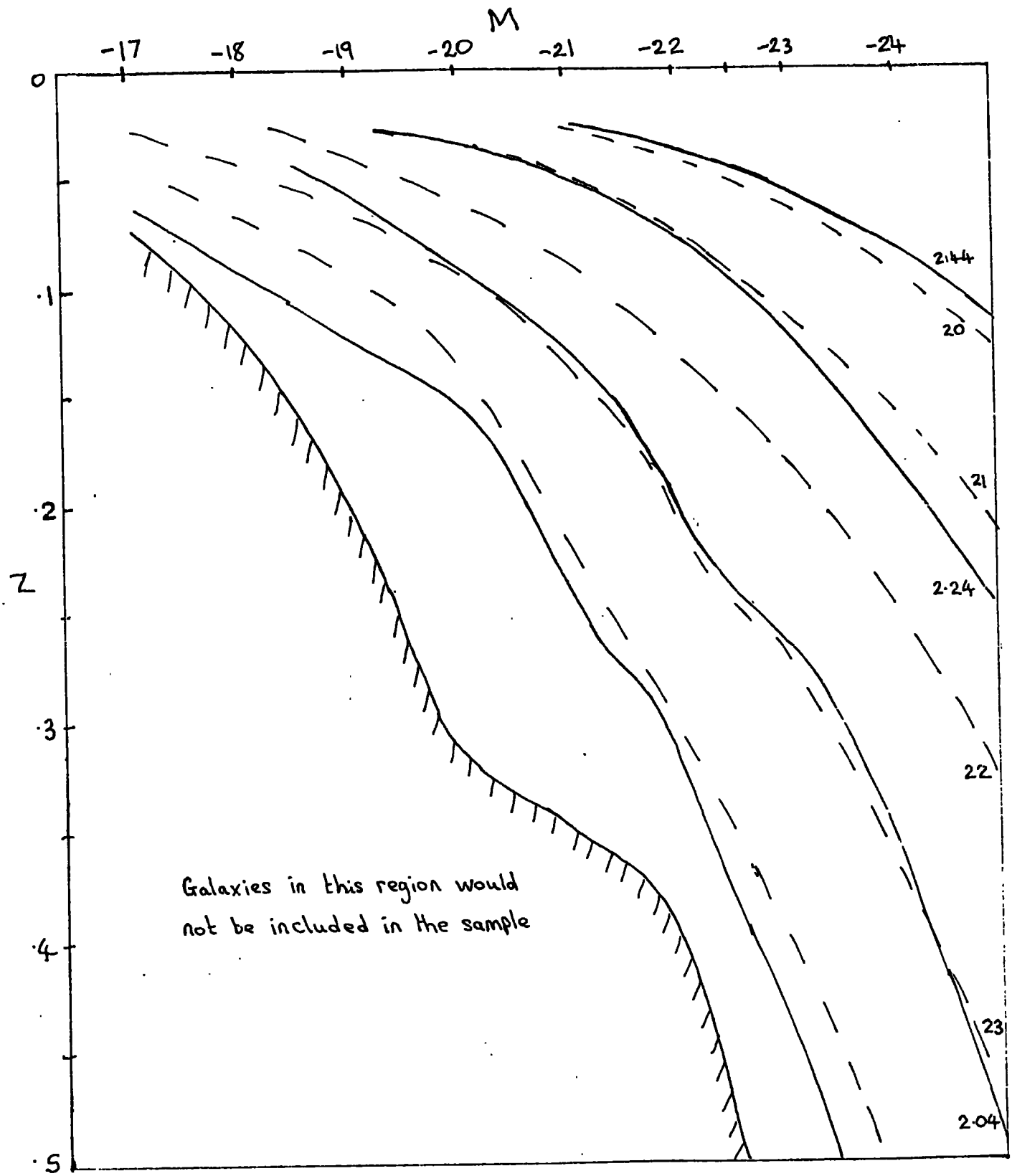

Joint distribution of central brightness S_o and angular diameter θ with absolute magnitude M and redshift z for ellipticals, for the model parameters used for the J1920 sample. The solid lines are curves of constant θ (labelled by $\log\theta(\mu m)$), the dashed lines are curves of constant S_o (labelled in magnitudes).

quite similar, so it is difficult to judge the correct (M,z), that is many different (M,z) combinations give approximately the same (θ,S_o). This is less so for spirals (figure 7.13) since they all have the same intrinsic central brightness, so S_o depends mainly on z and only on M through the radius parameter a(M) effecting the dilution due to seeing. In practice, there will be variations from the simple rules relating the radius parameter and intrinsic central intensity to the absolute magnitude which were used in section 5.4, so individual determinations will be uncertain.

The difficulties of solving for (M,z) given (θ,S_o) will be reduced when plates are obtained from outside the atmosphere to remove seeing - especially in the case of the more numerous spirals - and in this case, it could prove a useful method. Figures 7.14 and 7.15 show the expected results for ellipticals and spirals for zero seeing and the same limiting isophote as in figures 7.12 and 7.13. Furthermore, if the redshifts are known, further checks on the models used are possible.

Also since θ and S_o are known for each M and z, it follows that their joint distribution is given by

$$N(\theta,S_o)\ \Delta\theta\ \Delta S_o = \sum \Phi(M)\ \Delta M\ \rho\ \Delta V(z)$$

where ΔV is given by equation (5.22), $\Phi(M)$ is the integral luminosity function and the sum is over all (M,z) cells such that $\theta(M,z)$ and $S_o\ (M,z)$ are both in their

Figure 7.13

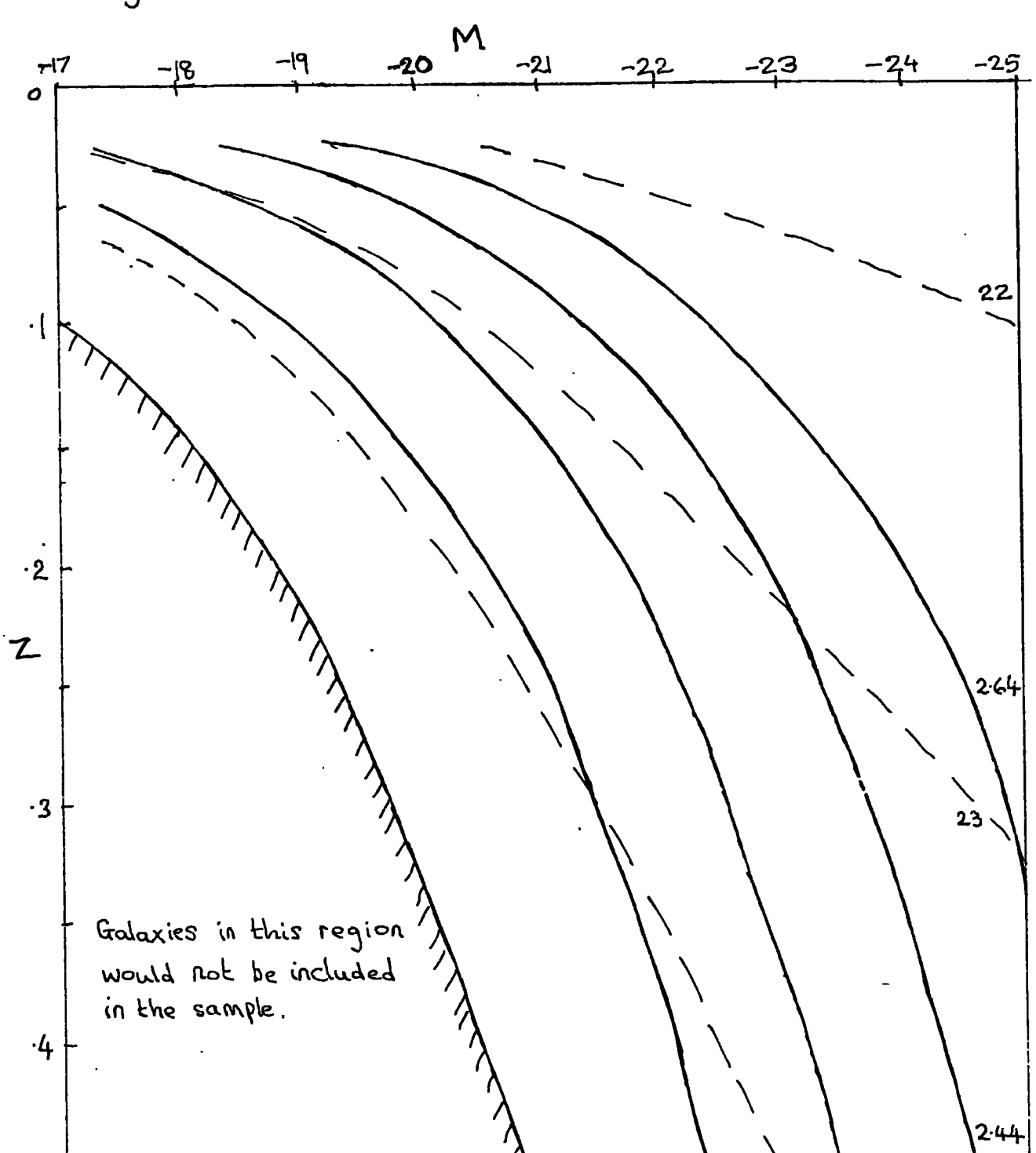

As figure 7.12 but for spiral (Sab) galaxies.

Figure 7.14

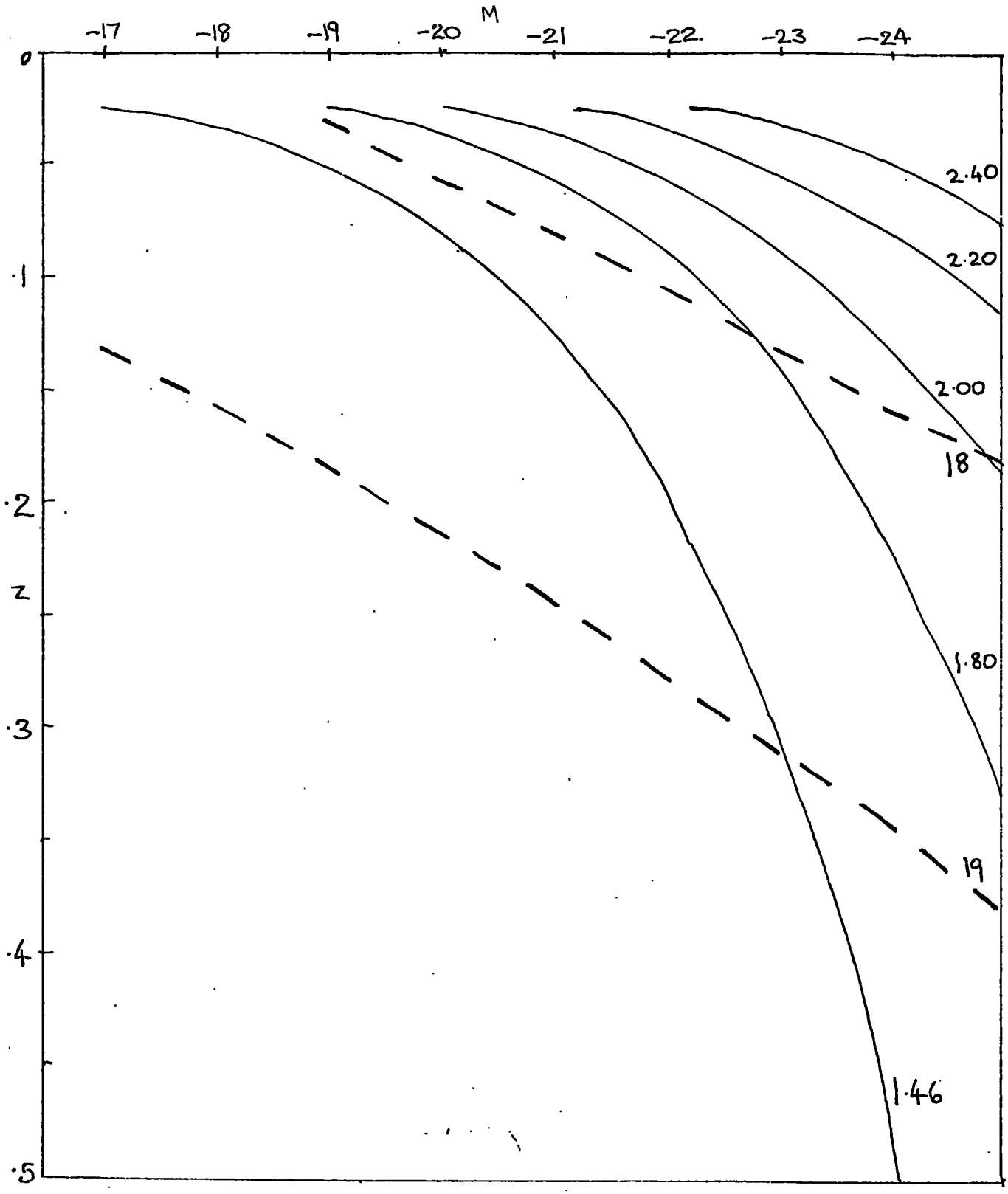

As figure 7.12 but for the case $s = 0$. The limiting angular size of galaxies included in the J1920 sample corresponds to the line $\log \theta(\mu m) = 1.46$.

Figure 7.15

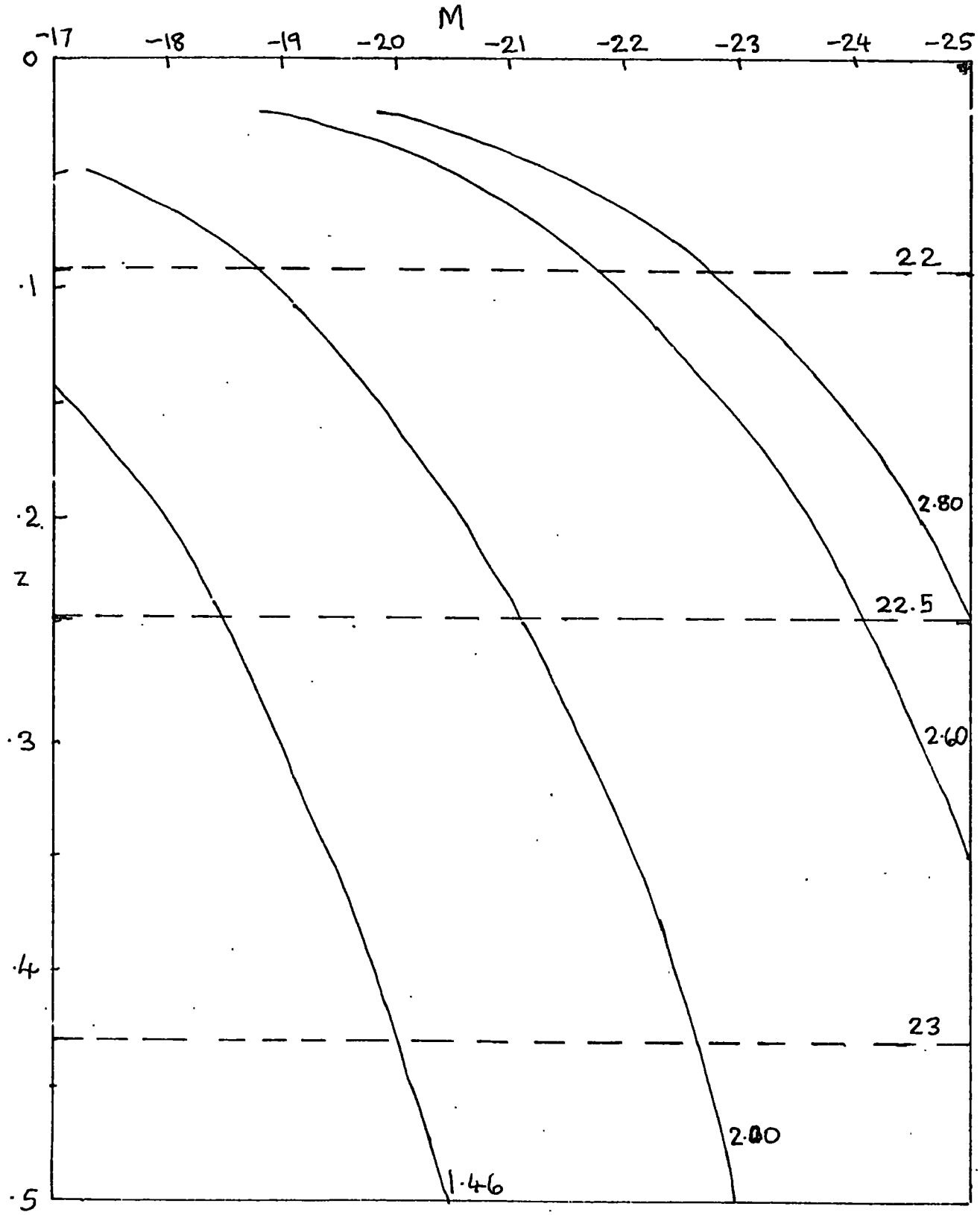

As Figure 7.14 but for spiral (Sab) galaxies.

respective ranges $(\theta, \theta + \Delta\theta)$, $(S_o, S_o + \Delta S_o)$.

This is clearly related to the (TMIN,AREA) plots used in the COSMOS softwave (chapter 3) and might be used to predict the distribution of points in this plane for different types of object, for given seeing and limiting isophote.

7.6 VARIATION OF ANGULAR DIAMETERS OF GALAXIES WITH DISTANCE

It was shown in chapter six that the samples considered in this thesis are not magnitude limited and that the 'apparent magnitude limit' varies with the redshift and type, due to the area limit imposed.

It is evident from table 6.1 that, for the J149 sample, m_{lim} decreases as z increases for each type. This was used in the determination of the function $\phi(m)$ in section 6.1 and implies that galaxies with faint apparent magnitudes are only visible out to some limiting distance.

However, this simple behaviour of m_{lim} is not universal. It may be seen from figure 7.15 that the shapes of the θ = constant curves for spirals, on the (M,z) plane, are very similar for all values of θ and it is easily shown that the lines m(apparent magnitude) = constant fall off more steeply than these. This implies

that m_{lim} decreases with z as above. This is shown schematically in figure 7.16.

On the other hand, figure 7.14 shows that some of the θ = constant curves for ellipticals are steeper than others and it is possible for them to be steeper than the m = constant curves, implying that m_{lim} increases with redshift. This is shown schematically in figure 7.17. Note that this means that very faint apparent magnitude objects must be at a large redshift.

The variation of angular diameters with distance may of course be easily determined for any given type and absolute magnitude, by the methods used in chapter five. This is shown for elliptical and Sab galaxies of various absolute magnitudes in figures 7.18 and 7.19, using the model parameters corresponding to plate J1920 as in sections 7.3 and 7.5. Figure 7.20 shows a comparison of $\theta(z)$ for an elliptical, a spiral, a naive $\theta \propto 1/z$ law and a 'star'. The star curve is for a point source whose apparent magnitude decreases as 5 log z (i.e. in this case z represents the distance), using equation (7.3) which gives

$$\theta^2 \propto \text{constant} - m$$

or

$$\theta^2 \propto \text{constant} - 5 \log z$$

It is clear that both ellipticals and spirals decrease in size less rapidly than the 1/z law, and that the ellipticals, which are relatively more centrally concentrated, have

Figure 7.16

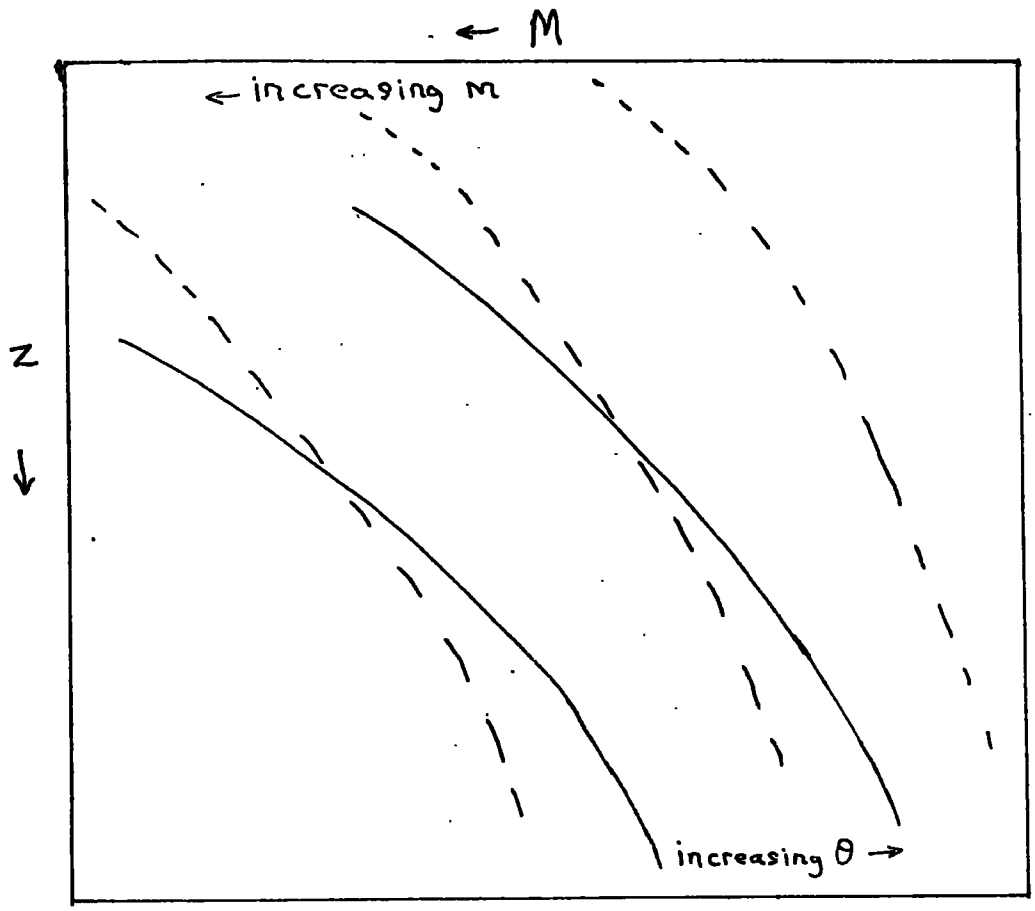

Variation of apparent magnitude and angular diameter on the (M, z) plane for spirals. The solid curves are lines of constant angular diameter, dashed curves are lines of constant apparent magnitude. With increasing z the constant θ lines move to lower values of M.

Figure 7.17

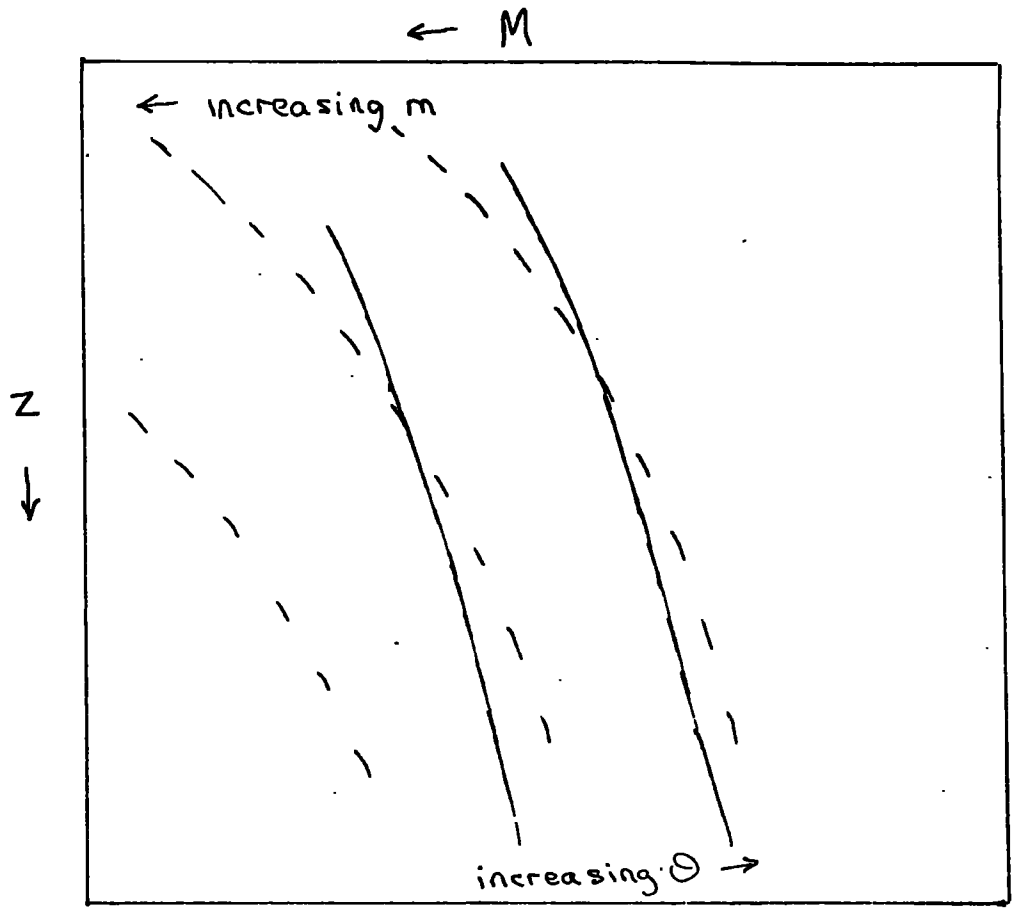

As Figure 7.16 but for ellipticals.
With increasing z the particular constant Θ curves shown moves to higher values of m.

Figure 7.18

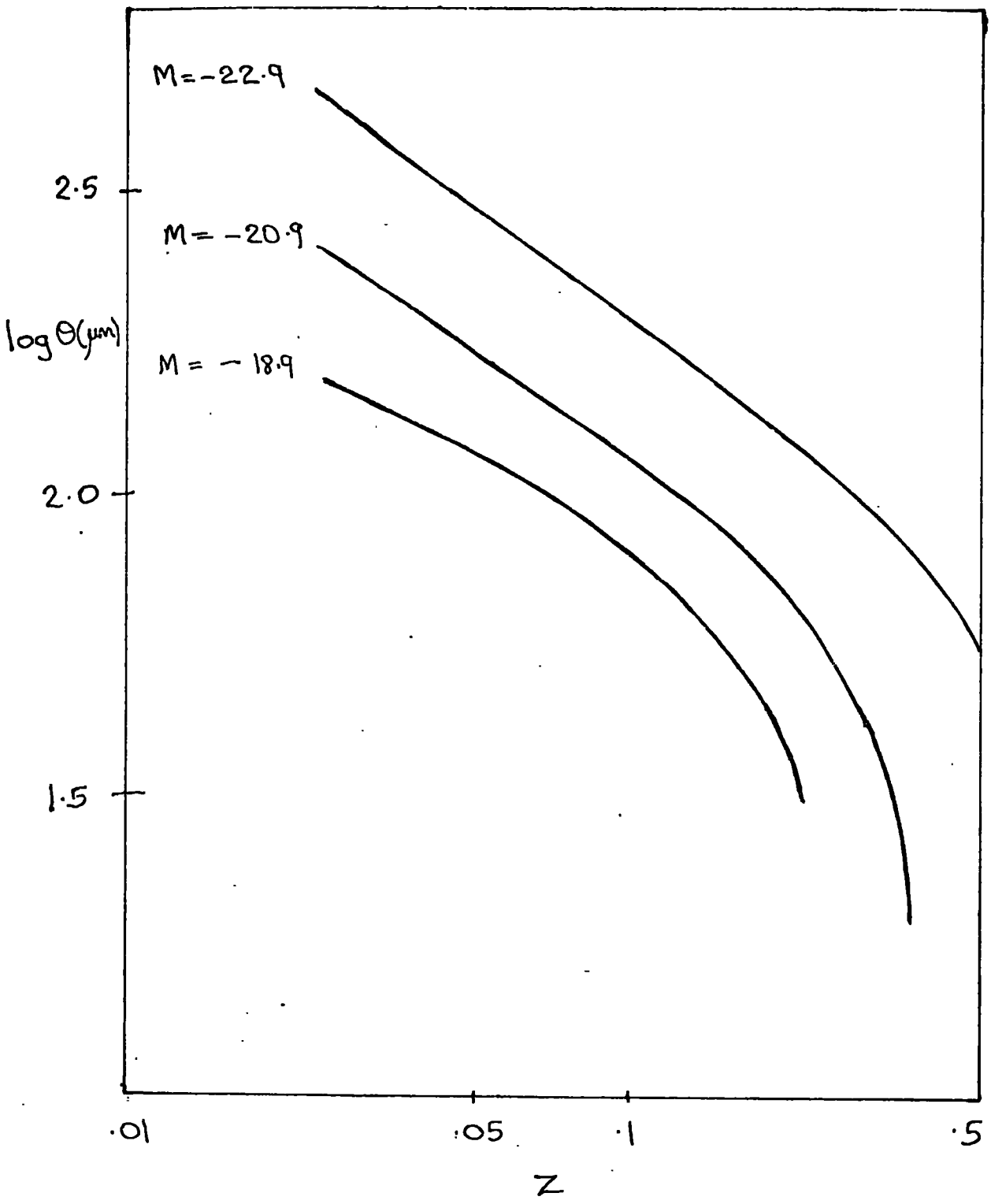

Variation of angular diameter with z for ellipticals of absolute magnitude −18.9, -20.9 and -22.9, with the model parameters of the J1920 sample.

Figure 7.19

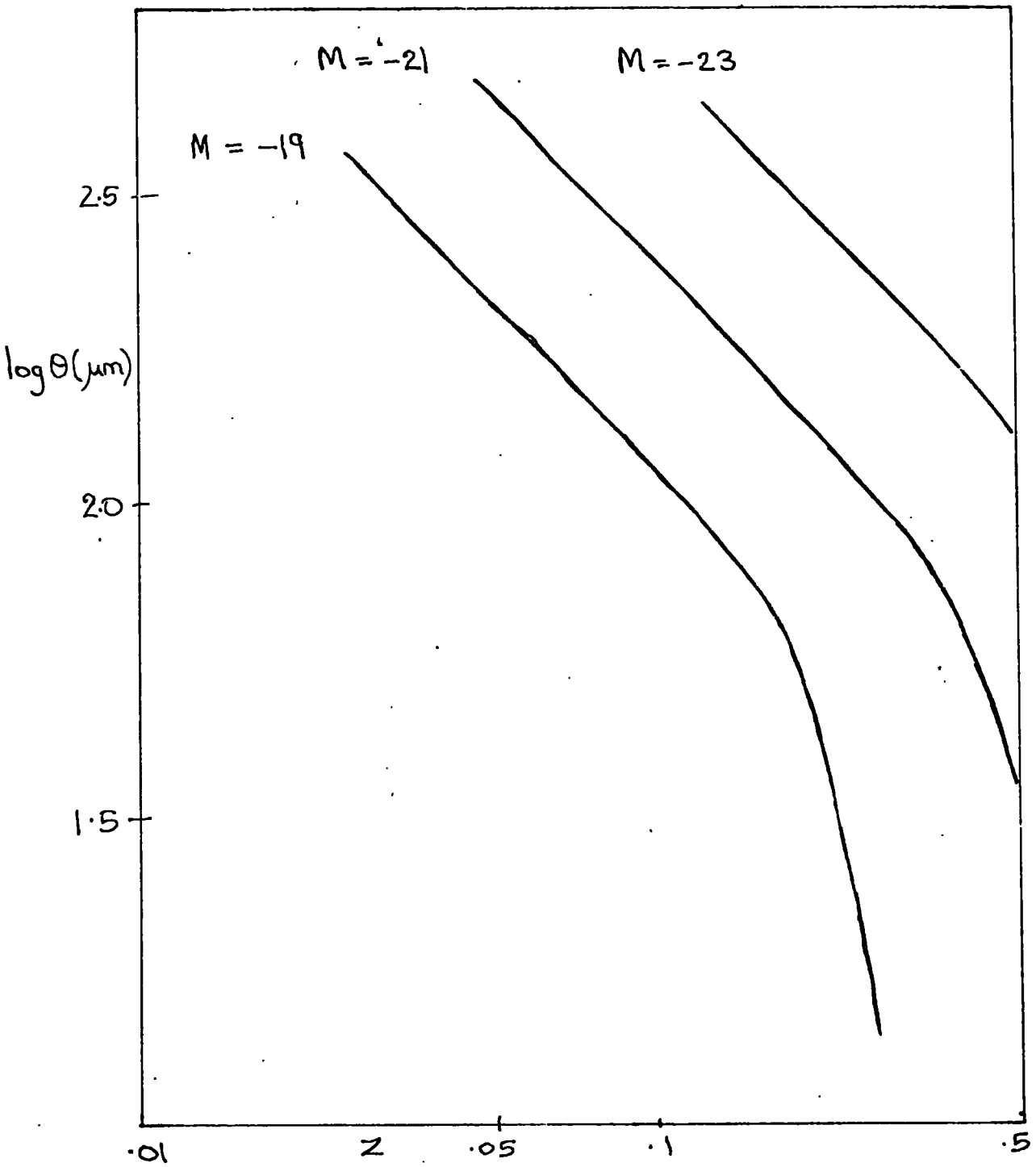

As figure 7.18 but for spirals of absolute magnitude −19, −21 and −23.

Figure 7.20

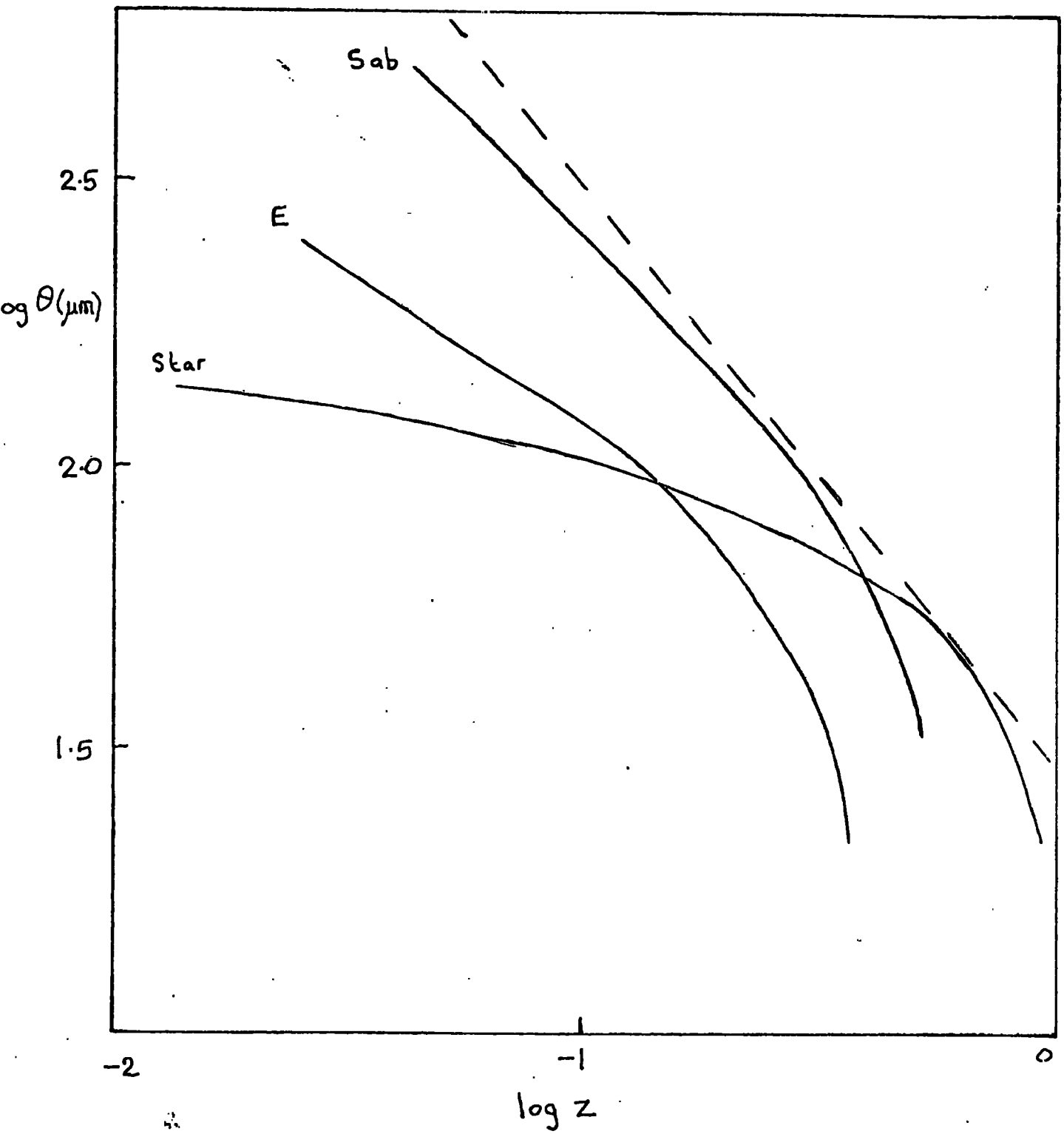

Variation of angular diameter with redshift for an elliptical (E), spiral (Sab) and 'star' (see text) compared to a 1/z law (dashed line).

angular diameters which decrease (initially) more slowly with z than those of spirals; nearer to the behaviour of 'stars' which are just point sources blurred by seeing. In all cases the fall-off is very rapid for $\theta \lesssim 50\mu m$, which is of the order of the seeing (3.''5).

Without seeing, both types decrease in angular size slightly faster than $1/z$. This is because the k-corrections and the $(1 + z)^4$ dependence of surface brightness on redshift cause the limiting isophote to move up the galaxy profile towards the centre of the galaxy, though this is partly compensated for by the evolution (working against the k-corrections) and the fact that the angular diameter distance D_A does not increase as fast as z in the cosmological models considered here.

This again demonstrates the importance of seeing on angular diameters in understanding and interpreting the angular diameter counts.

CHAPTER EIGHT

INTERPRETATION OF THE COVARIANCE FUNCTION RESULTS

'Those that hold that there are lies, damn lies and statistics, must be delighted that Abell could actually name a cluster that amounts to more than the figment of someone's covariance function'.

John Darius.

8.1 THE SPATIAL COVARIANCE FUNCTION

Peebles' basic assumption, that the space surveyed in a catalogue (or other sample), is a fair sample of the universe - in other words, that it would yield the same statistical results if obtained in the same fashion from any other point in the universe - may be stated as follows (Peebles 1973); (1) The distribution of objects (i.e. galaxies, clusters of galaxies, superclusters etc., if they exist) is described by a random stationary process. (2) The ensemble-average values defined by the process are good approximations to the values obtained from our observed sample of the universe.

The second may be reversed to suggest that if the individual results agree to within statistical uncertainties then they are likely to be a good approximation to the ensemble-average values. Peebles and co-workers' own results (see section 2.4) gave good agreement as to the form of the angular covariance function, and since the amplitudes also scaled in the way they were expected to, this implied that the same spatial covariance function was obtained from each. Hence it was assumed that this was a good approximation to the 'universal' spatial covariance function.

From Peebles and Hauser (1974) and Peebles (1974a) this was given by

$$\xi(r) = B r^{-\gamma} \qquad (8.1)$$

with $\gamma = 1{\cdot}77$, $B = 20h^{-\gamma}$ and $0{\cdot}03h^{-1} < r < 30h^{-1}$ Mpc and a possible error in the amplitude of a factor two either way (estimated by calculations with different luminosity functions). The revised calculations of Groth and Peebles (1977) reduced the amplitude to $B = 15h^{-\gamma}$.

Note that for Abell clusters a similar result was found but with an amplitude some ten times as large, while the cross correlation was intermediate (sections 2.9, 2.10).

8.2 DEVIATIONS FROM THE SIMPLE POWER LAW

Peebles (1974a) showed that the results for $w(\theta)$ for the Shane-Wirtanen catalogue, appeared to fall below a power law at angles of a few degrees. This corresponds to a 'typical' linear separation, $\theta D^* \approx 10h^{-1}$ Mpc (where D^* is the representative depth of the survey described in section 2.2, taken to be $220h^{-1}$ Mpc for the Shane-Wirtanen catalogue). Using their revised Shane-Wirtanen results Groth and Peebles (1977) obtained

$$\xi(r) = 15\,(hr)^{-1{\cdot}77}$$

with the power law holding over the range $0{\cdot}05 < hr < 9$ Mpc, the upper limit being the separation $\theta D\, h$ where θ was the angle at which the new results were found to break below the power law form for $w(\theta)$.

They noted that the 'break' defines a characteristic length $\sim 9h^{-1}$ Mpc and hence a characteristic value of $\xi \sim 0.3$ (to within a factor 2). As this is of the order of unity they suggested that this occurs at about the transition from non-linear to linear density fluctuations (Davis, Groth and Peebles 1977, see section 8.6 below).

Groth and Peebles fitted two power laws to the curve, i.e.

$$w(\theta) \propto \theta^{-0.75} \quad \theta \leq 2^{\circ}.5$$
$$w(\theta) \propto \theta^{-1.75} \quad \theta > 2^{\circ}.5 \qquad (8.2)$$

suggesting that $\xi(r)$ falls away from $r^{-1.75}$ to something like $r^{-2.75}$ at large r (though a two power law $\xi(r)$ such as this does not give rise to exactly the w given above, see section 8.6; it does however give quite a good fit to the observations (Efstathiou 1976 unpublished)).

Fall (1975) considered the correlation energy per particle of mass $\langle m \rangle$

$$W = \tfrac{1}{2} \rho \int_0^R \frac{-G \langle m \rangle}{r} \xi(r)\, 4\pi r^2\, dr \qquad (8.3)$$

where ρ is the mean matter density. This is the excess potential energy galaxies have when they are clustered compared to when they have a random distribution. With the power law covariance function $B r^{-\gamma}$ with $\gamma \leq 2$ this is

$$W = \frac{2\pi B}{(\gamma - 2)} G \langle m \rangle \rho R^{2-\gamma} \qquad (8.4)$$

which clearly diverges as $R \to \infty$ (and if $\gamma > 2$ it diverges at small separations). Hence in order for the correlation energy to be finite γ must be < 2 at small separations but change to $\gamma > 2$ at large separations, as was suggested above.

8.3 ANTI-CORRELATIONS

Though Peebles and Hauser noted that there was no evidence of new clustering effects when different scales were considered, the results (including the 3-point function; Peebles and Groth 1975, see note below) are consistent with the interpretation that in the range $\cdot 05h^{-1}$ to at least 5 or $10h^{-1}$ Mpc, there is no preferred scale of clustering and that galaxies are organised in a clustering hierarchy. This may be called the 'continuous clustering' model, the most noticeable characteristic being that the spatial covariance function is positive on all measured scales.

If clusters of galaxies are thought of as an accumulation from an initially more or less homogeneous medium, anti-clustering might be expected - that is sparsley populated regions around clusters giving rise to negative correlations on the corresponding scales. For example, if space is divided into cells and a fraction f

of galaxies in each cell is clustered near its centre, then $\bar{\xi}(r) \simeq -f^2$ on scales between the cluster diameter and the cell size. According to Peebles (1974a)

$$w(\theta) \approx -R_2 f^2 / D^* \qquad \text{for } R_1 \ll \theta D^* \ll R_2 \qquad (8.5)$$

where R_1, R_2 are the cluster and cell diameters. If $R_2 \approx 60h^{-1}$ Mpc (roughly the separation of Abell clusters) then for the Shane-Wirtanen catalogue the criterion is satisfied at $\theta D^* \sim 30h^{-1}$ Mpc or $\theta \sim 8^\circ$. Now $w(8^\circ) \approx \cdot 01$, so could not be consistent with $f = 1$ (all galaxies in the central cluster) as this would give $w \approx -\cdot 2$, though if $f \approx \cdot 2$, $w \approx -\cdot 008$, so could conceivably be within the statistical uncertainty of the estimated w. One possible way to remove this discrepancy is to cluster the clusters and possibly also the superclusters and so on.

NOTE

The 3-point covariance function is defined so that the probability of finding objects in solid angles $\delta\Omega_2, \delta\Omega_3$ separated by angle θ_{23} and distance θ_{12}, θ_{13} respectively from a given galaxy is

$$\delta P = \mathcal{N}^2 \left[1 + w(\theta_{12}) + w(\theta_{23}) + w(\theta_{31}) + z(\theta_{12}, \theta_{23}, \theta_{31})\right] \delta\Omega_2 \delta\Omega_3$$

In practice if the area to be studied is divided into equal cells and the number of objects in cell i is n_i, then

$$z(\theta_{ij}, \theta_{jk}, \theta_{ki}) = \frac{\langle n_i n_j n_k \rangle}{\langle n_i \rangle \langle n_j \rangle \langle n_k \rangle} - \frac{\langle n_i n_j \rangle}{\langle n_i \rangle \langle n_j \rangle} - \frac{\langle n_j n_k \rangle}{\langle n_j \rangle \langle n_k \rangle} - \frac{\langle n_k n_i \rangle}{\langle n_k \rangle \langle n_i \rangle} + 2$$

where the means are over triples of cells i,j,k separated by angles θ_{ij} , θ_{jk} , θ_{ki} .

8.4 THE DENSITY DISTRIBUTION IN CLUSTERS

A more important model proposed by Peebles in the same paper, depends on the density distribution inside individual clusters and is henceforth referred to as the 'cluster density distribution' model. Given that all galaxies are in identical clusters which are randomly distributed (no superclusters or subclusters) and that the density

$$n(r) = n_g E r^{-\varepsilon} \qquad r < R \qquad (8.6)$$

where n is the mean density of galaxies, E is a constant and R is the cluster radius, then

$$\gamma(r) = \frac{4\pi E^2 n_c I(R/r, \varepsilon)}{r^{2\varepsilon-3}} \qquad (8.7)$$

where n_c is the number density of clusters and if R is large

$$I(R/r, \varepsilon) \approx I(\infty, \varepsilon) \approx \pi^2/4 \qquad \text{for } \varepsilon \approx 2$$

Now comparing with the observational results $\gamma = 2\varepsilon - 3$ so with $\gamma = 1{\cdot}8$, $\varepsilon = 2{\cdot}4$. Hence according to this model a

power law density fall-off $n(r) \propto r^{-2.4}$ can give rise to an angular covariance function close to that observed, even with random cluster centres. This form of density fall-off is also consistent with the cross correlation between galaxies and Abell cluster centres (section 2.10), and it may be surmised that the contribution to $\xi(r)$ from individual Abell clusters is an appreciable fraction of the total on scales $\sim 1h^{-1}$ Mpc.

Peebles however, noted that as Abell clusters are themselves clustered the correlations on scales $\sim 10h^{-1}$ Mpc should be up by a factor of 2 or 3, and since the power law continues, the density fall-off in the cluster must fall below $r^{-2.4}$ just enough to compensate for the extra correlation from superclusters. Further the density appears to level off near the centre of clusters such as Coma at a radius of a few hundred kpc (Bahcall 1973, 1975), so the contribution from Abell clusters on these scales must also level off and in order to maintain ξ as a power law an additional (and just sufficient) contribution must be made by compact groups. A specific continuous clustering model of this nature was considered by Peebles (1974e).

In a refinement of this model, Seldner and Peebles (1977a) concluded that the covariance functions for galaxies and cluster centres and the cross correlation between the two could all be as observed if the galaxies had an $r^{-2.4}$ density fall-off inside clusters while the

clusters are clustered according to $\xi_A \propto r^{-1.8}$, with the amplitude E, in equation 8.6 approximately 165 to give the correct amplitude B in equation (8.1) using equation (8.7).

It might be noted that an isothermal sphere has a density fall-off fairly similar to this $r^{-2.4}$ law (e.g. Peebles 1971) and apparent density distributions are often fitted to projected isothermal type distributions (e.g. MacGillivray et al 1976b). Also most dynamical models of clustering seems to have similar fall-offs, $r^{-\varepsilon}$ with $\varepsilon \approx 2{\cdot}3$ or possibly slightly greater (e.g. White 1976, Aarseth and Binney 1978).

8.5 GALAXY FORMATION

The hypothesis that the clustering phenomenon is continuous was shown by Peebles 1974c) to fit into the gravitational instability picture of galaxy formation, and the particular form $\xi(r) \propto r^{-1.8}$ was shown to imply an initial 'white noise' spectrum of initial perturbations - that is the Fourier amplitude of the fractional deviation from the mean density, of perturbations of wavenumber k, δ_k, is such that the power spectrum $|\delta_k|^2 \propto k^n$ with $n = 0$ (Peebles 1974d). This is equivalent to totally random initial perturbations.

Fall (1975) also noted that the lack of significant features (i.e. peaks and dips; the 'break' discussed above is quite smooth and is not a feature in this sense) and anti-correlations and the long range natures of the correlations seemed to be consistent with the gravitational instability theory in which all large scale structure is assumed to be the result of gravitational attraction, which is itself featureless and long range.

Gott and Rees (1975) pointed out explicitly that if the spectrum was a power law then the perturbations had to be isothermal.

Peebles and Groth (1975) noted their 2- and 3-point functions appeared to be as predicted by a hierarchical model of the type proposed by de Vaucouleurs (1970), on small scales ($\lesssim 5h$ Mpc), with the index of the covariance function corresponding to de Vaucouleurs 'thinning' factor.

This idea of a finite hierarchy, that is a model where clusters have hierarchical structures, may correspond to the way in which clustering is built up in the isothermal gravitational instability theory (since in this theory, galaxies form first, then clusters).

Soneira and Peebles (1977) constructed the hierarchy as follows: Cluster centres are distributed randomly in space. In a sphere of radius r_1 about each centre randomly place η subcentres (where η is a random variate). In a sphere of radius $r_2 = r_1/\lambda$ (where λ is a constant) about each of these subcentres place η further subcentres and so on,

until the L th level where there are on average $\langle\eta\rangle^{L}$ points in $\langle\eta\rangle^{L-1}$ spheres each of radius $r_1 \lambda^{1-L}$.

In this model the points are distributed with a maximum correlation length $2r_1$ and the typical density within a cluster of size r varies as $r^{-\gamma}$ with $\gamma = 3 - \log\langle\eta\rangle/\log\lambda$ Note that the 'clusters' are not distinct, they may overlap considerably, making a "continuous sea of clustering".

Doreshkevich and Shandarin (1978) studied the problem from the point of view of the rival adiabatic theory of galaxy formation (e.g. Doroshkevich, Sunyaev and Zeldovich 1974). As their initial spectrum they used $|\delta_k|^2 \propto k^{n-2} \exp(-kR)$ where R is the minimum scale of surviving perturbations, but only considered the distribution of Abell type clusters - finding that their predictions agreed with Hauser and Peebles' (1973) results. In their theory the covariance function of individual galaxies on small scales is due to the relaxation of the rich clusters and is hence independent of the large scale correlations. They considered that $\xi \sim r^{-2}$ could arise in this way similarly to the distribution of stars in an elliptical galaxy (Binney 1976). Adiabatic theory also predicts a preferred scale of clusters, i.e. a preferred cluster size $\sim 25h^{-1}$ Mpc and, if $\Omega \sim .1$, a preferred mass $\approx 2 \times 10^{15}$ $M_\odot$.

The relevance of the statistical measures of clustering to galaxy formation theories was reviewed by Jones (1976).

8.6 EVOLUTION OF CORRELATIONS

The BBGKY (Bogolyubov, Born, Green, Kirkwood, Yvon) equations of the theory of non-ideal gases maybe used as a basis for theoretical considerations of the evolution of correlations.

The BBGKY equations (e.g. Montgomery and Tidman 1964) are a set of coupled equations

$$\left(\frac{\partial}{\partial t} + \sum \underline{v}_i \cdot \frac{\partial}{\partial \underline{x}_i} - \sum \frac{\partial \phi_{ij}}{\partial \underline{x}_i} \cdot \frac{\partial}{\partial \underline{v}_i}\right) f^{(n)} = \int \sum \frac{\partial \phi_{i\,n+1}}{\partial \underline{x}_i} \cdot \frac{\partial f^{(n+1)}}{\partial \underline{v}_i} \, d\underline{x}_{n+1} \, d\underline{v}_{n+1}$$

relating all orders of the mass correlation function, $f^{(n)}$, and the gravitational potential ϕ. The $f^{(n)}$ are directly related to the n-point correlation functions. The sequence can be truncated if the observed result that the 3-point correlation function ζ is a simple quadratic in ξ, i.e.

$$\zeta(r_1, r_2, r_3) = Q\,(\xi(r_1)\xi(r_2) + \xi(r_2)\xi(r_3) + \xi(r_3)\xi(r_1)) \qquad (8.8)$$

is assumed to be generally true.

In the case of an Einstein-de Sitter universe (i.e. $\Lambda = 0$, density parameter $\Omega = 1$ ($q_0 = \frac{1}{2}$), zero pressure) with no preferred scales in the initial irregularities in the matter distribution and certain other assumptions (non-gravitational forces can be neglected, the effect of discreteness of particles can be ignored, the growing mode of the density irregularities approximates a random Gaussian process with power spectrum k^n, bound virialized groups are stable over a Hubble time) the spatial two point

correlation function is

$$\bar{\xi}(s,t) \propto R(t)^{5+n} s^{-(3+n)} \quad \text{at large proper distance } s \qquad (8.9)$$

$$\bar{\xi}(s,t) \propto R(t)^{3} s^{-(9+3n)/(5+n)} \quad \text{at small proper distance } s \qquad (8.10)$$

(Peebles and Groth 1976, Davis and Peebles 1977). Note that this later form is exactly that which was assumed for the evolution of $\bar{\xi}$ in section 2.3 in the case $\eta = 3$.

Using computations with $n = -0{\cdot}1$ (so that $\gamma = 1{\cdot}776$; if $\gamma = 1{\cdot}8$ then $n = (9 - 5\gamma)/(\gamma - 3) = 0$ so the spectrum corresponds to 'white noise' (Peebles 1974c)), Davis, Groth and Peebles (1977) obtained numerically the form of $\bar{\xi}(s)$ between the limits at large and small s given above, and used these to obtain the expected shape of $w(\theta)$. Using different models of the behaviour of $\bar{\xi}$ in the 'transition region' where $\bar{\xi} \sim 1$ curves were found all of which agree well with Peebles' observed curves for the Zwicky, Shane-Wirtanen and Jagellonian catalogues. The value of Q arising from these models is around $0{\cdot}7$, in reasonable agreement with the observed $1{\cdot}0 \pm {\cdot}2$, bearing in mind the uncertainties in the observations and the models. The most impressive feature though is the agreement of the break point, that is where w falls below a $\theta^{-0{\cdot}8}$ law. This change of slope of w is also sharper than for a two power law model

$$\xi(r) \propto r^{-1.8} \qquad r \leq R_c \qquad (8.11)$$

$$\xi(r) \propto r^{-2.9} \qquad r > R_c \qquad (8.12)$$

(c f.equations 8.9, 8.10 with n = -0·1) where R_c is the value of r at which the two slopes intersect (which is very nearly the same as the two power law $\xi(r)$ mentioned previously in section 8.2). This is because with increasing r, ξ first rises above the $r^{-1.8}$ asymptote then falls more rapidly than $r^{-2.9}$ finally approaching this second asymptotic form from below.

The dispersion of velocities can also be obtained from the computations, and they were found to agree with that expected from Peebles' 'cosmic virial theorem' (Peebles 1976a, 1976b).

N-body experiments (Fall 1978) with $\Omega \approx 1$ have confirmed that for a 'white noise' spectrum, a power law covariance function with $\gamma = 1{\cdot}8$ is obtained on small scales, starting from various initial conditions. Other N-body experiments show that different values of n and Ω also give rise to power law correlation functions (Efstathiou 1977, private communication).

Davis, Groth and Peebles also considered models with $q_0 < \frac{1}{2}$. The computations were done as perturbations to the $q_0 = \frac{1}{2}$ solutions. As q_0 decreases the break occurs at higher ξ and w falls away from the power law sooner and

faster making the agreement with observation less satisfactory. This is in apparent disagreement with Fall (1975, 1976b) who used the correlation energy (which should be roughly equal to the random kinetic) and Peebles' estimates of B and γ to show that the observed velocity dispersion - $\sim$50 km s^{-1} for field galaxies (Sandage and Tammann 1975), $\sim$1000 km s^{-1} for galaxies in large clusters (Rood et al 1972) - was inconsistent with $\Omega \approx 1$ and Fall considered the most likely values to be $0{\cdot}01 \lesssim \Omega \lesssim 0{\cdot}05$.

Gott and Rees (1975) also favoured solutions for $\Omega \sim 0{\cdot}1$ rather than $\Omega \sim 1$ since they considered that over most of the range of separations where $\bar{\xi}(r)$ was known the density enhancements would not be truly virialised. The effective γ corresponding to a given n would then be steeper than Peebles' result for the virialised regime, so that $n = -1$ would be more appropriate than $n = 0$, and they claimed that any model with $\Omega \sim 1$ should have a 'spike', or at least a distinct feature at $\sim$ 50 Mpc (corresponding to a mass contained of $\sim 10^{17}$ $M_\odot$ since the Jeans mass remains at this value between the time when the baryon and photon densities were equal and the time of recombination, and perturbations above this mass grow relative to those below it) which would make w flatter than observed on large scales - numerical calculations on a 'spiky' $\bar{\xi}(r)$ show that a wide hump is produced in the $w(\theta)$ curve.

It might be noted here that Seldner and Peebles (1977b) attempted to calculate Ω directly from the covariance function. In section 2.11 the calculation by Seldner and Peebles (1977a) of the number density distribution of galaxies in Abell clusters was described. They found

$$n(r) = 165\, F_R \langle n \rangle (hr)^{-2.4}$$

where F_R depended on the richness of the cluster and was taken to be 1 for R = 1, and 1·6 for R = 2.

Assuming that the mass in clusters is distributed in the same way as galaxies

$$n(r) / \langle n \rangle = \rho(r) / \langle \rho \rangle$$

where ρ is the mass density. Also from the distribution of velocities in the cluster

$$\rho(r) = \sigma^2 / 2\pi G r^2$$

where σ^2 is the line of sight velocity dispersion. It follows that

$$\Omega = \frac{\langle \rho \rangle}{\rho_c} = \frac{4\ \sigma^2\ r_j^{0.4}}{3\ H_0^2\ F_R\ 165\ h^{-2.4}}$$

where r_j (taken to be $2h^{-1}$ Mpc) is a convenient radius (where both equations for ρ are valid) at which to evaluate σ^2. Data for 12 clusters with R = 1 or 2 gave a mean value

$$\Omega = 0{\cdot}69 \pm {\cdot}11$$

8.7 DISCRIMINATION BETWEEN ISOTHERMAL AND ADIABATIC THEORIES

The result for the three-point spatial covariance function ζ obtained by Peebles and Groth (1975) and Groth and Peebles (1977) from the Zwicky and Shane-Wirtanen catalogues i.e.,

$$\zeta(r_1, r_2, r_3) \propto \xi(r_1)\xi(r_2) + \xi(r_2)\xi(r_3) + \xi(r_3)\xi(r_1)$$

agrees with the hierarchical matter clustering expected from the isothermal gravitational instability picture, since it implies

$$\zeta(r, ru, rv) \propto \xi(r)^2 \qquad (8.13)$$

as required (Peebles 1974c, Davis and Peebles 1977, Groth et al 1977). Peebles and Groth (1975) used the observations

$$\xi(r) \propto r^{-1.8}, \quad \zeta(r, ru, rv) \propto r^{-3.6} \qquad (8.14)$$

to rule out the 'cluster density distribution' model in favour of the isothermal gravitational instability model since the calculations using the 'cluster' model with $n(r) \propto r^{-\varepsilon}$ implied

$$\xi \propto r^{-(2\varepsilon-3)}, \quad \zeta \propto r^{-(3\varepsilon-3)}$$

which can not give both observed indices for any choice of ε. The 'cluster density distribution' model may be

identified with adiabatic perturbation theory of galaxy formation (since the contribution at small r is mainly from galaxy clusters, as above), so this would seem to be definite observational evidence in favour of the 'isothermal' theory and against the 'adiabatic theory'. However equation (8.14) is not valid when a realistic cut-off for the cluster radius is applied.

Consider a model in which all galaxies are in clusters of diameter D which are distributed uniformly throughout space, each cluster containing n_g galaxies distributed spherically symmetrically with a power law fall-off of index ε.

Using calculations which simulated the Zwicky catalogue (see appendix for description of simulations), it was found by Shanks (1978) that rather than the $\varepsilon = 2{\cdot}4$ given by Peebles, $\varepsilon \simeq 2{\cdot}25$ gives the correct $w \propto \theta^{-0{\cdot}8}$ out to the required separation, $\theta = 6^{\circ}$ (i.e. the break) if $D = 25h^{-1}$ Mpc - which is comparable to the preferred cluster size on the adiabatic theory - and $n_g \approx 500$ - which gives a mass $\sim 5 \times 10^{14}\ M_{\odot}$, again comparable to the expected preferred mass, if $\Omega \sim {\cdot}1$.

Superclustering of smaller (e.g. $9h^{-1}$ Mpc) clusters was not found to be capable of reproducing the correct behaviour. The conclusion is that for a model of this type, the clusters must be of conventional supercluster size. The 3-point correlation $z \propto \theta^{-1{\cdot}6}$ from the Zwicky

catalogue was reproduced almost exactly by the same model - in clear disagreement with equation (8.14) which would predict $z \propto \theta^{-2.2}$ when $w \propto \theta^{-0.8}$.

Shanks noted that the ease with which the simulation was made to match the observations (i.e. no superclustering, ellipticity of clusters or mixtures of different cluster sizes were necessary) could even be taken as positive evidence for the 'adiabatic' theory and the observational results certainly do not rule it out as Peebles claimed.

Furthermore a hierarchical model - in the 'isothermal' theory - as proposed by Soneira and Peebles (1977) and simulated by Groth et al (1977)-requires more parameters and different types of clusters to obtain the desired results, using the same type of simulations. Note that this hierarchical model appears to be a good approximation to the distribution arising from N-body experiments (section 8.6).

A new analysis due to Mead (Mead 1974, Besag and Diggle 1977) was also applied to the same simulations and the real data by Shanks. This appears to give further support for the 'cluster density distribution' type of model, and evidence against the hierarchical model. This analysis is designed to detect clustering on various discrete scales and it was found to show clustering up to scales of $5.^{\circ}5$ and 1° for the real Zwicky and Jagellonian data, respectively, corresponding approximately to the

'break' points in $w(\theta)$.

The behaviour of the Mead's statistics for the corresponding 'cluster model' simulations was found to be much nearer to that for the real data than was that for hierarchical simulations. The statistics for the distribution of points resulting from N-body experiments, however, agree with those for the hierarchical models, confirming the correspondence noted earlier.

It appears then that the 'cluster density distribution' model - identified with adiabatic gravitational instability theory - can not be dismissed by the observed 2- and 3-point correlation functions. In fact the simulations show that it is easier to match the observations to that model than to a hierarchical model - identified with isothermal gravitational instability theory and, incidentally with the results of N-body experiments - and furthermore the results of the Mead's analysis pose a serious problem to this latter theory.

CHAPTER NINE

CONCLUSION

'To describe the Universe in terms of our present knowledge is to say almost nothing about everything'.

E. Schucking.

9.1 THE SHAPE OF THE COVARIANCE FUNCTION

The results for the covariance function for the very deep samples considered in this thesis are all found to be consistent with a power law form

$$w(\theta) = A\theta^{-\delta}$$

at small separations $\lesssim 0^{\circ}.1$.

Moreover they are consistent with the assumption

$$\delta = 0{\cdot}8$$

and while the $w(\theta)$ curves may be reasonably well fitted by any index from 0·7 to 0·9, the integrated (i.e. smoothed) curves $E(\theta)$, described in chapter 5, indicate that 0·8 is probably the most satisfactory; in agreement with previous observations (see section 2.4).

There is no significant evidence for any features on these small scales, but in each case the curve falls below the extrapolated $\delta = 0{\cdot}8$ power law on slightly larger scales $\sim 0^{\circ}.1$ to $0^{\circ}.2$. This is also reminiscent of the behaviour of the $w(\theta)$ curves obtained by Peebles' group especially for the Shane-Wirtanen catalogue (Peebles and Hauser 1974, Groth and Peebles 1977).

Beyond about $0^{\circ}.15$ or $0^{\circ}.20$ (depending on the sample) there is a region where the $w(\theta)$ estimates are negative. This feature was not present in the results presented by

Peebles' group for any of their samples, though it should appear as a consequence of the operational definition of w used for the estimates as was noted by Jones (1976).

Note that for the less deep samples 1920/100 and 1921 the break and the onset of negative values are moved to larger separations. This is not apparent for the other shallower subsample RS however.

In attempting to relate the break to a physical separation it is not clear what to choose as a 'typical' distance in the sense of Peebles' D^*. Choosing the median redshift z_{med} (i.e. half the galaxies in the sample have $z < z_{med}$) one 'typical' angular diameter distance is 500 h^{-1} to 600 h^{-1} Mpc for the very deep samples (using the z distribution obtained in chapter 6) giving a linear scale $\sim 1h^{-1}$ Mpc. It should be noted however that this is not a <u>maximum</u> or even <u>preferred</u> scale of clustering. This is shown by simulations (see appendix) with clusters of fixed size and power law fall-offs, as these show the same deviation below a power law $w(\theta)$ on the scale $\sim 0^\circ.1$ for much larger clusters of $\sim 25h^{-1}$ Mpc diameter. Hence the scale $\sim 1{\cdot}0h^{-1}$ Mpc can not be interpreted as the scale at which $\xi(r)$ drops below an $r^{-1.8}$ form. This is also a criticism of Peebles and Groth's (1977) estimation of $9h^{-1}$ Mpc as the maximum separation for which $\xi \propto r^{-1.8}$, found from the Shane-Wirtanen catalogue, as calculations simulating a survey to this depth show that $25h^{-1}$ Mpc diameter clusters

also mimic the $w(\theta)$ behaviour of this data. Shanks (1978) has also noted this from his Mead's analysis - where he finds the same scales of clustering $\sim 1^{\circ}$ for the Shane-Wirtanen catalogue depth and $\sim 0^{\circ}.1$ for the very deep simulations while using $25h^{-1}$ Mpc diameter clusters - and notes that these are the scales at which the density contrast remains significant against the background.

Also the fact that the break does not give a separation anywhere near $9h^{-1}$ Mpc seems to invalidate Groth and Peebles' statement that the break occurs at ξ of the order unity, since the present estimate would give ξ almost two orders of magnitude higher. However it should be noted that at the 'representative' distance for the deep samples, the total width of the plates is only $15h^{-1}$ Mpc so the behaviour on scales $\sim 9h^{-1}$ can not be reliably estimated.

It appears then that the present results do not give any clue as to the maximum scale at which

$$\xi(r) \propto r^{-1.8}$$

and in fact, various considerations suggest that previous estimates may be somewhat suspect.

Simulations show that the data may be best compared with a model in which the most important contribution to ξ is from the density distribution in individual clusters (or superclusters), which may be of either 'power-law' or hierarchical nature.

9.2 AMPLITUDE OF THE COVARIANCE FUNCTION

The amplitudes A_i of the angular covariance function estimates for the various samples are in all cases lower than would be expected by scaling Peebles' earlier results to the depth of the present ones using the methods of chapter 6 even if a certain amount of evolution is allowed for. The discrepancy increases with the depth when different depths are studied on the same plate, and for the deepest samples is a factor of about 2 to 2·5 for a non-evolving model ($\gamma = 3{\cdot}0$; see table 6.2).

This obviously implies a corresponding change in the amplitude of the spatial covariance function, given by equation (2.47)

$$B = \frac{A_i\,\Gamma(\gamma/2)}{S_i\,\sqrt{\pi}\,\Gamma((\gamma-1)/2)}$$

where S_i, given by equation (2.26), is the scaling factor. Now for $\gamma = 1{\cdot}8$ this gives

$$B = 0{\cdot}296\ \frac{A_i}{S_i} \qquad (9.1)$$

Note that the scaling factors calculated in chapter 6 for the Zwicky, Shane-Wirtanen and Jagellonian samples will be different from those obtained by Peebles and co-workers since the luminosity function, k-corrections and evolutionary effects used are different. However the scaling factor

for the Zwicky catalogue, for example, used in table 6.2, gives $B = 16h^{-1.8}$ which agrees fairly closely with Peebles and Hauser's (1974) estimate

$$B = 20h^{-1.8}$$

Note that the discrepancy is in the opposite direction when using the Shane-Wirtanen data, since from table 6.2

$$B = 22h^{-1.8}$$

while Groth and Peebles obtained

$$B = 15h^{-1.8}$$

In general the present data gives

$$B = 16h^{-1.8} \quad A / A_z^s \tag{9.2}$$

with A/A_z^s from table 6.2. For the deepest samples this then gives approximately

$$B = 7h^{-1.8} \tag{9.3}$$

where as noted above the difference between this and previous estimates is partly due to changes in the model of the galaxy distribution and partly to the discrepancy in the scaled amplitudes of the angular covariance function. It also depends to a degree on the amount of correlation evolution included, the present amplitude B being higher the greater the evolution allowed.

9.3 FINAL CONCLUSIONS AND THOUGHTS

The shape of $w(\theta)$ corresponds to earlier estimates and hence supports arguments based on the previous results, except in that the new results break below a power law of index - 0·8 earlier than would have been expected, giving rise to a rough linear scale of $1h^{-1}$ Mpc.

It is possible that this behaviour may be partly the result of the small area surveyed - estimates on the scale of the plate (only $15h^{-1}$ Mpc at a 'typical' distance) clearly being uncertain - but equally simulations with fixed cluster size give a break in $w(\theta)$ corresponding to smaller and smaller linear separations as the depth is increased.

The amplitude of $w(\theta)$ is lower than expected for all the present samples. It was initially hoped that behaviour of this kind could lead to an estimate of the rate of the growth of clustering - but the discrepancy is too large to be accounted for by any reasonable correlation evolution.

Possible sources of error in w are the estimate of the mean density $\mathcal{N}$ from a limited sample and the method of edge correction, but these will be small especially on the small scales where the amplitude is calculated.

Assuming that the scaling of the deep samples has been successfully carried out - and there is little room for change of $\gtrsim 10\%$ if the agreement of the angular diameter

counts, discussed in chapter five, is to be maintained - there appear to be three possible explanations for the discrepancy; (1) The space nearby or the space at a depth surveyed in the present samples are not representative of the overall average distribution throughout the universe, (2) the nearby samples or the distant samples are not representative of the average distributions at the corresponding depths, or (3) the samples are contaminated either by stars or random errors. The first explanation is rather unlikely as it requires inhomogeneities of extremely large scale, leaving the second as the most likely cause, i.e. poor sampling, although the third is also a serious possibility, as was discussed in sections 4.5 and 6.3.

Peebles (1974) has claimed that the Zwicky, Shane-Wirtanen and Jagellonian samples are 'fair samples' of the underlying distribution, mainly on the evidence of the good scaling between the amplitude estimates, and, despite some possible criticisms levelled at the samples by Phillipps et al (1978), it seems likely that this is the case.

Hence we are left with the most likely explanation; that the small areas surveyed are not of sufficient size - despite containing several thousand galaxies - to be a fair sample of galaxies at the depths sampled, and while it is obviously impossible to discern the fairness of a sample without a similarly processed larger sample, the subjective impression, when looking at the measured area

of the plate, is that it is relatively deficient in prominent clusters.

Despite this disappointing conclusion, the methods discussed in this thesis, when applied to much larger areas of the sky, e.g. several whole Schmidt plates, may indeed prove a valuable and powerful means of exploring the large scale distribution of matter in the universe at relatively recent epochs.

APPENDIX A

The Robertson-Walker Metric

The Cosmological Principle, which is central to much of cosmological theory, states that the universe is spatially homogeneous and isotropic (or equivalently is isotropic about every point).

Mathematically this implies that the universe is a four-dimensional space with three-dimensional maximally symmetric subspaces with constant cosmic time.

Thus it is possible to choose co-ordinates r, θ, ϕ, t such that the metric takes the form (see e.g. Weinberg chapters13,14)

$$ds^2 = c^2 dt^2 - R^2(t)\left[\frac{dr^2}{(1-kr^2)} + r^2 d\theta^2 + r^2 \sin^2\theta\, d\phi^2\right] \quad (A.1)$$

with $k = 0$ or ± 1, where R is an unspecified function of cosmic time. known as the cosmic scale factor.

Hence the infinitesimal comoving (co-ordinate) volume element

$$dV = \frac{dr}{(1-kr^2)^{1/2}}\, r\, d\theta\, r \sin\theta\, d\phi = \frac{r^2\, dr}{(1-kr^2)^{1/2}}\, d\Omega \quad (A.2)$$

and the corresponding proper volume element is

$$dV_p = R^3(t)\, dV \qquad (A.3)$$

At constant t and ϕ (this may be chosen to be the case for any pair of neighbouring points) the comoving separation at a distance r which subtends an angle θ at the origin is clearly given by

$$dy^2 = \frac{dr^2}{(1 - kr^2)} + r^2\, d\theta^2 \qquad (A.4)$$

and again the proper separation is

$$dy_p = R(t)\, dy \qquad (A.5)$$

Consider two photons emitted from a comoving distance r at cosmic times t_{em} and $t_{em} + \delta t_{em}$ and received at the origin at t_o and $t + \delta t_o$. For each the path is a null geodesic, ds = 0, so

$$\int_0^r \frac{dr_1}{(1 - kr_1^2)^{1/2}} = \int_{t_{em}}^{t_o} \frac{c\, dt}{R(t)} = \int_{t_{em}+\delta t_{em}}^{t_o+\delta t_o} \frac{c\, dt}{R(t)}$$

$$\therefore \quad \frac{\delta t_o}{R(t_o)} = \frac{\delta t_{em}}{R(t_{em})}$$

Thus the fractional change in wavelength of the light i.e. the redshift,

$$z = \frac{\lambda_o}{\lambda_{em}} - 1 = \frac{\delta t_o}{\delta t_{em}} - 1$$

i.e.

$$1 + z = \frac{R(t_o)}{R(t_{em})} \tag{A.6}$$

Since each photon has its energy (hc/λ) decreased by a factor (1+z) and they arrive at intervals a factor (1+z) longer than those at which they were emitted, the luminosity of an object at co-ordinate r as seen by an observer at the origin is

$$b = \frac{L}{4\pi r^2 R(t_o)^2 (1 + z)^2} \tag{A.7}$$

where L is the emitted luminosity (as the photons are spread over the surface of a sphere radius $R(t_o)r$ at the time the object is observed).

Hence the "luminosity distance" is defined by

$$D_L = r\, R(t_o)\, (1+z) \tag{A.8}$$

Similarly if an object of proper length y subtends an angle $\delta\theta$ at the origin

$$y = r\, R(t)\, \delta\theta \tag{A.9}$$

so define the "angular diameter distance" by

$$D_A = r\, R(t_o)\, (1+z)^{-1} \tag{A.10}$$

If the Cosmological Principle is supplemented by Einstein's equations of general relativity, then the

universes so described are known as Friedmann universes.

In the matter dominated era (i.e. when the energy density of radiation is negligible compared to the rest-mass density of matter) it may be shown that (see e.g. Weinberg 1972, eqn. 15.3.23)

$$r\,R(t_o) = c\,H_o^{-1}\,q_o^{-2}\left(zq_o + (q_o - 1)\left((2q_o z + 1)^{1/2} - 1\right)\right)(1 + z)^{-1} \qquad (A.11)$$

where Hubble's parameter $H = \dot{R}/R$ and the deceleration parameter $q = -\ddot{R}R/\dot{R}^2$ and the subscript o refers to the present epoch. This then gives D_L and D_A as functions of z.

APPENDIX B

Simulations

A useful way to analyse the data is by way of comparison with the results generated by simulations. Since the present data are for small areas of sky the simulated points are generated directly onto a flat 'plate' - no curvature or projection being necessary.

In general cluster centres (XC, YC) are generated randomly on a slightly larger area than that of the final 'plate' since cluster centres outside the 'plate' can have galaxies inside (if required superclustering can be introduced at this stage by generating a suitable distribution of cluster centres about supercluster centres).

A co-ordinate $x = c^{-1} H_o R_o r_1$ (where r_1 is the co-ordinate distance, see e.g. Weinberg 1972 chapter 14) is then chosen for the centre - in some range sufficiently large to include all galaxies that could possibly be visible - so that the co-moving density was kept constant

i.e. $$P(x) \propto x^2 (1 - (2q_o - 1)x^2)^{-1/2}$$

(this is equivalent to $P(r_1) \propto r_1^2 (1-kr_1^2)^{-1/2}$).
The redshift is then given by

$$z = \left[x - x^2 q_o^2 - 1 + q_o - (q_o - 1)(1 - x^2 - 2x^2 q_o)^{1/2}\right] (1 - xq_o)^{-2}$$

and

$$D_L = c \times H_o^{-1} (1 + z)$$

and

$$D_A = c \times H_o^{-1} (1 + z)^{-1}$$

are the luminosity and angular diameter distances.

Each cluster is assigned NG (either a constant or according to some distribution) galaxies as members and absolute magnitudes M for them are generated according to some suitable luminosity function (e.g. Schechter 1976) and the galaxy is said to be visible and hence on the 'plate' if

$$M < m_{lim} - 25 - k(z) - 5 \log D_L \qquad (B.1)$$

where k(z) is the k-correction (possibly including an evolutionary term) and m_{lim} is the limiting magnitude. (Samples are for simplicity taken to be magnitude limited. This is of course no problem when identifying with earlier observations but does not follow the selection criteria for the present samples as specified in the text. This should not be important for comparative, interpretive purposes however).

If NV of the NG magnitudes generated for the cluster satisfy inequality (B.1) then MV galaxy positions in the cluster are generated (the magnitudes are

generated first to save unnecessary generation of positions for 'invisible' galaxies - this does not, of course, effect the randomness of the positions).

For any particular model the distribution of galaxies about the centre can be determined and the NV positions generated accordingly (e.g. uniformly in a sphere radius RC or with an R^{-2} fall-off out to RC etc.). In practice, since the diameter of the cluster is negligible as far as detecting members is concerned (this would not be true for a shallow sample), the projected densities are used so that the generation of r (according to some law) and θ (uniformly) give the position

$XG = XC - r \cos \theta$

$XG = YC - r \sin \theta$

of the galaxy directly on the 'plate'.

Thus we have a set of positions XG, YG on the plate which simulate a magnitude limited survey.

REFERENCES

Aarseth, S.J. and Binney, J., 1978, Mon.Not.R.astr.Soc., 185, 227.

Abell, G.O., 1958, Astrophys.J.Suppl., 3, 211

Abell, G.O., 1961, Astron.J., 66, 607.

Abell, G.O., 1962, in Problems of extragalactic research, ed. G.C. McVittie (New York; McMillan).

Abell, G.O., 1975, in Stars and Stellar systems, Volume IX, ed. A. Sandage, M. Sandage and J. Kristian (Chicago: University of Chicago press).

Abell, G.O., 1977, private communication.

Abell, G.O. and Mihalas, D.M., 1966, Astron.J., 71, 635.

Allen, C.W., 1973, Astrophysical quantities, 3rd edition (London; Athlone Press).

Arakelyan, M.A. and Kalloglyan, A.T., 1970, Soviet Physics - Astronomy, 13, 953.

Bahcall, J.N. and Joss, P.C., 1976, Astrophys.J., 203, 23.

Bahcall, N.A., 1973, Astrophys.J., 180, 699.

Bahcall, N.A., 1975, Astrophys.J., 198, 249.

Baker, E.A., 1949, Publ. R.O.E. 1, No.2.

Benedict, G.F., 1976, Astron.J., 81, 89.

Besag, J. and Diggle, P.J., 1977, J.R.S.S.(C), 26, 327.

Binney, J., 1976, Mon.Not.R.astr.Soc., 177, 19.

Blackman, R.B. and Tukey, J.W., 1958, The measurement of power spectra (New York; Dover).

Bogart, R.S. and Wagoner, R.V., 1973, Astrophys.J., 181, 609.

Brown, G.S. and Tinsley, B.M., 1974, Astrophys.J., 194, 555.

Carnochan, D.J., Navach, C. and Wilson, R., 1975, Mon.Not. R.astr.Soc., 172, 27P

Charlier, C.V.I., 1908, Arkiv Mat.Astr.Fys., 4, No.24.

Christensen, C.G., 1975, Astron.J., 80, 282.

Code, A.D., Welch, G.A. and Page, T.L., 1972, in The Scientific results from the orbiting astronomical observatory, ed. A.D. Code (Washington National Aeronautics and Space Administration).

Davis, M., Groth, E.J. and Peebles, P.J.E., 1977, Astrophys.J. (Letters), 212, L107.

Davis, M. and Peebles, P.J.E., 1977, Astrophys.J.Suppl., 34, 425.

Deharveng, J.M., Laget, M., Monnet, G. and Vuillemin, A., 1976, Astron.Astrophys., 50, 371.

Disney, M.J., 1976, Nature, 263, 573.

Dodd, R.J., Morgan, D.H., Nandy, K., Reddish, V.C. and Seddon, H., 1975, Mon.Not.R.astr.Soc., 171, 329.

Dodd, R.J., MacGillivray, H.T., Ellis, R.S., Fong, R. and Phillipps, S., 1976, Mon.Not.R.astr.Soc., 176, 33P.

Doroshkevic, A.G. and Shandarin, S.F., 1978, Mon.Not.R.astr. Soc., 182, 27.

Doroshkevic, A.G., Sunyaev, R.A., and Zeldovich, Ya. B., 1974, in IAU symposium No. 63 Confrontation of cosmological theories with observational data, ed. M.S. Longair, (Dordrecht, Reidel).

Dreyer, J.L.E., 1888, New general catalogue, Memoirs R.A.S., 49, 1.

Efstathiou, G., 1976, unpublished.

Efstathiou, G., 1977, private communication.

Ellis, R.S., Fong, R. and Phillipps, S., 1976, Mon.Not.R. astr.Soc., 176, 391

Ellis, R.S., Fong, R. and Phillipps, S., 1977a, Nature, 265, 313.

Ellis, R.S., Fong, R. and Phillipps, S., 1977b, Mon.Not.R. astr.Soc. 181, 163.

Fall, S.M., 1975, Mon.Not.R.astr.Soc., 172, 23P.

Fall, S.M., 1976a, D.Phil. Thesis (University of Oxford).

Fall, S.M., 1976b, Mon.Not.R.astr.Soc., 176, 181

Fall, S.M., 1978, Mon.Not.R.astr.Soc., 185, 165.

Fall, S.M., Geller, M.J., Jones, B.J.T. and White, S.D.M., 1976, Astrophys.J.(Letters), 205, L121.

Fall, S.M. and Tremaine, S., 1977, Astrophys.J., 216, 682.

Freeman, K.C., 1970, Astrophys.J., 160, 811.

Geller, M.J. and Davis, M., 1976, Astrophys.J., 208, 13.

Gott, J.R. and Rees, M., 1975, Astron.Astrophys., 45, 365.

Groth, E.J. and Peebles, P.J.E., 1975, Astron.Astrophys., 41, 143.

Groth, E.J. and Peebles, P.J.E., 1977, Astrophys.J., 217, 385.

Groth, E.J., Peebles, P.J.E., Seldner, M. and Soneira, R.M., 1977,Sci.Am., 237, 66.

Gudehus, D.H., 1973, Astron.J., 78, 583.

Gudehus, D.H., 1975, Publ.Astr.Soc. Pac., 87, 763.

Gunn, J.E. and Gott, J.R., 1972, Astrophys. J., 176, 1.

Hauser, M.G. and Peebles, P.J.E., 1973, Astrophys.J., 185, 757.

Herschel,W., 1811, Phil.Trans.Roy.Soc.Lond., 101, 269.

Herschel, J., 1864, General catalogue of nebulae.

Holmberg, E., 1937, Ann.Obs.Lund., No.6, 1.

Holmberg, E., 1962, in Problems in extragalactic research, ed. G.C. McVittie (New York, McMillan).

Holmberg, E., 1969, Arkiv.Astr., 5, 305.

Holmberg, E., 1975, in Stars and Stellar systems, Volume IX, ed. A. Sandage, M. Sandage and J. Kristian (Chicago; Chicago University Press).

van Houten, G.J., 1961, Bull.Astr.Inst.Neth., 16, 1.

Hubble, E.P., 1924, Annual Reports of Mount Wilson Observatory.

Hubble, E.P., 1927, Proc.Nat.Acad.Sci., 15, 168.

Hubble, E. P., 1934, Astrophys.J., 79, 8.

Hubble, E.P., 1936, The realm of the nebulae (London; Oxford University Press).

Hubble, E.P. and Tolman, R., 1935, Astrophys.J., 82, 302.

Icke, V., 1973, Astron.Astrophys., 27, 1.

Johnson, H.M., 1961, Astrophys.J., 133, 314.

Jones, B.J.T., 1976, Rev.Mod.Phys., 48, 107.

Kalinkov,M., Kuneva, I.F. and Gelovska, E.G., 1975, Comptes rendues de l'accademie bulgare des sciences, 28, 1573.

Liller, M.H., 1960, Astrophys.J., 132, 306.

Limber, D.N., 1953, Astrophys.J., 117, 134.

Limber, D.N., 1954, Astrophys., 119, 655.

Lundmark, K., 1924, Mon.Not.R.astr.Soc., 84, 747.

MacGillivray, H.T., 1975, PhD. Thesis (University of Edinburgh).

MacGillivray, H.T., Martin, R., Pratt, N.M., Reddish, V.C., Seddon, H., Alexander, L.W.G., Walker, G.S. and Williams, P.R., 1976a, Mon.Not.R.astr.Soc., 176, 265.

MacGillivray, H.T., Martin, R., Pratt, N.M., Reddish, V.C., Seddon, H., Alexander, L.W.G., Walker, G.S. and Williams, P.R., 1976b, Mon.Not.R.astr.Soc., 176, 649.

Mead, R., 1974, Biometrica, 30, 295.

Messier, C., 1784, Catalogue des nebuleuses et des amas d'etoiles (Paris, l'Imprimerie Royale).

Montgomery, D.C. and Tidman, D.A., 1964, Plasma kinetic theory (New York, McGraw Hill).

Neyman, J., 1962, in Problems of extragalactic research, ed. G.C. McVittie (New York, McMillan).

Neyman, J. and Scott, E.J., 1952, Astrophys.J., 116, 444.

Neyman, J., Scott, E.J. and Shane, C.D., 1953, Astrophys.J., 117, 92.

Nilson, P., 1973, Uppsala general catalogue of galaxies (Uppsala Astr.Obs.Ann. Vol.6).

Oemler, A., 1974, Astrophys.J., 194, 1.

Peebles, P.J.E., 1971, Physical cosmology (Princeton, Princeton University Press).

Peebles, P.J.E., 1973, Astrophys.J., 185, 413.

Peebles, P.J.E., 1974a, Astron.Astrophys., 32, 197.

Peebles, P.J.E., 1974b, Astrophys.J.Suppl., 28, 37.

Peebles, P.J.E., 1974c, Astrophys.J.(Letters), 189, L51.

Peebles, P.J.E., 1974d, Astron. Astrophys., 32, 391.

Peebles, P.J.E., 1974e, Astrophys.Sp.Sci., 31, 403.

Peebles, P.J.E., 1975, Astrophys.J., 196, 647.

Peebles, P.J.E., 1976a, Astrophys.J.(Letters), 212, L107.

Peebles, P.J.E., 1976b, Astrophys.Sp.Sci., 45, 3.

Peebles, P.J.E. and Groth, E.J., 1975, Astrophys.J., 196, 1.

Peebles, P.J.E. and Hauser, M.G., 1974, Astrophys.J.Suppl., 28, 19.

Pence, W., 1976, Astrophys.J., 203, 39.

Petrosian, V., 1976, Astrophys.J.(Letters), 209, L1.

Phillipps, S., Fong, R., Ellis, R.S., Fall, S.M. and MacGillivray, H.T., 1978, Mon.Not.R.astr.Soc., 182, 673.

Pratt, N.M., Martin, R., Alexander, L.W.G., Walker, G.S. and Williams, P.R., 1975, in Image processing techniques in astronomy (Dordrecht, Reidel).

Press, W.H. and Schechter, P., 1974, Astrophys.J., 187, 425.

Rood, H.J., Page, T.L., Kinter, E.C. and King, I.R., 1972, Astrophys.J., 162, 411

Rubin, V.C., 1954, Proc.Nat.Acad.Sci., 40, 541.

Rudnicki, K., Dworak, T.Z., Flin, P., Baranowski, B. and Sandrakowski, A., 1972, Acta Cosmologica, 1, 7.

Sandage, A., 1961, Astrophys.J., 133, 355.

Sandage, A., 1972, Astrophys.J., 178, 1.

Sandage, A., 1975, Astrophys.J., 202, 563.

Sandage, A. and Hardy, E., 1973, Astrophys.J., 183, 743.

Sandage, A. and Tammann, G.A., 1975, Astrophys.J., 196, 313.

Schechter, P., 1976, Astrophys.J., 203, 297.

Schechter, P. and Press, W.H., 1976, Astrophys.J. 203, 557.

Seldner, M. and Peebles, P.J.E., 1977a, Astrophys.J., 215, 703.

Seldner, M. and Peebles, P.J.E., 1977b, Astrophys.J. (Letters), 214, L1.

Seldner, M., Siebers, B., Groth, E.J. and Peebles, P.J.E., 1977, Astron.J., 82, 249.

Shane, C.D., 1956, in Vistas in astronomy, Volume 2, ed.A.Beer (London and New York, Pergamon Press).

Shane, C.D. and Wirtanen, C.A., 1967, Pub.Lick obs., 22, Part 1.

Shanks, T., 1978, Mon.Not.R.astr.Soc., preprint.

Shapiro, S., 1971, Astron.J., 76, 291.

Shapley, H., 1933, Proc.Nat.Acad.Sci. U.S., 19, 591.

Shapley, H., 1972, Galaxies, 2nd edition (Cambridge, Mass, Harvard University Press).

Shapley, H. and Ames, A., 1932, Ann.Harvard obs, 88, 43.

Simkin, S.M., 1975, Astron.J., 80, 415.

Slipher, V.M., 1915, Popular.Astr., 23, 21.

Slipher, V.M., 1922, Proc.Am.Phil.Soc., 56, 403.

Soneira, R. and Peebles, P.J.E., 1977, Astrophys.J., 211, 1.

Thuan, T.X. and Oke, J.B., 1976, Astrophys.J., 205, 360.

Tinsley, B.M., 1976a, private communication.

Tinsley, B.M., 1976b, preprint.

Tinsley, B.M., 1976c, Astrophys.J.(Letters), 209, L7.

Tinsley, B.M., 1977, Astrophys.J., 211, 621.

Totsuji, H. and Kihara, T., 1969, Publ.Astr.Soc. Japan, 21, 221

Turner, E.L. and Gott, J.R., 1975, Astrophys.J. (Letters), 197, L89.

Turner, E.L. and Gott, J.R., 1976, Astrophys.J., 209, 6.

de Vaucouleurs, A. and de Vaucouleurs, G., 1964, Reference catalogue of bright galaxies (University of Texas Press).

de Vaucouleurs, G., 1953, Astron.J., 58, 30.

de Vaucouleurs, G., 1956, in Vistas in astronomy, Volume 2, ed.A.Beer (London and New York Pergamon Press).

de Vaucouleurs, G., 1958, Astron.J., 63, 253.

de Vaucouleurs, G., 1961, Astrophys.J.Suppl., 5, 233.

de Vaucouleurs, G., 1963, Astrophys.J., 138, 934.

de Vaucouleurs, G., 1970, Science, 167, 1203.

de Vaucouleurs, G., 1971, Pub.Astr.Soc.Pac., 83, 113.

de Vaucouleurs, G., 1975, in Stars and stellar systems, Volume IX, ed.A.Sandage, M. Sandage and J.Kristian (Chicago, Chicago University Press).

de Vaucouleurs, G., 1975, Astrophys.J., 202, 319.

Wagoner, R.V., 1967, Nature, 214, 766.

Weinberg, S., 1972, Gravitation and cosmology (New York, John Wiley and Sons).

White, S.D.M., 1976, Mon.Not.R.astr.Soc., 177, 717.

Wirtz, C., 1918, Astr.Nach., 206, 109.

Wirtz, C., 1924, Astr.Nach., 222, 22.

Wolf, M., 1902, Heidelberg Pub., 1, 125.

Wolf, M., 1906, Astr.Nach, 170, 211.

Yu, J.T. and Peebles, P.J.E., 1969, Astrophys.J., 158, 103.

Zealey, W., 1976, private communication.

Zwicky, F., 1938, Publ.Astr.Soc.Pacific, 50, 218.

Zwicky, F., Herzog, E., Wild, P., Karpowicz, M. and Kopal, C.T., 1961-68. Catalogue of galaxies and clusters of galaxies (6 volumes). (Pasadena: California Institute of Technology).

Zwicky, F. and Rudnicki, K., 1963, Astrophys.J., 137, 707.

ACKNOWLEDGEMENTS

I would like to thank Professor A. W. Wolfendale for being my initial supervisor and setting me off in this field of research, Dr R. Fong for supervising my research as it developed and Dr. R. S. Ellis for much assistance especially with the computing.

I also acknowledge very useful discussions with my colleagues Tom Shanks and George Efstathiou, as well as many astronomers in Edinburgh and Cambridge, especially Drs. H.T. MacGillivray, R.J. Dodd, S.M. Fall and B.M. Tinsley.

I would also like to thank my mother for the careful typing of this thesis.

I was supported by an SRC research studentship during the course of the research and by a Durham University studentship during the final writing of the thesis.